GENERATION OF SYNTHETIC ANTIBODIES AS POTENTIAL THERAPEUTICS TO BLOCK IL3–MEDIATED INNATE IMATINIB RESISTANCE IN CHRONIC MEYLOID LEUKEMIA

A Thesis Submitted to the
College of Graduate and Postdoctoral Studies
In Partial Fulfillment of the Requirements
For the Degree of Doctor of Philosophy
In the Department of Pathology and Lab Medicine
University of Saskatchewan
Saskatoon, Canada

By
MAHSA ABRISHAMI

PERMISSION TO USE

In presenting this thesis in partial fulfillment of the requirements for a Postgraduate degree from the University of Saskatchewan, I agree that the Libraries of this University may make it freely available for inspection. I further agree that permission for copying of this thesis in any manner, in whole or in part, for scholarly purposes may be granted by the professor or professors who supervised my thesis work or, in their absence, by the Head of the Department or the Dean of the College in which my thesis work was done. It is understood that any copying or publication or use of this thesis or parts thereof for financial gain shall not be allowed without my written permission. It is also understood that due recognition shall be given to me and to the University of Saskatchewan in any scholarly use which may be made of any material in my thesis.

Requests for permission to copy or to make other use of material in this thesis in whole or part should be addressed to:

Dean
College of Graduate and Postdoctoral Studies
University of Saskatchewan
116 Thorvaldson Building, 110 Science Place
Saskatoon, Saskatchewan S7N 5C9
Canada

Head of the Department of Health Sciences
University of Saskatchewan
Saskatoon, Saskatchewan S7N 5E5
Canada

ACKNOWLEDGMENTS

I would like to sincerely thank my supervisor Dr. Geyer. I am grateful for your great mentorship, guidance and support during my PhD program.

I am thankful to my advisory committee, Dr. John DeCoteau, Dr. Andrew Freywald, Dr. Franco Vizeacoumar, and Dr. Maruti Uppalpati for spending the time to read my thesis and for providing valuable advice throughout the course of my graduate program.

I would like to express my gratitude to all of the members of the Geyer Lab for the great teamwork and for making the lab an enjoyable place to work. Thanks to Ashley Sutherland for her outstanding talent in preparing beautiful signaling and phage display figures for my thesis.

A special thank-you to Dr. Landon Pastushok whose constant help and support added considerably to my graduate experience. As well, I would like to thank Lindsay Pelzer and Karen Mochoruk for the encouragement, help and friendship. Thank you for taking the time out to help and support me when I needed it most.

I would like to thank my husband, Dr. Behzad Toosi, for all his great help at home and in the lab, for his understanding and patience. Our engraftment assays could not go so remarkable without his perfect tail vein injections. Thank you.

A very special thank-you to my wonderful son, Armaan, for making my days brighter with big smiles and hugs.

ABSTRACT

This thesis was focused on generation of novel antibodies as therapeutics to block innate imatinib resistance in chronic myeloid leukemia (CML). Tyrosine kinase inhibitor (TKI), imatinib, is the standard therapy for CML. Although many patients respond to the conventional TKI chemotherapy, the majority relapse upon withdrawal of treatment (Ross et al., 2013) implicating the inability of TKIs in eradication of leukemic stem cells (LSCs). Accumulating evidence demonstrates that bone marrow stromal cell secreting factors, such as Interleukin 3 (IL3) hinder TKI activity and support CML–LSCs to survive the therapy with innate drug resistance. Therefore, the overall objective of this work was to target IL3 receptor as the biomarker of LSCs in CML. We generated anti–IL3Rα and anti–IL3Rβ antibodies against IL3R using solid phase phage display selection. The phage–displayed antibodies were affinity–matured human anti–mIL3Rα and –β antibodies with nanomolar dissociation for the target proteins that bound to IL3 cell surface receptor on multiple CML cell lines. Anti–IL3Rα and anti–IL3Rβ antibodies successfully impaired IL3 downstream signaling, inhibited IL3–mediated CML cell proliferation, and promoted cell apoptosis and targeted LSCs by disruption of colony formation *in vitro*. Engraftment of cells treated with anti–IL3Rα and anti–IL3Rβ antibodies showed a prolonged survival of C57BL/6 mouse models that received antibody–treated CML cells. Encouraged by anti–leukemic activity of anti–IL3Rα and anti–IL3Rβ antibodies on CML cells, we used our novel antibodies to engineer anti–IL3Rα–IL3Rα and anti–IL3Rβ–IL3Rβ bivalent and anti–IL3Rβ–IL3Rα bispecific antigen binding fragments (Fabs) to enhance targeting of CML cells. SpyCatcher-SpyTag system was used to join IL3Rα / IL3Rβ mono–Fabs by a covalent bond. The bivalent and bispecific Fab formats against IL3Rα, IL3Rβ, or IL3Rα and IL3Rβ elicited nanomolar dissociation for the targets, bound to CML cells, and impaired IL3 signaling in CML cells *in vitro*. Remarkably, bivalent Fabs and bispecific Fab induced direct cytotoxicity on CML cells in a dose–dependent manner *in vitro*. In testing the Synergy / additive effect of Fabs and TKIs, adding imatinib to anti–IL3Rβ–IL3Rβ bivalent or anti–IL3Rβ–IL3Rα bispecific (but not anti–IL3Rα mono–Fab or anti–IL3Rα–IL3Rα bivalent Fab) augmented their cytotoxic potential on CML cells *in vitro*, suggesting the potential key role of targeting IL3Rβ to deplete CML–LSC.

This work provided novel anti–IL3Rα and anti–IL3Rβ antibodies, IL3Rα and IL3Rβ bivalent or bispecific Fabs to specifically target malignant CML blast cells and CML–LSCs. Future studies will advance preclinical strategies for targeted therapy and eradication of LSCs in CML patients.

TABLE OF CONTENTS

LIST OF FIGURES

LIST OF TABLES

LIST OF ABBREVIATIONS

2YT	2x yeast extract and tryptone
A loop	Activation loop
ABD	Actin-binding domain
ABL	Abelson murine leukemia viral oncogene
ABS	Absorbance
ADC	Antibody-drug conjugate
ADCC	Antibody-mediated cellular cytotoxicity
ADP	Adenosine diphosphate
ALL	Acute lymphoid leukemia
AML	Acute myeloid leukemia
AP	Accelerated phase
ATP	Adenosine triphosphate
ATP	Adenosine triphosphate
BC	Blast crisis
BCR	Breakpoint cluster region
BLI	Biolayer interferometry
BM	Bone marrow
BMSF	Bone marrow stromal factor
BRCA	Breast cancer associated
BSA	Bovine serum albumin
C-terminus	Carboxyl-terminus
CaLB	Calcium-dependent lipid-binding site
CAR	Chimeric antigen receptor
Carb	Carbenicillin
CC	Coiled-coil
CCC-dsDNA	Covalently closed circular dsDNA
CDC	Complement-dependent cytotoxicity
cDNA	Complementary DNA
CDR	Complementarity determining region
CFU	Colony forming unit
CH	Constant heavy chain
CL	Constant light chain
CLL	Chronic lymphoid leukemia
CML	Chronic myeloid leukemia
Cmp	Chloramphenicol
CNL	Chronic neutrophilic leukemia

CP	Chronic phase
CRM1	Chromosome region maintenance 1; also referred to as exportin1
DBD	DNA-binding domain
Dbl / CDC24	Diffuse B-cell lymphoma / Cell division control protein 24
DNA	Deoxyribonucleic acid
DNA-PK_{cs}	Catalytic subunit of DNA-dependent protein kinases
dNTP	Deoxyribonucleotide triphosphate
DSB	Double-strand break
DSBR	Double-strand break repair
dsDNA	Double stranded DNA
DTT	Dithiothreitol
dU-ssDNA	Deoxyuracil-containing ssDNA
E. coli	*Escherichia coli*
ECD	Extracellular domain
EGF	Epidermal growth factor
ELISA	Enzyme-linked immunosorbent assay
EML1	Echinoderm microtubule-associated protein-like 1
ETV6	Translocation-Ets-leukemia virus
F-actin	Filamentous-actin
Fab	Fragment antigen binding
FBS	Fetal bovine serum
Fc	Crystalizable fragment
FcγR	Fc gamma receptor
FDA	Food and Drug Administration
FTK	Fusion tyrosine kinase
FW	Framework
FYN	Src family tyrosine kinase
G-actin	Globular-actin
G.A.	Gibson assembly
GAP	Guanosine triphosphatase-activating protein
GFP	Green fluorescent protein
GM-CSF	Granulocyte-macrophage colony stimulating factor
GRB	Growth factor receptor-bound protein
HCK	Hematopoietic cell kinase
HEK	Human embryonic kidney
HER	Human epidermal growth factor receptor
HOXA9	Homeobox A9

HR	Homologous recombination
HRP	Horseradish peroxidase
HSC	Hematopoietic stem cells
IC_{50}	Half-maximal inhibitory concentration
Ig	Immunoglobulin
IGF-1	Insulin-like growth factor
IgG	Immunoglobulin G
IL	Interleukin
IPTG	Isopropyl β-D-1-thiogalactopyranoside
Kan	Kanamycin
K_D	Dissociation constant
Koff	Dissociation rate constant
Kon	Association rate constant
LB	Luria Broth
LMB	Leptomycin B
LSC	Leukemic stem cell
LYN	Lck/Yes novel tyrosine kinase
M	Molar
mAb	Monoclonal antibody
MBP	Maltose binding protein
MHC	Major histocompatibility complex
min	Minute
Myr	Meristotylation modification site
N-terminal	Amino-terminal
N-terminus	Amino-terminus
NES	Nuclear export signal
NGS	Next generation sequencing
NK	Natural killer
NLS	Nuclear localization signal
NUP98	Nucleoporin 98
OD	Optical density
ON	Over night
P	Proline
PBT	Phosphate buffered saline with BSA and tween 20
PCR	Polymerase chain reaction
PD-L	Programmed death-ligand
PDGFR	Platelet-derived growth factor receptors
PE	Phycoerythrin

PEG	Polyethylene glycol
PFU	Plaque forming units
PGM	Personal Genome Machine
Ph	Philadelphia chromosome
PIP2	Phosphatidylinositol 4,5-bisphosphate
PPs	Proline-rich SH3 binding sites
PRDX1	Peoxiredxin1
PSTPIP	Phosphate-interacting adaptor protein
PTD	Protein transduction domain
PxxP motifs	Proline-rich motifs
R	Receptor
RAB	RAS in the brain
RAC	RAS-related C3 botulinum toxin substrate
RAD	Radiation sensitive
RAS	Rat sarcoma
RIN	RAS and RAB interactor
RNA	Ribonucleic acid
ROS	Reactive oxygen species
rpm	Rotations per minute
RPMI	Roswell Park Memorial Institute
RT	Room temperature
RTK	Receptor tyrosine kinase
scFv	Single-chain variable fragment
SDS-PAGE	Sodium Dodecyl Sulphate Polyacrylamide Gel Electrophoresis
sec	Second
SFK	SRC family kinase
SH	SRC homology
SOC	Super Optimal Broth with Catabolic Repression
SP	Secretion signal peptide sequence
SRC	Sarcoma inducing gene of rous sarcoma virus
ssDNA	Single stranded DNA
STAT	Signal transducer and activator of transcription
Tet	Tetracycline
TKI	Tyrosine kinase inhibitor
TMB	3,3', 5,5'-tetramethylbenzidine
TNF	Tumor necrosis factor
TUSC2	Tumor suppressor protein FUS1
Tyr	Tyrosine

v-ABL	Ableson murine leukemia virus
VDJ	Variable, diversity, joining gene segments
VH	Variable heavy chain
VL	Variable light chain
WT	Wild-type
Y	Tyrosine
YFP	Yellow fluorescent protein

1. CHAPTER 1. INTRODUCTION

1.1 Scientific and clinical significance of the work

The reciprocal chromosomal translocation t(9;22)(q34;q11) produces the BCR-ABL oncogene, which is responsible for the onset of chronic myelogenous leukemia (CML) (Calabretta & Perrotti, 2004). CML initiates as a chronic phase (CP) disease and progresses to an accelerated phase and then to a more aggressive, treatment-resistant, blast crisis (BC) phase. The BCR-ABL tyrosine kinase inhibitor (TKI) imatinib is the standard therapy for CML. Imatinib is effective in suppressing CP-CML but does not completely eliminate BCR-ABL$^+$ leukemic stem cells (LSCs), which leads to drug resistance and disease relapse (Kreuzer et al., 2003).

BCR-ABL$^+$ LSCs can be resistant to imatinib despite no prior exposure to the drug (Elrick, Jorgensen, Mountford, & Holyoake, 2005; Kreuzer et al., 2003). The innate resistance of CML cells to imatinib can be mediated by cytokines secreted by bone marrow stromal cells (Weisberg et al., 2008). Bone marrow stromal-derived cytokines are associated with the long-term survival and proliferation of BCR-ABL$^+$ B-lineage acute lymphoblastic leukemia (B-ALL) (M. Y. Konopleva & Jordan, 2011) and prevent apoptosis of acute myeloid leukemia (AML) cells (M. Y. Konopleva & Jordan, 2011). In CML stem / progenitor cells, pro-survival and self-renewal pathways downstream of BCR-ABL are maintained in an activated state by cytokines (Belloc et al., 2009; Jorgensen & Holyoake, 2007; H Konig et al., 2008; Weisberg et al., 2008), which decreases their "addiction" to BCR-ABL (H Konig et al., 2008; Heiko Konig et al., 2008). Taken together, these studies implicate the association of bone marrow cytokines with innate imatinib resistance in CML cells and argue that elimination of these cells is crucial for developing curative strategies.

Antibodies have emerged as potent and effective molecular-targeted therapies for human cancers and are usually used in combination with chemotherapy (Finn, 2008). For example, promising results have been observed when anti-IGF-1R (insulin-like growth factor receptor 1) antibodies are combined with other drugs, such as carboplatin and paclitaxel (Chitnis, Yuen, Protheroe, Pollak, & Macaulay, 2008; Rodon, DeSantos, Ferry, & Kurzrock, 2008). Antibodies are particularly valuable for inhibition of cell surface receptors and recruitment of the host immune response to induce cellular cytotoxicity (Cheson & Leonard, 2008). This is particularly

important when targeting CML stem cells, where inhibition of a specific signaling pathway can be compensated by bone marrow cytokine stimulation of alternative pathways.

This chapter is an overview on CML, drug resistance in CML, the role of interleukin–3 signaling in innate drug resistance in CML, therapeutic antibodies, and antibody phage display as an effective method of generation of synthetic antibody inhibitors.

1.2 Chronic myeloid leukemia (CML)

Chronic myeloid leukemia (CML) is characterized by a neoplastic transformation of hematopoietic stem cells (HSCs) to leukemic stem cells (LSCs). This neoplastic transformation is the result of a reciprocal chromosomal translocation that was first discovered as Philadelphia chromosome [Ph^+], an abnormal shortened chromosome 22 (Nowell & Hungerford, 1961; Rowley, 1973). The reciprocal chromosomal translocation occurs by transposition of the 3' sequence from *ABL1* proto-oncogene on chromosome 9 with the 5' sequence of *BCR* gene on chromosome 22. The t(9;22)(q34;q11) translocation is the genetic hallmark of CML that generates *BCR-ABL1* oncogene (Bartram et al., 1983; S. E. Hernandez, Krishnaswami, Miller, & Koleske, 2004; Nowell & Hungerford, 1961; Rowley, 1973; Shtivelman, Lifshitz, Gale, Roe, & Canaani, 1986). BCR-ABL causes constitutive expression of *BCR-ABL* fusion tyrosine kinase protein that promotes CML pathogenesis (Bartram et al., 1983; Groffen et al., 1984; Heisterkamp et al., 1983; Kurzrock, Gutterman, & Talpaz, 1988; Nowell & Hungerford, 1961; Rowley, 1973; Shtivelman et al., 1986) (Figure1.1).

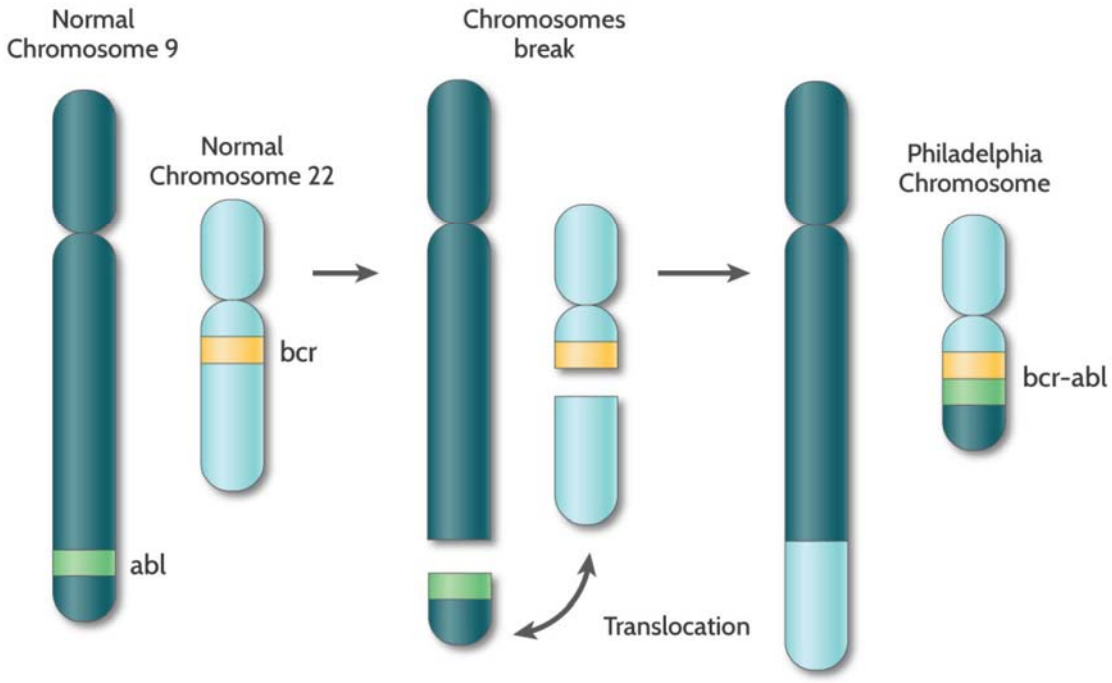

Figure 1.1. Philadelphia chromosome (Ph). Reciprocal chromosomal translocation between *BCR* gene on chromosome 22 and *ABL* gene on chromosome 9 results in the Philadelphia chromosome. The t(9;22)(q34;q11) translocation produces the *BCR-ABL1* fusion gene that encodes the *BCR-ABL* fusion protein.

1.2.1 Three phases of CML: Chronic Phase, Accelerated Phase, and Blast Crisis

CML initiates as a chronic phase (CP) and progresses to an accelerated phase followed by blast crisis phase (Kurzrock et al., 1988; Radich, 2007; Shet, Jahagirdar, & Verfaillie, 2002). The chronic phase is characterized by an elevated count of myeloid progenitor cells in the peripheral blood and an increase in the number of mature granulocytes. As the disease progresses to accelerated phase (AP), myeloproliferative acceleration develops as a result of myeloid cells losing their differentiation capacity. By disease progression to blast crisis (BC), the patient undergoes hematopoietic differentiation arrest, immature blast cell accumulation into the bone marrow, and blast cell spillage to the blood circulation (Kurzrock et al., 1988; Radich, 2007).

1.2.2 BCR-ABL and its oncogenic activity

1.2.2.1 BCR protein

BCR (breakpoint cluster region) is a signaling protein with complex modular domains, containing a coiled-coil oligomerization domain, a serine / threonine kinase domain with a Dbl / CDC24 guanine-nucleotide exchange factor homology domain, a pleckstrin homology domain, a putative calcium dependent lipid binding portion, and a RAS-related C3 botulinum toxin substrate (RAC) guanosine triphosphatase activating domain (Quintás-Cardama & Cortes, 2009; Ren, 2005). Tyrosine 177 (Y177) on BCR can be phosphorylated, producing a binding site for growth factor receptor-bound protein 2 (GRB2), GRB10, 14-3-3, and ABL1 proteins through its SRC homology 2 (SH2) domain (Figure 1.2) (Y. He et al., 2002; Quintás-Cardama & Cortes, 2009; Ren, 2005). The most common fusion sites on BCR are p185, p210, and p230 that generate BCR-ABL variants associated with ALL (acute lymphoblastic leukemia), CML, and CNL (chronic neutrophilic leukemia), respectively (Figure 1.2) (Advani & Pendergast, 2002; Quackenbush et al., 2000).

1.2.2.2 ABL family kinases

1.2.2.2.1 Structure and regulation of ABL kinase activity

The Abelson (ABL) non-receptor family kinases, ABL1 and ABL2, are closely related to each other and are >90% identical with unique and overlapping functions in cellular context

(Greuber, Smith-Pearson, Wang, & Pendergast, 2013; Quintás-Cardama & Cortes, 2009). Both ABL1 and ABL2 have SRC homology 3 (SH3), SH2, and SH1 tyrosine kinase domains. On the carboxyl terminal, both ABL1 and ABL2 have a conserved filamentous-actin (F-actin)–binding domain. The domain upstream of the F-actin domain is different in ABL1 and ABL2. ABL1 contains a globular (G)-actin binding domain, whereas ABL2 has a second internal F-actin binding domain. In addition, ABL1 contains nuclear localization signal motifs (NLS) and one nuclear export signal motif (NES) that enables nuclear and cytoplasmic localization of ABL1 (Figure 1.2). The major difference between ABL1 and ABL2 is that ABL2 lacks the NLS motif and hence, lacks the nuclear localization ability. Therefore, ABL2 is primarily localized in the cytoplasm. ABL1 and ABL2 have multiple isoforms formed by alternative splicing of the first exons, forming isoforms 1a and 1b (Colicelli, 2010; Greuber et al., 2013; Oliver Hantschel and Giulio Superti-Furga, 2000; Quintás-Cardama & Cortes, 2009).

ABL1 (v-ABL) was first discovered as the Ableson murine leukemia virus over 30 years ago (Abelson & Rabstein, 1970; Goff, Gilboa, Witte, & Baltimore, 1980). In the 1980's, Baltimore's team identified the human ortholog of ABL1 and its translocation product (BCR-ABL) in leukemias (Ben-Neriah, Daley, Mes-Masson, Witte, & Baltimore, 1986). The ABL1 fusion gene encodes the ABL1 tyrosine kinase that is constitutively activated in leukemia and induces cellular transformations (Colicelli, 2010; Ann Marie Pendergast, 2002). This non-receptor tyrosine kinase has two isoforms, human ABL1a and ABL1b, that are alternatively spliced at the first exon (Colicelli, 2010; Quintás-Cardama & Cortes, 2009; Ren, 2005). Aside from the spliced N-terminal, both ABL1a and ABL1b contain tandem SH3 and SH2 domains with a rigid scaffold and a tyrosine kinase domain (Figure 1.2) (Hantschel et al., 2003; Nagar et al., 2003). At the N-terminus, a short amino-terminal 'cap' maintains the stable conformation of the inactive ABL through surface interactions (Colicelli, 2010; Oliver Hantschel and Giulio Superti-Furga, 2000). Downstream of 'cap', SH2 and SH3 domains together generate an autoinhibitory structure that locks the kinase domain in the 'off state' (Nagar et al., 2003; Kristen M Smith, Yacobi, & Van Etten, 2003). Therefore, this intramolecular autoinhibition is a result of a SH3-SH2-SH1 'clamp structure' (Hantschel & Superti-Furga, 2004). The release of the kinase domain (SH1) from the SH2-SH3 tandem unlocks the active conformation (Hantschel et al., 2003; Hantschel & Superti-Furga, 2004; Nagar et al., 2003). ABL1b contains an extra myristoylation modification site at the extreme end of the N-terminal segment (Myr-HH). The

myristoyl group forms a ‘latch’ to the hydrophobic ‘pocket’ of the C-terminal lobe of the ABL kinase domain to reinforce the inhibitory ‘lock’ and stabilize the inactive conformation of the kinase domain (Colicelli, 2010; Greuber et al., 2013; Hantschel et al., 2003; Nagar et al., 2003; Quintás-Cardama & Cortes, 2009; Ren, 2005).

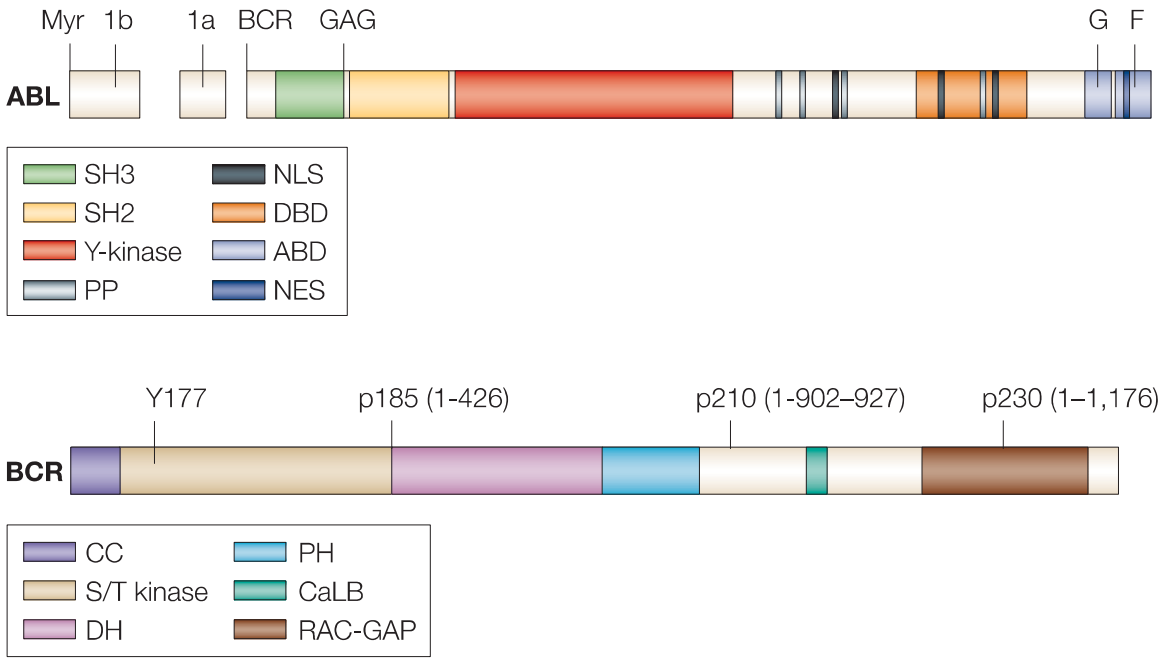

Figure 1.2. Schematic view of important domains in BCR and ABL proteins. Top panel: ABL. Myr (Meristoylation modification site) is the docking site for the amino-terminal glycine of the protein. Following an alternatively spliced sequences, the N–terminus of ABL protein has the tandem SRC homology 3 and 2 (SH3 and SH2), GAG (the fusion point of ABL to BCR), and tyrosine kinase domain (Y–kinase). On the C–terminal of ABL comprises of four proline-rich SH3 binding sites (PPs), three nuclear localization signals (NLSs), a nuclear exporting signal (NES), one DNA-binding domain (DBD), and the actin-binding domain (ABD) for monomeric (G) and filamentous (F) forms of actin. **Bottom panel: BCR**. BCR contains a coiled-coil (CC) oligomerization domain, a serine/threonine (S/T) kinase domain, a Dbl/CDC24 guanine-nucleotide exchange factor homology (DH) domain and a pleckstrin homology (PH) domain, a putative calcium-dependent lipid-binding site (CaLB) and a RAC guanosine triphosphatase-activating protein (RAC-GAP) domain. The numbers in brackets indicate the number of amino acids. Figure reprinted and modified with permission from Nature Reviews Cancer, 2005, vol.5 (3), p.172 (Ren, 2005).

1.2.2.2.2 Activation of ABL kinase

ABL (c-ABL or cellular ABL) is normally in a low catalytic activity state and is not phosphorylated on tyrosine residues (Dorey et al., 2001; Hantschel et al., 2003; Oliver Hantschel and Giulio Superti-Furga, 2000; Schindler et al., 2000). In the inactive conformation of a kinase domain, the activation loop (A loop) is inwardly folded into the active site and impairs ATP and peptide substrate binding to the active site (Levinson et al., 2006; Schindler et al., 2000). A loop lies at the interface of the small N-terminal and larger C-terminal of the catalytic domain of protein tyrosine kinase (Dorey et al., 2001; Oliver Hantschel and Giulio Superti-Furga, 2000),

ABL self-association via autophosphorylation is reported to be crucial for ABL tyrosine kinase activity (Brasher & Van Etten, 2000; Tanis, Veach, Duewel, Bornmann, & Koleske, 2003), whereby tyrosine residue(s) can be autocatalytically trans-phosphorylated in the activation loop (Colicelli, 2010; Dorey et al., 2001; Greuber et al., 2013). Active forms of ABL autophosphorylate *in trans* and stabilize the active conformation to promote its catalytic activity and enable various signaling pathways (Brasher & Van Etten, 2000; Colicelli, 2010; Dorey et al., 2001; Schindler et al., 2000). Sequential phosphorylation of ABL1 Tyr412, residing in the activation loop of SH1, and Tyr245, located in linker segment between the SH2 and the kinase domain, correlates with full catalytic activity of ABL and elevated kinase activity (Brasher & Van Etten, 2000; Colicelli, 2010). The key role of autophosphorylation has been further confirmed by chemically inducing dimerization of ABL1, which enhances the ABL tyrosine kinase activity and transformation capacity (K M Smith & Van Etten, 2001). Phosphorylation of Tyr412 and Tyr245 increases the ABL kinase activity by altering the ABL protein stability through ABL ubiquitylation and degradation (Echarri & Pendergast, 2001).

Cytoskeleton components of ABL allow direct binding of ABL to cytoskeletal elements(Colicelli, 2010). F-actin and G-actin domains are located at the C-terminal of ABL and provide binding sites for G-actin and F-actin bundle formations (Van Etten et al., 1994). ABL kinases engage actin polymerization in response to growth factor-mediated stimulations and other extracellular signals that promotes intracellular rearrangements, such as membrane protrusions, cellular morphology, and motility (W. D. Bradley & Koleske, 2009; Colicelli, 2010;

Greuber et al., 2013). Actin bundle formation may have a regulatory role on ABL kinase activity since binding to F-actin impairs ABL kinase activity in detached fibroblast cells (W. D. Bradley & Koleske, 2009; Woodring, Hunter, & Wang, 2001).

Signal transduction among ABL partners have been detected through engagement of phosphotyrosines or proline-rich motifs (PxxP motifs) on other ABL partner proteins (Colicelli, 2010). In addition to intramolecular interactions via SH3 and SH2 (Meyn et al., 2006; Ren, 2005; Kristen M Smith et al., 2003), ABL kinase activity can be regulated by multiple intermolecular interactions such as, ABL interactor proteins (ABI2 and ABI2) (Colicelli, 2010), adaptor proteins RAS and RAB interactor1 (RIN1) (Cao, Tanis, Koleske, & Colicelli, 2008), peroxiredoxin1 (PRDX1; also known as PAG) (Wen & Van Etten, 1997), the tumor suppressor protein FUS1 (or TUSC2) (Lin et al., 2007), phosphate-interacting adaptor protein PSTPIP1, and Phosphatidylinositol 4,5-bisphosphate (PIP2) (Colicelli, 2010; Greuber et al., 2013).

ABL kinase protein has 42% overall sequence homology with SRC family kinases and structurally resembles the inactive configuration of SRC family kinases (Melo & Deininger, 2004; Nagar et al., 2003; Quintás-Cardama & Cortes, 2009). ABL can be phosphorylated by SRC family of tyrosine kinases (S. Chen, O'Reilly, Smithgall, & Engen, 2008; Meyn et al., 2006; Tanis et al., 2003) and PDGFR (Platelet-derived growth factor receptor) (Plattner, Koleske, Kazlauskas, & Pendergast, 2004). Phosphorylation of ABL1 Tyr89 by SRC family kinases enhances the tyrosine kinase activity through disruption of SH3-SH2 autoinhibitory interactions (S. Chen et al., 2008; Colicelli, 2010; Meyn et al., 2006). Interestingly, this phosphorylation site (i.e. Tyr89) is associated with CML cell transformations (Meyn et al., 2006) and is phosphorylated by SRC family members, providing a critical regulatory mechanism in ABL signaling cascades (Colicelli, 2010; Meyn et al., 2006). In addition, ABL fusion proteins kinase activity can be widely stimulated by elimination of autoinhibition, myristoylation group, N-terminal Cap, transphosphorylation, oligomerization of ABL fusion proteins, or consistent SH3 retention (Colicelli, 2010; Greuber et al., 2013; Ren, 2005).

1.2.2.2.3 BCR-ABL oncoprotein

BCR-ABL contains the N-terminal 927 amino acids of BCR and the ABL sequence with the loss of its first exon (Ren, 2005). Several fusion proteins of BCR-ABL are characterized by

the most common fusion points on BCR (M. W. Deininger, Goldman, & Melo, 2000). Translocation-derived ABL1 and ABL2 oncoproteins are BCR-ABL1 p190 (also P185 in ALL and CML) (Dhingra et al., 1991; Puil et al., 1994), p210 (in CML), p230 (in CNL or chronic neutrophilic leukemia) (Pane et al., 1996), ETV6-ABL1 (CML and AML) (Golub et al., 1996; Janssen et al., 1995), Nup214-ABL1 (T-ALL) (Graux et al., 2004), EML1-ABL1 (T-ALL) (De Keersmaecker et al., 2005), and ETV6-ABL2 (AML)(Iijima et al., 2000).

Fusion of BCR and ABL proteins brings together multiple functional domains that serve as key essential motifs for leukemogenesis (Greuber et al., 2013; Hantschel & Superti-Furga, 2004; Quintás-Cardama & Cortes, 2009; Ren, 2005). The fusion of BCR to ABL releases the intramolecular inhibitory contacts, such as N-terminal Cap, SH3-SH2 clamp and myristoylation group leading to activation of ABL kinase domain (Greuber et al., 2013; Hantschel & Superti-Furga, 2004; Quintás-Cardama & Cortes, 2009; Ren, 2005). Unlike ABL, in the oncogenic BCR-ABL protein, the amino-terminal coiled-coil domain facilitates oligomerization that activates the ABL kinase activity (Y. He et al., 2002; McWhirter, Galasso, & Wang, 1993). ABL Tyr177 and the coiled-coil domain on BCR are the two key motifs for BCR-ABL activation (Oliver Hantschel and Giulio Superti-Furga, 2000; X. Zhang, Subrahmanyam, Wong, Gross, & Ren, 2001). The coiled-coil domain enables the autophosphorylation and dimerization of BCR-ABL proteins and Tyr 177 serves a docking site for downstream signaling proteins (Calabretta & Perrotti, 2004; Y. He et al., 2002; McWhirter et al., 1993; Ren, 2005). Therefore, full activation of BCR-ABL protein and ABL kinase activity requires dimerization and tetramerization of the protein through the coiled-coil domain of BCR (Y. He et al., 2002; McWhirter et al., 1993; Muller et al., 1991; Ren, 2005) and BCR phosphorylation at Tyr177 in order to induce the downstream signaling cascades (Quintás-Cardama & Cortes, 2009; Ren, 2005).

Similar to ABL, BCR-ABL contains three NLS and one NES on the C-terminal (described in 1.2.2.2.1). However, the nuclear-cytoplasmic shuttling of BCR-ABL is impaired by leptomycin B (LMB) through inhibition of NES receptor (also known as CRM1 or exportin 1) (Colicelli, 2010; Taagepera et al., 1998). This abrogation of BCR-ABL nuclear localization promotes DNA damage response functions and contributes to mitogenic and anti-apoptosis cascades and promote BCR-ABL cell transformation functions (Colicelli, 2010; Van Etten, Jackson, & Baltimore, 1989). Therefore, BCR-ABL nuclear entrapment may offer a potential

therapeutic strategy by targeting the BCR-ABL$^+$ LSCs and induction of apoptosis (Z.-L. Huang et al., 2013; Vigneri & Wang, 2001).

1.2.3 BCR-ABL and CML disease progression

The underlying mechanisms responsible for disease progression and transformation are poorly understood (Calabretta & Perrotti, 2004; Shet et al., 2002). The disease progression could be highly heterogeneous and is characterized by multiple chromosomal abnormalities, molecular defects, and cytogenetic alterations (H. M. Kantarjian et al., 1987; Shet et al., 2002), such as mutations, epigenetic changes, deregulation of lineage profiles, clonal hemopoiesis, DNA damage, or inflammatory responses (Beerman et al., 2013; Grover et al., 2016; Notta et al., 2016; Rossi et al., 2005).

1.2.3.1 BCR-ABL expression

BCR-ABL has an indispensable role in the onset and pathogenesis of CML. The unrestrained continual expression / activity of BCR-ABL kinase is a key to continuation and progression of CML. Elevated BCR-ABL RNA transcripts and BCR-ABL protein levels have been detected in blast crisis phase as compared with CP-CML (Gaiger et al., 1995; Guo, Wang, & Arlinghaus, 1991). Despite the critical role of BCR-ABL in CML, BCR-ABL-independent mechanisms may also contribute to CML cell transformations and disease progression. Overexpression of SFK (SRC family kinase), HCK (hematopoietic cell kinase), LYN (Lck/Yes novel tyrosine kinase), and FYN are involved in disease progression and drug resistance (Ban et al., 2008; Dai, Rahmani, Corey, Dent, & Grant, 2004; Donato et al., 2003, 2004).

1.2.3.2 BCR-ABL and chromosomal abnormalities

BCR-ABL promotes non-random chromosomal abnormalities; however, the pathogenetic association of chromosomal abnormalities to disease progression are not known (Calabretta & Perrotti, 2004; Shet et al., 2002). The most frequent chromosomal aberrations occur in chromosomes 8, 17, 19, and 22 with Philadelphia chromosome duplication (38%) or trisomy 8 (34%), and isochromosome 17 (20%) being the most common (Johansson, Fioretos, & Mitelman, 2002; Quintás-Cardama & Cortes, 2009).

Furthermore, secondary genetic alterations are corroborated to be relevant in survival of myeloid progenitors, dysregulation of differentiation and differentiation arrest in BC-CML cells, and disease progression (Mitani et al., 1994; Nakamura et al., 1996). Particularly, t(3;21)(q26;q22) translocation and expression of AML-1/EVI-1 protein appears to block differentiation in blast cells and to contribute in leukemogenesis upon coexpression with BCR-ABL (Cuenco & Ren, 2001; Kurokawa, Mitani, Imai, et al., 1998; Kurokawa, Mitani, Irie, et al., 1998). The t(7;11)(p15;p15) is another secondary chromosomal translocation in BC-CML and the chimeric NUP98/HOXA9 protein is associated with disease progression (Dash et al., 2002; Kroon, Thorsteinsdottir, Mayotte, Nakamura, & Sauvageau, 2001). BCR-ABL–NUP98/HOXA9 coexpression leads to expansion of progenitor cell population and differentiation arrest in BC-CML cells (Dash et al., 2002; Kroon et al., 2001; Mayotte, Roy, Yao, Kroon, & Sauvageau, 2002).

1.2.3.3 BCR-ABL and genomic instability / DNA repair

In 1992, Laneuville *et al*. demonstrated that genomic instability is highly associated with BCR-ABL translocation (Laneuville, Sun, Timm, & Vekemans, 1992). Since then, there have been many studies investigating roles of DNA damage and genetic instability as a key drivers for progression of CML to blast crisis (Burke & Carroll, 2010). Studies suggested that BCR-ABL compromises the efficiency or fidelity of DNA double sttand break (DSB) repair pathways, leading to misrepair of DSBs (Artur Slupianek, Nowicki, Koptyra, & Skorski, 2006), accumulation of other genetic defects, and disease progression (Shet et al., 2002). Multiple mechanisms have been suggested to promote genomic instability and defective DSB repair, such as BCR-ABL down-regulation of DNA-PK_{cs} levels (catalytic subunit of DNA-dependent protein kinases) (E Deutsch et al., 2001; Melo & Barnes, 2007), BCR-ABL down-regulation of BRCA-1 (a protein that participates in genomic integrity surveillance) (Risch et al., 2006),(Eric Deutsch et al., 2003), and activation of BCR-ABL–dependent pathways leading to enhanced expression / activity of RAD51 (a protein involved in homologous recombination repair (HRR)) (Shinohara & Ogawa, 1995; A Slupianek et al., 2001). Additionally, BCR-ABL may cause DNA damage by generation of endogenous reactive oxygen species (ROS) (Nowicki et al., 2004; Sattler et al., 2002). Furthermore, BCR-ABL abrogates DNA damage checkpoints through inhibition of the DNA-damage sensor kinases and disruption of cellular response to DNA damage by impairing

the inactivation of cell division cycles (Burke & Carroll, 2010; Dierov, Dierova, & Carroll, 2004; Quintás-Cardama & Cortes, 2009).

1.2.3.4 BCR-ABL and inactivation of tumor suppressor function

The most common gene mutations associated with BC-CML are in the tumor suppressor P53 (Calabretta & Perrotti, 2004; Quintás-Cardama & Cortes, 2009). P53 is located on the short arm of chromosome 17 (Ahuja, Bar-Eli, Advani, Benchimol, & Cline, 1989; Mashal et al., 1990) , which becomes genetically and functionally inactivated in 25–30% of BC-CML patients (Calabretta & Perrotti, 2004; Quintás-Cardama & Cortes, 2009). Several studies confirmed heterogeneous alterations in the structure of P53, such as reduced or undetectable expression of P53 or progressive expansion of P53 loss that contribute to blastic transformation (Ahuja et al., 1989; Mashal et al., 1990; Stuppia et al., 1997). Loss of P53 function can be linked to mutations (Foti, Bar-Eli, Ahuja, & Cline, 1990), deletions, or rearrangements (Fioretos et al., 1999). P53 mutation in CML disease progression has been extensively studied in various mouse models of P53-deficient ($P53^{-/-}$) (Skorski et al., 1996), P53 heterozygous ($P53^{+/-}$) (Honda et al., 2000), or cross heterozygous BCR-ABL ($BCR\text{-}ABL^{+/-}$) / heterozygous P53 ($P53^{+/-}$) (Donehower et al., 1992). These studies demonstrate the ability of BCR-ABL to accelerate leukemogenesis and CML blastic transformation upon P53 mutation (Calabretta & Perrotti, 2004). $BCR\text{-}ABL^{+}$ P53 deficient cells show a loss of lineage commitment and differentiation, higher level of resistance to apoptosis, and growth factor-independent high clonogenic potential (Calabretta & Perrotti, 2004; Skorski et al., 1996; Wlodarski et al., 1998). However, differentiation arrest in BC-CML cells is confirmed to be due to genomic instability caused by cumulative effect of BCR-ABL and loss of P53 function, not P53 inactivation alone (Wlodarski et al., 1998).

Another common mutation in BC-CML is a homozygous deletion of exon 2 at INK4A/ARF locus that occurs in about 50% of lymphoid blast crisis (Calabretta & Perrotti, 2004). This mutation eliminates P14/ARF and P16 proteins that regulate cell cycle progression and G1/S checkpoint by P53 upregulation and G1 phase Cyclin D inhibition, respectively (Serra, Gottardi, Della Ragione, Saglio, & Iolascon, 1995; Sill, Goldman, & Cross, 1995). Although ARF and P16 are both essential for lymphoid transformation in BC-CML, the relative

participation of ARF- or P16-dependent P53 activity is not known (Calabretta & Perrotti, 2004; Quintás-Cardama & Cortes, 2009; Radich, 2007).

1.2.4 BCR-ABL kinase downstream signaling pathways

BCR-ABL interacts with many signaling proteins via its functional domains / motifs and activates multiple downstream signaling pathways (Quintás-Cardama & Cortes, 2009; Rowley, 1973; Sattler et al., 2002). Two functional key motifs that are essential for BCR-ABL leukemogenesis are the coiled-coil oligomerization domain and Tyrosine 177 (Y. He et al., 2002; Quintás-Cardama & Cortes, 2009; Ren, 2005). The N-terminal coiled-coil oligomerization domain of BCR serves as an activator of ABL kinase and a plays a key role in dimerization of BCR-ABL through association of BCR-ABL with actin fibres (Figure 1.2) (McWhirter et al., 1993; Zhao, Ghaffari, Lodish, Malashkevich, & Kim, 2002). Therefore, the coiled-coil oligomerization domain mediates dimerization, cross-phosphorylation, and activation of BCR-ABL and stimulates cellular signaling. BCR Tyr177 serves an essential role in BCR-ABL leukemogenesis upon autophosphorylation (Sattler et al., 2002). BCR Tyr177 provides a docking site to engage the GRB2 protein that couples with GAB2 and activates phosphatidylinositol 3-(PI3K) and SHP2 (SH2 containing a ubiquitously expressed tyrosine-specific protein phosphatase) signaling pathways (Sattler et al., 2002) (Figure 1.3). The leukemogenic potential of BCR-ABL is markedly impaired by mutation of coiled-coil domain or Tyr177 (Y. He et al., 2002; Sattler et al., 2002; Kristen M Smith et al., 2003).

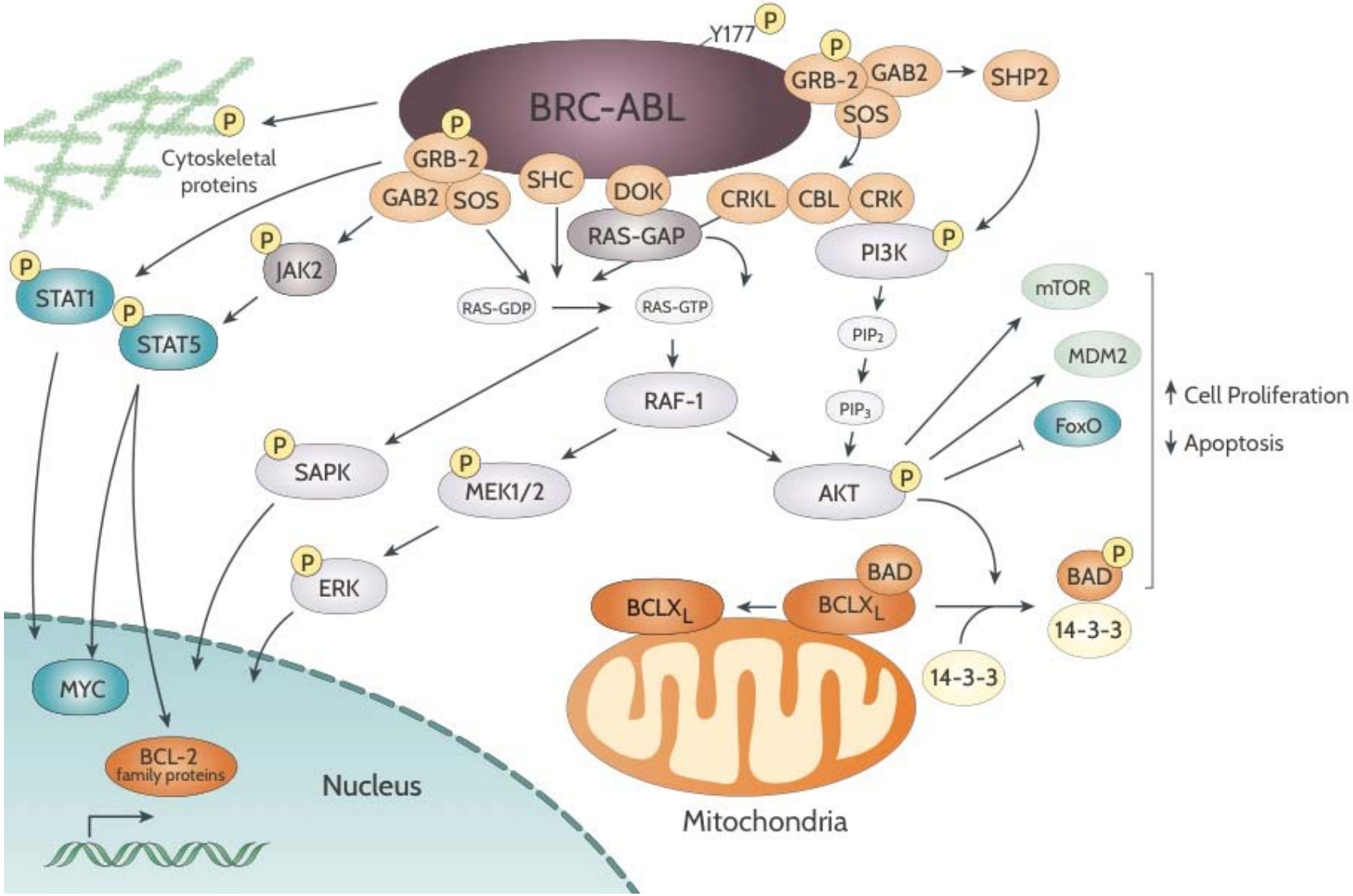
BRC-ABL
Y177
P
GRB-2
GAB2
SHP2
SOS
Cytoskeletal proteins
GRB-2
SHC
DOK
CRKL
CBL
CRK
GAB2
SOS
RAS-GAP
PI3K
JAK2
STAT1
STAT5
RAS-GDP
RAS-GTP
PIP2
PIP3
mTOR
MDM2
FoxO
RAF-1
SAPK
MEK1/2
AKT
ERK
BAD
BCLXL
14-3-3
MYC
BCL-2 family proteins
Nucleus
Mitochondria
Cell Proliferation
Apoptosis

Figure 1.3. BCR–ABL signaling. Upon dimerization of BCR–ABL, autophosphorylation of tyrosine 177 (Y-177) activates the kinase domain and generates a docking site for adapter proteins (light orange) such as GRB2. BCR-ABL–GRB2 is a stable complex that recruits SOS (Son of Sevenless; a guanine-nucleotide exchanger of RAS) and GRB2-associated binding protein 2 (GAB2) into the complex via the SH3 domain of GRB2. GRB2–SOS–GAB2 complex recruits multiple downstream pathways upon BCR–ABL dimerization that enhances cell survival, proliferation, and inhibition of apoptosis. A subset of the downstream BCR–ABL pathways and their constituent transcription factors (green) and apoptosis–related proteins (dark orange) are illustrated. The downstream serine / threonine–specific kinases such as RAS/ RAF, MEK / ERK, and PI3K / AKT signaling cascades (light grey) promote cell proliferation, regulate anti–apoptotic events and cell cycle progression. Constitutive activation of PI3K triggers serine / threonine kinases AKT, and activation of AKT phosphorylates multiple downstream signaling pathways, such as mTOR, FOXO, MDM2, BAD, and JAK / STAT pathways. These pathways are involved in increased cell proliferation, decreased apoptosis, and altered cell adhesion properties. Of note, this is a simplified illustration of BCR–ABL signaling and there are multiple other signaling cascades associated with BCR–ABL reported.

1.2.4.1 PI3K / AKT pathway

Autophosphorylation of Tyr177 residue on BCR-ABL generates a high-affinity binding site that is specifically recognized by the SH2 domain of GRB2. BCR-ABL–GRB2 is a stable complex that recruits SOS (Son of Sevenless; a guanine-nucleotide exchanger of RAS) and GRB2-associated binding protein 2 (GAB2) into the complex via the SH3 domain of GRB2 (Figure 1.3). Coupling of GRB2 and GAB2 scaffolding protein recruits SHP2 and PI3K cascades that both contribute to leukemogenesis. Constitutive activation of PI3K converts phosphatidylinositol bi-phosphate (PIP2) to phosphatidylinositol triphosphate (PIP3), which in turn triggers serine / threonine kinases AKT and 2-phosphoinositide-dependent protein kinase-1 (PDK1) that enables phosphorylation and activation of AKT (Figure 1.3). Activation of AKT phosphorylates multiple downstream signaling pathways, such as mTOR, FOXO, MDM2, BAD, and JAK / STAT pathways. These pathways increase cell proliferation, decrease apoptosis, alter cell adhesion properties, and migration that leads to premature release of immature myeloid cells, loss of growth factor dependence, HSC transformation, and CML progression (Ahmed & Van Etten, 2013; Calabretta & Perrotti, 2004; M. W. Deininger et al., 2000; Helgason, Karvela, & Holyoake, 2011; Quintás-Cardama & Cortes, 2009; Sattler et al., 2002; Skorski et al., 1997). In addition, GRB2 – GAB2 complex constitutively activates PI3K / AKT, as well as, extracellular signal-regulated kinase (ERK) in primary CML cells (Notari et al., 2006; Quintás-Cardama & Cortes, 2009). The downstream MEK / ERK signaling pathway is cytokine-dependent in chronic phase of CML, but becomes directly activated in accelerated and blast crisis phase (Notari et al., 2006; Quintás-Cardama & Cortes, 2009) (Figure 1.3).

1.2.4.2 RAS / RAF / MAP kinase pathway

As described above (section 1.2.4.2), BCR-ABL–GRB2 complex recruits SOS and GAB2 through the SH3 domain of GRB2. GRB2 / SOS complex initiates RAS (Helgason et al., 2011; Puil et al., 1994), which leads to downstream mitogen-activated protein kinase (MAPK) pathway. Growth factor-dependent stimulation of hematopoietic cells activates RAS and serine / threonine kinase RAF that leads to serine / threonine kinases MEK and ERK signaling cascades (Cahill, Janknecht, & Nordheim, 1996; M. W. Deininger et al., 2000; Marais, Light, Paterson, &

Marshall, 1995; Mizuchi et al., 2005; A M Pendergast et al., 1993; Quintás-Cardama & Cortes, 2009). Moreover, SH2 domains on ABL together with a tyrosine phosphorylation site on ABL kinase domain (Tyr1294 on BCR-ABL) are alternative activators of RAS.

RAS signaling pathway promotes growth and proliferation of myeloid cells. Moreover, RAS and downstream effectors of its signaling pathway regulate anti-apoptotic events and cell cycle progression(McCubrey et al., 2007). In particular, this pathway affects survival or apoptosis of cells, depending on the phosphorylation of specific residues on BCL2-like protein-11 (BIM) (K. Lei & Davis, 2003; Putcha et al., 2003) (Figure 1.3). Additionally, oncogenic RAS induces cell cycle arrest at G1 phase through various molecular mechanisms (Chang & McCubrey, 2001; Malumbres et al., 2000). As further support for the significance of RAS signaling, RAS antagonists (such as JUNB) or MEK / ERK inhibitors act as tumor suppressors in CML cells (Puil et al., 1994; Schorpp-Kistner, Wang, Angel, & Wagner, 1999).

1.2.4.3 JAK / STAT pathway

BCR-ABL phosphorylates the SRC family hematopoietic cell kinases (HCK) directly or indirectly through Janus kinase 2 (JAK2) (Calabretta & Perrotti, 2004; Ilaria & Van Etten, 1996; Klejman et al., 2002; S. Xie et al., 2001). Upon activation, phosphorylated HCK triggers the transcription factor signal transducer and activation of transcription 5 (STAT5) by phosphorylation of Tyr699 residue of STAT5B (Klejman et al., 2002; Nieborowska-Skorska et al., 1999). STAT5B then translocate to the nucleus to function as a transcription factor. Once in the nucleus, STAT5 induces transcription of various target genes (Beerman et al., 2013; Calabretta & Perrotti, 2004; Ilaria & Van Etten, 1996; Klejman et al., 2002; Nieborowska-Skorska et al., 1999) (Figure 1.3). BCL-XL is one of the STAT5 target genes with anti-apoptotic properties. BCL-XL is normally repressed by the transcription factor interferon consensus sequence binding protein (ICSBP) (Gabriele et al., 1999), but becomes transcriptionally activated by STAT5 (Gesbert & Griffin, 2000; Quintás-Cardama & Cortes, 2009). The constitutive phosphorylation of STAT5 leads to BCL-XL overexpression in CML cells and reduces susceptibility of CML cells to apoptosis (Calabretta & Perrotti, 2004; Horita et al., 2000; Klejman et al., 2002; Quintás-Cardama & Cortes, 2009). Similarly, BCR-ABL abrogates ICSBP-mediated inhibition of BCL-2 gene in the nucleus that causes BCL-2 transcription activation and

survival of CML progenitor cells (Calabretta & Perrotti, 2004; Quintás-Cardama & Cortes, 2009). In addition, BCR-ABL controls progenitor cell expansion and survival through controlling the expression of genes, such as Cyclins and CDK inhibitors (Calabretta & Perrotti, 2004; M. W. Deininger et al., 2001; Nosaka et al., 1999; Quintás-Cardama & Cortes, 2009). Modulation of gene transcription and upregulation of Cyclin D1 by BCR-ABL leads to cell cycle entry of primitive hematopoietic cells from G1 to S phase (Nosaka et al., 1999; Quintás-Cardama & Cortes, 2009). However, there is a discrepancy among several studies about the direct role of STAT5 in the gene transcription modulations of Cyclin D1 and alteration of cell cycle entry in CML cells (Frank & Varticovski, 1996; Grebien et al., 2008; Hoelbl et al., 2006; Sexl et al., 2000; Z. Yao et al., 2006). JAK / STAT pathway is negatively regulated by suppressors of cytokine signaling (SOCS) and cytokine-induced SH2 containing (CIS) family of proteins and protein phosphatases, such as CD45 (Steelman et al., 2004) (Figure 1.3).

1.3. Tyrosine kinase inhibitors and therapeutic implications

From 1960s to 1980s, busulfan, hyroxyurea, Interferon α (IFNα), and allogeneic hematopoietic stem cell transplantation were used as the standard therapies for CML (Bolin, Robinson, Sutherland, & Hamman, 1982; Goldman, 1992; H. M. Kantarjian et al., 1995). As the pivotal role of BCR-ABL in Philadelphia$^+$ leukemias was confirmed, BCR-ABL–mediated tyrosine kinase inhibition became an attractive target in many studies (Daley, Van Etten, & Baltimore, 1990; Krause & Van Etten, 2005; Pear et al., 1998). However, the inhibition of BCR-ABL kinase activity may lead to off–target activity and toxicity, largely due to tyrosine kinases being an indispensable part of various mechanisms in normal cells (Krause & Van Etten, 2005).

The protein tyrosine kinase family binds adenosine triphosphate (ATP) and catalyzes the phosphate transfer to tyrosine residues on proteins and induces tyrosine phosphorylation (Manley et al., 2002). Receptor tyrosine kinases (RTKs) and protein phosphatases regulate the reversible protein phosphorylation (Hunter, 2000; Pawson & Nash, 2000) and mediate signaling transductions that contribute to cell survival, growth, and differentiation (Lemmon & Schlessinger, 2010; Schlessinger, 2000). Dysregulation of these signaling pathways leads to oncogenesis (Blume-Jensen & Hunter, 2001). RTK activation requires ligand-induced receptor

oligomerization and tyrosine autophosphorylation of the receptor subunits (Hubbard & Till, 2000). Crystal structure of FGFR (Fibroblast growth factor receptor) and VEGFR (Vascular endothelial growth factor receptor) revealed a *cis* inhibition / *trans* activation mechanism that dictates the catalytic activity of the receptor through phosphorylation. When tyrosine residues in the activation catalytic loop are bound in *cis*, the substrate access to the binding sites and the ATP binding are blocked (Blume-Jensen & Hunter, 2001; Hubbard & Till, 2000). Upon ligand stimulation and dimerization of the receptor, tyrosine residues in the activation loop are phosphorylated in *trans* (Blume-Jensen & Hunter, 2001; Hubbard & Till, 2000). Point-mutations in the activation loop disturbs the balance in the *cis / trans* controlling system, leading to receptor activation and oncogenic outcomes (Blume-Jensen & Hunter, 2001). Disruption of RTK tyrosine phosphorylation by occluding the catalytic loop blocks the downstream signaling pathways required for cell proliferation and inhibition of apoptosis (M. Deininger, Buchdunger, & Druker, 2005; Shawver, Slamon, & Ullrich, 2002).

Since the first drug discovery by scientists at Ciba Geigy, now known as Novartis, protein tyrosine kinases have been attractive molecular targets for drug discovery (Traxler et al., 2001; Zimmermann et al., 1996). Originally, a 2-phenylaminopyrimidine derivative raised against protein kinase C (PKCα) was discovered by random screening and showed inhibition of both serine / threonine and tyrosine kinases with low potency and poor specificity (Buchdunger et al., 1996; M. Deininger et al., 2005). This lead structure was then further modified to enhance the tyrosine kinase activity (M. Deininger et al., 2005). The final compound lost its activity against PKCα and significantly increased the potency for inhibition of ABL tyrosine kinase. STI571 (formerly known as CGP57148B, now imatinib mesylate; Gleevec® or Glivec®, Novartis, Basel, Switzerland) emerged as a promising compound to approach further clinical development (M. Deininger et al., 2005; Traxler et al., 2001).

1.4. BCR-ABL tyrosine kinase inhibitors: CML frontline therapy

BCR-ABL is a non-receptor tyrosine kinase located in the cytoplasm of CML stem cells. Therefore, a soluble low molecular weight inhibitor is required to selectively target the intracellular BCR-ABL kinase activity in CML cells. Tyrosine kinase inhibitors (TKIs)

competitively target the intrinsic ATP-binding sites on tyrosine residues and block ATP binding to the kinase (Blume-Jensen & Hunter, 2001; M. Deininger et al., 2005; Shawver et al., 2002). ABL kinase inhibitors are classified into three groups based on their function: i) Inhibitors targeting the active conformation of the ABL kinase domain. Dasatinib and Bosutinib are type 1 inhibitors (Greuber et al., 2013); ii) Inhibitors targeting the inactive conformation of the ABL kinase domain and inhibit the kinase activation by stabilizing the closed conformation. Imatinib, nilotinib, and ponatinib are type 2 inhibitors (Greuber et al., 2013); iii) Allosteric inhibitors that are non-ATP competitive inhibitors of kinase domain targeting the regulatory domains to inhibit ABL kinase activity and decrease the BCR-ABL kinase activity. GNF2 and GNF5 are type 3 ABL kinase inhibitors that bind the myristoyl-binding pocket (J. Zhang et al., 2010).

1.4.1. Imatinib mesylate

Imatinib mesylate is the first generation BCR-ABL kinase inhibitor (M. Deininger et al., 2005; Traxler et al., 2001). Studies on the *in vitro* profile of imatinib confirmed its ability to inhibit the kinase activity at the cellular level. Particularly, imatinib inhibits ABL tyrosine kinase activity in BCR-ABL fusion proteins, such as p185 $^{BCR-ABL}$, p210 $^{BCR-ABL}$, and translocated (TEL)-ABL (Beran et al., 1998; Buchdunger et al., 1996; Carroll et al., 1997; Druker et al., 1996), but has no or weak inhibitory effect on tyrosine kinase activity of EGFR (Epidermal growth factor receptor) or VEGFR (Vascular endothelial growth factor receptor) (M. Deininger et al., 2005; Traxler et al., 2001). Furthermore, imatinib showed a preferential suppression of ligand-activated PDGFR (Platelet-derived growth factor receptor) and inhibition of stem cell factor (SCF)-mediated growth events such as KIT autophosphorylation and MAP kinase activation (Carroll et al., 1997; Heinrich et al., 2000; Traxler et al., 2001). In contrast, signaling pathways mediated by EGF (Epidermal growth factor), IGF (Insulin-like growth factor), FGF, (Fibroblast growth factor), and phrobol ester are non-responsive to imatinib (M. Deininger et al., 2005). Likewise, signal transduction mediated by FLT3 or CSF1 (colony stimulating factor 1), non-receptor tyrosine kinases SRC and JAK2 are insensitive to imatinib (Traxler et al., 2001). However, several other studies showed imatinib inhibited cell proliferation and induced apoptosis in BCR-ABL–expressing CML and ALL cells *in vitro* (Beran et al., 1998; Gambacorti-Passerini et al., 1997) and had anti-tumor activity *in vivo* (Wolff & Ilaria, 2001; X. Zhang & Ren, 1998). Based on the successful preclinical findings, an imatinib dose-escalating phase I clinical

trial started in IFNα (Interferon α)-resistant CML patients and revealed high response rates in all phases of CML (Traxler et al., 2001). Imatinib received food and drug administration (FDA) approval May 21, 2001 (Traxler et al., 2001).

Imatinib functions as a competitive inhibitor of the ATP-binding sites on ABL kinase domain (M. Deininger et al., 2005). The crystal structure of imatinib within the ATP-binding site of ABL kinase domain was solved by Cowan Jacob's research team (Manley et al., 2002) and revealed the underlying molecular mechanisms of imatinib activity. A key finding in Cowan-Jacob's report was that imatinib locks the receptor tyrosine kinase in a non-functional closed conformation, a kinase-inactive conformation whereby the N-terminal of the A-loop is folded into the ATP-binding site (Cowan-Jacob et al., 2004; Manley et al., 2002). They demonstrated that imatinib exploits the enlarged hydrophobic pocket (also called selectivity pocket in most kinases) for its selective binding, while the A-loop blocks the catalytic domain. This binding conformation of imatinib is highly selective for ABL kinases (Cowan-Jacob et al., 2004; M. Deininger et al., 2005; Manley et al., 2002). Imatinib interaction with ABL disrupts the ligand binding and prevents kinase phosphorylation and blocks the downstream BCR-ABL signaling (M. Deininger et al., 2005). The inhibition constant value (K_i) of imatinib is estimated 85 ± 19 nM for c-ABL (Manley et al., 2002). Mutations in the kinase domain have been discovered in 50-90% of the patients with secondary imatinib resistance (M. Deininger et al., 2005). The four most distinguishable hot spot clusters of mutations are in the ATP-binding loop (P-loop), T315, M351, and in the A loop, where mutations disrupt the binding of ABL kinase inhibitors (M. Deininger et al., 2005; Weisberg, Manley, Cowan-Jacob, Hochhaus, & Griffin, 2007).

1.4.2. Other tyrosine BCR-ABL kinase inhibitors as therapeutics for CML

Despite the success of imatinib as a first-line treatment for Ph^+ CML, imatinib resistance and / or lack of therapeutic response led to the development of additional TKIs specific for BCR-ABL. Two second generation TKIs gained FDA approval in 2007 and offered advantages over imatinib, including improved targeting of CML progenitors and in susceptibility to common imatinib resistance mutations (Hamad, Sahli, El Sabban, Mouteirik, & Nasr, 2013; Milojkovic & Apperley, 2009). Dasatinib is a dual SRC / ABL kinase inhibitor that binds ABL irrespective of conformation, as compared with imatinib that exclusively binds the closed / inactive

conformation (Shah et al., 2004). Further to the conformational flexibility, dasatinib was found to be over 300–fold more potent than imatinib at inhibiting ABL kinase activity *in vitro* (Milojkovic & Apperley, 2009). The other second generation TKI, nilotinib, binds the ABL kinase domain in the closed conformation but with 20 – 50 fold increase in potency over imatinib (Elias Jabbour, Cortes, & Kantarjian, 2009; Weisberg et al., 2005). A newer second generation TKI, bosutinib, recently gained FDA approval in 2012 but as with the aforementioned Dasatinib and Nilotinib, a common ABL kinase resistance mutation, T315I, renders it ineffective (Puttini et al., 2006). To overcome this problematic "gatekeeper" mutation, a third generation TKI named Ponatinib was designed with a structural feature that circumvents the bulk imparted by T315I (W.-S. Huang et al., 2010). However, mutations are emerging that lead to Ponatinib resistance (Korfi et al., 2015) and it is clear that complementary therapeutic approaches for CML should be explored.

1.5. Drug resistance

Imatinib is the best model of targeted cancer therapy with 85% eight-year overall survival in patients newly diagnosed with CML (Milojkovic & Apperley, 2008), yet there are several ways in which resistance occurs, including acquired and innate (*de novo*) mechanisms. Many studies are elucidating reasons by which resistance to imatinib may occur, but it is important to note that resistance mechanisms may not be mutually exclusive.

1.5.1 Acquired drug resistance

1.5.1.1 Mutations in ABL1 kinase domain

Point mutations within the kinase domain as a result BCR-ABL genomic instability are seen in 40 – 90% of drug resistant CML (Quintás-Cardama & Cortes, 2009; Quintas-Cardama, Kantarjian, & Cortes, 2009). This wide range is due to detection methods, nature of resistance, and disease phase (Quintas-Cardama et al., 2009). The ABL kinase mutations are detected in all phases during the course of CML (Milojkovic & Apperley, 2009). This high frequency of kinase domain mutations that affect imatinib binding is not surprising given the "rigid" structure of the ATP binding site and high selectivity of imatinib binding to the kinase domain (discussed in

1.4.1) (Schindler et al., 2000). Mutations that occur prior to TKI therapy (Kreuzer et al., 2003; Roche-Lestienne et al., 2002) in the kinase domains have been detected in some CML patients, including high Sokal risk (Carella et al., 2010), but most of the mutations occur following TKI treatment due to selective pressure (Griswold et al., 2006; Willis et al., 2005).

Kinase mutations cause resistance to imatinib in two ways. The first type of mutations alters essential residues in the kinase domain from contacting imatinib (Milojkovic & Apperley, 2009; Quintas-Cardama et al., 2009). The second type of mutations prevents the ABL kinase domain existing in a closed/inactive conformation necessary for imatinib binding. These mutations are generally classified in four categories depending on their ABL1 location. *i) Mutations in the P-loop* (*phosphate loop* or ATP binding site): 48% of all mutations in imatinib resistance cases are mapped to the *P-loop* (M. Deininger et al., 2005; O'Hare et al., 2005). Mutations of the P-loop are involved in disease transformation and confer poorer clinical outcome compared to other categories (Branford et al., 2003; Soverini et al., 2005), with the exception of M244V, which may not generally confer a poor prognosis. These mutations destabilize the conformation of ATP binding site (E Jabbour et al., 2006; Milojkovic & Apperley, 2009; Quintas-Cardama et al., 2009). *ii) imatinib binding site*, and *iii) catalytic domain mutations*: These two categories inhibit imatinib binding through destabilizing the binding conformation (Milojkovic & Apperley, 2009; Quintás-Cardama & Cortes, 2009). *iv) Mutation in the A-loop (Activation loop):* mutations in the A-loop affect the regulatory component of ABL and result in an open/active conformation that prevents imatinib binding (Milojkovic & Apperley, 2009; Quintas-Cardama et al., 2009). Conformational changes in the A-loop block imatinib binding, although dasatinib still binds to this active conformation (Quintás-Cardama & Cortes, 2009; Schindler et al., 2000).

T315I (Threonine-315–Isoleucine) is the most significant and frequently identified point mutation that occurs in 48% of imatinib resistance cases (Branford et al., 2003). T315I was first identified in 2001(Gorre et al., 2001). T315 is also known at the 'gatekeeper' residue, situated at the periphery of the nucleotide-binding site of ABL1 within the imatinib binding site (E Jabbour et al., 2006; Elias Jabbour et al., 2008). This residue is particularly significant because T315 forms a key H-bond interaction with imatinib and dasatinib (Nagar et al., 2002). T315 mutation to isoleucine blocks the H-bond and make it insensitive to imatinib, and impairs its binding to the

second generation of TKIs dasatinib, nilotinib, bosutinib, and INNO406 (Gorre et al., 2001; H. Kantarjian et al., 2006; Lombardo et al., 2004; O'Hare, Eide, & Deininger, 2007; Shah et al., 2004; Talpaz et al., 2006; Weisberg et al., 2005). T315I has been reported in up to 19% of patients with persistent imatinib-resistant CML (Cortes et al., 2007).This phenotype has spurred the invention of the third generation of ABL1 TKIs, such as Ponatinib that are not be susceptible to T315I/A (Isoleucine/Alanine)-mediated resistance (O'Hare, Deininger, Eide, Clackson, & Druker, 2011; Patel, O'Hare, & Deininger, 2017).

Taken together, high frequency of point-mutations causing imatinib resistance and the numerous sites of mutations in the BCR-ABL kinase domain underscores the importance of developing other therapeutics for TKI-resistant CML.

1.5.1.2 Bioavailability / intracellular availability of imatinib

Multidrug efflux transporters of the ATP-binding cassette (ABC) transporter family are involved in restricting drug uptake by pumping imatinib out of the CML cells (Arceci, 1993). ABCB1 transporter or multidrug resistance 1 (MDR-1) are overexpressed in blast phase patients (Soverini et al., 2005) and lead to reduced efficacy of chemotherapy in advanced phase CML (Kuwazuru et al., 1990) and imatinib resistance (Mahon et al., 2003). In addition, inhibition of imatinib influx by OCT-1 (organic cation transporter) (Crossman et al., 2005; Thomas, Wang, Clark, & Pirmohamed, 2004) may disrupt imatinib transport into the CML cells (Sakata et al., 2004). Higher doses of imatinib are required to overcome the low OCT-1 activity (White et al., 2007).

1.5.1.3 Amplification of BCR-ABL

Increased expression of BCR-ABL mostly occurs in accelerated phase of CML (Jamieson et al., 2004). High levels of BCR-ABL expression is generally correlated with lower sensitivity to imatinib and more tendency toward imatinib resistant mutant sub-clones (Barnes et al., 2005). Similarly, Nilotinib resistance has been identified in BCR-ABL overexpressing CML cells *in vitro* (Mahon et al., 2008).

1.5.1.4 Alternative signaling pathways that promote cell survival and proliferation

BCR-ABL–independent mechanisms that promote CML progression can contribute to drug resistance. Members of SRC family kinase, such as HCK, LYN, and FYN (Ban et al., 2008; Dai et al., 2004; Donato et al., 2003, 2004) are expressed on myeloid cells (Danhauser-Riedl, Warmuth, Druker, Emmerich, & Hallek, 1996; Quintás-Cardama & Cortes, 2009), and have a key role in imatinib resistance and disease progression to blast crisis. In particular, lymphoid blast phase is promoted by LYN and HCK upregulation (Donato et al., 2003; Hu et al., 2006). In addition, overexpression of LYN occurs in imatinib resistant cells lines *in vitro* (Dai et al., 2004).

1.5.2 Innate drug resistance (*de novo* resistance)

Despite the importance of acquired drug resistance and disease relapse after prolonged cytotoxic therapies, there is increasing evidence that mechanisms behind the initial escape of cancer stem cells from the therapies represent a more promising target for real curative therapies (Meads, Gatenby, & Dalton, 2009). Cancer stems cells are an important topic in cancer research today and were first identified by Bonnet and Dick in studies of AML (Bonnet & Dick, 1997). As such, much of what has been studied regarding these leukemic stem cells (LSC) may be applied to CML. A core concept of LSC is that a distinct population of leukemic cells retains long-term self-renewal capacity and the ability to give rise to differentiated leukemic progeny. In addition to the dynamic heterogeneity, there are several innate intrinsic (or intracellular) and extrinsic (or extracellular) properties that make LSCs difficult therapeutic targets (Meads et al., 2009). Clearly, targeting the primary events contributing to LSC survival could prevent the emergence of secondary acquired phenotypes with poorer outcomes.

1.5.2.1 Intrinsic innate resistance properties of LSCs

The cell cycle status of LSCs is thought to be a prominent contributor to intrinsic innate resistance. LSCs reside in a quiescent state in the cell cycle with no active cell replication or division. Repopulation studies using transplanted quiescent primitive AML cells confirmed the leukemic potential of these cells (Guan, Gerhard, & Hogge, 2003). Similarly, quiescent cell populations are found in the primitive CML cells (Holyoake et al., 2001; Holyoake, Jiang, Drummond, Eaves, & Eaves, 2002). Quiescence, therefore, plays a key role in innate immunity since therapies mostly target cycling cells, as is the case for imatinib and BCR-ABL (Holyoake et al., 2001, 2002). The result is persistence of quiescent cells in the presence of drugs.

Activation of pro-survival and self-renewal signaling pathways are common distinguishing features of LSCs over normal stem cells (Monica L Guzman & Allan, 2014; M. Y. Konopleva & Jordan, 2011). NF-κB pathway is one of the central pro-survival and proliferation pathways activated in LSCs. NF-κB pathway is upregulated in primitive AML cells (M L Guzman et al., 2001) and is suggested to be downregulated by proteasome inhibitors, leading to elimination of LSCs (Monica L Guzman et al., 2002). In particular, studies show that protein kinase CK2 inhibition leads to downregulation of stem cell-regulating protein BMI-1, which, in turn, causes inhibition of NF-κB, STAT3, and AKT, resulting in poor survival of LSCs (Quotti Tubi et al., 2017). This confirms that LSC survival is associated with multiple pro-survival pathways mediated by NF-κB, STAT3, and AKT (Quotti Tubi et al., 2017).

Other innate properties of LSCs that confer intrinsic resistance to therapy are excessive self-renewal and anti-apoptotic activities. Some self-renewal pathways that are aberrantly expressed or over-activated in LSCs include WNT/β-catenin, NOTCH/Hedgehog, and members of the clustered HOX gene family and the polycomb group protein BMI1 (Huntly & Gilliland, 2005; Krause & Van Etten, 2007). For example, a mouse model of AML was used to demonstrate the requirement of WNT/β-catenin for LSC self-renewal, and the β-catenin expression inhibitor indomethacin caused LSC impairment (Yingzi Wang et al., 2010). While self-renewal allows LSCs to persist, anti-apoptotic activity allows LSCs to counter therapy-mediated effects, such as imatinib-induced apoptosis in BCR-ABL expressing cells (Dan, Naito, & Tsuruo, 1998). LSCs are found to overexpress key anti-apoptotic proteins Bcl-XL and Bcl-2, and the ABT-737 inhibitor of Bcl-2 was found to effectively and selectively kill AML blast, progenitor, and stem cells (M. Konopleva et al., 2006). In CML, the self-renewal regulator Musashi has a major role along with Numb in the transition to CML blast crisis (T. Ito et al., 2010). Finally, oxidation and oxidative stress in LSCs has a role in inhibiting self-renewal (K. Ito et al., 2004).

1.5.2.2 Intercellular / Microenvironment-mediated properties of LSCs

The influence of tumor microenvironment on tumor cell survival has been elucidated by several studies as a passive cross–talk, meaning that LSCs benefit from the same molecular conditions that enable self-renewal, differentiation and cell survival of normal HSCs (Tlsty &

Coussens, 2006). Understanding this microenvironmental cross–talk is of great importance since a small subset of cancerous stem cells do not succumb to the therapy and survive. The interaction of these cells with their microenvironment is one of the major factors that allows them to stay in a quiescent protected state during the therapy that leads to their survival and disease relapse (Meads et al., 2009). Cells survival and drug resistance may reflect the separate or additive effect of cell-cell, cell-extracellular matrix, or cell-growth factor interactions (Meads et al., 2009; Y Nefedova, Landowski, & Dalton, n.d.). These interactions can be classified in two categories:

1.5.2.2.1 Cell adhesion-mediated drug resistance

A number of studies have elucidated that cell survival can be regulated by the microenvironment. Cell adhesion to the extracellular matrix component, fibronectin, has been widely investigated as a multi-drug resistant phenotype in human myeloma and leukemia cells (de la Fuente et al., 2002; Hazlehurst, Damiano, Buyuksal, Pledger, & Dalton, 2000; G. Scott, Cassidy, & Busacco, 1997; Shain, Landowski, & Dalton, 2002). Furthermore, studies have confirmed the engagement of integrin by fibronectin (Damiano, Cress, Hazlehurst, Shtil, & Dalton, 1999) and adhesion-mediated reduction of apoptosis in direct contact with normal bone marrow stromal cell (Damiano et al., 1999; Lagneaux, Delforge, Bron, De Bruyn, & Stryckmans, 1998; Matsunaga et al., 2003). These studies confer that higher expression of integrin α4β1 is correlated with disease relapse and poorer outcome in both solid tumors and leukemia (Folgiero et al., 2008; Graf et al., 2006; Nikkola et al., 2004; Oshita et al., 2002; Vuoristo et al., 2007; E. S. Yao et al., 2007).

Various other mechanisms are implicated with *de novo* resistance through integrinβ. G1 cell cycle arrest through p21 or p27 upregulation (Hazlehurst et al., 2000; Yulia Nefedova, Cheng, Alsina, Dalton, & Gabrilovich, 2004), modulation regulators of apoptosis and proliferation such as FAS (CD95) (Shain et al., 2002), CASP8, and FADD-like apoptosis regulator (FLIP) (Shain et al., 2002), or degradation of BCL2-interacting mediator of cell death (BIM) (Hazlehurst et al., 2000) are all induced by β1 integrin-mediated adhesion in myeloma and leukemia cells. Other extracellular matrix components such as collagen, and laminin bestow *de novo* drug resistance phonotypes, as well (Meads et al., 2009).

1.5.2.2.2 Soluble factor-mediated drug resistance (SFM-DR)

Since the first discovery of soluble factors stimulating the proliferation of bone marrow hematopoietic cells by Metcalf's group (T. R. Bradley & Metcalf, 1966), bone marrow cells, microenvironment, and various soluble factors have been extensively studied. In 2003, Nefedova *et al*. demonstrated that direct contact of myeloma cells with conditioned media from stromal cells protected them against drug-induced apoptosis (Y Nefedova et al., n.d.). A number of other studies on solid tumors and hematopoietic malignancies confirmed the effect of soluble factors (such as Interleukin–6, IL6) on tumor cell desensitization to cytotoxic drugs (Borsellino et al., 1999; Catlett-Falcone et al., 1999; Duan et al., 2006; Frassanito, Cusmai, Iodice, & Dammacco, 2001; Perez et al., 2008). Similarly, bone marrow stromal cell-mediated survival of BCR-ABL expressing cells in response to TKIs have been corroborated in several studies (Liesveld, Harbol, & Abboud, 1996; Weisberg et al., 2008).

Soluble factors are cytokines, chemokines, and growth factors that are highly produced by various cells in the stem cell microenvironment (Meads et al., 2009). Bone marrow is a complex heterogeneous dynamic microenvironment, consisting of mesenchymal stem cells, mesenchymal stromal cells, pericytes, advetitial cells, endothelial cells, fibroblasts, marrow adipocytes, and hematopoietic and immune cells (Sobacchi, Palagano, Villa, & Menale, 2017). The regulatory system of the normal HSCs (and LSCs) is a complex interplay of cells, extracellular matrix compartments, and secreted soluble factors in bone marrow niche (M. Y. Konopleva & Jordan, 2011). Multiple proliferation and prosurvival signaling pathways modulate the normal hematopoietic cell survival, proliferation, and apoptosis, through cytokine receptors (such as CD123 and CD47), which could potentially lead to drug resistance in LSCs. Moreover, some of the self-renewal cascades (such as WNT) may augment LSC survival (Yingzi Wang et al., 2010) or even be mediated by bone marrow niche (Fleming et al., 2008). The bone marrow niche cell-cell and cell-microenvironment interactions and cross–talks have provided a framework for researchers to identify and validate novel therapeutics targeting the LSC itself or its microenvironment (M. Y. Konopleva & Jordan, 2011; Meads et al., 2009). These novel targeted therapies may trigger: a) Prosurvival pathways regulated by stromal cells in the bone marrow; b) The critical self-renewal signaling cascaded in the LSCs promoted by bone marrow niche; c) The homing, adhesion, and migration of LSCs controlled by chemokines and adhesion molecules; d) The hypoxic milieu of bone marrow niche; e) The aberrant intracellular signaling pathways activated in bone marrow cells (M. Y. Konopleva & Jordan, 2011).

Interleukin 3 (IL3) is one of the cytokines secreted by bone marrow stromal cells (Moore, 2005). IL3 is an emerging cytokine that may have an crucial role in the prosurvival and self-renewal of CML-LSCs against TKI therapies (Nievergall et al., 2014).

1.6 Interleukin–3 (IL3)

1.6.1 IL3 cytokine and its physiological relevance in normal hematopoiesis

Interleukin–3 (IL3) is a product of activated T cells and mast cells that bridges the immunity and hemopoietic machinery (T. R. Hercus et al., 2013, 2017; Murphy & Young, 2006). IL3 has a regulatory function on hematopoietic cells / stem cells (Ihle, 1992; Rothenberg et al., 1988) and a key role in immunological response by development and recruitment of mast cells and basophils (S. Kim et al., 2010; Lantz et al., 1998). IL3 is a key cytokine in early hematopoiesis and proliferation of myeloid lineages and supports myeloid cell differentiation (Ihle, 1992; Lachmann et al., 2014).

1.6.2 IL3 cytokine and its biological relevance in CML

IL3 is a member of four-helical bundle family of cytokines that includes other cytokines / growth factors such IL5 and GM-CSF, as well as, IL4 and erythropoietin (Mott & Campbell, 1995) IL3 has crucial roles in regulation of hematopoietic cell growth and contributes to development of leukemia in animal models and in humans (Alexander & Nicola, 1998; Zhu & Emerson, 2002). Specifically, IL3 is shown to have relevance in leukemogenesis of BCR-ABL expressing cells (Holyoake et al., 2001; Wong et al., 2003). The connection between IL3 signaling and AML is well-established (Jin et al., 2009) and it remains to be seen if similar connection exists in CML.

Why is IL3 emerging as a therapeutic target for CML? CML evolved as a paradigm for targeted therapies since treatment with first generation TKIs lead to significant patient survival (Hughes et al., 2006), and even faster and higher molecular response rate (MMR) was found in patients treated with second and third generation TKIs (Larson et al., 2012; Shah et al., 2016). Nonetheless, TKIs do not completely eradicate LSCs. LSCs persistence and disease relapse after imatinib cessation is observed in 61-66% of patients, despite the prolonged treatment and durable complete molecular response (CMR) (Chomel et al., 2011; Chu et al., 2011; Mahon et al., 2010).

The TKI-refractory subset of cells that evade the therapy may be the source of post-treatment relapse and drug resistance. This subset of cells represents a promising target for further investigation in terms of surface markers, intra / intercellular regulatory mechanisms, and interactions / cross–talk with their microenvironment. Some studies have elucidated that a cytokine-induced JAK / STAT signaling mediates $CD34^+$ CML-LSCs drug resistance (Hiwase et al., 2010; Traer et al., 2012; Ying Wang et al., 2007). IL3, as a strong inducer of JAK / STAT cascade, represents a promising target with pathophysiologic relevance in CML (Horita et al., 2000). Importantly, multiple studies have shown that CML-LSCs with $CD34^+$ and $CD34^+$ / $CD38^-$ immunophenotype produce IL3 and granulocyte-stimulating factor (G-CSF) that activate autocrine activation loops linked to innate imatinib resistance in CML (Holyoake et al., 2001; Jiang et al., 2007; Jiang, Lopez, Holyoake, Eaves, & Eaves, 1999).

1.6.3 IL3 receptor structure

IL3 / GM-CSF / IL5 family of cytokines have multiple roles in cell survival, proliferation, differentiation, and cell migration. Generally, their pleiotropic functions initiate by ligand binding to the receptor through two subunits, which in turn triggers a cascade of intracellular signaling events, leading to their key cellular functions (Broughton et al., 2012; Murphy & Young, 2006).

The structure of a functional analog of IL3 was solved by NMR spectroscopy (Feng, Klein, & McWherter, 1996). IL3 receptor belongs to type I cytokine receptor superfamily (Murphy & Young, 2006). The fold of these proteins is arranged in a way that four α–helices are situated anti-parallel in sets of two, an "up-up-down-down" topology (Abdel-Meguid et al., 1987). This family of receptors is characterized by a cytokine–receptor module (CRM) with a conserved sequence arrangement in the ectodomain (Murphy & Young, 2006), and a cytoplasmic domain lacking catalytic activity (Murphy & Young, 2006). Studies have discovered several conserved key residues on human IL3 cytokine that are required for IL3 binding to the receptor α–subunit (Glu22) (Klein et al., 1997) and β–subunit (GLu43, Glu44, Arg94, and Lys110) binding motifs (Olins et al., 1995). IL3 receptor contains two heterodimeric polypeptide chains: cytokine-specific α–subunit and signal transducing β–subunit.

1.6.3.1 Cytokine-specific α subunit and its functional implications

IL3 binds to IL3 receptor α–subunit that confers binding specificity and forms a low affinity binary complex with K_d ~ 20–100 nM. The complex then engages the β_c (common β subunit) to form a high affinity ternary complex with K_d ~ 100 pM for IL3 (Broughton et al., 2015; T. R. Hercus et al., 2013; Murphy & Young, 2006). The β_c – subunit, which contains a larger intracellular domain, recruits the downstream IL3 signaling components. Nevertheless, the α–subunit intracellular domain has an essential role in signaling (Broughton et al., 2015; T. R. Hercus et al., 2013; Murphy & Young, 2006).

In 2014, the crystal structure of IL3Rα was revealed in a binary complex bound to a neutralizing monoclonal antibody by Broughton et al (Broughton et al., 2014). IL3Rα was discovered to have three Fibronectin type-III domains: N-terminal (NTD), D2, and D3. Surprisingly, the crystal structure disclosed two different conformations of IL3Rα, where an alternative ~40° angle between the NTD and D2 domains creates an "open" or "closed" conformation (Broughton et al., 2014). The position of NTD is due to the NTD-D2 linker being highly flexible, which leads to the receptor adopting both closed and open conformations and a potential constant dynamic between the two forms (Broughton et al., 2014). In the open conformation model, NTD leans backwards and opens the surface area for IL3 binding. The open conformation IL3Rα contains extra 12 residues in contact with IL3 when compared to the closed conformation. In the closed conformation IL3Rα binding to IL3 is more restricted because of fewer points of interaction (Broughton et al., 2014, 2015) (Figure 1.4).

IL3 receptor α–subunit (also known as cluster of differentiation–123 or CD123) is the major binding protein for IL3 and leads to the receptor activation that promotes cell survival and proliferation (Lopez, Hercus, Ekert, Littler, Guthridge, Thomas, Ramshaw, Stomski, Perugini, D'Andrea, et al., 2010). Elevated expression of CD123 has been observed on CML early progenitors and stem cells as compared to normal HSCs (Nievergall et al., 2014). In particular, $CD34^+$ / $CD38^-$ cells from CP- and BC-CML and $CD34^+$ cells from lymphoid or myeloid BC-CML patients showed elevated expression of CD123 (Nievergall et al., 2014). Moreover, CD123 overexpression has been widely investigated in AML and found to be correlated with poorer prognosis (U Testa et al., 2004). Recently, monoclonal antibodies targeting IL3Rα have been reported to inhibit the proliferation of AML-LSCs by complex pathways via inhibition of

homing, activation of innate immunity, or altering intracellular signaling cascades (Broughton et al., 2014; Jin et al., 2009).

Taken together, IL3Rα (CD123) has major biological relevance in leukemogenesis of stem and progenitor cells and represents a promising target for monoclonal antibody therapy of CML.

1.6.3.2 Signal–transducing common βc subunit and its functional implications

The signal transducing β common (βc / CD131) family of cytokines is the key signaling receptor subunit for IL3, IL5 (Interleukin–5), and GM–CSF (granulocyte macrophage colony-stimulating factor). This prototypic signaling subunit revealed several structural models and binding paradigms for other receptor families, such as Interleukin–2, –4, and –6, which also share one or more signaling subunits (T. R. Hercus et al., 2017; Murphy & Young, 2006). β_c–subunit has a key role in activation of oligomeric IL3 receptor (IL3R) and transactivation of the signals directly through Janus kinases (JAKs).

The x-ray structure of β_c ectodomain was solved in 2001 by Carr *et al.*(Carr et al., 2001) and revealed an intertwined homodimer in the absence of the cytokine ligand (Murphy & Young, 2006). The two β_c–subunits ectodomain make an elaborate intertwining homodimer that contains complex non-covalent interactions forming an arch-like structure with D4 domains ~120Å apart and positioned at a 60° angle adjacent to the membrane (Broughton et al., 2015; Murphy & Young, 2006). β_c subunit is a common subunit that is shared by IL3, GM-CSF, and IL5. Thus, it is presumed that receptor β_c–subunit is unable to bind to the corresponding cytokine in the absence of its α–subunit (Murphy & Young, 2006).

Although, β_c is not detectable in the circulation, and does not show a significant role in hemopoietic and immune functions, genetic ablation of β_c in mice has lead to disruption of IL3, IL5, and GM-CSF functions and dramatically reduced the level of eosinophils (Nishinakamura, Miyajima, Mee, Tybulewicz, & Murray, 1996). β_c dynamically participates in normal IL3 receptor activation and mutations in β_c reduce its responsiveness to the ligand binding *in vitro* (Murphy et al., 2004). Understanding the structure, modeling, and biological relevance of β–subunit as an indispensable part of IL3 signaling is critical in targeted therapy of CML.

1.6.4 IL3:IL3R assembly

There are multiple models proposed for activation of β_c upon ligand binding to the α–subunit. Murphy *et al*. have extensively discussed these models and reported the most feasible β_c activation model based on the crystal structure of β_c and the conformation of β_c homodimer (Carr et al., 2001; Murphy & Young, 2006). In this model, IL3 cytokine binds to the α–subunit with low (nM) affinity and this binary complex is recruited by β_c homodimer. The ligand binds to the interface between domains 1 and 4 of β_c dimer to form a high affinity (pM) ternary complex (Murphy & Young, 2006). As reported by Broughton *et al*. in 2015, the two hexameric ternary complexes pack together to form the dodecameric complex (Broughton et al., 2015; Murphy & Young, 2006) (Figure 1.4).

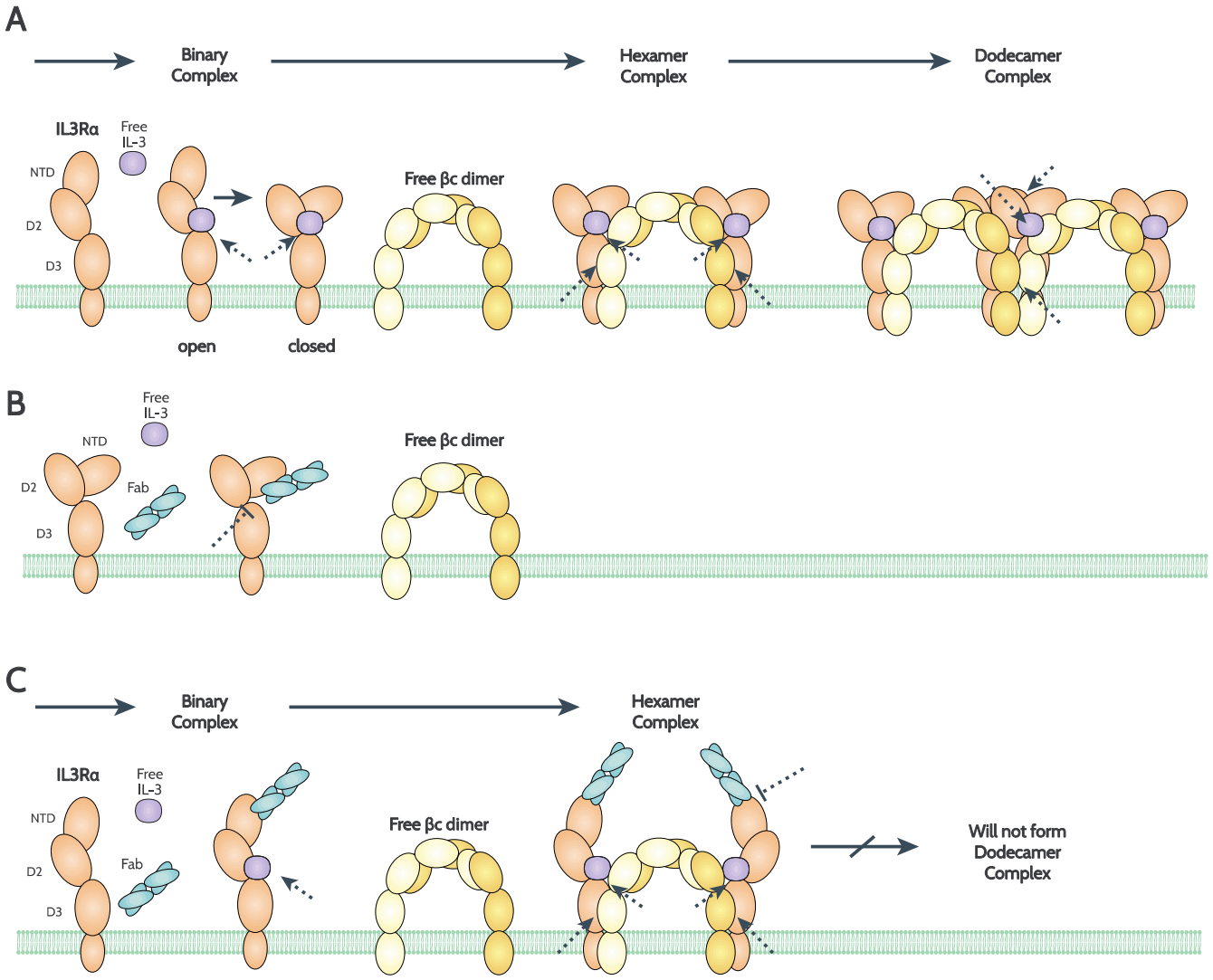
A
Binary Complex
Hexamer Complex
Dodecamer Complex
IL3Rα
Free IL-3
NTD
D2
D3
Free βc dimer
open
closed
B
Free IL-3
NTD
D2
Fab
D3
Free βc dimer
C
Binary Complex
Hexamer Complex
IL3Rα
Free IL-3
NTD
D2
Fab
D3
Free βc dimer
Will not form Dodecamer Complex

Figure 1.4. Schematic model of IL3: IL3Rα assembly and the mechanism of actin of an anti–IL3Rα Fab.

(A) Upon ligand binding to IL3Rα sequential assembly of IL3 receptor initiates with engagement of β_c free dimers and heterodimerization. The two ternary complexes form the hexameric complex that assembles into a higher–order active dodecameric complex. The active dodecameric complex is associated with JAK2 signaling activation. Arrows indicate the multiple interaction sites of ligand and receptor on IL3R subunits. (**B)** The closed conformation of IL3Rα is a result of the conformational flexibility of IL3Rα and highly mobile NTD that tilts forward. The placement of NTD in a closed conformation locks in the Fab and prevents heterodimerization of the receptor subunits **(C)** The open conformation of IL3Rα occurs when NTD is laterally twisted away to facilitate locking of the ligand. Binding of anti–IL3Rα Fab to open conformation of IL3Rα leads to heterodimerization and formation of hexameric complex but not to higher order complexes. Fab binding to open conformation IL3Rα blocks the activation of downstream JAK2 signaling. Figure reconstructed from Broughton *et al.* with permission from Elsevier group (Broughton et al., 2014).

1.6.5 IL3 signaling

The sequential assembly of the IL3 receptor into an active signaling dodecamer allows full IL3 receptor signaling by bringing together the cytoplasmic juxtamembrane regions of α–subunit and β_c into a closer proximity to transactivate (Broughton et al., 2012, 2014; Lopez, Hercus, Ekert, Littler, Guthridge, Thomas, Ramshaw, Stomski, Perugini, D'Andrea, et al., 2010) (Figure 1.5). Following formation of the active dodecameric IL3R, receptor activation initiates with pre-associated Janus kinases (JAK) on β_c coming into close proximity to transactivate (P.-H. Chen et al., 2012). Upon JAK2 transphosphorylation, JAK2 coincidently phosphorylates multiple sites on the β_c. Phosphorylation of various tyrosine residues on β_c is the key step in multiple signal initiations because the tyrosine residues serve as docking sites for multiple downstream pathways including JAK2 / STAT5, RAS / RAF/ MAPK, PI3K / AKT, and NF-κB (nuclear factor kappa light chain enhancer of activated B-cells) (T. Hercus & Thomas, 2009; Lopez, Hercus, Ekert, Littler, Guthridge, Thomas, Ramshaw, Stomski, Perugini, D'Andrea, et al., 2010). Mutagenesis analyses and phosphotide competition assays have elucidated the outcome of phosphorylation in various key tyrosine residues on β_c (Bone & Welham, 2000; T. R. Hercus et al., 2013). Following IL3:IL3R activation and JAK2 transphosphorylation, JAK2 triggers phosphorylation of Y612, Y750, Y806, and Y866 in order to recruit STAT5 and activate JAK2 / STAT5 downstream signaling pathways (Itoh, Liu, Yokota, Arai, & Watanabe, 1998). JAK / STAT is mainly involved in anti-apoptotic events via BCL-X_L (Kamizono et al., 2001; Steelman et al., 2004; Ungureanu, Saharinen, Junttila, Hilton, & Silvennoinen, 2002). JAK / STAT signaling is under tight negative regulation with ubiquitination and degradation through suppressors of cytokine signaling (SOCS) (Kamizono et al., 2001; Ungureanu et al., 2002), autophosphorylation (Ungureanu et al., 2011) , and ubiquitination and endocytosis of β_c (J. T. Lei, Mazumdar, & Martinez-Moczygemba, 2011).

IL3-mediated activation of the receptor β_c recruits SHC/GRB2/SOS coupling complex (McCubrey et al., 2007) SHC interacts with β_c via its SH2 domain and phosphotyrosine binding (PTB) domain via tyrosine 577 and tyrosine 612 (Y577 and Y612) of β_c, respectively (Bone & Welham, 2000; T. R. Hercus et al., 2013). Y577 and S585 are mutually exclusive

phosphorylation sites that constitute a molecular switch between survival and proliferation or survival only. This switch is thought to be cytokine dose-dependent such that low concentrations of cytokine lead to steady state maintenance of survival and high cytokine levels induced survival and proliferation (Mark A Guthridge et al., 2006).

SHC / GRB2 / SOS complex stimulation induces a conformational change in the inactive RAS through GDP-GTP (guanosine diphosphate to guanosine triphosphate) exchange and activates the RAS / RAF/ MAPK signaling pathway (T. R. Hercus et al., 2013; McCubrey et al., 2007). This signaling cascade promotes proliferation of myeloid cells, and RAS downstream effectors regulate cell cycle progression and anti-apoptotic events (McCubrey et al., 2007). SHC / GRB2 / SOS coupling complex is also associated with activation of PI3K / AKT pathway. Phosphorylation of β_c S585 (Serine 585) and association of chaperone molecule 14-3-3 are both required for engagement of PI3K to β_c and IL3-mediated activation of PI3K / AKT pathway (M A Guthridge et al., 1998; Mark A Guthridge et al., 2004). Moreover, Y612 is important for SHP2 interaction. PI3K / AKT activates multiple other pathways associated with hematopoietic cell survival, proliferation, and anti-apoptotic phenotypes (Steelman et al., 2004).

Furthermore, IL3 binding activates NFκB and inhibitors of κB kinase (IKK) (Sandow et al., 2012). In an inactive state, NFκB dimers are sequestered in the cytoplasm, which are known as IκBs (inhibitors of κB) (T. R. Hercus et al., 2013). Upon IL3-mediated phosphorylation of JAK2s, IκBβα is phosphorylated on two serine residues by κB kinase (IKK) complex (Hacker & Karin, 2006). IKK complex consists of two related catalytic domains IKK1, IKK2, and an NFκB essential modulator (NEMO) (DiDonato, Hayakawa, Rothwarf, Zandi, & Karin, 1997; Yamaoka et al., 1998; Zandi, Rothwarf, Delhase, Hayakawa, & Karin, 1997). IKK phosphorylates IκB, leading to ubiquitination and proteasomal degradation of IκBβα, which releases NFκB transcription factors. The released NFκB transfers to the nucleus to activate the transcription of its target genes (Hacker & Karin, 2006). IKK and NFκB activation by IL3R stimulation is associated with maintaining cell survival (Besancon, Atfi, Gespach, Cayre, & Bourgeade, 1998; T. R. Hercus et al., 2013) and blocking NFκB leads to cell apoptosis (Besancon et al., 1998; T. R. Hercus et al., 2013). Studies have demonstrated that IKK complex is essential for activation of pro-apoptotic events by B-cell lymphoma 2 (BCL2) family, PUMA, and BBC3.

Phosphorylation and degradation of PUMA via IKK complex enhances cell survival through NFκB activation (Fricker, O'Prey, Tolkovsky, & Ryan, 2010; Sandow et al., 2012) (Figure 1.5)

Taken together, IL3 receptor signaling and BCR-ABL activate redundant downstream signaling cascades (Wong et al., 2003). Particularly, activation of RAS / RAF / MAPK via SHC / GRB2 / SOS adaptor complex has been elucidated in IL3R signaling and BCR-ABL activation in fibroblast cells lacking the IL3 expression (M A Guthridge et al., 1998; Maru, 2001). Similar to IL3, BCR-ABL upregulates STAT and MYC expression and promote cell growth, proliferation, and anti-apoptotic events (Maru, 2001). Moreover, IL3 upregulation contributes to the development of BCR-ABL–induced leukemogenesis and disease progression (M A Guthridge et al., 1998). Overexpression of both RAS / RAF/ MAPK and PI3K / AKT pathways has been reported in AML and conferred to poorer prognosis than overexpression of the single pathway (Kornblau et al., 2006). IL3 receptor represents a promising target for potential therapeutic monoclonal antibodies to inhibit multiple signaling pathways associated with CML LSC survival, proliferation and differentiation in the bone marrow.

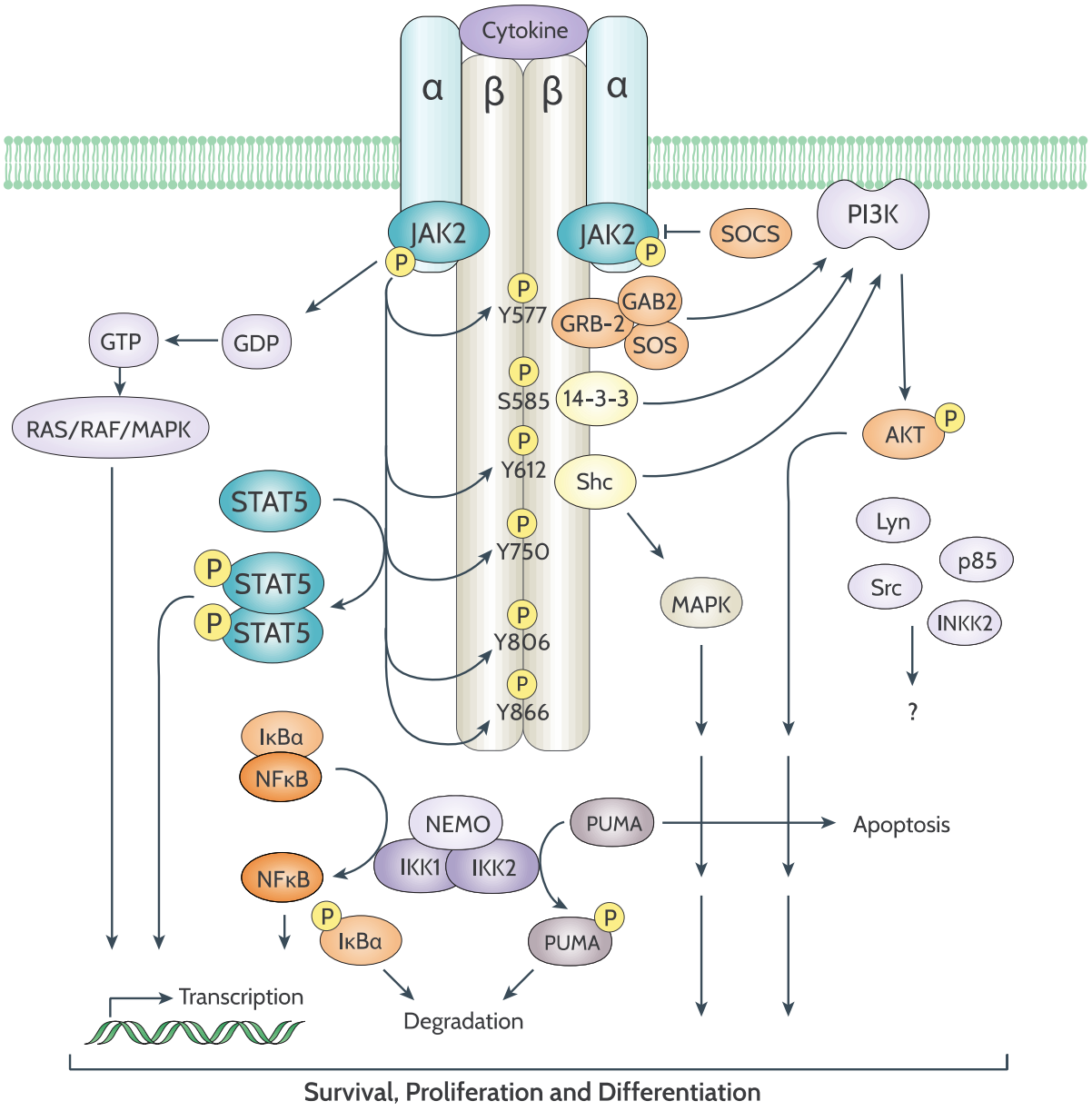
Cytokine
α
β
β
α
JAK2
JAK2
P
SOCS
PI3K
GTP
GDP
RAS/RAF/MAPK
P
Y577
GRB-2
GAB2
SOS
P
S585
14-3-3
AKT
P
P
Y612
Shc
STAT5
P
Y750
P
STAT5
P
STAT5
MAPK
Lyn
p85
Src
INKK2
?
P
Y806
P
Y866
IκBα
NFκB
NEMO
IKK1
IKK2
PUMA
Apoptosis
NFκB
P
IκBα
PUMA
P
Transcription
Degradation
Survival, Proliferation and Differentiation

Figure 1.5. IL3 downstream signaling pathways. The presence of IL3 cytokine leads to heterodimerization of IL3Rα and β_c subunits and JAK2 transphosphorylation that triggers multiple tyrosine and serine sites on β_c tail (Lopez, Hercus, Ekert, Littler, Guthridge, Thomas, Ramshaw, Stomski, Perugini, Andrea, et al., 2010). Phosphorylation of Y577, Y612, Y750, Y806, and Y866 leads to STAT5 recruitment and activation of JAK2 / STAT5 downstream signaling pathways (Itoh et al., 1998). At the same time, IκBβα is phosphorylated on two serine residues by κB kinase (IKK) complex (Hacker & Karin, 2006) with two catalytic IKK1, IKK2 domains, and a NFκB essential modulator (NEMO) (DiDonato et al., 1997; Yamaoka et al., 1998; Zandi et al., 1997). IKK phosphorylates IκB leading to IκBβα ubiquitination and proteasomal degradation and releasing NFκB transcription factors. NFκB transfers to the nucleus to activate the transcription of its target genes (Hacker & Karin, 2006). Activation of the receptor β_c also launches SHC/GRB2/SOS coupling complex, a docking site for recruitment of PI3K / AKT pathway (McCubrey et al., 2007). SHC/GRB2/SOS complex also induces conformational changes in the inactive RAS through GDP-GTP exchange and activates the RAS / RAF/ MAPK signaling pathway (T. R. Hercus et al., 2013; McCubrey et al., 2007). Of note, this is a simplified illustration of IL3 downstream signaling pathways and multiple other signaling cascades are associated with IL3R signaling. GFP: guanosine diphosphate; GTP: guanosine triphosphate. Figure reconstructed from Hercus *et al.* Cytokine and Growth Factor Reviews, 24 (2013) with permission from Science Direct group.

1.7 Antibodies as therapeutics

In 1975, the first report of monoclonal antibodies (mAbs) by Kohler and Milstein lead to a Nobel prize (Kohler & Milstein, 1975). The first therapeutic monoclonal antibody, muromonab – CD3 was approved by the FDA for treating acute organ transplant rejections in 1992 (Hongrong Cai, 2016). The first FDA-approved monoclonal antibody that was broadly used in cancer treatment was Rituximab, a chimeric anti-CD20 antibody, that showed up to 48% overall response rate in patients with relapsed low-grade non-Hodgkin's B-cell lymphoma (McLaughlin et al., 1998).

As of May 2016, over sixty monoclonal antibodies are approved by FDA for therapeutic purposes in the United States and Europe, and more than fifty are currently under investigation in late clinical trail stages that are expected to drive an emerging trend of 6 to 9 monoclonal antibody approvals per year in the near term (Ecker, Jones, & Levine, 2015; Hongrong Cai, 2016; Reichert, 2017).

The use of monoclonal antibody therapy offers the promising feature of directly targeting specific antigens on cancer cells, increasing specificity and efficacy (Rogers, Veeramani, & Weiner, 2014). Her2 / neu, EGFR, VEGFR, CD20, CD52, and CD33 are currently the most relevant targets for antibody therapy of solid and haematological malignancies that are approved by FDA (Mellman, Coukos, & Dranoff, 2011). Other than targeting cancer cells, various other antibody-based therapeutic strategies have been investigated for angiogenesis inhibition, T-cell checkpoint blockade, radioimmunotherapy, antibody-drug conjugates, bispecific antibodies, and chimeric antigen receptor T-cells (G. J. Weiner, 2015).

1.7.1 Immunoglobulin isotypes

Antibodies are a dimer of heterodimeric protein with complex structure and function that belong to the immunoglobulin superfamily. Immunoglobulins are produced by B-cells and secreted into the plasma for their immune system functions. The five major immunoglobulin isotypes are IgG, IgA, IgE, IgD, and IgM classified based on their crystallisable fragments (Fc)

(Figure 1.6) and have distinct structures, activities, and biodistributions. (Schroeder & Cavacini, 2010; Woof & Burton, 2004). IgG is a monomeric immunoglobulin mostly found in the serum (~12 mg/mL) and has a key role in immunity against bacteria and viruses (Gorham, 2005; Woof & Burton, 2004). IgA is the another predominant antibody in the serum (~3 mg/mL) that forms a monomer or dimer and functions in mucosal areas by preventing the colonization of pathogens (Underdown & Schiff, 1986; Woof & Burton, 2004). IgE is a monomeric immunoglobulin involved in allergic responses (Schroeder & Cavacini, 2010; Woof & Burton, 2004). The role of IgD is less clear, but mainly functions as an antigen receptor on B-cells (Geisberger, Lamers, & Achatz, 2006; Woof & Burton, 2004). IgM is the largest in size and exists as a pentamer, and is therefore restricted to the circulation and is associated with the initial humoral immune response against bacterial and fungal infection (Geisberger et al., 2006; Gorham, 2005).

1.7.2 Structure of Immunoglobulin gamma (IgG)

The IgG is a Y-shaped monomeric glycoprotein with an approximate mass of 150 kD. It is comprised of two identical heavy and two identical light chains (Figure 1.6). Each chain has an N-terminal variable domain (*VH* and *VL*) followed by a single constant light (CL) domain or three constant heavy domains (CH1, CH2, CH3). Each variable or constant domain contains two sandwiched β-pleated sheets with conserved disulphide bonds for stability. A spacer hinge adds flexibility between CH1 and CH2 (Schroeder & Cavacini, 2010; Woof & Burton, 2004). IgG is arguably the best-studied class of immunoglobulin and most therapeutic antibodies are IgGs (Schroeder & Cavacini, 2010; Williams & Barclay, 1988). There are four human IgG subclasses – IgG1, IgG2, IgG3, and IgG4 – with the difference among them being their distinct constant heavy chains for the purpose of modulating effector functions (Woof & Burton, 2004). Based on classical protease digestion experiments, Papain digestion of IgG is characterized as having an antigen binding fragment (Fab) and one Fc fragment. (Schroeder & Cavacini, 2010).

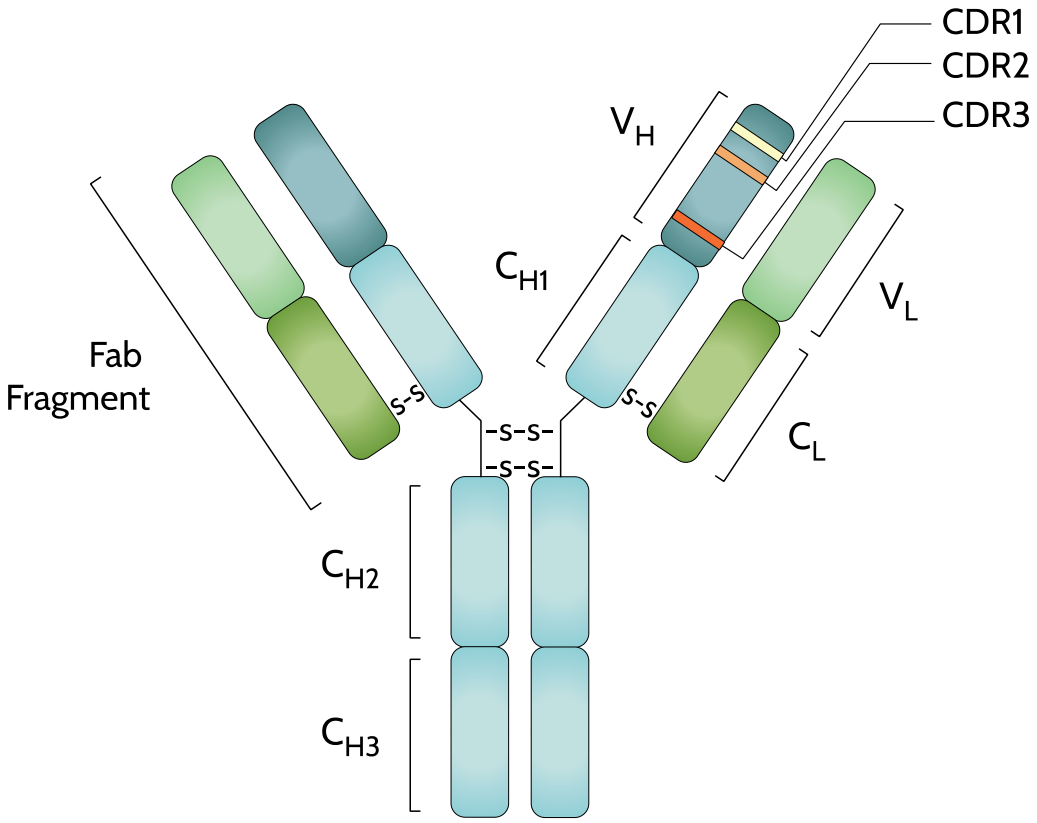

Figure 1.6. Structure of Immunoglobulin gamma (IgG). IgG is a Y-shaped dimer of heterodimers with two Fabs linked to one Fc portion. The Fab portion contains two identical light chains with N-terminal variable domains (*VH* and *VL*). VH and VL contain hypervariable intervals known as complementarity-determining regions (CDR1, CDR2, and CDR3) (Schroeder & Cavacini, 2010) that it used to bind to its corresponding antigen. The C-terminal of the Fab comprises of a single constant light (CL) domain or a constant heavy domains (CH1). Fc portion of antibody contains constant heavy chains 1 and 2 (CH1 and CH2). Heavy and light chains are covalently bound with disulphide bonds (S-S) (Schroeder & Cavacini, 2010; Woof & Burton, 2004). Fc: Fragment crystalizable.

The Fab portion of IgG contains the entire light chain (VL and CL), and the VH and CH1 portions of the heavy chain. The N-terminal part of the Fab contains the variable fragment (Fv) that contains the individual determinants (idiotype) of each antibody in order to recognize their specific antigen epitope (Schroeder & Cavacini, 2010). As such, the Fv is the minimal portion of an IgG that can constitute the antigen-binding properties of its parental antibody (K. A. Smith et al., 2004). The specific point of antigen binding occurs within three hyper-variable loops known as complementarity-determining regions (CDR1, CDR2, and CDR3) (Schroeder & Cavacini, 2010).

The Fc domain denotes the isotype of antibodies and bears the recognition motifs for mediating the effector function(s) of the antibody. The Fc binds to Fc receptors (FcR such as FcγRs, C1q, and neonatal FcR or FcRn) on immune effector cells to activate other immune mediators and enhance antibody stability (Ghetie & Ward, 2000; Idusogie et al., 2000; Jefferis, Lund, & Pound, 1998; J. K. Kim, Tsen, Ghetie, & Ward, 1994; Lund et al., 1991). Fc engineering and modulation of effector function modifies the function of antibodies for specific applications and optimized therapeutic potential (H. Liu, Saxena, Sidhu, & Wu, 2017; Presta, 2002; Torres & Casadevall, 2008).

1.7.3 Mechanism of action of antibody

Immunomodulatory approaches to target cancer cells without affecting normal cells have been broadly investigated. Targeted therapies are particularly important when they specifically inhibit the oncogenic signaling pathways and trigger the antitumor immunity (Reis, Mastellos, Ricklin, Mantovani, & Lambris, 2017).

1.7.3.1 Complement-dependent cytotoxicity (CDC)

Complement activation initiates with the classical component pathways. As the Fab portion of antibody binds to the antigen, the Fc portion binds to C1q (Reis et al., 2017; S.-Y. Wang & Weiner, 2008), a glycoprotein complex with 18 polypeptide chains that is a part of the C1 complex (Thielens, Tedesco, Bohlson, Gaboriaud, & Tenner, 2017). C1q mediates a number of

immunomodulatory pathways by enhancing phagocytosis, cytokine production via antigen presenting cells, mediating the “eat-me” signal for apoptosis and uptake / clearance of apoptotic cells, and disrupting T lymphocyte maturation (Thielens et al., 2017).

Fc binding to C1q promotes the activation of the C1 complex. Activation of C1 cleaves C4 into C4a and C4b and C2 into C2a and C2b. C4b and C2a then bind and form C3 convertase. C3 convertase (C4bC2a) induces cleavage in C3 and splits it into C3a and C3b. C3b has a dual function: (i) Opsonisation of target cells and promoting phagocytosis and cytotoxicity, (ii) promoting complement-dependent cytotoxicity (CDC). As a part of C1 complex activation, C3b binds to C4bC2a and forms C5 convertase, which cleaves C5 into C5a and C5b. C5b incorporates into C5 convertase and leads to sequential formation of C6 to C9 to create a terminal complex or assembly of the pore-forming membrane attack complex (MAC), a process that leads to CDC. On the other hand, C3a and C5a act as potent pro-inflammatory mediators that employ phagocytic properties such as neutrophils and macrophages (Reis et al., 2017; Rogers et al., 2014).

Regulators of CDC control the excessive amplification and activation of complement activity via membrane-bound regulators and soluble regulators. Membrane-bound regulators of complement activation (mRCA), such as CD46 (membrane cofactor protein), CD55 (decay acceleration factors or DAF), and CD59 (protectin) prevent formation of MAC pore through C3b degradation (CD46 and factor I), inhibition of C3 convertase, and MAC formation downstream of C5b deposition, respectively (J. Liu et al., 2005; Varela et al., 2008). Soluble regulators, such as C1 inhibitor, C4 binding protein (C4BP), factor I, factor H are associated with complement regulations that hinder the classical pathway of C1 complex activation by protease activity, degradations or decay acceleration or dissociation of convertase at various stages of the pathway (Davis, 2004; Heinen et al., 2009; Rogers et al., 2014; Skerka, Chen, Fremeaux-Bacchi, & Roumenina, 2013).

There are a number of studies on the role of CDC in antibody-mediated therapy. The effect of CDC cell killing in solid tumours needs to be ascertained since the expression or even overexpression of membrane-bound CDC regulators (descried above) on the tumour cells may prevent MAC pore formation. Multiple studies have demonstrated the antibody-mediated CDC

as a critical anti-tumour mechanism for anti-CD20 antibodies, such as alemtuzumab, combination therapy with Trastuzumab and Pertuzumab, and Ofatumumab in treatment of CLL. However, antibodies such as Rituximab and Obinutuzumab (anti-CD20 antibodies) are poorly effective complement activations. Furthermore, several groups have elucidated a depleted / exhausted complement during Rituximab and Ofatumumab treatment of CLL (Baig et al., 2012; Middleton et al., 2015; Tempescul et al., 2016). Antibody engineering on the constant region or glycosylation of the antibody may alter the effect of these antibodies on CDC (Reis et al., 2017; Rogers et al., 2014; Taylor & Lindorfer, 2016; G. J. Weiner, 2015).

1.7.3.2 Antibody-dependent cellular cytotoxicity (ADCC)

ADCC is induced by interaction of Fc region of antibody with the FcR on immune effector cells. FcRs are expressed on different types of immune effector cells such as natural killer cells (NK cells), granulocytes, monocytes, and macrophages (G. J. Weiner, 2015). In human, stimulatory FcRs are FcγRIA, FcγRIIA, FcγRIIC, and FcγRIIIA (Nimmerjahn & Ravetch, 2006). Cross-linking of antibody bound to the target and activation of FcγRs leads to phosphorylation of immunoreceptor tyrosine-based activation motifs (ITAMs) that activate downstream signaling cascades. The main immune effector cells associated with ADCC are NK cells, although macrophages, dendritic cells, neutrophils, and eosinophils also express FcγRs (Nimmerjahn & Ravetch, 2006). ADCC begins with the production of pro-inflammatory cytokines (i.e. IFNγ or Interferonγ) and the release of cytotoxic compounds such as perforin and granzymes (Rogers et al., 2014; S.-Y. Wang & Weiner, 2008; G. J. Weiner, 2015). Upon degranulation, perforin bind to the cell membrane and form oligomers in a calcium (Ca^{2+})-dependent manner that creates pores on target cells. Pore formation on target cells induces diffusion of pro-apoptosis protease and granzyme B into targeted cells. The perforin / granzyme cell killing system is mediated by direct or indirect activation of intracellular cell death proteases, Caspase 3 and Caspase 7, leading to substrate proteolysis and induction of apoptosis and cell death (Cullen, Brunet, & Martin, 2010; Rogers et al., 2014; Trapani, 1995).

Taken together, NK cell FcR binding to the Fc portion of antibody leads to activation of immune effector cells that contributes to (i) exocytosis of cytotoxic granules and induction of tumour cell apoptosis, (ii) production of pro-inflammatory cytokine release (i.e. IFNγ), (iii)

recruitment and activation of other immune effector cells (by IFNγ) to promote antigen presentation and adaptive immune response, and (iv) activation of tumor necrosis factor (TNF) family death receptor signaling and induction of apoptosis (Bowles & Weiner, 2005; W. Wang, Erbe, Hank, Morris, & Sondel, 2015).

1.7.4 Generation of antibodies

1.7.4.1 *In vivo* generation of antibodies

1.7.4.1.1 Animal immunization

The simplest manner in which to generate antibodies is to take advantage of the natural adaptive immune system of animals. Following injection with a target antigen, an animal's primary immune response typically results in the expansion of polyclonal B-cells, each producing a single antibody clone. Animals are then re-immunized with the same antigen so that immune serum can be harvested with a high titre of polyclonal antibodies (heterogeneous isotype and antigen specific antibody) with affinity to the target antigen. The immunization of rodents, rabbits, goats, and sheep is a common method for producing polyclonal antibodies that may be of limited use as lab reagents due to their finite supply and polyclonal nature. This heterogeneous population contains antibodies with varying affinity and epitope specificity. Nonetheless, immunization for a polyclonal antibody response in animals is almost always the first step toward producing antibodies *in vivo*, and provides an early opportunity to assay for monoclonal antibody potential (Birch & Racher, 2006; Gerdes, Schwab, Lemke, & Stein, 1983; W. Wang, Xu, & Li, 2010; Yokoyama, 2001).

1.7.4.1.2 Transgenic mice

In 1989, Bruggemann *et al.* demonstrated the expression of a repertoire of human heavy chains and generation of transgene-encoded immune response in mice in the absence of the endogenous genes (Bruggemann et al., 1989). A number of studies have exploited the same method to produce human antibodies. In this platform, a fragment of human heavy and light chain antibody gene is introduced into genetically modified mouse germline. The human antibody gene sequence enters the mouse machinery of antibody recombination and expression. This system creates transgenic mice that are capable of producing a wide repertoire of fully

human antibodies that are antigen specific. Transgenic mice could in part overcome the obstacle of immunogenicity of rodent antibodies for human. *In vivo* expression of full-length human antibodies and convenience of the method are highly advantageous; however, this approach limits the use of toxic immunogens, antibody-drug conjugates, or targeting an antigen with high level of homology between mouse and human (Chames, Van Regenmortel, Weiss, & Baty, 2009; Lonberg, 2005; Nelson, Dhimolea, & Reichert, 2010).

1.7.4.1.3 Hybridoma technology

Assuming a productive challenge with target antigen, each immunized animal contains a population of B-cells that contains individual B-cell clones that produce a single antibody to a single antigenic epitope. Such monoclonal B cells can be isolated, and their secreted monoclonal antibody recovered. However, normal B cells have a finite lifespan and eventually stop producing the antibody. To address this hurdle in monoclonal antibody production, Kohler and Milstein published a novel hybridoma technology in 1975 (Kohler & Milstein, 1975; Strebhardt & Ullrich, 2008). In their revolutionary work, they fused specific antibody-producing cells from immunized animals with immortal myeloma cells. The resulting antibody-producing cells had immortality and the ability to provide a constant supply of highly specific monoclonal antibody (Kohler & Milstein, 1975; Strebhardt & Ullrich, 2008).

Commercial providers of monoclonal antibodies numbers in the dozens, and many have hundreds, or thousands of monoclonal antibodies listed for sale. Certainly, monoclonal antibodies have become indispensable research and diagnostic tools. However, because nearly all monoclonal antibodies are derived from mice, their use as therapeutic agents in humans faces major obstacles. First, mouse monoclonal antibodies are affected by immunogenicity, hypersensitivity, and a human anti-murine antibody (HAMA) response (Milstein, 1999; L. M. Weiner, 2006). Second, with dependency on immunoglobulin isotype, using mouse antibodies in humans leads to lower ADCC. Third, mouse antibodies have a considerably shorter half-life in humans. To alleviate these problems, several approaches to "humanize" mouse monoclonal antibodies are undertaken in order to make mouse monoclonal antibodies useful as human therapeutics (Almagro & Fransson, 2008; Riechmann, Clark, Waldmann, & Winter, 1988). In such cases, the antibody-encoding sequence is recovered from the hybridoma cells of interest and

recombinant DNA technology is used for protein engineering of the immunoglobulin (K. A. Smith et al., 2004). In first-generation humanized antibodies, the mouse variable region is fused as a chimera to the constant regions of a human antibody. Taking this concept further, second generation hyper-chimeric antibodies are created by grafting the CDR sequences from the murine monoclonal onto a human immunoglobulin framework (Gavilondo & Larrick, 2000; Kipriyanov & Le Gall, 2004). These humanization techniques have been essential to making antibodies the successful therapeutic agents they are today.

Despite the success in generating monoclonal antibodies for therapy, several disadvantages have led to the emergence of *in vitro* alternatives (discussed below). Most notably, in order for humanization, the antibody DNA sequence needs to be cloned from hybridoma RNA (Orlandi, Gussow, Jones, & Winter, 1989). The process requires a labour intensive amplification of variable gene segments and pairing of compatible heavy and light chains (Krebber et al., 1997). Further, the existence of aberrant or non-functional but expressed immunoglobulin RNAs make the process unreliable (Ding, Chen, Zhu, & Cao, 2010). Another problem for *in vivo* generated antibodies is the lack of control over the antigen used for immunization. Upon injection, the antigen is in a "black box" and may be poorly presented to the immune system, misfolded, or degraded. Such conditions may lead to poor antigenicity or the production of antibodies that recognize non-native target conformations. Finally, antigens too similar to the host may elicit a poor immune response (Silvestri & Taniuchi, 1988), and others may be unusable due to host toxicity.

1.7.4.2 *In vitro* generation of antibodies

1.7.4.2.1 Library generation

Antibodies generated *in vitro* are typically selected from a library or pool of antibody clones. Antibody libraries generally fall into two categories, as they are either derived from natural or "synthetic" sources. Natural libraries are generated through the cloning of antibody sequences (Andris-Widhopf, Steinberger, Fuller, Rader, & Barbas, 2011) from natural B-cell populations harvested from various tissues including the bone marrow (Marks et al., 1991) and spleen (Clackson, Hoogenboom, Griffiths, & Winter, 1991). These include naïve B cells from unchallenged animals, which yield antibodies suited for selections against de novo targets.

Alternatively, natural libraries may be created from B cells from the spleen of immunized animals, so that a library is "directed" and contains antibodies to the immunized target antigen within a polyclonal background, facilitating the selection of target binding antibodies (Moon et al., 2011).

Synthetic antibody libraries are not derived directly from natural B-cell immunoglobulin sequences. Instead, they are created using extensive antibody structure and function knowledge as the basis for library design (Chen, G; Sidhu, 2014; Johnson & Wu, 2000; Sachdev S Sidhu & Fellouse, 2006). The earliest examples were semi-synthetic libraries, which used natural human antibody repertoires as the basis to incorporate minor diversity elements such as the "artificial" rearrangement of VH and VL domains (Griffiths et al., 1994; Marks et al., 1991), or additional diversity within particular CDRs (Andris-Widhopf et al., 2011). So-called fully synthetic libraries employ more aggressive "hard randomization" to generate antibody diversities that deviate further from natural repertoires, but still retain natural elements (Knappik et al., 2000; Tiller et al., 2013).

Since the CDR regions are normally targeted for synthetic antibody libraries, diversity is usually incorporated with the use of mutagenic oligonucleotides (Miersch & Sidhu, 2012). Chemical synthesis of DNA enables the randomization of the four basic nucleotides such that degenerate codons have the potential to encode all 20 amino acids. The use of trinucleotide phosphoramidites in mutagenic oligonucleotide synthesis allows a controlled distribution of all 20 amino acids and the avoidance of unwanted stop codons (Virnekas et al., 1994). These mutagenic oligonucleotides enable incredible diversity up to 20n possible members, where "n" equals the number of positions equally mutated across the 20 amino acids. Since this often yields theoretical CDR diversities much larger than can be used in practice, tailored diversity is often employed to customize the antibody libraries (Koide & Sidhu, 2009). The main approaches used to incorporate mutagenized CDRs involve PCR-mediated assembly of "cassettes" that require restriction-based or recombination mediated-cloning to generate the library (Soderlind et al., 2000), or whole plasmid mutagenesis (Krebber et al., 1997; Orlandi et al., 1989) such as Kunkel mutagenesis. In Kunkel mutagenesis, site-specific mutagenic primers anneal to a single stranded DNA (ssDNA) template and after *in vitro* synthesis of the mutant strand, the wild-type template is preferentially eliminated from *E. coli* (Kunkel, 1985).

Synthetic antibody libraries offer several advantages over their natural counterparts. These include customization of CDR diversity outside "natural" constraints (Miersch & Sidhu, 2012) that may lead to higher antigen affinities down to low picomolar dissociation constants as compared with lower thresholds of ~100 picomolar for natural antibodies (Bradbury, Sidhu, Dubel, & McCafferty, 2011; Ebersbach, H; Proetzel, 2012). The ability of focused diversity in synthetic libraries has also revealed the nature of antibody–antigen interactions (Persson et al., 2013), and may facilitate easier screening of selected antibody clones (unpublished data from our laboratory). Synthetic libraries are normally built upon a single well-characterized antibody isotype and subclass. Using a constant antibody framework can help the success of selected antibodies in therapy for example, as one can tailor a library for desired effector functions (such as ADCC). Particular antibody frameworks are also robust and have optimal protein express properties (Desiderio et al., 2001; Lee et al., 2004). Designing synthetic libraries on a single framework also permits features that can facilitate clone screening, DNA sequencing, and downstream recombinant DNA manipulations (Ebersbach, H; Proetzel, 2012).

1.7.4.2.2 Phage display

A bacteriophage or "phage" is a virus that infects and replicates in a bacterial host. A common example is the M13 filamentous phage (Figure 1.7). M13 is an elongated phage with thousands of major coat proteins (pVIII) surrounding a capsid that contains a circular ssDNA (single stranded DNA) phage genome. A minor coat protein (pIII), containing 3–5 copies, is situated at one end of the virion and is responsible for infection via attachment to the E. coli F-pilus. Upon retraction of the pilus, the bacteriophage enters the cell and releases (+) strand phage ssDNA that is converted to a replicative double stranded DNA (dsDNA) form that allows transcription of phage proteins and serves as a substrate for rolling-circle replication of the (+) strand. Following expression of phage proteins and genomic replication, phage progeny are assembled and packaged in the periplasm (about 1000 per cell), and released from their host in a non-lytic fashion (Rakonjac, Bennett, Spagnuolo, Gagic, & Russel, 2011).

In 1985, George Smith published a breakthrough method exploiting M13 phage biology in order to display peptide fusions to the pIII protein (G. P. Smith, 1985). In this approach, "fusion phage" contained peptide coding DNA sequences fused to the M13 pIII gene. The resulting

phage could then display a library of peptides on the phage surface while retaining infection through pIII. Importantly, the peptide displayed (phenotype) would be connected to the phage genome (genotype) encoding it. Not long after this discovery, phage display was extended to antibody fragments (McCafferty, Griffiths, Winter, & Chiswell, 1990), and antibody phage display selections became commonplace for generating target-binding antibody fragments *in vitro* (Hoogenboom et al., 1998).

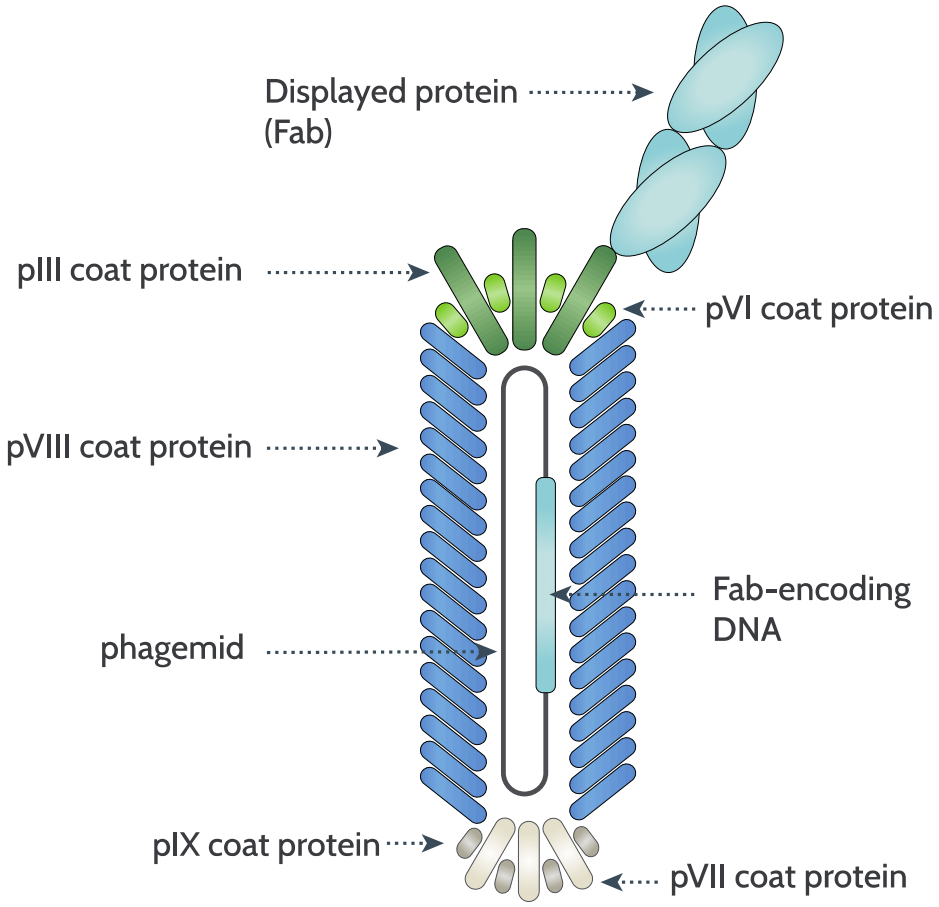

Figure 1.7. M13 filamentous phage. M13 is an elongated phage. PVIII is the major coat protein surrounding a capsid with a circular ssDNA phage genome (phagemid). PIII is a minor coat protein with 3–5 copies positioned at one end of the virion (Rakonjac et al., 2011). Fusion of peptide coding DNA sequences to the M13 pIII gene displays the peptides on the phage surface and links the encoding genotype to the displayed phenotype (McCafferty et al., 1990). Other phage coat proteins include pVI, pVII, and PIX.

Phage display selections are simply cycles of affinity purification and phage amplification (Figure 1.8). Phages that display a library of fusions (e.g. antibody fragments) are incubated with an immobilized target. Phage displaying target-binding entities are isolated from the unbound phage by washing, and then amplified in *E. coli*. This enriched pool of target binding phage is subsequently used in additional rounds of selection (typically 3–5) and at the end of the process, the DNA encoding the target-binding entity can be easily recovered due to the phenotype–genotype connection (Fellouse & Sidhu, 2006). A notable advantage in the phage display selection methodology is the *in vitro* control over the target, such that conditions can be customized to create the best opportunity for the desired binding to take place. This includes random or uniform orientation of the target, modulation of temperature or buffer conditions, and even selections against cell-surface based targets (Chan, Lim, MacAry, & Hanson, 2014; Jones et al., 2016; Miersch & Sidhu, 2012).

Initial phage display systems utilized vectors that carried all the genetic information for the displayed entity as well as all the phage components (Clackson et al., 1991; McCafferty et al., 1990). However, most modern phage display is performed using a phagemid (Barbas, Kang, Lerner, & Benkovic, 1991). Phagemid is a small plasmid-like vector that contains the genetic fusion of the displayed entity to the pIII sequence, and origins of replication for ssDNA and dsDNA production. Because phagemids do not encode other phage components, they are normally partnered with helper phage that provides the remaining essential genetic information to reconstitute a viable phage. A key advantage to this set-up is that phagemid libraries can be constructed and electroporated into high-efficiency *E. coli* to yield phage diversities greater than 10^{10} members (Fellouse & Sidhu, 2006). In addition, phagemids facilitate dsDNA propagation, recovery of clones, DNA sequencing, subcloning and may also be directly amenable to pIII-independent protein expression (Hoogenboom et al., 1991). Phagemid-mediated phage display also enables a range of displayed valencies, from mono- to multivalent (Miersch & Sidhu, 2012).

Phage display has been used successfully in the selection of Fab (Lee et al., 2004), scFv (Sachdev S Sidhu et al., 2004), and single-domain VH antibody fragments (Bond, Wiesmann, Marsters, & Sidhu, 2005). Although full-length antibodies are not applicable in phage display without shortcomings (Mazor, Van Blarcom, Carroll, & Georgiou, 2010), antibodies can be easily subcloned since the DNA sequence encoding antibody fragments is readily available. It

has been 15 years since adalimumab (Humira®), the first of six phage-developed antibodies, was approved for clinical therapy. However, advances in phage display technology and synthetic library generation has resulted in dozens of antibodies currently in clinical trials (Frenzel, Schirrmann, & Hust, 2016).

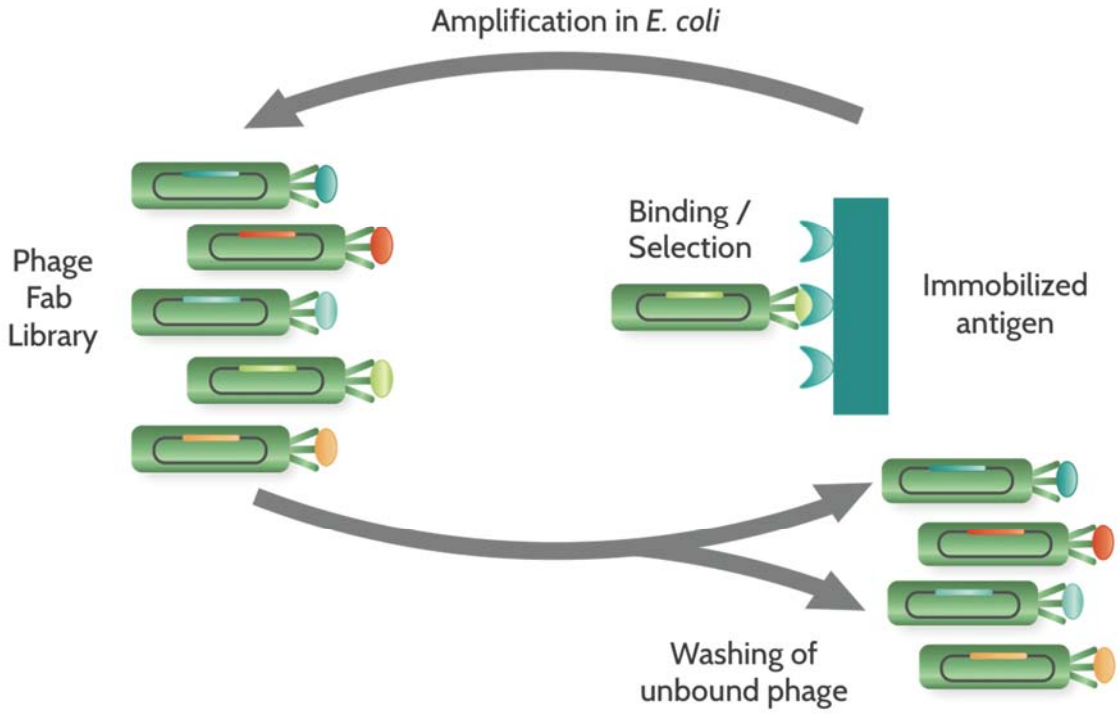

Figure 1.8. Phage display selection. . Libraries of antigen-binding fragments (Fabs) are screened for target-binding entities. The target-binding phage are isolated and amplified in *E. coli*, while the unbound phage is washed away. In order to enrich the pool of target-binding phage, the amplified target-binding phage pool undergoes additional rounds of selection.

2. CHAPTER 2. HYPOTHESES AND OBJECTIVES

Hypothesis 1. Synthetic antibodies can be raised against IL3 receptor α and β subunits with high specificity and affinity

Objective 1.1. Generation of synthetic antibodies against IL3 receptor -α and -β subunits by phage display

Objective 1.2. *In vitro* validation and characterization of anti–IL3R antibodies

Objective 1.3. *In vivo* validation and characterization of anti–IL3R antibodies

Hypothesis 2. Anti–IL3Rα or IL3Rβ antibodies eliminate CML stem cells protected by IL3–mediated innate Imatinib resistance

Objective 2.1. To test the *in vitro* function of synthetic IL3R antibodies in eradication of CML stem cells via cell proliferation, apoptosis, and self-renewal capacity

Objective 2.2. To compare the *in vitro* function of synthetic IL3R antibodies alone, in combination, or as co–drugs with imatinib

Hypothesis 3. Anti–IL3R antibodies inhibit IL3 signaling in CML stem cells

Objective 3.1. To test whether anti-IL3Rα / IL3Rβ antibodies inhibit downstream JAK/STAT signaling in the presence of IL3

Hypothesis 4. Engraftment of anti–IL3R antibody treated BC–CML cells increases disease latency in the mouse model

Objective 4.1. To test the efficacy of IL3Rα / IL3Rβ antibodies, alone, in combination or as co-drugs with imatinib on mouse survival in the murine CML model

Hypothesis 5. Bispecific anti–IL3R antibody fragments can replace the combinatorial anti–IL3Rα and anti–IL3Rβ antibody therapy in CML

Objective 5.1. Generation of mono-specific Fab (mono–Fab), bispecific and bivalent antibody fragments (bi-Fabs) against IL3 receptor -α and -β subunits

Objective 5.2. Validation and characterization of mono-Fabs and bi-Fabs

Objective 5.3. To test the *in vitro* function of mono-Fabs or bi-Fabs in eradication of CML stem cells via cell proliferation, apoptosis, and self-renewal capacity assays

Objective 5.4. To test the additive or synergistic effect of mono-Fab / bi-Fabs with imatinib on CML cells

3. CHAPTER 3. MATERIALS AND METHODS

3.1.Reagent and suppliers for generation of antibodies and antibody fragments

Table 3.1. Required materials and reagents

Reagent	Supplier
0.2 cm gap electroporation cuvette	ThermoFisher Scientific
10 mM dNTP mix (10 mM of each dATP, dCTP, dGTP and dTTP)	Fermentas
10% (w/w) Ethidium Bromide	Sigma Aldrich
100 mM HCl	ThermoFisher Scientific
293F FreeStyle™ Medium	ThermoFisher Scientific
2xYT	BD DifcoTM
Agarose	ThermoFisher Scientific
Amicon® Ultra-0.5 mL centrifugal filter	Millipore
Amicon® Ultra-4 mL centrifugal filter	Millipore
Anti-Human Fab-CH1 2nd Generation (FAB2G) biosensors	PALL Forté Bio®
Anti-Human IgG Fc Capture (AHC) biosensors	PALL Forté Bio®
Anti-M13 mouse monoclonal antibody, HRP conjugate [B62-FE2]	Abcam
BCA Protein Assay Kit	ThermoFisher Scientific
Blasticidin	ThermoFisher Scientific
Bovine Serum Albumin (BSA)	Sigma Aldrich
Carbinocilin	Sigma Aldrich
Chloramphenicol	Sigma Aldrich
Citric acid	Sigma Aldrich
cOmplete™ His-Tag Purification Resin	Roche
Dibasic sodium phosphate	Sigma Aldrich
Dip and Read™ Biosensors	FortéBio
Dulbecco phosphate buffered saline (PBS)	Sigma Aldrich
Expi 293F expression medium	ThermoFisher Scientific
Expifectamine™ 293 transfection kit	ThermoFisher Scientific
Falcon tube 15 and 50 mL conical tubes	ThermoFisher Scientific
Fast SYBR® Green Master Mix	ThermoFisher Scientific
Gibson Assembly® HiFi 1 Step Master Mix	VWR
Glycerol	Sigma Aldrich
Granulated Agar	Sigma Aldrich
H_3PO_4 (1M)	ThermoFisher Scientific
HCl, Concntrated	Sigma Aldrich

Hepes PH 7.4	Sigma Aldrich
High sensitivity protein 250 chip kit	Agilent
High sensitivity protein chip	Agilent
HisTrap™ HP column, 1 mL	GE Healthcare
HiTrap™ Protein A column, 1 & 5mL	GE Healthcare
HiTrap™ Protein L column, 1 mL	GE Healthcare
IgG Elution buffer	ThermoFisher Scientific
Imidazole	ThermoFisher Scientific
IRDye® 800CW Protein Labeling Kit	LI-COR Biosciences
Kanamycine	Sigma Aldrich
KOH	Sigma Aldrich
MACSQUANT running buffer	Miltenyi Biotec
MACSQUANT washing buffer	Miltenyi Biotec
Monobasic sodium phosphate	Sigma Aldrich
Na_2HPO_4	Sigma Aldrich
Nalgene® Polyether sulfon (PES) filters	ThermoFisher Scientific
Nalgene™ Rapid-Flow™ Sterile Disposable Filter Units with PES Membrane	ThermoFisher Scientific
NaOH	Sigma Aldrich
Nitrocellulose	Bio-Rad
Nunc MaxiSorp® Flat-Bottom 96-Well Plate	ThermoFisher Scientific
Odyssey Blocking Buffer	LI-COR Biosciences
Oligonucleotides	Integrated DNA Technologies
Opti-MEM™ I Reduced Serum Medium	ThermoFisher Scientific
Overnight ExpressTM Instant TB Medium	Novagen
PBT	
PCR Cleanup Kit	ThermoFisher Scientific
PCR Purification Kit	ThermoFisher Scientific
PEG_{8000}	ThermoFisher Scientific
Pierce Zeba® Desalting Spin Columns	ThermoFisher Scientific
Plasmid Maxiprep DNA extraction Kit, Endonuclease free	Qiagen
Plasmid Miniprep DNA extraction Kit	Qiagen
Protease inhibitor tablets	Sigma Aldrich
Protein A biosensors	PALL Forté Bio®
Protein L biosensors	PALL Forté Bio®
QIAPrep Spin M13 Kit	Qiagen
QIAquick Gel Extractio Kit	Qiagen
Rapid flow filter units 0.45 um	ThermoFisher Scientific
Recombinant Human Fc gamma RIIIA/CD16a Protein, CF	R&D Systems
Recombinant human IL3Rα–Fc Chimera CF	Sino Biological

Recombinant mouse IL3Rα–Fc Chimera CF	R&D systems
Recombinant mouse IL3Rβ–Fc Chimera CF	R&D systems
Salts Na_2CO_3, 0.1 M $MgCl_2$, 0.5 M Tris (pH 7.5), 1.0 M Tris (pH 8.0), Tris-HCl, 1.0 M $MgSO_4$, KCl, KH_2PO_4, K_2HPO_4, Na Citrate·$2H_2O$, NaCl, EDTA, Tris Acetate,	Sigma Aldrich
Shaking baffled flasks	ThermoFisher Scientific
SnakeSkin™ dialysis tubing 10K MWCO, 22m	ThermoFisher Scientific
SnakeSkin™ dialysis tubing 30K MWCO, 22m	ThermoFisher Scientific
Sodium dodecyl sulfate (SDS)	ThermoFisher Scienctific
Tetracycline	Sigma Aldrich
Tissue Culture Flat-Bottom 96-, 48-, 24-, 12-Well Microplates	Corning
TMB (Tetramethylbenzidine)	Sigma Aldrich
Tris-acetate	Sigma Aldrich
Tris-HCl	Invitrogen
Tryptone	ThermoFisher Scientific
Tween 20	Sigma Aldrich
Ultra Low Cell Culture Flask, 25 & 75cm^2	Corning
Ultra Low Cell Culture Flask, 25 & 75cm^2	Corning
Ultrapure Glycerol	Invitrogen
Uridine	Sigma Aldrich
Zeocin	ThermoFisher Scientific

Table 3.2 Reagent setup

Reagent	**Materials** (Tonikian, Zhang, Boone, & Sidhu, 2007)
10 × PCR buffer	600 mM Tris-HCl pH 8.3, 250 mM KCl, 15 mM $MgCl_2$
10 × TM buffer	0.1 M $MgCl_2$, 0.5 M Tris pH 7.5
Oligonucleotide design	The criteria used for designing oligonucleotides: (i) The minimal length of oligonucleotide 19 bases (ii) The maximal length of the PCR primer depended on its melting temperature (T_m) (iii) The optimal GC content for a PCR primer is between 35% and 60% (iv) Annealing temperature (T_a) is 5 °C below the lowest T_m of the pair of primers used. PCR primers with a T_m of 58–72 °C
PBS	137 mM NaCl, 3 mM KCl, 8 mM Na_2HPO_4 and 1.5 mM KH_2PO_4. Adjust pH to 7.2 with HCl
PBT	PBS + 0.05% Tween 20, 0.5% BSA. Filter-sterilize.
PT	PBS + 0.05% Tween20
PEG_{8000} / NaCl	20% PEG-8000 (w/v), 2.5 M NaCl. Mix and autoclave
SOC medium	5 g bacto-yeast extract, 20 g bacto-tryptone, 0.5 g NaCl, 0.2 g KCl + H2O up to 1 liter and adjust pH to 7.0 with NaOH, autoclave; add 5.0 ml of autoclaved 2.0 M $MgCl_2$ and 20 ml of filter-sterilized 1.0 M glucose
TAE buffer	40 mM Tris-acetate, 1.0 mM EDTA; adjust pH to 8.0; autoclave
2xYT	31 gr of 2xYT media in 1 L of Milli-Q water (Millipore); autoclave
2xYT solid medium plates	18 gr/L agar in 2YT, autoclave
SOC medium (Super Optimal Broth with Catabolic Repressor medium)	5g bacto-yeast extract, 20g bacto-tryptone, 0.5g NaCl, 0.2g KCl, H2O, and 2.0M MgCl2, 1.0M glucose; PH 7.0; autoclave
2xYT Carbenicillin	50 mg/L in 2xYT
2xYT Kanamycin	25 mg/L in 2xYT
2xYT Zeocin	50 mg/L in 2xYT
2xYT Blasticidin	100 mg/L in 2xYT
2xYT Tetracycline	5 mg/L in 2xYT
2xYT Chloramphenicol	10 mg/L in 2xYT
2xYT Carbenicillin / Kanamycin	50 mg/ L Carb/ 25 mg/L Kan in 2xYT
Overnight Express™ Instant TB (auto-induction) Medium	60 g Overnight Instant TB Medium in 1 L Milli-Q water + 10 mL glycerol; vacuum filtered

Table 3.3 Enzymes

Enzyme	Supplier
Restriction Endoncleases (*Bam*HI, *XHO*I, *Eco*RI, *Eco*RV, *Not*I, *Sac*I)	ThermoFisher Scientific
HotStarTaq® DNA Polymerase	Qiagen
Phusion High-Fidelity DNA Polymerase	ThermoFisher Scientific
T4 DNA Ligase	New England Biolabs
T4 Polynucleotide Kinase (PNK)	New England Biolabs
T7 DNA Polymerase	New England Biolabs

Table 3.4 Cellular strains

Strain	Genotype	Supplier / Reference
NEBαF'	F´ *pro*A+B+ *lac*Iq Δ(*lac*Z)M15 *zzf*::Tn10 (TetR) / *fhu*A2Δ(*arg*F-lacZ)U169 *pho*A *gln*V44 Φ80Δ(*lac*Z)M15 *gyr*A96 *rec*A1 *rel*A1 *end*A1 *thi*-1 *hsd*R17	New England Biolabs (NEB)
XL1-blue	*rec*A1 *end*A1 *gyr*A96 *thi*-1 *hsd*R17 *sup*E44 *rel*A1 *lac* (F´ *pro*AB *lacI*qZΔM15 T*n*10 (T*et*^{r}))	Stratagene
DH5αF'	*F- φ80lacZΔM15 Δ(lacZYA-argF) U169 deoR recA1 endA1 hsdR17 (rk-, mk+) phoA supE44 λ- thi-1 gyrA96 relA1*	Invitrogen
MC1061	F-*ara*D139 Δ(*ara*A-*leu)7697 gal*E15 *gal*K16 Δ(*lac*)X74 *rps*L (S*trr*) *hsd*R2 (*r*K-*m*K+) *mcr*A *mcr*B1	(Wertman *et al.*, 1986)
SS320	*hsd*R *mcr*B *ara*D139 Δ(*ara*ABC-*leu*)7679 Δ*lac*X74 *gal*U*gal*K *rps*L *thi*	Lucigen
CJ236	FΔ(HindIII)::cat (*Tra*$^{+}$ *Pi*$^{I+}$ *Cam*^{R})/ *ung*-1 *rel*A1 *dut*-1 *thi*-1 *spo*T1 *mcr*A	NEB
BL21(DE3)	F-*ompT hsdSB*(r_B^-, m_B^-) *gal dcm (DE3[lacI lac*UV5-*T7 gene* 1 *ind*1 *sam*7 *nin*5])	Novagen
DH10B	F^{-}*mcr*A Δ(*mrr-hsd*RMS-*mcr*BC) Φ80*lac*ZΔM15 Δ*lac*X74 *rec*A1 *end*A1 *ara*D139Δ(*ara*, *leu*)7697 *gal*U *gal*K λ^{-}*rps*L *nup*G	ThermoFisher Scientific
Exp293F	Mammalian cell line; Human embryonic kidney	ThermoFisher Scientific

Table 3.5 Oligonucleotides and primers. Oligonucleotides were ordered from Integrated DNA Technologies. Their sequences represent in 5′ to 3′ orientation and serial numbers are used to refer theoligonucleotides in the text. Oligonucleotides are represented by one letter nucleotide codes, where M = (A, C), R = (A, G), V = (A, C, G) and S = (G, C). NGS forward primers contain adaptor (blue), key (red), barcode (grey) and antibody framework (black). The barcode sequence is an example of multiple unique barcodes used for NGS of various phage pools. NGS reverse primers contain truncated P1 (Green) and antibody framework (black) regions. Adaptor and truncated P1 sequences were used for circumventing PCR amplification. Kunkel and library oligos were suspended at 1 µg / µl concentration and primers at 200 µM concentration in ddH2O.

Primer	Primer Sequence (5′ → 3′)
FabHCupF forward	GGACGCATAGTGGCCC
FabHCupF reverse	GGGCCACTATGCGTCC
pFUSE-CHIg-VH forward	CTAAGTCTTGCACTTCTCACGAATTCGATTGAGATCTCCGAGGTTCAGCTGG
pFUSE-CHIg-VH reverse	CGATGGGCCCTTGGTGCTAGCACTCGACATCGAGGAGACGGTGACCAGGG
pFUSE-CLIg-VL forward	CTTGCACTTGTCACGAATTCACCGGTCACGTCCGATATCCAGATCACCCAGTCC
pFUSE-CLIg-VL reverse	AGATGGTGCAGCCACCGTACGTTTGATTTCCACCTTGGTACCCTGTCCGAACG
pFUSEssUPF	GTCCGCCGTCTAGGTAAGTTT
L3-forward	CCATCTCATCCCTGCGTGTCTCCGACTCAGATCCGGAATCCCGGAAGACTTCGCAACTTA
L3-reverse	CCTCTCTATGGGCAGTCGGTGATATCTCCACCTTGGTACCCTG
H1-forward	CCATCTCATCCCTGCGTGTCTCCGACTCAGATCCGGAATCCGTTTGTCCTGTGCAGCTTC
H1-reverse	CCTCTCTATGGGCAGTCGGTGATCCCTTACCCGGGGCCTGACG
H2-forward	CCATCTCATCCCTGCGTGTCTCCGACTCAGATCCGGAATCCCCCGGGTAAGGGCCTGGAA
H2-reverse	CCTCTCTATGGGCAGTCGGTGATCTTATAGTGAAACGGCCCTTGACGCT
H3-forward	CATCTCATCCCTGCGTGTCTCCGACTCAGATCCGGAATCAGGACACTGCCGTCTATTAT
H3-reverse	CCTCTCTATGGGCAGTCGGTGATACGGTGACTAGTGTACCTG
IL3Rα forward	CACCATGGTCCTCCTTTGGCTCACGC
IL3Rα reverse	TCAAGTTTTCTGCACGACCTGTACTTC
Kunkel CDRL3-mIL3Rα–2 mut	GGAAGACTTCGCAACTTATTACTGTCAGCAATGGTACAGCTACCACCACATCACGTTCGGACAGGGTACCAAG
Kunkel CDRH1-mIL3Rα–2 mut	TCCTGTGCAGCAGCTTCTGGCTTCAACATCAGCAGCTACTACCTGCACTGGGTGCGTCAGGCC
Kunkel CDRH2-mIL3Rα–2 mut	GGGCCTGGAATGGGTTGCATTCATCTACCCCTACTACGACAGCAGCCAGTATGCCGATAGCGTCAAGGG
Kunkel CDRH3-mIL3Rα–2 mut	GCCCTCTATTATTGTGCTCGCGGCGTGTGGGCCTACAGCGCCTGGAGCAGCAAGATCGGCTTCGACTACTGGGGTCAA

TGS 157 forward	TCCAGATGACCCAGTCCCCGAGCTCCCTG
TGS 160 reverse	CAAATCTTGTGACAAAACTCACACGGGTGGTTCGCACCA CCACCACCACCACTGAG
TGS 160-SpyCatcherΔN reverse	ataaacctgataaggtatcaaccatCGAACCACCTGTGTGAGTTTTGTCACAA GATTTG
pCW-SpyCatcher forward	AGCTCTAGCTAGGCTGGCTGGCTCGAGgatagtgctacccatattaaattc
pCW SpyCatcher reverse	ATACTCAGTGGTGGTGGTGGTGGTGCGAACCACCaatatgagcgtcac ctttagttgc

Figure 3.1 Plasmids

The following plasmids were created using Geneious software..

Figure 3.1.1. A map of phagemid-F STOP. Phgemid-F STOP is shown with annotations and unique restriction enzyme sites as indicated. PhoA: E. coli phosphotase promoter, BLA: beta lactamase, ORI: *E. coli* origin of replication pMB1, f1 ORI: filamentous phage m13 origin of replication, LC/HC: antibody secretion signal, *VL* and CL: antibody variable and constant light chains, *VH* and CH1: antibody variable and constant heavy chains, p3: phage pIII minor coat protein.

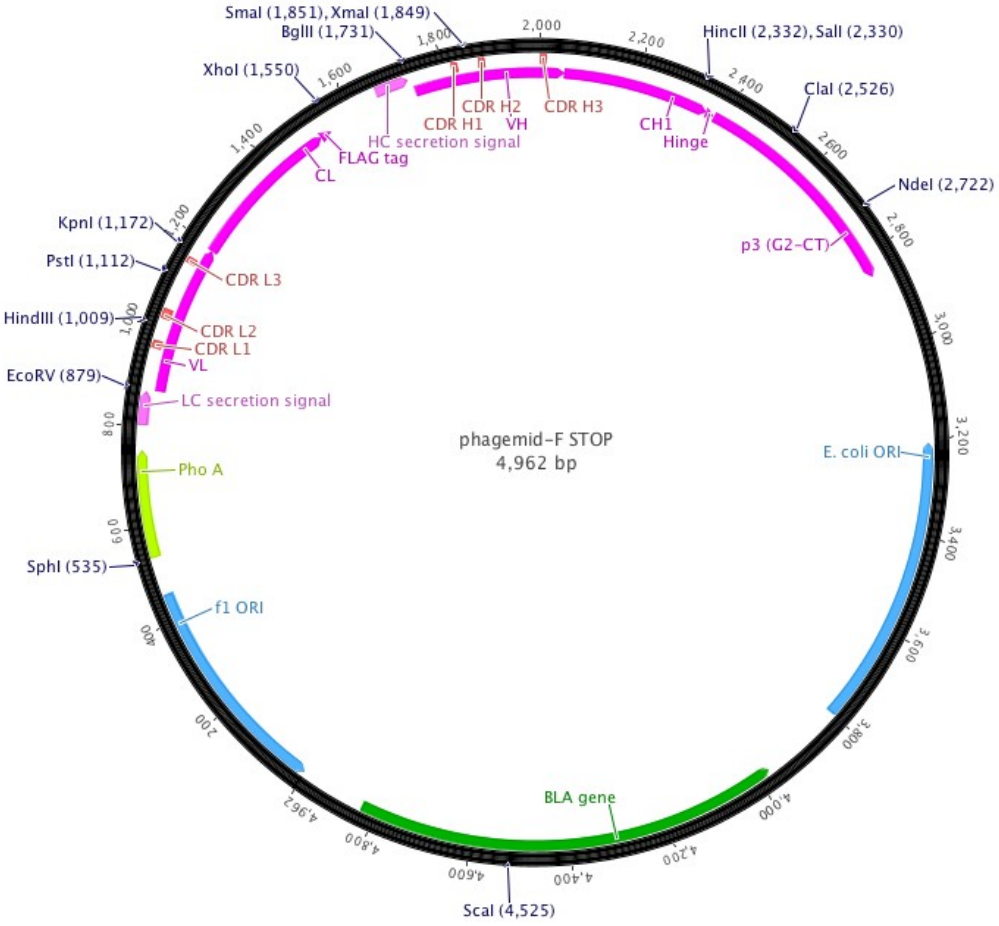

Figure 3.1.2. A map of pCW-FABV for sub-cloning of antibody fragments. To prepare pCW-LIC for sub-cloning of antibody fragments, the *Sac*B gene was deleted and replaced with a portion of the phagemid-F STOP including the LC secretion signal and 5' *VL* until the *Sac*I restriction site. This new destination vector, called pCW-FabV, was also constructed to include an *Nde*I restriction site followed by a 6X poly-His tag and stop codon (see Figure for Fab-phagemid). pCW-FabV was digested with *Sac*I and *Xho*I (unpublished data from Geyer laboratory) to prepare it as the Gibson Assembly® destination vector for PCR amplified Fab fragments from phagemid F clones using TGS157 and TGS160 primers.

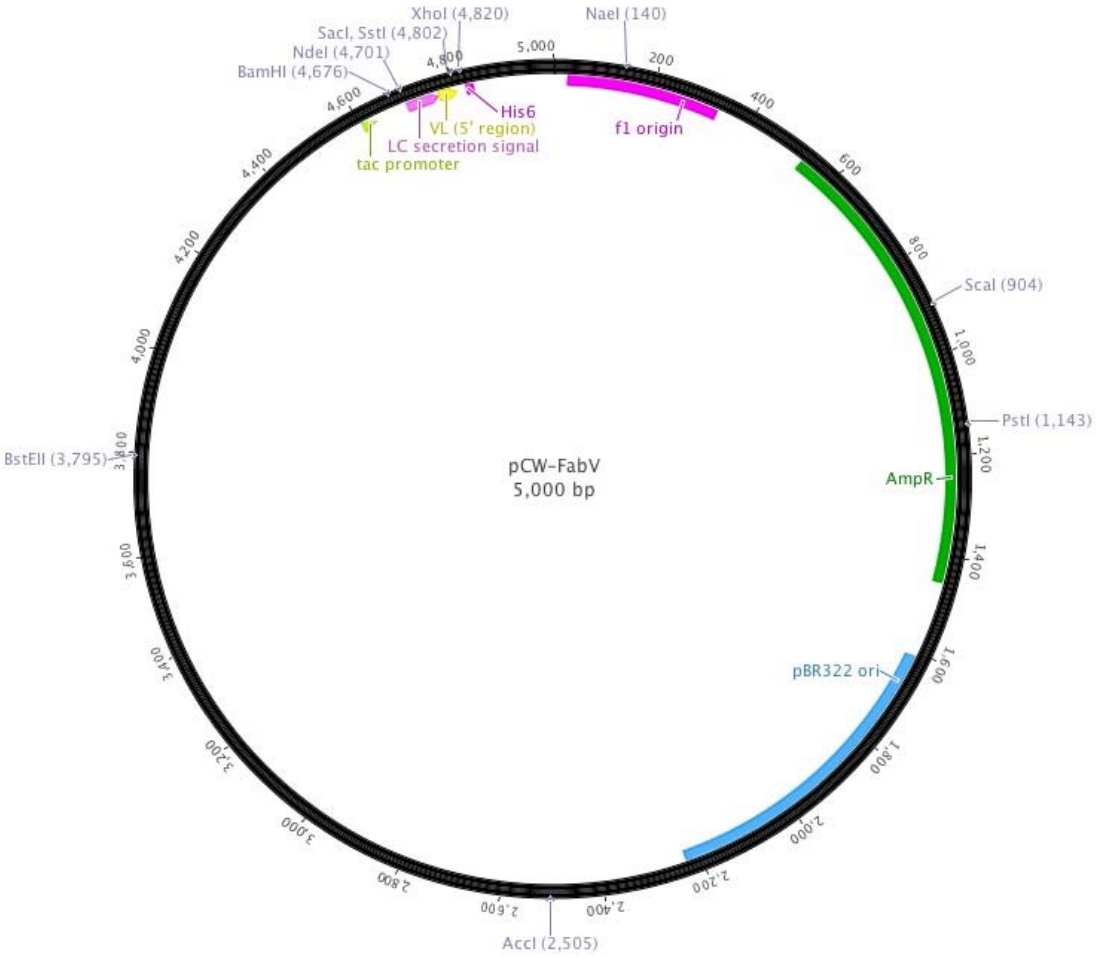

Figure 3.1.3. pFUSEss-CHIg-hG1 vector for cloning the variable heavy domain of the antibody of interest. The constant region of the human IgG1 heavy chain is preceded by a multiple cloning site containing four restriction sites: *Eco*RI, *Eco*RV, *Xho*I and *Nhe*I. *Eco*RI was used for 5' cloning site to ensure the *VH* will follow the hIL2 signal sequence without unwanted amino-acids. *Nhe*I must be used for insertion of the 3'end of the variable region to maintain the integrity of the constant region. Figure adapted from NEB (NEB# pfuse-hchg1).

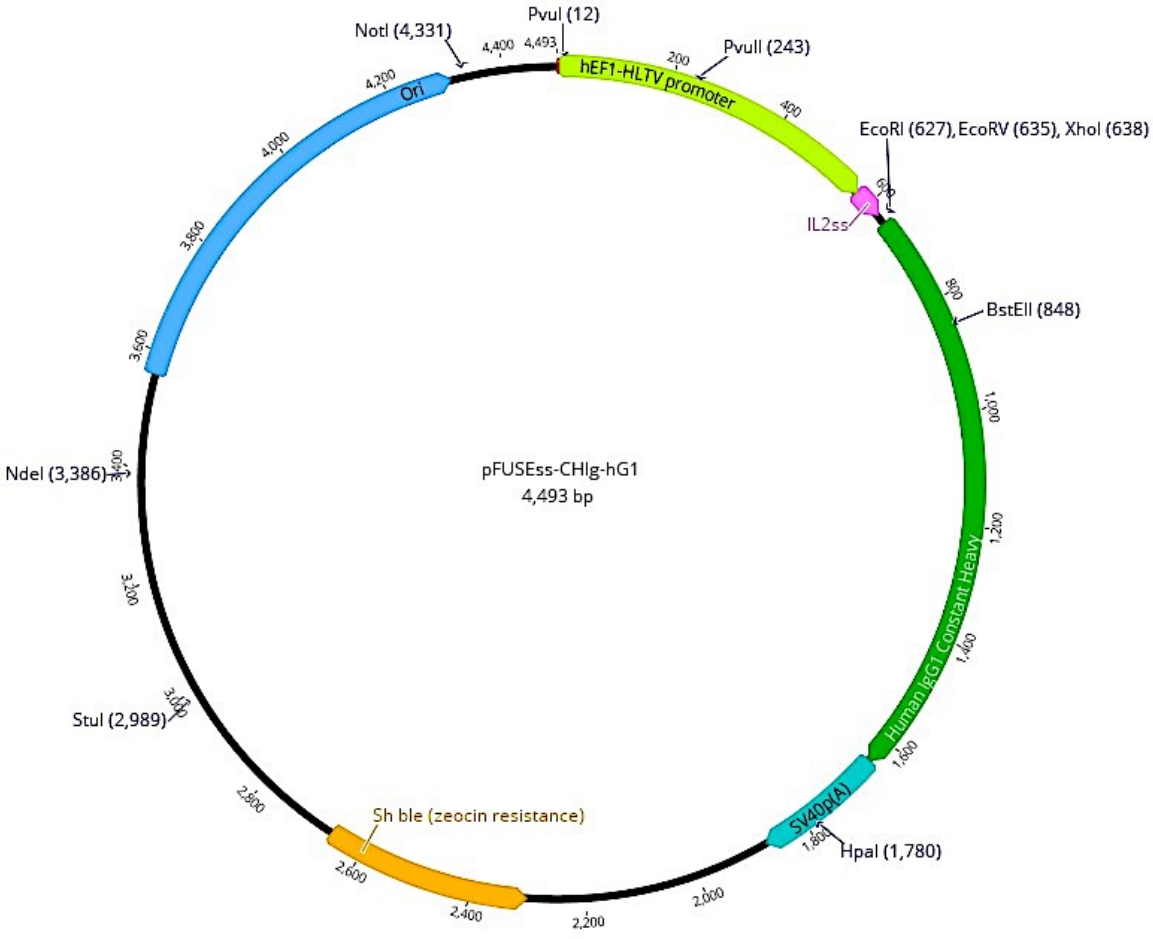

Figure 3.1.4. pFUSE2ss-CLIg-hk vector for cloning the variable light domain of the antibody of interest. The constant region of the human kappa light chain contains multiple cloning site containing five restriction sites: *Eco*RI, *Age*I, *BstE*II, *Nco*I, and *BsiW*I. *NcoI* restriction site was used as the 5' cloning site to ensure that the cloned *VL* will follow the hIL2 signal sequence with no unwanted amino acids. *BsiW*I was used as the 3' cloning site for the *VL* in order to preserve the immunoglobulin kappa constant amino acid sequence. Figure adapted from NEB (NEB # pfuse2ss-hclk).

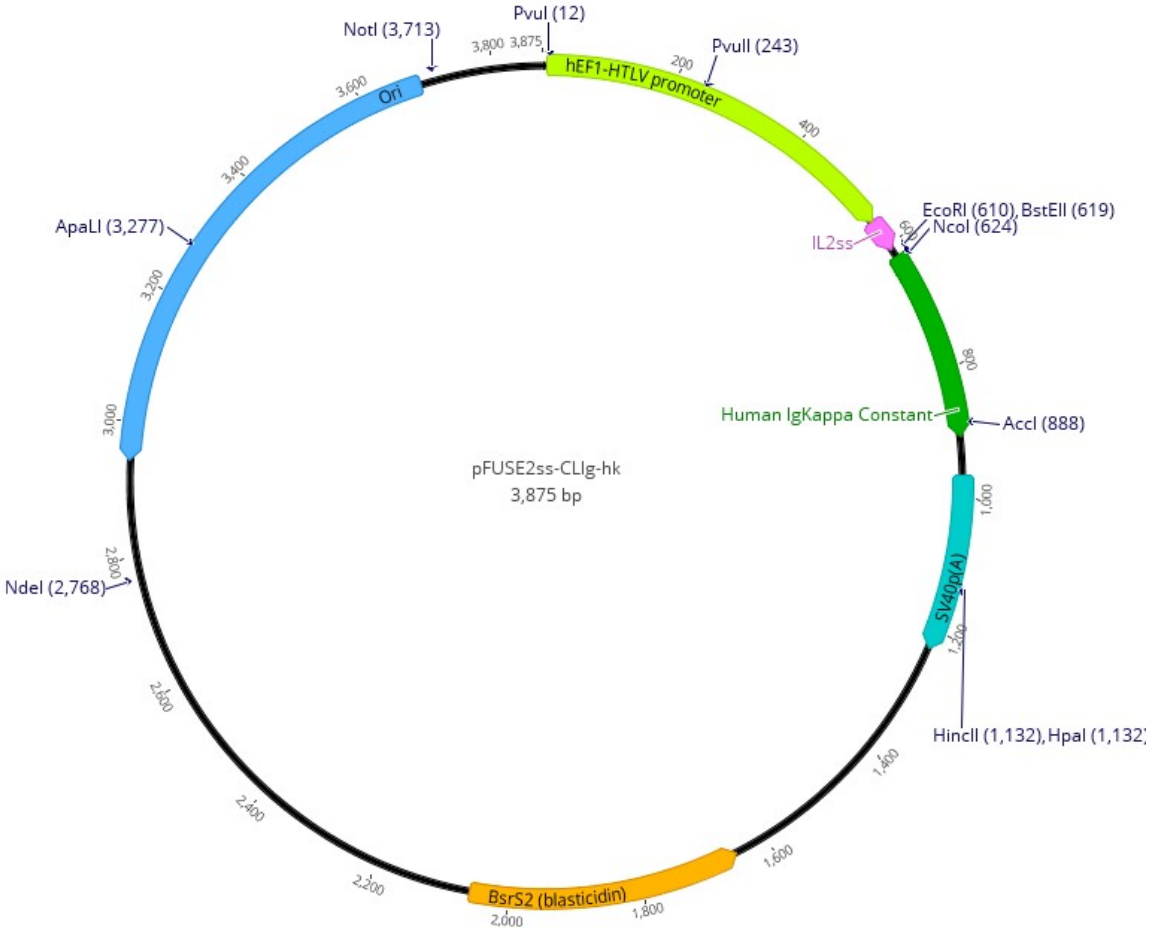

Figure 3.1.5. pcDNA^{TM}3.2 / V5 / GW/ D-TOPO vector- The vector used as a destination plasmid for cloning of IL3Rα DNA coding sequence. The vector contains Cytomegalovirus (CMV) promoter for high-level expression and is adapted for directional TOPO® cloning that enables cloning of a PCR product in a specific orientation. Neomycin resistance gene is used for stable selection, and C-terminal V5 tag facilitates its detection. Ampicillin resistance gene and pUC origin are for selection and maintenance in *E. coli* cells. (ThermoFisher #K244020)

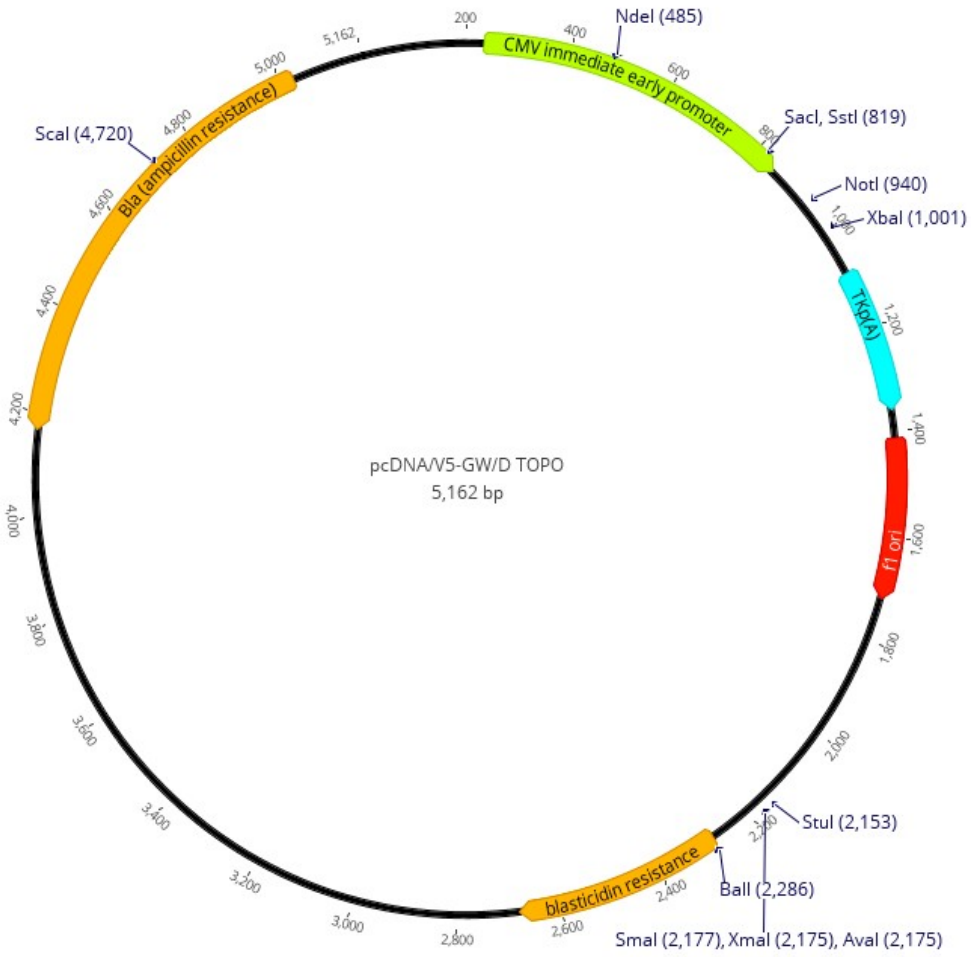

Figure 3.1.6. pCMV expression plasmid (8917 bp) used for cloning human CD131 / CSF2RB/ IL3Rβ/ IL5Rβ Gene. CMV promoter and a hygromycin-resistance (*hygro*) gene allow direct use of the plasmid in mammalian cell expression (freestyle^{TM} 293F cells) of IL3Rβ. (Sino biological #HG10516-NM).

3.2. General protocols for generation of antibodies and antibody fragments

3.2.1 Preparation of electrocompetent Escherichia coli (*E. coli*) cells

E. coli (e.g. SS320) were cultured as described according to standard methods(Elbing & Brent, 2002). Electrocompetent *E. coli* cells were optimized for high transformation efficiency by electroporation. A single *E. coli* colony was used to inoculate 500 mL 2xYT liquid medium and incubated at 200 rpm shaking. Upon reaching the OD_{600} of 0.35 – 0.4, the culture was transferred on ice for 20 – 30 minutes with occasional swirling. The cells were harvested by centrifugation at 5000 g at 4 °C for 10 minutes in a Sorvall GS-3 rotor and cells were washed with ice-cold Milli-Q water three times. The cells were then collected after centrifugation at 5000 g in 4 °C for 10 minutes. Cells were resuspended in 50 mL of ice-cold 10% ultrapure glycerol and stored at -80 °C.

3.2.2 Preparation of Plasmid DNA

Individual colonies were inoculated in 5 – 10 mL of 2xYT media with appropriate antibiotic. Cells were collected by centrifugation at 5000 g for 10 minutes. Plasmid DNA was extracted using Plasmid Miniprep Kits (ThermoFisher Scientific) according to manufacturer's instructions. The concentration of plasmid was measured using a NanoDrop 2000c spectrophotometer at OD_{260} Nanometer (nm) l(ThermoFisher Scientific).

3.2.3 *E. coli* Electroporation

Electrocompetent DH10B or SS320 *E. coli* cells were used as 50 µL aliquots for plasmid transformations. One µL of 50 – 150 ng/µL plasmid DNA was mixed with the cells and electroporated in an ice-cold 0.2 cm gap electroporation cuvette at 12.5 kV/cm (Ec2 on Bio-Rad Micro Pulser). The cells were then incubated at 37 °C in 500 – 1000 µL of SOC medium and sub-cultured into 2xYT with proper antibiotic or plated onto 2xYT agar plates containing the required antibiotics.

3.2.4 Polymerase Chain Reaction (PCR)

3.2.4.1 High fidelity PCR reactions

The following high fidelity (HF) reactions were used for gene amplification and library creations. PCR products were amplified using following program in the thermal cycler.

Reagents	Amount	Final Concentration
5x Phusion HF buffer	10 µL	1x
10 mM dNTPs	0.5 µL	200 µM each
10 µM forward primer	1.5 µL	400 nM
10 µM reverse primer	1.5 µL	400 nM
Phusion HF DNA polymerase	0.5 µL	2.5 Unit / reaction
Template	Variable	50–200 ng complex DNA 1–10 ng plasmid DNA
Nuclease-free water	Up to 50 µL	
Total volume	50 µL	

	Steps	Temperature	Time
	Initial denaturation	98 °C	30 sec
25 Cycles	Denaturation	98 °C	10 sec
	Annealing	55 °C	30 sec
	Extension	72 °C	15-30 sec/kb
	Final extension	72 °C	10 min
	Hold	4 °C	

3.2.4.2 Low Fidelity PCR

Low fidelity PCR was used to check the plasmids for the correct insert, cloning of small DNA fragments and for generating libraries.

Reagents	Amount	Final Conc.
10x PCR buffer (with $Mgcl_2$)	5 µL	1x
10 mM dNTPs	1 µL	200 µM each
10 µM forward primer	1.2 µL	0.5 µM
10 µM reverse primer	1.2 µL	0.5 µM
HotStart Taq DNA polymerase	0.4 µL	2.5 Unit / reaction
Template	Variable	50-200 ng
Nuclease-free water	Up to 50 µL	
Total volume	50 µL	

	Steps	Temperature	Time
	Initial denaturation	95 °C	15 min
25 Cycles	Denaturation	94 °C	30 sec
	Annealing	55 °C	30 sec
	Extension	72 °C	1.5 min/kb
	Final extension	72 °C	8 min
	Hold	4 °C	

3.2.4.3 *E. coli* colony PCR

Colony PCR was used as a rapid test to verify the correct insertion of a DNA segment into a plasmid prior to plasmid purification and sequencing. Single colonies from 2xYT agar plates were picked and resuspended in 100 µL of sterile distilled water and 1uL of the colony suspension was then used as the template for PCR reaction.

3.2.5 Agarose gel electrophoresis

PCR products and plasmids were visualized using agarose gel electrophoresis. Samples were mixed with 6x loading dye (50% (v/v) glycerol, 0.2 M EDTA pH 8.3, 0.05% (w/v) bromophenol blue) for a 1x final concentration of the dye. Samples were resolved in an agarose gel consisting 0.8 – 1% (w/v) ultrapure agarose in 1x TAE Buffer (40 mM Tris-acetate, 1 mM EDTA, pH 8.0) and 0.5 µg/mL Ethidium bromide. Gels were run at 88 V for 30 to 60 minutes in 1x TAE Buffer and photographed using a UV light transilluminator Gel-Doc (Bio-Rad).

3.2.6 Purification and extraction of DNA

PCR products were purified using a PCR cleanup kit (Qiagen/Bio-Basic) as per manufacturer's instructions. Restriction enzyme-digested plasmids were purified using a gel purification kit (Qiagen/Bio-Basic), according to manufacturer's instructions. Similarly, Gel purification was performed using a Gel Purification kit as per manufacturers instructions.

3.2.7 Phage display selection

Phage display selection approach allows finding novel antibodies specifically bind to the target of interest. The phagemid library (library F) used for this project was a gift from Dr. Sidhu's laboratory, Toronto, Canada. Library F is a M13-based phagemid library with PIII fusions to the antibody fragment (Antigen binding fragment or Fab) sequences that contain completely randomized CDRL3, CDRH1, CDRH2, and CDRH3(Fellouse & Sidhu, 2006). The library was re-amplified with SS320 cells using M13KO7 helper phage at 10:1 ratio (helper phage:*E coli*) as per instructions by Dr. Sihu's laboratory (Fellouse & Sidhu, 2006; Tonikian et al., 2007). The library was then used for solid-phase immunoplate-based selections against immobilized target (Recombinant mouse IL3Rα Fc chimera, or human IL3Rα Fc chimera, or mouse IL3Rβ Fc ectodomain) following the protocol outlined in Tonikian *et al.*(Fellouse & Sidhu, 2006; Tonikian et al., 2007). Briefly, the "target" was pre-adsorbed onto the immunoplate wells at final concentration of 5 ug/ml in PBS at 4 °C overnight or room temperature for 2 hours. Subsequently, The target-coated wells were blocked with 0.5% BSA and washed with PT buffer as per standard protocols(Fellouse & Sidhu, 2006; Tonikian et al., 2007). The wells were then incubated with 100 μL of the amplified phage displaying the fab library at a concentration of 10^{13} phage/mL in PBT buffer (the library was pre-adsorbed on Fc-coated wells prior to each selection), and incubated at room temperature for 2 hours shaking at 200 rpm. The phage solution was then removed from the wells and the unbound phages were washed away. The remaining phage bound to the target through the displayed Fab was eluted using 100 mM HCl and neutralized with 1.0 M Tris–HCl (pH 8.0). Half the eluted phage solution was added to 10 volumes of actively growing *E. coli* XL1-blue, NEBαF', or DH5αF' (OD_{600} ~0.8) in 2xYT/Tet medium and incubated for 30 minutes. In order to evaluate the enrichment, 10–fold serial dilutions of the infected *E. coli* culture were plated on 2xYT/Carb plates followed by overnight incubation. The remaining culture was infected with M13K07 helper phage in a final concentration of 10^{10} phage/mL followed by incubation for 45 minutes till sub-culture into 25 volumes of 2xYT/Carb/Kan medium overnight incubation. The amplified phage was then extracted by PEG_{8000}/NaCl ($1/5^{th}$ the culture volume) and underwent another round of selection. The selection process was then repeated in the same manner until the retrieved phage titre

in a given round yielded an enrichment of phage bound to the target versus a negative control (**Figure 1.8**). Generally, 3 – 5 rounds of selection were performed to enrich the bound phage for various targets. Fc and BSA were used as controls for each round of selection. Ten clones from the last round of selection were picked for single clone sequencing. In addition, the pool of phage from the final round of selections was prepared for NGS. These two types of sequencing were performed to identify the CDR sequences for the lead binding clones and evaluate their frequency in the pool of phage.

3.2.8 Phage ELISA (Enzyme-Linked Immunosorbent Assay)

In order to monitor the selections for the enrichment of specific binding clomes, a phage ELISA was performed at the last round of selections following the standard protocols for Phage ELISA. The 96-well Maxisorp plate was coated with target proteins at 5 ug/mL. In parallel, control wells were coated with BSA and Fc as controls for each sample (5 ug/mL each) and incubated at 4 °C overnight. The wells were then blocked by 0.5% BSA for one hour at room temperature following by several washes with PT buffer. 10^{11} phage / well was added to the target-coated and control wells and incubated for 2 hours at room temperature. The wells were then washed 6 times with PT buffer according to the standard protocols (Fellouse & Sidhu, 2006). 50 μL of anti-M13 antibody HRP conjugate (1:3000 in PBT buffer) was added to the coated wells and incubated for ½ hours at room temperature. Next, the wells were washed with PT (8 times wash) and PBS (2 times wash). 50uL of TMB (Tetramethylbenzidine) substrate was added to the wells and monitor the color to develop for 1-5 minutes depending on the signal strength for the target-coated well. Upon color development, reaction was stopped by 5uL of 1.0 M H3PO4 and the signal was measured spectrophotometrically using SpectraMax 340PC384 microplate reader at 450nm.

3.2.9 Kunkel mutagenesis

3.2.9.1 Design and generation of softly-randomized oligonucleotides

To mutate the lead Fab clones, Kunkel oligonucleotides were designed using a spreadsheet and formula (provided by Kris Barreto; unpublished formula) to generate the

secondary phage Fab libraries. These oligonucleotides contain softly randomized CDRs based upon the particular lead clones that are flanked by annealing regions (indicated in Table 3.5 for primers). The formula determines the extent of the amino acid mutagenesis over a given length using variable frequencies of each nucleotide at each position. The hand-mix ratio formula allowed us to randomize the nucleotides of the particular lead Fab in a way that resulted in a minimum number of fully mutated CDRs and approximately 1% – 8.3% wild type CDRs. Using these parameters, the hand mixed oligonucleotides were ordered with 76% wild type frequency and 8% frequency for the remaining three nucleotides at each position. The oligonucleotides were ordered through Integrated DNA Technologies (IDT) and directly used for Kunkel mutagenesis.

3.2.9.2 **Purification of Uracil-containing single stranded DNA (dU-ssDNA)**

A single colony of *E. coli* CJ236 harboring the appropriate Fab-phagemid inoculated into 1 mL of the 2xYT Carb / Comp media along with $1x10^{10}$ phage/mL of M13K07 helper phage which carries kanamycin resistance gene. This media contains Carbenicillin to select for phagemids carrying β-lactamase gene and chloramphenicol to select for F' episome of CJ236 *E. coli* cells. After 2 hours, kanamycin was added to select for clones that have been co-infected with helper phage, and the culture was incubated for 6 hours. The culture was then sub-cultured into 30 mL of 2xYT Carb / Kan / Uridine and incubated overnight at 37 °C with 200rpm shaking. Phages were purified from cell culture supernatant using PEG_{8000} / NaCl precipitation as per instructions by Rajan and Sidhu in 2012 (Rajan & Sidhu, 2012). The dU-ssDNA was extracted from the purified phage using QIAPrep Spin M13 Kit following manufacturer's instruction and measured using NanoDrop 2000c spectrophotometer. 20ug of dU-ssDNA Kunkel template (phagemid–F STOP) was used for the construction of each library (Figure 3.1.1).

3.2.9.3 ***In vitro* synthesis of heteroduplex covalently closed circular - double stranded DNA (CCC-dsDNA)**

Mutagenic oligonucleotides were incorporated into heteroduplex CCC-dsDNA using a three-step procedure following the published technique by Kunkel et al. (Kunkel, Roberts, & Zakour, 1987). Full conversion of ssDNA to dsDNA is a successful reaction.

In this step, synthetic oligonucleotides are annealed into the dU-ssDNA to mutate CDRL3, CDRH1, CDRH2, and CDRH3 within the variable domains in CCC-dsDNA. See Appendix A for mutated oligonuceatide sequences ordered from IDT.

(i) *Phosphorylation of mutagenic oligonucleotides with T4 polynucleotide kinase:* 0.6 μg of the oligonucleotide, 2.5 μL of 10x TM buffer, 2.0 μL of 10 mM ATP, 1.0 μL of 100 mM DTT, and Milli-Q water were combined to a total volume of 25 μL. Subsequently, T4 polynucleotide kinase was added and the mixture was incubated at 37 °C for an hour.

(ii) *Annealing of the oligonucleotides to the template:* 1μg of ssDNA, 2 μL of 10x TM buffer, 2 μL of the phosphorylated oligonucleotide were mixed in and Milli-Q water to a total of 20 μL. The molar ratio 3:1 (oligonucleotide:ssDNA) was used for optimal condition. The mixture is then incubated at 90 °C for 3 minutes, 50 °C for 3 minutes and 20 °C for 5 minutes.

(iii) *Enzymatic synthesis of CCC-dsDNA:* Following annealing, primer extension occurred in the annealed oligonucleotide / template mixture by adding 1 μL of 10 mM ATP, 1 μL of dNTPs, 1.5 μL of 100mM DTT, 3 units of T4 DNA ligase, and 3 units of T7 polymerase. The reaction was then incubated overnight at 20 °C. CCC-dsDNA was affinity purified and desalted using the QIAquick DNA purification kit (Qiagen) as instructed in manufacturer's protocol.

3.2.9.4 **Secondary phage library generation**

In order to convert the kunkel DNA library product into the phage library, the heteroduplex CCC-dsDNA was introduced into SS320 *E. coli* cells by electroporation. SS320 is constructed by Dr. Sidhu's laboratrory using standard bacterial mating method (Low, 1974) to contain high efficiency electroporation of *E. coli* Mc1061 and F' episome from *E. coli* XL1-blue (S S Sidhu, Lowman, Cunningham, & Wells, 2000). Immediately following electroporation, 1mL of SOC (no antibiotics) was added to cells and the cells were then sub-cultured into 25 mL of SOC medium for 30 minutes. In order to determine the library diversity, serial dilutions were plated on 2xYT/Carb plates and incubated

overnight to select for the phagemid. The remaining culture was transferred to 500 mL of 2xYT/Carb/Kan supplemented with M13K07 helper phage to incubate overnight. The phage library was purified using PEG_{8000}/NaCl precipitation(Rajan & Sidhu, 2012). The library was used immediately or frozen and stored with glycerol (to a final concentration of 10%) at –80 °C.

3.2.10 Selection of antigen-specific mutated antibodies

Phage displayed antibody libraries created by soft randomization of the most frequent Fabs were screened against immobilized target as previously described in for phage display selections (3.1.3.7), and the best binding mutated fab phagemids were then identified by NGS.

3.2.11 Single clone sequencing

Applied Biosystems 3500XL genetic analyzer and manufacturer's protocol XX was used for capillary electrophoresis DNA sequencing. Sequencing primers are listed in TableX. Primer Fab-HCupF and Fab-HCupF reverse was used to respectively sequence the heavy and light chains of all phagemid and pCW clones. All pFUSE clones were sequenced with primer pFUSE-CHIg / CLIg 5'.

3.2.12 Next Generation Sequencing (NGS)

NGS was performed to sequence CDRs form multiple clones simultaneously. Ion Torrent™ Personal Genome Machine™ (PGM) system was used for next generation sequencing on 314™ or 316™ Chip v2 for 200 or 400 base reads. To prepare products for NGS, each CDR was PCR-amplified using primers annealing to regions just upstream and just downstream of each individual CDR (see Table 3.5 for primer annealing sequences). In addition to annealing sequence, the forward primers contained an adaptor and key sequences, as well as, sample-specific barcode. Barcode sequences were chosen from the ion express barcode list. In addition to the annealing regions, reverse primer contained the truncated P1 sequence. The adaptor and truncated P1 sequences are necessary for the downstream NGS emulsion PCR. The key sequence is for

bioinformatics analysis. The reaction contained a ready reaction premix (2.5x), Big dye sequencing buffer (5x), 3.2 pmol of primer, and 150-300 ng of phagemid DNA template in a total of 20 µL. The thermal cycler program performed by 96 °C for 1 minute initial denaturation, 25 cycles of 96 °C for 10 seconds, 50 °C for 5 seconds, 60 °C for 4 minutes, followed by rapid thermal ramp to 4 °C and hold until the PCR product was purified using PCR purification kit and quantified by Bioanalyzer and used as per manufacturer's protocols for NGS.

3.2.13 Gibson Assembly® cloning

Gibson assembly is an *in vitro* iso-thermal enzymatic approach to join overlapping DNA molecules. In this one-step reaction, exonuclease enzyme chews back the end of the DNA fragments and exposes the ssDNA overhangs to anneal to their ssDNA complement. Subsequently, DNA polymerase fills the gaps in the annealed products and DNA ligase then covalently ligates the resulting nicks in the assembly. In this project, Gibson assembly was used to clone *VH* and *VL* into mammalian cell expression vectors, and to clone Fabs and SpyCathcer or SpyTag in their corresponding destination pCW vectors.

3.2.13.1 **Cloning of *VH* and *VL* in mammalian cell expression vectors**

Once the *VH* and *VL* sequence were known, the inserts were cloned into mammalian cell expression vectors pFUSEss–CHIg-hg1 and pFUSE2ss–CLIg-hk (InvivoGen), respectively, to convert into full immunoglobulin G in mammalian cells. In pFUSE-CHIg-hG1, the constant region of the human IgG1 heavy chain is preceded by a multiple cloning site containing four restriction sites: *Eco*RI, *Eco*RV, *Xho*I and *Nhe*I. In order to clone the *VH*, *Eco*RV was used for insertion of the 5'end and *Nhe*I was used for insertion of the 3'end. *Nhe*I is associated with maintaining the integrity of the constant region. In pFUSE2ss-CLIg-hk, the constant region of the human kappa light chain is preceded by a multiple cloning site containing five restriction sites: *Eco*RI, *Age*I, BstEII, *Nco*I, and *BsiW*I. In order to clone *VL* into pFUSE2ss–CLIg-hk, *Nco*I was used for insertion of as the 5' end and *BsiW*I for the 3' cloning site.

Gibson Assembly® reaction was employed to clone *VH* or *VL* into pFUSE-CHIg or CLIg as per manufacturer's instructions. Briefly, the pFUSEss–CHIg-hg1 and pFUSE2ss–CLIg-hk were digested at *Eco*RV and *Nco*I respectively, as per FastDigest instruction prtocols (ThermoFisher Scientific). The digested plasmids were cleaned up with PCR purification kit. In order to perform the Gibson Assembly® reaction, 50 ng of the *VH* / *VL* insert was mixed with the corresponding linearized pFUSEss-CHIg or -CLIg vector at 1:3 molar ratio (insert: backbone template), 10 µL of Gibson Assembly® mix, and milli-Q water up to 20 µL total volume. The reaction mix was incubated at 50 °C for one hour and transformed into DH10B cells. The transformed cells were plated on 2xYT/Zeocin plates for *VH*-CHIg and 2xYT/Blastocidin for *VL*-CLIg. The single colonies from the plates were inoculated into 2-3 mL of proper media (2xYT/ Zeocin or Blastocidin) and sub-cultured into higher volumes (100-500 mL) to extract the DNA by Endofree plasmid Maxiprep kit according to manufacturer's protocol (Qiagen).

3.2.13.2 **Cloning Fab into bacterial expression vector**

DNA encoding Fab domains generated by phage display against IL3Rα and IL3Rβ were PCR-amplified from the Fab phagemid using the appropriate forward and reverse primers (TGS157 and TGS 160; see Table 3.5). pCW-FabV (Figure 3.1.3), digested with *Sac*I and *Xho*I, was used as the Gibson Assembly® destination vector for PCR amplified Fabs. Details of cloning Fabs into bacterial expression vector are described below in 3.2.14.

3.2.14 Generation of mono-Fab–SpyCatcher and mono-Fab–SpyTag

The SpyCatcher–SpyTag system is an engineered protein ligation system based on *Streptococcus pyogenes* collagen adhesion domain (CnaB2) of fibronectin-binding protein that naturally forms intramolecular isopeptide bonds. The Howarth lab was able to manipulate the protein to create a 138 amino acid domain, called SpyCatcher, that retains the ability to covalently "capture" a small 13 amino acid portion of the original protein, called SpyTag (Zakeri et al., 2012). The reaction is robust, irreversible, and has been successfully performed on the surface of mammalian cells through fusion to the intercellular adhesion molecule (ICAM) cell surface receptor(Zakeri et al., 2012). The

SpyTag also has good positional flexibility, as it can be placed at the N- or C- terminus of (or internal to), fusion proteins (Zakeri et al., 2012), and can function adjacent to a variety of tags (Reddington & Howarth, 2015). In this project, SpyTag–SpyCatcher system was used to ligate SpyTag– or SpyCatcher–labeled monoFabs to generate bivalent or bispecific Fabs.

In order to label the mono-Fabs with SpyTag, the Fab was PCR amplified using a forward primer (TGS157) and a reverse primer (TGS 160-SpyTag) to add the SpyTag sequence (AHIVMVDAYKPTK) at the 3' end, and the suitable restriction sites for sub-cloning into the bacterial expression vector pCW-FabV (See Figure 3.1.3).

In order to add SpyCatcher to the mono-Fab, PCR amplified Fab was cloned into pCW-SpyCatcher (*Xho*I-*Sac*I)(Alam et al., 2017) with the appropriate primers (pCW-SpyCatcher forward and pCW-SpyCathcer reverse). We used a special N-terminus truncated form of SpyCatcher, herein called SpyCatcherΔN, to limit its immunogenicity (Reddington & Howarth, 2015; Zakeri et al., 2012). In addition, SpyCatcherΔN contained a N-terminal His Tag (6x His), while SpyTag lacked the His Tag to facilitate nickel affinity chromatography of bi-Fabs (See 3.1.2.2 for details).

The resulting mono-Fab–SpyCatchers or mono-Fab–SpyTags were transformed into BL-21 *E. coli* cells and propagated in 10 mL of 2xYT/carb medium for 6-8 hours with 200 rpm shaking at 37 °C. The medium was then completely removed by centrifugation and *E. coli* was sub-cultured into 1L of Overnight Express^{TM} Instant TB Medium, supplemented with carbenicillin (50 mg / L). The culture was then incubated for 20-24 hours at 30 °C. The cells were harvested by centrifugation at 10000 g for 10 minutes at 4 °C and resuspended in binding buffer (20 mM sodium phosphate pH 7.0, 0.15 M NaCl) supplemented with protease inhibitors, and prepared for immediate purification (details of protein purification in 3.2.17.2).

3.2.15 Generation of full-length antibody in mammalian cells

The plasmid constructs *VH*-pFUSEss–CHIg and *VL*-pFUSE2ss–CLIg were transiently co-transfected onto the high-density culture of HEK (human embryonic kidney) cells as per manufacturer's instruction. Briefly, the 293F cells were transferred into new medium one day prior to transfection at a final concentration of 2 x 10^6 cell /

mL. Upon reaching the cell concentration of 3 x 10^6 cell / mL or more, 15 ug of each *VH*-pFUSEss–CHIg and *VL*-pFUSE2ss–CLIg (total of 30 ug) were mixed and diluted into Opti-MEM medium at a total volume of 1.5 mL. The DNA mixture was then combined with 80uL of ExpiFectamine™ pre-diluted into Opti-MEM. The DNA–ExpiFectamine mixture was incubated for 20 minutes in room temperature and subsequently added drop-wise to the 293F cell culture. 16-20 hours post-transfection, enhancers 1 and 2 were added to the cells as per manufacturer's instructions. The cells were incubated for 4-5 days shaking 200 rpm at 37 °C and 8% CO_2. The high-efficiency, cationic, lipid-based transfection reagent and transfection enhancers are designed to power the highest possible level of protein expression from Expi293F™ cells cultured in Expi293™ Expression Medium. The antibody was purified from the culture medium by affinity chromatography.

3.2.16 Generation of Bi-Fab using SpyCatcher–SpyTag reaction

The conditions in which the most efficient covalent bond between SpyTag–mono-Fab and SpyCatcher–mono-Fab occurs was optimized by altering pH, salt, and buffer type. Protease inhibitors and considerable effort was also necessary to determine conditions to avoid denaturation and / or aggregation during purification. The SpyTag–SpyCatcher reaction was resolved with an optimal ratio of 2:1 mono-Fab–SpyTag to mono-Fab–SpyCatcher. Final conditions for the optimal attachment of mono-Fab–SpyTag to mono-Fab–SpyCatcher was in citrate phosphate buffer pH 7.0, at 4 °C overnight. The bi-fab were purified using HisTag purification. The ligation of various SpyTag– or SpyCatcher–labeled monoFab resulted in generation of bivalent and bispecific Fabs.

3.2.17 Protein purification

3.2.17.1 **Purification of monoclonal antibodies**

In order to purify the monoclonal antibodies, the Exp293F cells transfected by co-expression of *VH*-pFUSEss-CHIg and *VL*-pFUSE2ss-CLIg vectors were incubated at 37 °C for 4 – 5 days. The supernatant was then collected after centrifugation and filtration of

the excess debris with low protein binding filters (Nalgene® PES). The supernatant was combined with binding buffer (10mM sodium biphosphate, 10mM sodium monophosphate in milliQ water, PH 7.0) at 1:1 ratio (v/v), and immobilized on HiTrapTM Protein A HP column using ÄKTA pure chromatography system (GE HealthCare). The monoclonal antibody was eluted off the column by elution buffer and neutralized by neutralization buffer (1M Tris-NaOH, pH 8.0). The purified Fabs were dialyzed using 10K MWCO SnakeSkin dialysis tubing and concentrated using ultra-centrifugal filters. Ultimately the monoclonal antibodies were stored in sterile PBS at 4°C for further analysis. The full-length monoclonal antibodies were labeled as mIL3R-α and mIL3R-β.

3.2.17.2 **Purification of mono-Fabs**

Mono-Fabs (labeled with SpyTag or SpyCatcher – details in 3.2.14) were expressed in BL-21 *E. coli* using Overnight Express auto-Induction media. Following centrifugation, the cells were resuspended in binding buffer (20 mM sodium phosphate pH 7.0, 0.15 M NaCl) supplemented with protease inhibitors, and were homogenized using French press disrupter (Constant Systems LTD) as per manufacturer's instruction. Cell debris was removed by centrifugation at 10000 g for 30 – 40 minutes at 4°C. mono–Fab was purified from supernatant by affinity chromatography using 1 mL HiTrap^{TM} Protein L–affinity column by ÄKTA pure chromatography system. Fab was eluted in elution buffer (0.1 M glycine pH 2.5) and neutralized in neutralization buffer (1 M Tris-Amine, pH 8.0). The purified Fabs were dialyzed using 10K MWCO SnakeSkin dialysis tubing and concentrated using ultra-centrifugal filters (Amicon®, Millipore). The mono–Fabs were ultimately stored in citrate phosphate buffer at 4°C for further analysis or production of bi-Fabs.

3.2.17.3 **Purification of bi-Fabs**

In order to facilitate bi-Fab purification, the SpyCatcher was tagged with a poly histidine (6xHis) Tag to allow the unreacted excess Fab–SpyTag to be removed using metal ion affinity chromatography (IMAC) by ÄKTA pure chromatography system. The bi-Fabs were immobilized on 1 mL HisTrap HP column using binding buffer (20 mM

sodium phosphate, 0.5 M NaCl, 5 mM imidazole, pH 7.4), and then eluted with elution buffer (20 mM sodium phosphate, 0.5 M NaCl, 0.5 M imidazole, pH 7.4). The eluted bi-Fabs were dialyzed using 30K MWCO SnakeSkin dialysis tubing into citrate phosphate buffer. The dialyzed bi-Fabs were then concentrated using ultra-centrifugal filters, and ultimately stored in citrate phosphate buffer at 4 °C for further analysis. Purification using His-Tag removed unfused mono-Fab, and spin columns removed the low molecular weight SpyCatcher and cleaned the impurities. The bi-Fabs were herein named bivalent Fabs mIL3RαΔN-α (mouse IL3Rα SpyCatcherΔN – IL3Rα SpyTag) and mIL3RβΔN-β (mouse IL3Rβ SpyCatcherΔN – IL3Rβ SpyTag), and the bispecific Fab mIL3RβΔN-α (mouse IL3Rβ SpyCatcher ΔN – IL3Rα SpyTag).

3.2.18 Validation of size and purity of synthetic antibodies and Fabs

Full antibodies, mono-Fabs and bi-Fabs were validated for purity and size with an automated electrophoresis system (Agilent 2100 Bioanalyzer System) using a High Sensitivity Protein 250 kit as per manufacturer's instructions. The run employed reductive conditions and the resulting band sizes were expected (~25kDa for individual light chains, ~63kDa for heavy chains connected by SpyCatcher–SpyTag).

3.2.19 Kinetics characterization of antibodies and Fabs by Biolayer Interferometry

Biolayer interferometry (BLI) platform was used for real-time measurement of antibody binding to the appropriate biosensor tip as a wavelength shift in nm. The binding between a ligand immobilized on the biosensor tip surface and an analyte in solution creates an increase in optical thickness at the biosensor tip, which results in a wavelength shift, Δλ. Evidently, association or dissociation of molecules from the biosensor shits the interference pattern and changes the wavelength and generates a response profile on the system. The wavelength shift is a direct measure of the change in thickness of the biological layer. We precisely monitored the binding specificity, association and dissociation rates, and accurately measured the concentration of the antibodies using Octet® BLI platform (FortéBio Inc). The analysis was performed at 30 °C with a stirring speed at 1000 RPM in a tilted-bottom 384-well plates (FortéBio Inc)

containing 80 μL of solution. PBS buffer (pH 7.0) was used to dilute analytes and to wash the sensors.

In order to measure the concentration of antibodies, purified antibody was loaded on protein A biosensor and compared to titration series of BSA. The results were compared to BCA protein assay kit to reassure the accuracy.

3.2.19.1 **Kinetic characterization of monoclonal antibodies**

Kinetic characterization of purified antibodies was performed by immobilization of 20 ug/mL of antibody on Anti-human Fab-CH1 2nd Generation biosensors for 30 – 180 seconds (depending on the binding rate of antibody). The biosensors were then washed by PBS and dipped into titration series of the target protein (antigen) at 0, 125, 250, and 1000 nM to associate to the immobilized antibody. The biosensors were then placed into PBS and the dissociation rates were monitored until the wavelength shift was stable. The generated binding profile was analyzed by global curve-fitting software (version 7.1- FortéBio,) for affinity measurement parameters, thereby K_a (association), K_d (dissociation), and K_D.

3.2.19.2 **Kinetic characterization of mono-Fabs and bi-Fabs**

Kinetic characterization of purified mono- or bi-Fabs was performed by immobilization of recombinant target proteins (mouse IL3Rα–Fc Chimera or recombinant mouse IL3Rβ–Fc Chimera) onto Anti-human IgG Fc biosensors at serial titration of 0, 125, 250, 500, and 1000nm. Following by a PBS wash, Fabs were associated against the target antigen for 20-60 seconds, depending on the binding profile of various fabs. The dissociation rates were monitored in PBS until the wavelength shift was stable. The generated binding profile was analyzed by global curve-fitting software (version 7.1- FortéBio,) for affinity measurement parameters, thereby K_a (association), K_d (dissociation), and K_D.

3.3. REAGENTS AND SUPPLIERS FOR *IN VITRO* AND *IN VIVO* ASSAYS IN MAMMALIAN CELLS

Table 3.6 Reagents and suppliers for *in vitro* and *in vivo* assay

Reagent	Supplier
12-, 24, 48-, 96-well flat bottom plates	ThermoFisher Scienctific
293fectin™	Invitrogen
Annexin V APC	BD Biosciences
Annexin V FITC	BD Biosciences
10X Binding Buffer 0.1 (M HEPES, pH 7.4; 1.4 M NaCl; 25 mM CaCl) for Annexin V staining)	BD Biosciences
Bovine Serum Albumin (BSA)	ThermoFisher Scienctific
G418, Geneticin®	ThermoFisher Scienctific
Gibco™ Fetal Bovine Serum, ultra-low IgG, US Origin	ThermoFisher Scienctific
Gibco™ Penicillin-Streptomycin (10,000 U/mL)	ThermoFisher Scienctific
Gibco™ RPMI (Roswell Park Memorial Institute Medium) 1640	ThermoFisher Scienctific
Gibco™DMEM (Dulbecco's Modified Eagle Medium), High glucose	ThermoFisher Scienctific
Gibco™Trypsin-EDTA (0.25%), Phenol red	ThermoFisher Scienctific
Goat anti-human IgG (H+L) secondary Alexa Fluor 546 / FITC / PE antibody	ThermoFisher Scientific
Goat anti-human IL3Rα antibody	R&D Systems
Goat anti-human IL3Rβ antibody	R&D Systems
Hygromycin	ThermoFisher Scienctific
Imatinib (Gleevec ®)	
MethoCult™ GF M3434 (Methylcellulose-based medium with recombinant cytokines (including EPO) for mouse cells)	Stem cell Technologies
MTT[(3-(4,5-Dimethylthiazol-2-yl)-2,5-Diphenyltetrazolium Bromide)]	Sigma Aldrich
Phosphate Buffered Saline (PBS), 10X powder pH 7.4	ThermoFisher Scienctific
Recombinant mouse IL3 cytokine protein (rmIL3)	R&D Systems
Sodium dodecyl sulfate (SDS)	ThermoFisher Scienctific

Sytox blue dead cell DNA dye	ThermoFisher Scienctific
Tissue culture flasks 25, 75, and 175 cm^2	ThermoFisher Scienctific
Trypan blue solution, 0.4%	ThermoFisher Scienctific
Vacuum filter 0.45nm	ThermoFisher Scienctific
Mini-protein TGX gels	#456-1084 BioRad
Nitrocellulose membrane	Amersham, GE Healthcare Life Sciences
Bovine Serum Albumin (BSA)	#9048-46-8 Sigma Aldrich
Phospho-Stat5 (Tyr694) (C11C5) Rabbit mAb	#9359 Cell Signaling Technologies
Phospho-Stat5 (Tyr694) (14H2) Mouse mAb	#9356 Cell Signaling Technologies
Phospho-Jak2 (Tyr1007/1008) Antibody	#3771 Cell Signaling Technologies
α-Tubulin (DM1A) Mouse mAb	#3873 Cell Signaling Technologies
GAPDH D16H11 XP® Rabbit mAb	#5174 Cell Signaling Technologies
IRDye® 800 CW Goat anti-mouse or rabbit IgG (H+L) antibody, 0.1 mg	Li-COR Biosciences
IRDye® 680 CW Goat anti-mouse or rabbit IgG (H+L0, 0.1 mg	Li-COR Biosciences

Table 3.7 Mammalian cell lines and mouse strains for *in vitro* and *in vivo* assay

Cell line / Mouse strain	Specifications	Supplier
Craig Jordan's mouse BC-CML cell line (CJ)	Mouse HSCs retrovially transfected with BCR-ABL and *NUP98/HOAXA9*	A gift from Dr. Craig Jordan laboratory(Neering et al., 2007)
TONB210	Murine CML cell line	ATCC®
KU812	Human CML cell line	ATCC®
KCL22	Human CML cell line	ATCC®
HEK293T	Human embryonic kidney cell line	ATCC®
Free style™ 293-F	A variant of 293 cell line (kidney embryonic cell)	ThermoFisher Scientific
Exp293F	A variant of 293 cell line (kidney embryonic cell)	ThermoFisher Scientiffic
C57BL/6J mice	#000664 – 6 to 8 weeks old female	The Jackson Laboratory

Table 3.8 Reagents set up for Signaling assays

Reagents	Reagent setup
Blocking Buffer	TBST, 7% BSA
Lysis buffer	0.1M EDTA, 0.3M Tris, 0.1M NaCL, 6mM PMSF, and 3 mM Sodium ortho-vandate
Primary Antibody Dilution Buffer	1X TBST
Running buffer	Running buffer: 25 mM Tris, 192 mM glycine, 0.1% SDS, pH 8.3
Sample buffer	Sample buffer: 62.5 mM Tris-HCl, pH 6.8, 2% SDS, 25% glycerol, 0.01% bromophenol blue
Secondary antibodies	IRDye® 680RD or IRDye® 800CW Goat anti-mouse IgG (H + L): # P/N926-68070 and #P/N926-32210 LI-COR, respectively
Secondary antibody dilution buffer	1X TBST, 5% BSA
TBS	50mM Tris-HCl (6.05gr), 150mM NaCl (8.76 gr), up to 1L ddH2o, pH 7.5 up
TBST or washing buffer	Tris Buffered Saline (TBS), 0.01% Tween® 20
Transfer Buffer	100 ml 10X running buffer, 200 ml methanol, 700 ml dH2O, mix.

3.4. Genaral procotols for *in vitro* and *in vivo* assays in mammalian cells

3.4.1 IL3 Receptor cloning

3.4.1.1 **pcDNA–IL3Rα**

The human IL3Rα coding sequence was ordered from OpenBiosystems (MHS1010-7507705). It was received as a clone in plasmid pCMV-SPORT6, which was used as a template to amplify the entire IL3Rα coding DNA sequence with IL3Rα forward and IL3Rα reverse primers (see Table 3.5). These primers contained annealing regions as well as an additional 5' "CACC" required for cloning into pcDNA/D-TOPO (see plasmid map), and a stop codon "TGA" on the 3' end. An 1138 bp amplicon corresponding to a full-length IL3Rα was cleaned and used to clone into the pcDNA/D-TOPO mammalian expression vector according to manufacturer instructions. Sanger sequencing was performed to confirm the correct sequence.

3.4.1.2 **pCMV1-IL3Rβ**

The human IL3R β coding sequence was ordered from SinoBiological as a pCMV1-IL3Rβ mammalian expression clone.

3.4.2 Receptor over-expression on mammalian cell lines

In order to evaluate the binding efficacy of the antibody / antibody fragments to the cell surface receptors, we generated Free style293F^{TM} cell over-expressing human IL3Rα or IL3Rβ (Broughton et al., 2014). 293fectin^{TM} was used to transfect the pcDNA–IL3Rα or pcDNA–IL3Rβ to Free style 293F^{TM} human embryonic kidney cells as per manufacturer's protocol. Briefly, adherent cell were plated 1-2 days prior to transfection at a density of 1-2 x 10^6 cells in 10 cm culture plates in high glucose DEMM with 10% FBS, in order to reach 90% cell confluence for the transfection. On the day of transfection, fresh culture medium (DMEM, high glucose) without FBS was added to the cells 6-8 hours prior to transfection. In order to make DNA-293fectin transfection complex, 5-10 ug of DNA in 250 µL of Opti-MEM® was mixed with 10-15 µL of

293fectin in 250 µL of Opti-MEM® and the complex was incubated for 20-30 minutes. DNA-293fectin complex was gently added to the cells and incubated at 37 °C with 8% CO2 for 72 hours. The appropriate antibiotic was then added to select for the transfected cells. G418 was used at a concentration of 1000 µg / mL for 293F cell over-expressing hIL3Rα, and Hygromycin was used at a concentration of 100 µg / mL for 293F cell over-expressing hIL3Rβ.

3.4.3 Characteristics of "CJ" murine CML cells

Neering et al developed a murine CML cell line by retroviral transfection of BCR-ABL–GFP and Nup98 / HOXA9–YFP translocation products on normal murine HSC cells. BCR-ABL and Nup98 / HOXA9 translocations are two genetic abnormalities associated with aberrant hematopoietic cellular differentiation in CML patients (See details in introduction) (Ahuja et al., 1989; Neering et al., 2007). This CML model, referred to as Craig Jordan (CJ) cells, was used for the *in vitro* and *in vivo* assays for this project. This model co-expresses both BCR-ABL and Nup98 / HOXA9 translocation products that identifies a distinct population of leukemic stem cells with aberrant immunotypes of lin^{-}, $Kit^{+/-}$, Sca^{+}, $CD34^{+}$, and $CD150^{-}$ (T. Ito et al., 2010; Neering et al., 2007). The green and yellow fluorescent protein labels on BCR–ABL and NUP98 / HOXA9, respectively, allowed histological analysis, imaging, and detection of leukemic stem cells by Flow cytometry. CJ cells are capable of initiating leukemogenesis, homing in the bone marrow, and development of blast crisis in recipient mice when injected intravenously. Hence, CJ cells provide a platform to demonstrate the effect of targeted antibody therapies and imatinib on leukemic stem cells viability, proliferation, and self-renewal *in vitro* and disease latency *in vivo* (Neering et al., 2007).

3.4.4 Cell surface receptor binding of antibodies and Fabs

In order to analyze the binding efficacy of antibody / Fab to cell surface receptors, 1 ug of antibody or Fab was incubated with the mammalian cells (at a final concentration of 10 µg / mL) at room temperature for 30 minutes. The cells were then washed twice with PBS buffer and labeled with a secondary fluorescence-labeled goat anti-human IgG (H+L) antibody (See Table 3.6) for 30 min at room temperature. The cells were then

washed twice with PBS and antibody / Fab binding to the cell surface receptor was analyzed by flow cytometry (MACSQuant® VYB; Miltenyi Biotec). Cell lines used for this assay were 293F–human IL3Rα or 293F– human IL3Rβ, CJ (murine CML cell line), human CML cell lines such as KU812, KCL-22, JURL-MK1.

3.4.5 *In vitro* functional assays on murine CML cell line

In order to determine the effect of synthetic antibodies or antibody fragments on IL3–mediated imatinib resistance, multiple functional assays were performed *in vitro*. Prior to treatment, CJ cells were cultured in medium, containing RPMI 1640 supplemented with 20% fetal bovine serum (FBS), to reach cell viability of $\geq$ 95% within 2-3 passages. The cells were then transferred to fresh RPMI 1640 with 20% FBS to proceed with the treatments. CJ cells received consecutive treatment of antibody or Fab (10 μg / mL), 10 ng / mL recombinant mouse IL3 (rmIL3), and 1uM imatinib every 3 hours. The treated cells were incubated at 37 °C with 5% CO_2 for 48 hours. The final cell concentration was 5 x 10^5 cells / mL.

For Fab experiments, a common optimal treatment condition was determined; CJ cells (5 x 10^5 cells / mL) were incubated with 50 nM of bi–Fab for 48 hours at 37 °C. After 48 hours, the cells were analyzed for viability, apoptosis, or colony formation.

3.4.5.1 *In vitro* cell survival and proliferation assays

To determine the viability of CJ cells, treated as indicated, cells were counted by Countess II FL Automated Cell Counter (ThermoFisher) using Trypan blue cell exclusion dye. All the assays were done in triplicates.

In addition, MTT assay was performed in triplicates to determine cell viability and proliferation following treatments. Briefly, at 48 h ours after indicated treatment of cells, MTT (3-(4,5-Dimethylthiazol-2-yl)-2,5- Diphenyltetrazolium Bromide)) was added (10 μL or 1:10 v/v) to be reduced to purple formazan in live cells. Next, 10% SDS / HCl (Sodium dodecyl sulphate in diluted hydrochloric acid) was added (at 1:1 v/v ratio) to dissolve the insoluble purple formazan. The absorbance (nm) was measured using SpectraMax 340PC384 microplate reader at wavelengths 570 and 650 nm.

3.4.5.2 **Apoptosis (programmed cell death) assay**

CML cells, treated as indicated, were incubated at 37 °C with 5% CO_2 for 48 hours. Cells were washed with cold PBS and resuspended in 100 µL of 1x binding buffer (BD Bioseinces) at concentration of 1 x 10^6 cells / mL. The cells were labeled with 5 µL of Annexin V–APC apoptosis dye (Annexin conjugated with Allophycocyanin) and 1 µL of SYTOX™ blue dead-cell nucleic acid stain for 15 minutes in the dark. 400 µL of 1x binding buffer added to each tube and the cells were analyzed by flow cytometry (MACSQuant® VYB; Miltenyi Biotec) within an hour. Double-negative populations defined as viable cells. Early apoptotic cells were identified with Annexin V APC positive population excited with blue laser (561nm) and no Sytox blue staining. The cells in late apoptosis or already dead were defined by both Annexin V apoptosis and Sytox blue excited by violet laser (excited with 405nm) and blue laser (excited with 561nm).

3.4.5.3 **Colony forming unit (CFU) assay**

Mouse blast crisis CML cells (CJ) were treated as indicated and after 48 hours of treatment, 2000 cell / mL from each treatment were plated in semi-solid complete methylcellulose medium (Methocult™, containing mSCF, rmIL3, rhIL6, rh EPO, rh insulin, human transferrin, GFM3434 from StemCell Technologies). The cells were cultured in methylcellulose for 10 – 14 days in humidified conditions supplied with 5% CO_2 to allow colony formation, and colonies of more than 40 cells were counted (T. Ito et al., 2010). All treatment conditions were plated in triplicates. The number of colonies counted in CFU assay provid information about frequency of individual progenitor cells (Conly forming units or CFUs) and their potential to proliferate and differentiate after indicated treatments.

3.4.6 Cytokine signaling assays

Phosphorylation of signaling proteins was detected by immunoblots. CJ were washed and rendered quiescent by serum deprivation 3 – 4 hours prior to treatments. Cells were incubated

with antibody or Fabs (0 – 400 nM) for 20 min on ice. Next, cells were stimulated with 1 nM IL-3 for 10 min at 37 °C, as described by Jin *et al.* (Jin et al., 2009), and the treated cells were then immediately lysed in lysis buffer (See Table 3.8). The cell lysates were then resolved using SDS-PAGE, by adding 1:1 sample buffer. The lysates were heated at 95 °C for 8 minutes and subjected to immunoblotting. The samples were then transferred to nitrocellulose membrane, blocked and incubated with the primary antibodies at 4 °C overnight according to manufacturer's instructions. The proteins were visualized using fluorescent-labeled secondary antibody and images were acquired with LI-COR Odyssey® CLx imaging system (LI-COR Biosciences). Carestream software was used to perform the densitometry analysis. Anti α–Tubulin or Glyceraldehyde 3 phosphate dehydrogenase (GAPDH) monoclonal antibody was used as a loading control to confirm the purity of the nuclear fractions.

3.4.7 Engraftment assays

CJ cells, treated with antibody or Fab as indicated, were incubated for 48 hours at 37 °C and 5% CO_2. Forty-eight hours after treatment, the cells were washed with PBS. The cells in the control group (No treatment or control non-specific Ig) were counted and the dilution ratio to make a cell suspension with 1 x 10^6 cell / mL was calculated. Cells from other treatment groups were diluted in PBS using the same dilution ratio as that of the control groups. Sub-lethally irradiated C57BL/6J mice (600 RAD, XRAD 225, Precision X-Ray Inc.) received 100 µL of each diluted cell suspension via tail vein transplantation. Five mice were considered for each treatment group. The mice were monitored for symptoms of leukemia and mouse survival / death was analyzed by Kaplan meier survival curve.

3.4.8 Statistical analysis

Graphpad prism software was used for statistical analysis. Data were represented by the mean ± S.D. (Standard Deviation) based on at least three independent experiments. A P-value of less than 0.05 was considered significant (*$P < 0.05$, **$P < 0.001$).

4. CHAPTER 4. RESULTS

4.1. Growth factor–induced suppression of imatinib activity

4.1.1 Bone marrow stromal cell factor (BMSF) conditioned media suppresses imatinib activity

In order to gain insight into mechanisms of innate imatinib resistance in CML cells, we first investigated effects of secreted bone marrow stromal cell factors (BMSF) on imatinib suppression. CML cells (K562 human CML cell line) were serum–starved and then incubated with medium combined with BMSF conditioned media in the presence or absence of imatinib. BMSF-conditioned media reversed cytotoxic effects of imatinib on K562 cell viability as assessed Trypan blue exclusion assay. We observed a significant increase in cell viability in the presence of 50% BMSF at various concentration of imatinib ranging from 0.5 to 2 μM (Figure 4.1A).

We also stained K562 cells with Annexin V–PE and 7AAD to determine how BMSF-conditioned media alter levels of apoptosis and cell death, respectively. The control treatment group showed negligible apoptosis and cell death (Figure 4.1B top panel), and imatinib caused a significant increase in cell apoptosis as determined by a shift in Annexin V PE positive cells (Figure 4.1B middle panel). Treatment with 50% BMSF-conditioned media decreased the apoptotic cell sub–population (Figure 4.1B bottom panel). To see the effect of BMSF-conditioned media on the progenitor cell population of K562 cells, we used a colony formation assay. K562 cells were treated as described above and 300 cells were seeded in cytokine–enriched methylcellulose medium (MethoCult^{TM} GF; a medium formulated to support the growth of primitive hematopoietic cells with Interleukin (IL)–3, IL–6, Stem cell factor (SCF), and erythropoietin (EPO)) and incubated at 37ºC for 7 – 10 days. BMSF conditioned media + imatinib treated cells showed a significant increase in colony number compared to imatinib–treated cells (Figure 4.1C). In summary, BMSF-conditioned media reversed effects of imatinib by increasing cell viability and colony formation and by decreasing apoptosis.

4.1.2 IL3–induced suppression of the imatinib activity

The ability of BMSFs to reverse the effects of imatinib suggested that growth factors, cytokines, or chemokines in the BMSF-conditioned media were responsible for rescuing CML cells from imatinib activity. To test this, we treated the K562 human CML cell line with imatinib in the presence or absence of various recombinant human cytokines. Viability assay showed that IL3, Granulocyte macrophage–Colony stimulating factor (GM–CSF), and Granulocyte–Colony stimulating factor (G–CSF) desensitized K562 cells to imatinib and lead to significantly lower cell death compared to imatinib treatment alone (Figure 4.2).

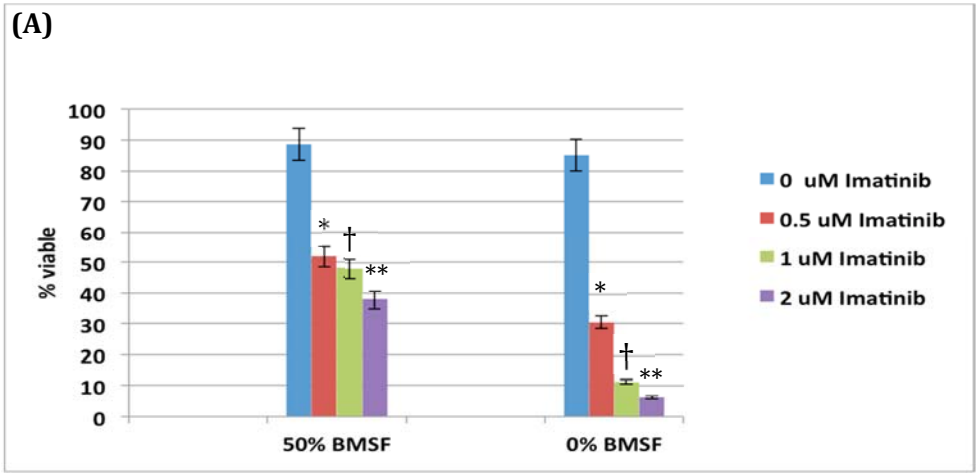
(A)
% viable
100
90
80
70
60
50
40
30
20
10
0
50% BMSF
0% BMSF
0 uM Imatinib
0.5 uM Imatinib
1 uM Imatinib
2 uM Imatinib

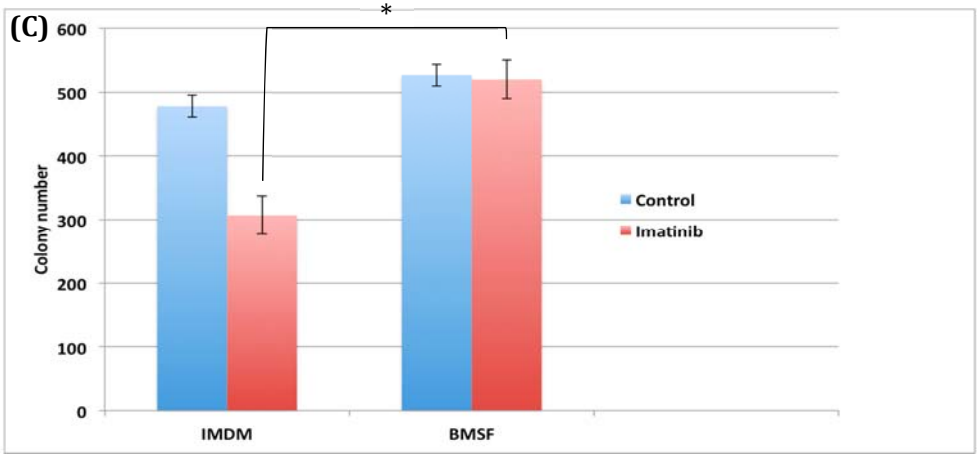
(C)
Colony number
600
500
400
300
200
100
0
IMDM
BMSF
Control
Imatinib

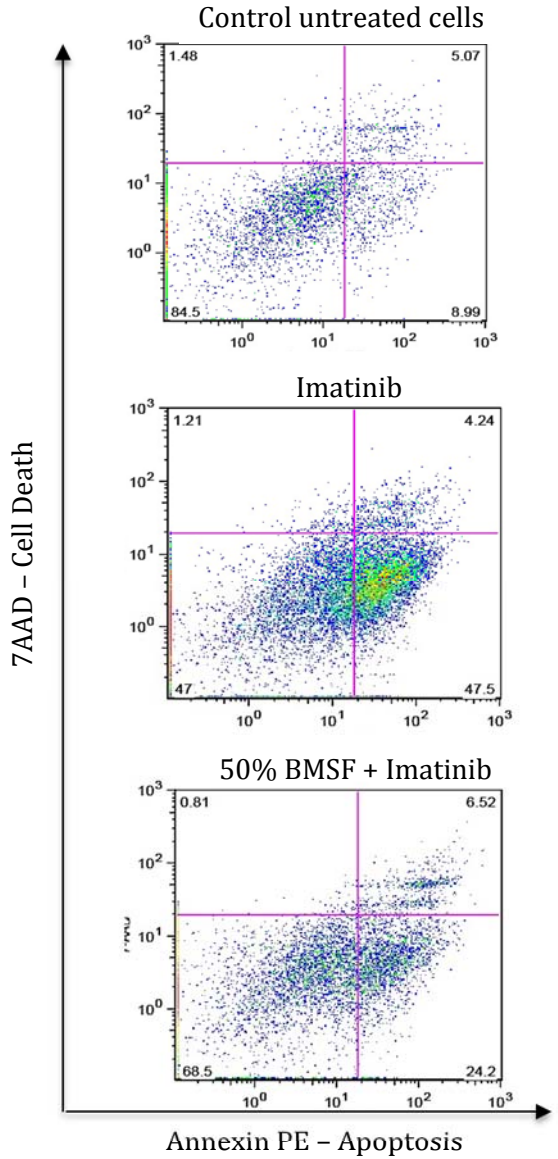
(B)
Control untreated cells
1.48
5.07
84.5
8.99
Imatinib
1.21
4.24
47
47.5
50% BMSF + Imatinib
0.81
6.52
68.5
24.2
7AAD – Cell Death
Annexin PE – Apoptosis

Figure 4.1. Suppression of Imatinib activity by bone marrow stromal cell secreted factors (BMSF) on CML cells *in vitro*. (A) Viability assay. Serum–starved K562 human CML cells were cultured in medium combined with BMSF-conditioned media ranging 0% – 50% in the presence and absence of 0 – 2 μM of imatinib for 72 hours. Cell viability was assessed by the trypan blue exclusion assay. Bar graphs represent the percentage of CML cell survival at various concentrations of imatinib; $*P < 0.0001$, $\dagger P < 0.0001$, $**P < 0.0001$; Y–axis numbers denote the percentage cell viability and X–axis indicates various treatments. (B) Annexin V Apoptosis assay. Cells stained with Annexin V–PE and 7AAD to determine apoptosis and cell death, respectively. Top panel: Control (No treatment) group; Middle panel: imatinib treatment; bottom panel: imatinib + 50% BMSF-conditioned media. Y–axis indicates 7–AAD staining for cell death and X–axis denotes Annexin V PE staining of apoptotic cells. (C) Colony formation **assay**. CML cells treated with imatinib in the presence or absence of BMSF. After 72 hours of treatment, cells were washed and 300 cells were seeded in cytokine–enriched methylcellulose for 7 – 10 days ($*P < 0.0001$). Bar graphs are representative of colony number quantification by optical microscopy; Y–axis numbers denote the number of colonies and X–axis indicates various treatments. Error Bars represent Mean ± SD; Significant difference between groups were determined using one-way ANOVA followed by Tukey *post hoc* test. IMDM: Iscove's Modified Dulbecco Medium; μM, micro–Molar; PE, Phycoerythrin; 7–AAD: 7–Aminoactinomycin D.

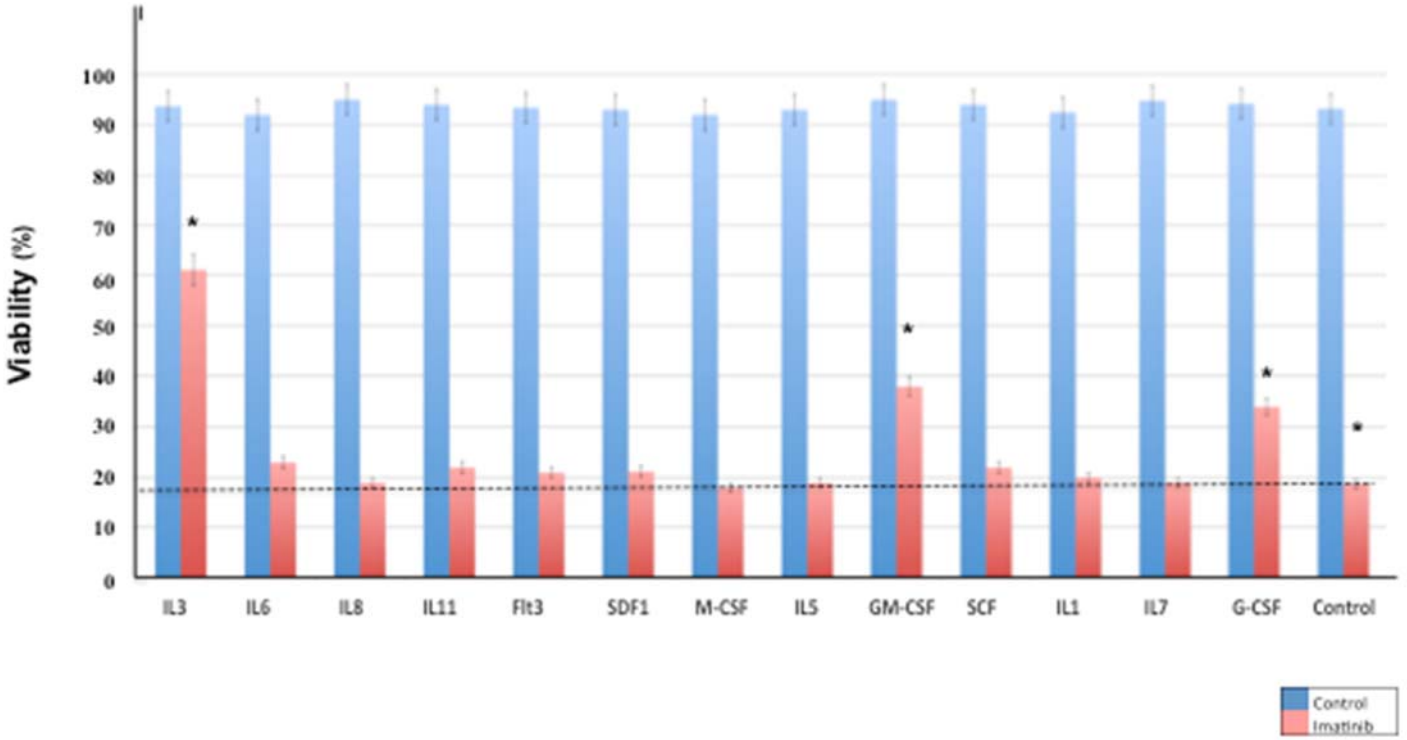

Figure 4.2. Cytokine–induced survival of CML cells. Cell survival analysis of K562 cells treated with imatinib in the presence or absence of various recombinant human cytokines for 48 hours. Red bars represent the survival of cells treated with imatinib in the presence or absence of various cytokines. Blue bars indicate the cell survival with no treatment. Bars represent the mean cell viability in triplicate; Error Bars represent Mean $\pm$ SD; *$P < 0.0001$. Significant differences between groups were determined using one-way ANOVA followed by Tukey *post hoc* test. Y–axis numbers denote the number of percentage of viable cells and X–axis indicates various treatments.

4.2. Generation of novel synthetic human antibodies against murine IL3R–α and IL3R–β using phage display

We used IL3Rα and IL3Rβ as our target proteins in solid phase phage display selections to screen for antigen binding fragments (Fabs) that bound each subunit of IL3 receptor independently.

4.2.1 Primary phage display selections to enrich for antigen–binding fragments

Phage Fab library F (Rajan & Sidhu, 2012) was used in phage display selections against purified mouse IL3Rα and IL3Rβ. Library F is well characterized with a diversity of over 10^{10} Fabs and has been used in phage display to successfully generate antigen–binding antibody fragments against EGFR receptor (Sachdev S Sidhu et al., 2004). A solid-phase panning approach was used whereby targets were immobilized by adsorption to an immunoplate and incubated with the phage library or phage amplified from the previous round of panning. Following each round of selection the enrichment of target binding phage was determined in order to monitor the selection process (Figure 1.8).

Our selections were complete after four rounds as we observed very strong enrichment of 2500– and 3500–fold against mouse IL3Rα and IL3Rβ targets, respectively. No enrichment at the first round of selection was expected since the number of binders in the naïve library was sufficiently low compared to the background. The resulting phage pools collected at the end of final selections contained phage Fabs enriched for members that bound to IL3Rα or IL3Rβ subunits of IL3R. Phage pools underwent next generation sequencing (NGS) to rank–order the phage clones based on their sequence frequency.

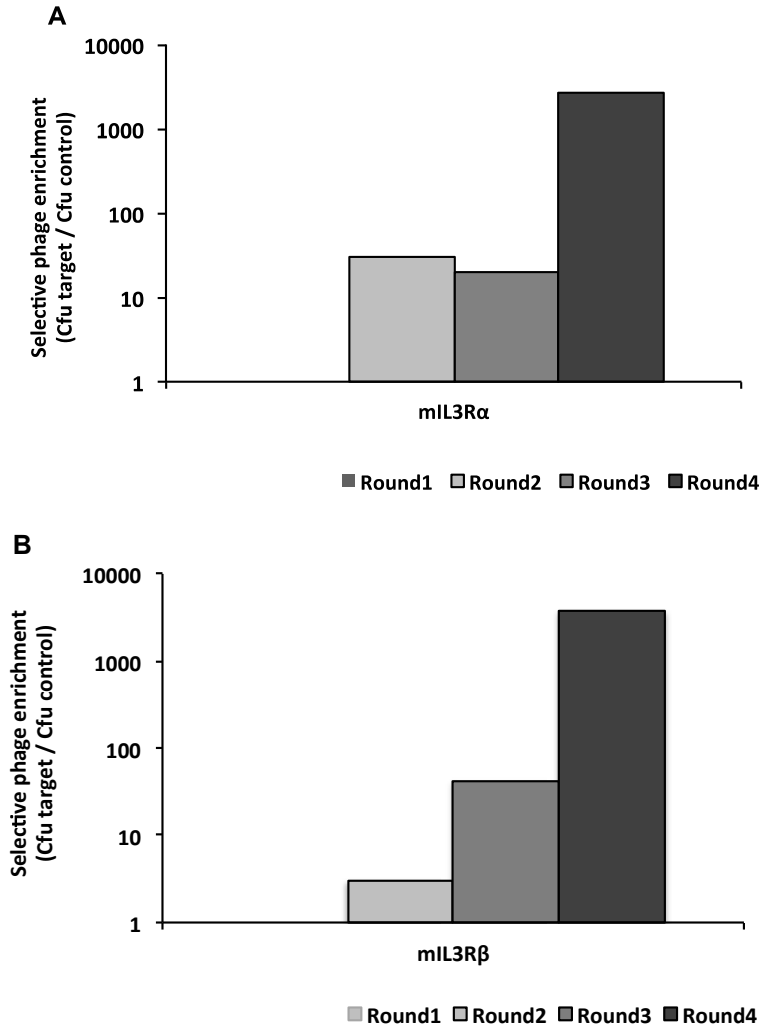

Figure 4.3. Selection of phage-displayed Fabs. Libraries of antigen–binding fragments (Fabs) displayed on the surface of phage are retained by immobilized Fc–fused target and amplified by infection of an *E. coli* host. The amplified pool is used for additional rounds of selection to enrich for a phage population that is dominated by IL3R–α or IL3R–β binding clones. Phage enrichment is calculated by titering the number of phage binding the target (represented by Cfu) divided by the number of phage binding the corresponding negative control target (BSA), and is shown for selections against (A) recombinant mouse IL3 receptor–α (mIL3Rα) and (B) recombinant mouse IL3 receptor–β (mIL3Rβ). Cfu: Colony forming units.

4.2.2. Identification of Fab sequences within enriched phage pools

We used Ion Torrent NGS and Sanger single–clone DNA sequencing in order to identify and recover the most abundant Fab clones from enriched phage pools after four rounds of selection.

4.2.2.1 Ion Torrent NGS

Since NGS makes it possible to perform DNA sequencing of large populations of templates at the same time, we used Ion Torrent NGS to determine the frequency of unique CDRH3 sequences in the repertoire of Fabs in the phage pool from the final round of panning. As compared with single-clone Sanger DNA sequencing, we reasoned that the NGS data would allow us to rank–order potential Fabs based on their relative frequency and also provide sequence convergence information on Fab CDRH3s.

The phage pool was amplified with primers flanking CDRH3 and these templates were sequenced using the Ion Torrent NGS platform. Raw nucleotide sequences were merged, aligned, and trimmed to remove low quality short sequences, frame shifts, and premature stop codons. We rank-ordered CDRH3 sequences by frequency to determine the most abundant Fabs.

The most abundant 20 – 30 CDRH3 sequences obtained from the enriched Fab phage pool after four rounds of selection against Fc–fused mouse IL3R–α or –β targets, respectively are shown Table 4.1 and 4.3. In our initial NGS analysis, we focused on CDRH3 because it is the most diverse CDR in Library F and for its importance in antibody diversity and specificity (Xu & Davis, 2000).

The DNA sequence encoding the CDRH3 "TVRGSKKPYFSGWAM" was the most abundant CDRH3 sequence found in the mIL3R–α phage Fab pool with a frequency of 18.4% (Table 4.1). This sequence encodes the CDRH3 for the anti–maltose binding protein (anti–MBP) library phagemid template and therefore was excluded from the analysis. The anti–MBP encoding sequence was not frequently observed in the mIL3R-β Fab phage pool after the fourth round of selection.

4.2.2.2 Sanger DNA sequencing

Sanger DNA sequencing was used to identify corresponding CDRL3, H1, and H2 sequences for abundant Fabs. To accomplish this, *E. coli* was infected with phage from the round four phage pool to isolate single–clone colonies. Twenty to thirty single colonies were arbitrarily picked and sequenced using the Sanger method with primers that amplified a region of DNA encoding all CDRs randomized in the library. A list of unique CDR sequences found by single clone sequencing from the primary selections against mIL3Rα or mIL3Rβ target, respectively is shown in Table 4.2 and Table 4.4. Two clones corresponding to the most abundant CDRH3, provided by NGS data were selected and recovered for further investigations.

mIL3R–α phage pool (Round 4)	
CDRH3 sequence	% Frequency
ARTVRGSKKPYFSGWAMDYWGQG	18.4%
ARYSAYYGAVALDYWGQG	15.4%
ARYWWYGLDYWGQG	14.5%
ARGVWSYAGWSSAVGFDYQGQG	10.8%
ARYYYSYSVSWSFSGLDYWGQG	8.2%
ARGVYYYYWSGYYSGVYGLDYWGQG	4.4%
ARHPWPWYGLDYWGQG	3.5%
ARYWYPGSYSYVWAIDYWGQG	3.0%
ARTVRGSKKPYFSGWLWTDWGQG	2.5%
ARAPYSWSHGPYWYGYYSGLDYWGQG	1.8%
ARYAPGYYWYGLDYWGQG	1.8%
ARSYPGPWAGAWYGAMDYWGQG	1.4%
ARGWYYPYPGSSSVSGAMDYWGQG	1.3%
ARSSYWGSWSSYPAYVSGGLDYWGQG	1.2%
ARWWSFGYWWHAFDYWGQG	1.2%
ARGWFYWSFVAPSGGGAIDYWGQG	1.1%
ARHHHAFDYWGQG	1.0%
ARYWSWSGAGGSSGMDYWGQG	0.8%
ARFWWPGMDYWGQG	0.5%
ARGGGGYYWYSGLDYWGQG	0.5%
ARYHYGYGLDYWGQG	0.5%
ARAWWGPAPGSAVGHVYGAMDYWGQG	0.4%
ARTVRGSKNRTSLVGLWTDWGQG	0.4%
ARAPSYSGAGGFDYWGQG	0.3%
ARGVYVYGSSYSFVGLDYWGQG	0.3%
ARGYYYGASYGYYYVASAGMDYWGQG	0.3%
ARGSSYSYYSVPYAWPPFHALDYWGQG	0.2%
ARGVYYYYWSGYYSWLFTVWTYWGQG	0.2%

Table 4.1 NGS analysis of CDRH3 sequences from the final round of panning against mIL3Rα. The frequency of CDRH3 sequences from the round four pool of phage was ranked in descending frequency. Highlighted CDRH3 sequences were selected as leads for further experimentation. The CDRH3 domains were aligned based on AR– and –DYWGQG as the framework–CDR junction sequences up and downstream, respectively. Subsequent NGS analysis of CDL3R, CDRH1, and CDRH2 for this mIL3Rα phage pool can be found in Appendix B.

(A)

Clone ID	CDRL3	CDRH1	CDRH2	CDRH3
mIL3Rα-1	SAGLITF	ISYSSM	SIYPSYGYTY	**YSAYYGAVAL**
mIL3Rα-2	WHSSHPI	ISSYYM	SIYPYYGSTY	**GVWSYAGWSSAVGF**
mIL3Rα-3	SFYYYPF	ISYYSI	SISSYYGYTS	TVRGSKKPYFSGWAM*
mIL3Rα-4	AYWSSPF	IYSYYM	SIYSYYGSTS	AWWGPAPGSAVGHVYGAM
mIL3Rα-5	WYSGAPI	ISSYYM	SIYPYYGSTY	GVYYYYWSGYYSGVYGL
mIL3Rα-6	SYPYYPF	ISYYSI	SISSYYGYTS	TVRGSKKPYFSGWAM*
mIL3Rα-7	SYPYYPF	ISYYSI	SISSYYGYTS	TVRGSKKPYFSGWAM*
mIL3Rα-8	SYPYY	ISYYYI	SISSYYGYTS	TVRGSKKPYFSGWAM*
mIL3Rα-9	SFYYYPF	LSYYSI	SISSSYGYTS	TVRGSKKPYFSGWAM*
mIL3RA-10	SYPYYPF	ISYYSI	SISSYYGYTS	TVRGSKKPYFSGWAM*

(B)

	CDRL3	CDRH1	CDRH2	CDRH3
Anti–MBP	SSYSLI	FSSSSI	SISSSYGYTY	TVRGSKKPYFSGWAM

Table 4.2 CDR sequences for single clones randomly selected from the primary phage pool selected against mIL3Rα. (A) Random clones were picked from the fourth round of primary phage display against immobilized mIL3Rα and subjected to Sanger DNA sequencing. Highlighted clones were identified as two of the four most abundant CDRH3s analyzed by NGS. The corresponding CDRL3, CDRH1, and CDRH2 for selected CDRH3 encoding sequences are also shown. Clones containing library template sequences (anti-MBP) are indicated. **(B)** CDR sequences encoded by anti–MBP (anti–Maltose–binding protein) Fab template.

mIL3Rβ phage pool (Round 4)	
CDRH3 sequence	% Frequency
ARSSSGWYGFDYWGQG	49.5%
ARSSWGYYYPYGLDYWGQG	23.6%
ARSGSPSAYSFGALDYWGQG	11.2%
ARTVRGSKKPYFSGWAMDYWGQG	4.7%
ARYGLDYWGQG	1.8%
ARSSSWLYGFDYWGQG	1.1%
ARSSYFGHAIDYWGQG	0.9%
ARWPGAYWYSFGMDYWGQG	0.8%
ARYSYYYAHYGWGYFAGAYALDYWGQG	0.7%
ARSHYWHGMDYWGQG	0.6%
ARSWYYVVGLDYWGQG	0.5%
ARWYGGPYHAGMDYWGQG	0.5%
ARAHASWYWPWVGYHVWYGMDYWGQG	0.4%
ARYGYHSFWAMDYWGQG	0.4%
ARGYYSSGYWYYYGLDYWGQG	0.3%
ARSWPWFGGSYAMDYWGQG	0.3%
ARYSYHYVGGGSYHYWYVYGFDYWGQG	0.3%
ARFWSYSYSYYSYSSYAMDYWGQG	0.2%
ARHGGAYAMDYWGQG	0.2%
ARSWYGGAYVGWSSPAYVAFDYWGQG	0.2%
ARYGMDYWGQG	0.2%
ARYSYGYYFVSGFASSYAFDYWGQG	0.2%
AHSSSGWYGFDYWGQG	0.1%
ARAHASWYWPWVGYHVWYDMDYWGQG	0.1%
ARAPWYSAIDYWGQG	0.1%
ARSCFWLYGFDYWGQG	0.1%
ARSFYYHAFDYWGQG	0.1%
ARSGSPSALLFRCLDYWGQG	0.1%
ARSGSPSAYSFGASDYWGQG	0.1%
ARSGSPSDLLFRCLDYWGQG	0.1%
ARSHYSYHSWAWYYWSGAMDYWGQG	0.1%
ARSSCGWYGFDYWGQG	0.1%

Table 4.3 NGS analysis of CDRH3 sequences from the final round of panning against mIL3Rβ. The frequency of CDRH3 sequences from the round four pool of phage was ranked in descending frequency. Highlighted CDRH3 sequences were selected as leads for further experimentation. CDRH3 domains were aligned based on AR– and –DYWGQG as the framework–CDR junction sequences up and downstream, respectively. Subsequent NGS analysis of CDL3R, CDRH1, and CDRH2 for this mIL3Rβ phage pool can be found in 4.

Clone ID	CDRL3	CDRH1	CDRH2	CDRH3
mIL3Rβ-1	YSYSYYYPI	LSSSSM	SIYSYYSYTS	SSSGWYGF
mIL3Rβ-2	WSYGVPI	IYSSSI	YISPYSSYTY	SSWGYYYPYGL
mIL3Rβ-3	N/A	LSSSSM	SISSYSGYTS	Frame-shift
mIL3Rβ-4	GYAPF	LSYYYM	SIYPSSSYTY	SGSPSAYSFGAL
mIL3Rβ-5	YSYSYYYPI	LSSSYM	SIYSYYSYTS	SSSGWYGF
mIL3Rβ-6	GWVPF	ISSSYI	YIYSYSGYTY	SSYFGHAI
mIL3Rβ-7	*SYGVPI	LYSSSI	SISPYSSYTY	SSWGYYYPYGW
mIL3Rβ-8	N/A	LSSSYM	SIYPSSSYTS	SASGW
mIL3Rβ-9	GYAPF	LSYYYM	SIYPSSSYTY	SGSPSAYSFGAL
mIL3Rβ-10	YSYSYYYPI	LSSSYM	SIYSYYSYTS	SSSGWYGF

Table 4.4 CDR sequences for single clones randomly selected from the primary phage pool raised against mIL3Rβ. Random clones were randomly picked from the fourth round of primary panning against immobilized mIL3Rα and subjected to Sanger DNA sequencing. Highlighted clones were identified as the two most abundant CDRH3s analyzed by NGS. The corresponding CDRL3, CDRH1, and CDRH2 for the selected CDRH3 encoding sequences is also shown. A stop codon is indicated with an asterisk. N/A: Not Applicable; * Stop codon.

4.2.2.3. Selected lead Fabs bind to their targets in phage ELISA

Phage ELISAs were performed to confirm the binding of selected Fabs to their respective targets. Phage from several clones identified by Sanger sequencing were propagated and incubated with mIL3R–Fc chimeras or BSA (negative control) immobilized on immunosorp plates. The Fc domain was used as a control for Fc binding since the IL3R proteins used for selections were Fc chimeras. All phage displaying selected Fabs bound to their cognate target with signals > 5–fold higher than BSA and Fc controls. Moreover, strongest ELISA signals were detected from Fabs bearing the highest CDRH3 frequency by NGS analysis, for both mIL3Rα and mIL3Rβ (Figure 4.4).

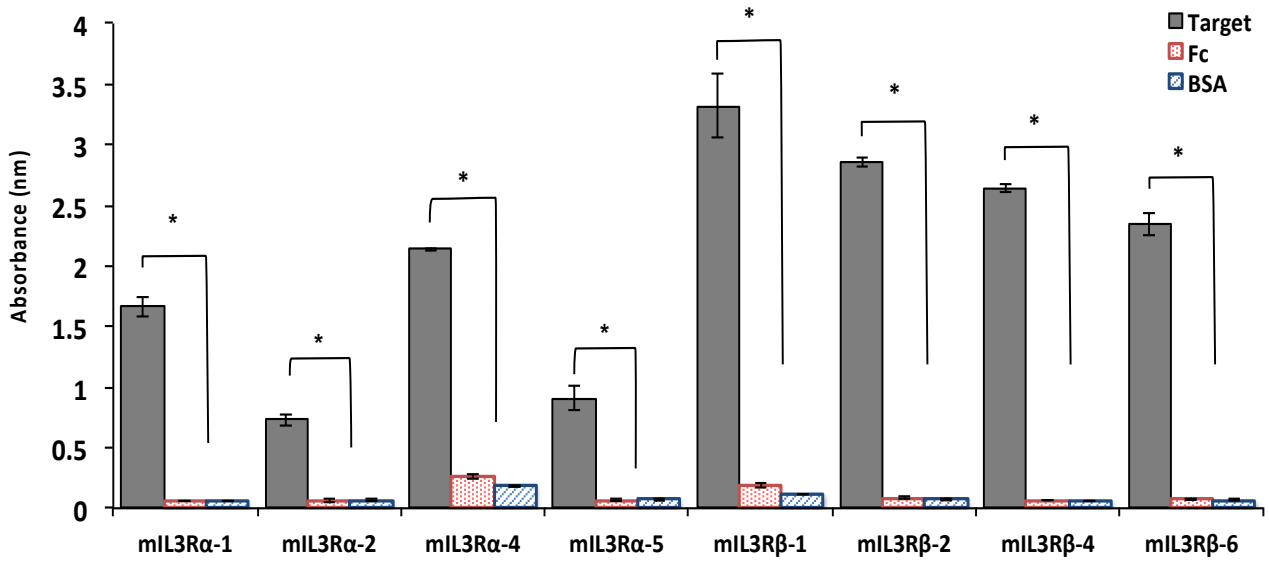

Figure 4.4. Phage clones from the primary selections bind their targets by ELISA. Phage clones recovered from the fourth round of selection were used in an ELISA against immobilized recombinant mIL3Rα or mIL3Rβ Fc chimeras. An irrelevant antigen (BSA) and Fc served as negative controls. Phage Fab binding was detected with peroxidase–conjugated anti–His tag antibody as measured by absorbance at 450nm. Bar graph represents the mean and standard deviation of duplicate experiments; * $P < 0.0001$; BSA: Bovine serum albumin; Fc: Fragment crystallization.

4.2.3. **Affinity maturation of selected Fabs using phage display**

With the goal to achieve the tightest binding antibodies for the purposes of therapy and testing the innate resistance hypothesis, we decided to mutate our lead candidate sequences in order to achieve tighter target binding affinity. To perform "affinity maturation", we created new mutated phage Fab libraries constructed from the soft randomization of CDRL3, CDRH1, CDRH2, and CDRH3 of the top two Fabs from each of the primary mIL3Rα and mIL3Rβ selections. Using software to achieve the desired level of mutagenesis (section 3.2.9), we synthesized oligonucleotides to create new mutated phagemid libraries with soft randomized CDRL3, CDRH1, H2, and H3 using Kunkel mutagenesis. More details on CDR diversification and soft–randomization are denoted in Appendix A. We transformed the Kunkel reaction product (Figure 4.5A) into *E.* coli, determined the number of transformants (> 10^{10} for each library), and amplified the phage library. Based on their respective lead Fabs, mutagenic libraries were labeled *mutated* mIL3Rα–1 (mIL3Rα–1*mut*), *mutated* mIL3Rα–2 (mIL3Rα–2*mut*), *mutated* mIL3Rβ–1 (mIL3Rβ–1*mut*), and *mutated* mIL3R β–2 (mIL3Rβ–2*mut*). Using the same targets and selection protocol as the primary phage display selections, we performed three rounds of panning against each target for secondary selections. We obtained enrichment of over 2500- and 600–fold for the mIL3Rα–1*mut* and mIL3Rα–2*mut* libraries targeting mIL3Rα, respectively. For the mIL3Rβ target, we obtained over 1300- and 250–fold enrichment for mIL3Rβ–1*mut* and mIL3Rβ–2*mut* libraries, respectively (Figure 4.5 B and 4.5 C).

A

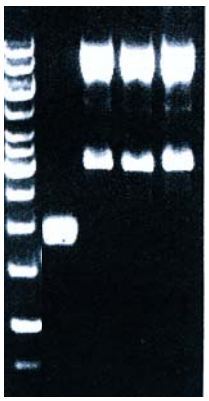

Strand-displaced dsDNA

dsDNA

dU-ssDNA

DNA Ladder

B

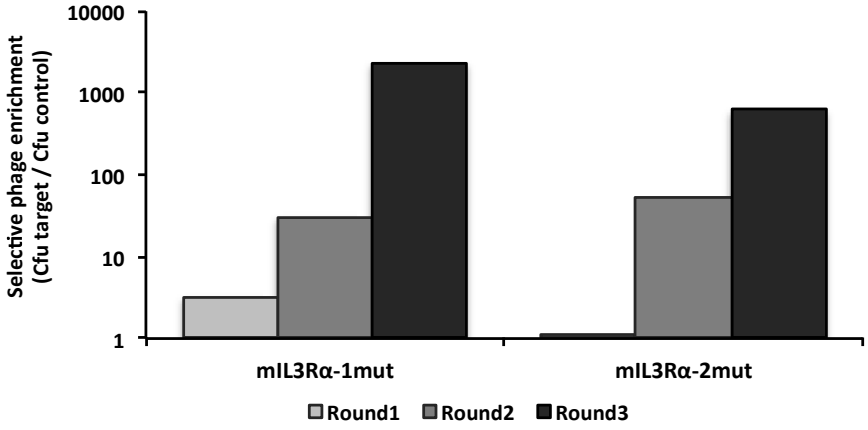

C

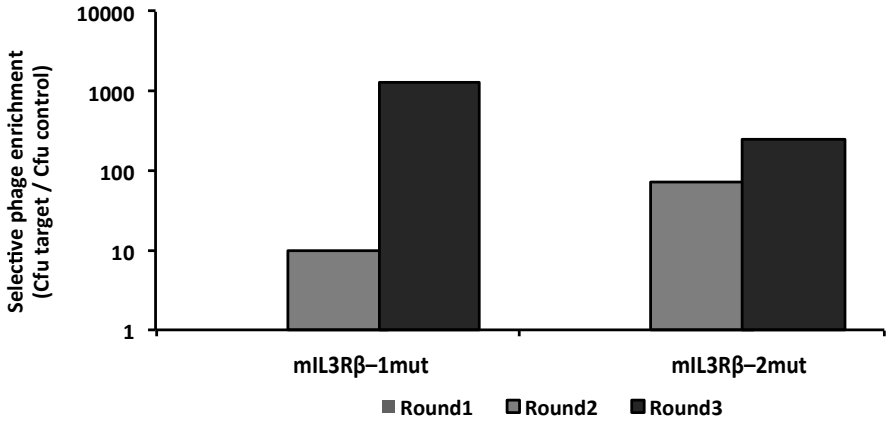

Figure 4.5. Secondary library construction and selection of phage displayed Fabs. (A) Gel electrophoresis to analyze conversion of the ssDNA Kunkel template to covalently closed circular, double–stranded DNA (CCC–dsDNA) for mIL3Rα–1*mut*, mIL3Rα–2*mut*, and mIL3Rβ–1*mut* (left to right). **(B–C)** The secondary phage Fab libraries were panned against immobilized target and amplified by infection of an *E. coli* host. The amplified pool was used for additional rounds of selection to enrich for a phage population that was dominated by IL3 receptor –α or –β binding clones. Phage enrichment was calculated by titreing the number of phage binding the target (represented by Cfu) divided by the number of phage binding the corresponding negative control target (BSA), and was shown for selections against (B) recombinant mouse IL3 receptor α (mIL3Rα) and (C) recombinant mouse IL3 receptor β (mIL3Rβ). The corresponding secondary libraries were indicated on the X-axis. Cfu: Colony forming units.

4.2.4. NGS analysis of the secondary phage display selections

Phage pools from the final round of the secondary selections were sequenced by NGS. The frequency of CDRH3 sequences identified for each selection is shown in Tables 4.5 and 4.6. In all selections, except for the mIL3Rβ–2mut selection, the most frequent CDRH3 was "softly" mutated from the originally isolated Fab. Sanger sequencing of single clones was used to retrieve Fabs containing the most frequently mutated CDRH3 sequence along with identifying the other CDRs for that particular clone. Because we found that particular CDRH3 sequences were matched with different CDRs of varying frequency by NGS analysis (Appendices A.4 through A.7), final clones were selected as summarized below:

- *Fab anti-mIL3Rα–1mut* contained the most abundant mutated CDRH3, CDRL3, and CDRH2. The CDRH1 was identified as the 10th most abundant at 1.8% (Appendix D).
- *Fab anti-mIL3Rα–2mut* contained the most abundant mutated CDRH3, CDRL3, CDRH1, and CDRH2 sequences (Appendix E).
- *Fab anti-mIL3Rβ–1mut* contained the most abundant mutated CDRH3, CDRL3, CDRH1, and CDRH2 sequences (Appendix F).
- *Fab anti-mIL3Rβ–2mut* contained the most abundant mutated CDRH3 sequence and all other CDRs were softly mutated but not among the most frequent.

CDRH3 sequence	Frequency
YTAYYGAVALDYWGQG	**14.8%**
ARYAAYFGPVTLDYWGQG	10.3%
ARYTAYYGTVALDYWGQG	8.1%
ARYSAYYGAVALDYWGQG	7.4%
ARYSAYYGSVALDYWGQG	4.5%
ARHSSYYGAVALDYWGQG	1.8%
ARYSAYYGAVSLDYWGQG	1.8%
ARHSAYYGAVAFDYWGQG	1.6%
ARYSAYYGSIALDYWGQG	1.6%
ARYSGYYGAVALDYWGQG	1.6%
ARYTAYYGPVSLDYWGQG	1.6%
ARYAAYYGAVALDYWGQG	1.3%
ARYSDYYGAVALDYWGQG	1.3%
ARHSAYYGAVDLDYWGQG	1.1%
ARYSAYYGPVALDYWGQG	1.1%
ARHSAYYGTVSLDYWGQG	0.9%
ARHSVYYGSVALDYWGQG	0.9%
ARYSAFYGAAYLDYWGQG	0.9%
ARYSAYYGVVALDYWGQG	0.9%
ARHSAYYGAVSLDYWGQG	0.7%
ARHSAYYGSVSLDYWGQG	0.7%
ARHSTYYGSVALDYWGQG	0.7%
ARYSAFYGFVALDYWGQG	0.7%
ARYSAYFGAVALDYWGQG	0.7%
ARYSAYYGAVSFDYWGQG	0.7%
ARYSAYYGAVVLDYWGQG	0.7%
ARYSGYYGFVAFDYWGQG	0.7%
ARHSAFYGPIALDYWGQG	0.4%

CDRH3 sequence	Frequency
AR **GVWAYSAWSSKIGFDYWGQG**	**24.2%**
AR GIWYNAGLSSTVGFDYWGQG	17.0%
AR GVWSYAGWSSAVGFDYWGQG	13.8%
AR GFWYLAGRSSAVGFDYWGQG	6.9%
AR GFWSYDGWSSAVGFDYWGQG	6.3%
AR GFWSYQGWSLAAGFDYWGQG	3.6%
AR GVWSYADRSPFVGFDYWGQG	2.0%
AR GVWSYAVWSSAVGFDYWGQG	2.0%
AR GVWYYSGWTPTVGFDYWGQG	1.7%
AR GFWSYAGWSSAVGFDYWGQG	1.4%
AR GFWYYTGWTSAVGFDYWGQG	1.0%
AR GIWSYAGLSSVVGFDYWGQG	1.0%
AR GVWSYLDGSSAVGFDYWGQG	0.9%
AR GVWSYSGWSSAVGFDYWGQG	0.9%
AR GVWSSRAISFLVGFDYWGQG	0.8%
AR GFWSYAGWSPAAGLDYWGQG	0.7%
AR GVWFAYAWSFAVGFDYWGQG	0.7%
AR GVWYYAAWAPAVGFDYWGQG	0.7%
AR GIWSYDGWSYAVGFDYWGQG	0.6%
AR GVWSFAGWASAVGFDYWGQG	0.6%
AR GVWYLAGRSSAVGFDYWGQG	0.6%
AR GVWYYTGWSSAIGFDYWGQG	0.5%
AR GIWFYSSWSSAVGFDYWGQG	0.3%
AR GIWSYTGWSFAVGFDYWGQG	0.3%
AR GVWNHGRWYSAVSFDYWGQG	0.3%
AR GVWSYSGRASAVGFDYWGQG	0.3%
AR GVWSYVGSSSAVGFDYWGQG	0.3%
AR GFGIWLVGLLQSVLDYWGQG	0.2%

Table 4.5 NGS analysis of CDRH3 sequences from the final round of secondary selections against mIL3Rα. CDRH3 sequences from the round three pool of phage were ranked in descending frequency. The most frequent mutated CDRH3 sequences from secondary selections (*highlighted yellow*) were selected for future study. The original unmutated CDRH3 sequences from primary selections are highlighted red and blue for mIL3Rα–1 and mIL3Rα–2, respectively. CDRH3 regions were aligned based on AR– and –DYWGQG as the framework–CDR junction sequences up and downstream, respectively. Additional NGS analysis of CDRL3, CDRH1, and CDRH2 for this pool can be found in Appendix B.

mIL3Rβ–1*mut* phage pool (Selection 2: Round3 pool)	
CDRH3	**Frequency**
ARSSSGWYGFDYWGQG	26.7%
ARSSSGRYGFDYWGQG	4.4%
ARSASGWYGFDYWGQG	4.3%
ARSSSGWYGLDYWGQG	4.1%
ARSTSGWYGFDYWGQG	3.4%
ARSSSGWFGFDYWGQG	2.6%
ARSPSGWYGFDYWGQG	2.4%
ARSYSGWYGFDYWGQG	2.3%
ARSFSGWYGFDYWGQG	1.9%
ARSLSGWYGFDYWGQG	1.6%
ARSSSGWYGIDYWGQG	1.4%
ARSSSGFYGFDYWGQG	1.3%
ARSSSGYYGFDYWGQG	1.0%
ARSSSGWHGFDYWGQG	0.8%
ARSSSGWYGYDYWGQG	0.8%
ARSSSGWYGVDYWGQG	0.7%
ARSSSGWNGFDYWGQG	0.7%
ARASSGWYGFDYWGQG	0.7%
ARSISGWYGFDYWGQG	0.7%
ARSASGRYGFDYWGQG	0.6%
ARSFSGRYGFDYWGQG	0.6%
ARSPSGRYGFDYWGQG	0.5%
ARSVSGWYGFDYWGQG	0.5%
ARSLSGRYGFDYWGQG	0.4%
ARSSSGRFGFDYWGQG	0.4%
ARSSSGRNGFDYWGQG	0.4%
ARSSSGRYGLDYWGQG	0.4%
ARSSSGRDGLDYWGQG	0.4%
ARSTSGWYGLDYWGQG	0.4%

mIL3Rβ–2*mut* phage pool (Selection 2: Round3 pool)	
CDRH3	**Frequency**
ARSSWGYYYPYGLDYWGQG	21.60%
ARSSWGYYYPFGLDYWGQG	18.18%
ARTPWGYYYPYGMDYWGQG	15.91%
ARSSWGYYYPYGMDYWGQG	9.44%
ARSAWGYYYPYGLDYWGQG	5.24%
ARSGWGYYYPYGLDYWGQG	4.92%
ARTPWGYYYPYGLDYWGQG	3.75%
ARSTWGYFYPYGLDYWGQG	3.10%
ARSPWGYYYPYGLDYWGQG	1.88%
ARSSWGYYYPHGLDYWGQG	1.81%
ARSSWGFYYPYGLDYWGQG	1.68%
ARSTWGYYYPYGLDYWGQG	1.42%
ARTPWGYYYPFGLDYWGQG	1.23%
ARASWGYYYPYGLDYWGQG	1.10%
ARSGWGYYYPFGLDYWGQG	0.78%
ARSSWGYHYPYGLDYWGQG	0.58%
ARSAWGFYYPYGLDYWGQG	0.52%
ARTPWGYFYPYGLDYWGQG	0.52%
ARSSWGYFYPYGLDYWGQG	0.45%
ARSTWGYCYPYCLDYWGQG	0.45%
ARSPWGYYYPYGMDYWGQG	0.39%
ARTPWGYFYPYGMDYWGQG	0.39%
ARSAWGYYYPYGMDYWGQG	0.32%
ARSTWGYYYPYGMDYWGQG	0.32%
ARTPWGYYYPHGLDYWGQG	0.26%
ARSSWGYYYPYGFDYWGQG	0.19%
ARTSWGYYYPYGLDYWGQG	0.19%
ARSAWGFYYPYGMDYWGQG	0.13%
ARSGWGYYYPYGMDYWGQG	0.13%

Table 4.6 NGS analysis of CDRH3 sequences from the final round of secondary selections against mIL3Rβ. CDRH3 sequences from the round three pool of phage were ranked in descending frequency. The most frequent mutated CDRH3 sequences from secondary selections (*highlighted yellow*) were selected for future study. The original unmutated CDRH3 sequences from the primary selections are highlighted red and blue for mIL3Rβ–1 and mIL3Rβ–2, respectively. The CDRH3 regions were aligned based on AR– and –DYWGQG as the framework–CDR junction sequences up and downstream, respectively. Additional NGS analysis of CDRL3, CDRH1, and CDRH2 for this pool can be found in Appendix C.

4.2.5. **Cloning, expression, and purification of full–length anti–mIL3Rα and anti–mIL3Rβ antibodies**

In order to generate full immunoglobulins (IgGs), V_H and V_L sequences identified in phage display selections were sub–cloned into mammalian cell expression vectors, pFUSEss–CHIg–hG1 and pFUSE2ss–CLIg–hk (InvivoGen), which encode constant regions of human IgG1 heavy and light chains, respectively. This resulted in a two-plasmid expression system that expresses high levels of secreted IgG. Plasmids and inserts used for the Gibson Assembly cloning are shown in Figure 4.6. Correct clones were evaluated for sizing by colony PCR and confirmed with Sanger sequencing.

We expressed IgGs by co–transfecting V_L–pFUSE2ss–CLIg and V_H–pFUSE2ss–CHIg plasmids into *Expi*293 mammalian cells. Secreted IgGs were purified using Protein A affinity chromatography of culture supernatants after five days. Upon generation and purification of IgGs, two IgGs showed extremely low yield. Since low yield was a major drawback cost–wise and could limit use in our mouse model, the anti–mIL3Rβ–2, and anti–mIL3Rβ–2*mut* antibodies were not pursued beyond initial validation and characterization.

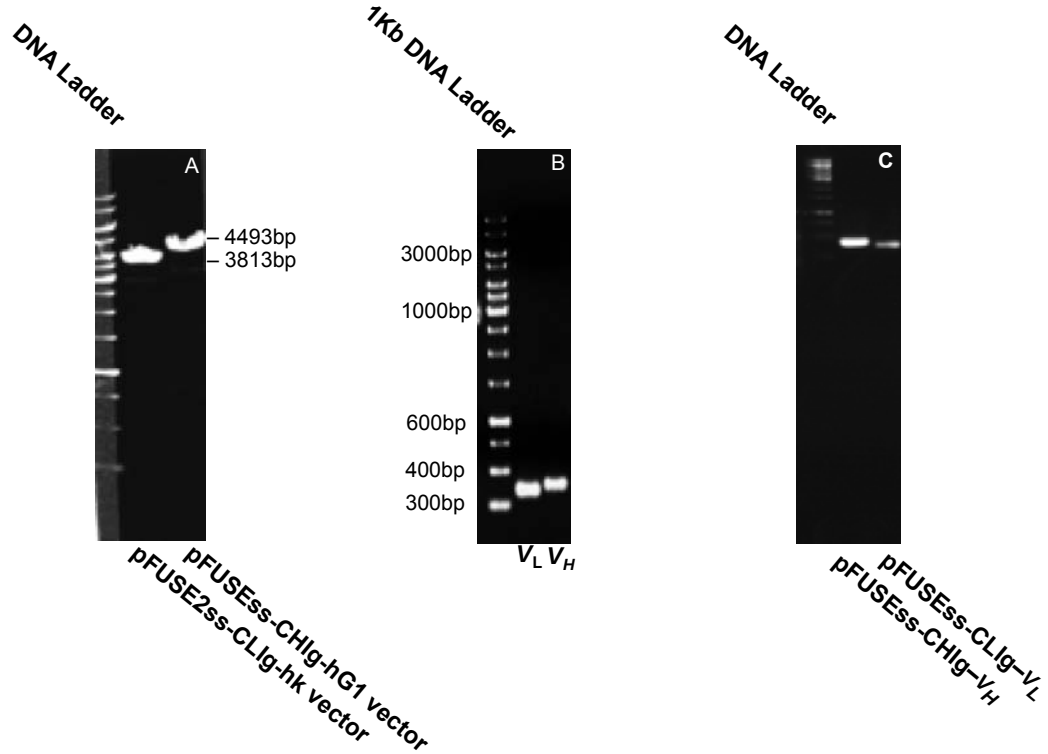

Figure 4.6. Gel electrophoresis of DNA fragments used for mammalian expression plasmid cloning. (A) Backbone plasmid restriction digestion. Plasmids pFUSE–CHIg–hG1 and pFUSE–CLIg–hk were linearized with *EcoR*V and *Nco*I, respectively. Digest reactions were confirmed by electrophoresis on 1% agarose gel. (B) Amplification of the inserts. V_H and V_L inserts were PCR–amplified and confirmed by electrophoresis on a 1% agarose gel and used for cloning into digested mammalian expression plasmids. (C) Colony PCR of the Gibson assembly products. V_H and V_L were cloned into the corresponding linearized pFUSE–CHIg and pFUSE–CLIg plasmids and transformed into *E. coli.* Clones were confirmed for sizing prior to sequencing analysis.

Synthetic IgG	Phage display Selection – Round	Randomization	CDRL3	CDRH1	CDRH2	CDRH3
mIL3Rα-1	Selection 1 – Round 4	Non-randomized	SAGLI	ISYSSM	SIYPSYGYTY	YSAYYGAVAL
mIL3Rα-1mut	Selection 2 – Round 3	Softly Randomized	SAGRI	LTFSSI	SIYPSYGSTY	YTAYYGAVAL
mIL3Rα-2	Selection 1 – Round 4	Non-randomized	WHSSHPI	ISSYYM	SIYPYYGSTY	GVWSYAGWSSAVGF
mIL3Rα-2mut	Selection 2 – Round 3	Softly Randomized	WYSYHPI	ISSYYL	FTYPYYDSSQ	GVWAYSAWSSKIGF
mIL3Rβ-1	Selection 1 – Round 4	Non-randomized	YSYSYYYPI	LSSSSM	SIYSYYSYTS	SSSGWYGF
mIL3Rβ-1mut	Selection 2 – Round 3	Softly Randomized	YSYSYYYPI	LSSSFM	SIYSYYGYRS	SSSGWYGF
mIL3Rβ-2	Selection 1 – Round 4	Non-randomized	WSYGVPI	IYSSSI	YISPYSSYTY	SSWGYYYPYGL
mIL3Rβ-2mut	Selection 2 – Round 3	Softly Randomized	WYYGVPI	IFSSTI	YISPYTGYTF	SSWGYYYPFGL

Table 4.7 Summary and CDR sequences of novel antibodies selected against mIL3Rα and mIL3Rβ by phage display.

4.3 Validation and characterization of synthetic antibodies

4.3.1. Size and purity

Synthetic antibodies were evaluated for purity and size using the automated electrophoresis system with a High Sensitivity Protein 250 kit. The electrophoresis was performed under reducing conditions and resulting band sizes were found as expected: approximately 28 kDa for light chains and 65 kDa for heavy chains (Figure 4.7A). In addition, we confirmed the expected size of full–length IgG of approximately 150 kDa under non–reducing conditions (Figure 4.7A).

Antibody size and purity was validated prior to every *in vitro* or engraftment assay. We observed impurities antibodies that correlated with storage conditions. For example anti–mIL3Rα–2 antibody upon storage at 4°C showed impurities of 20 and 55 kDa (Figure 4.7B). The impurity was not considered process–related since the size and purity of antibodies were closely monitored after purification and buffer exchange, hence the shorter shelf life was considered a disadvantage of this antibody. Anti–mIL3Rα–1 antibody showed impurities and degradation upon short–term refrigeration or freezing storage as well (data not shown).

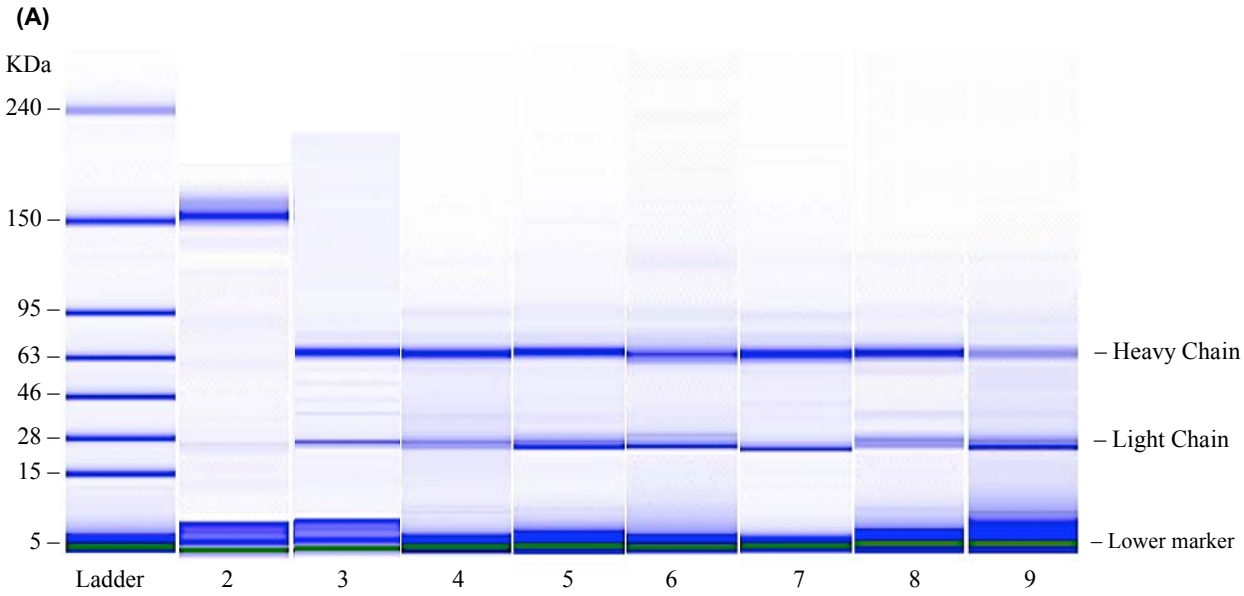
(A)
KDa
240 –
150 –
95 –
63 –
46 –
28 –
15 –
5 –
Ladder
2
3
4
5
6
7
8
9
– Heavy Chain
– Light Chain
– Lower marker

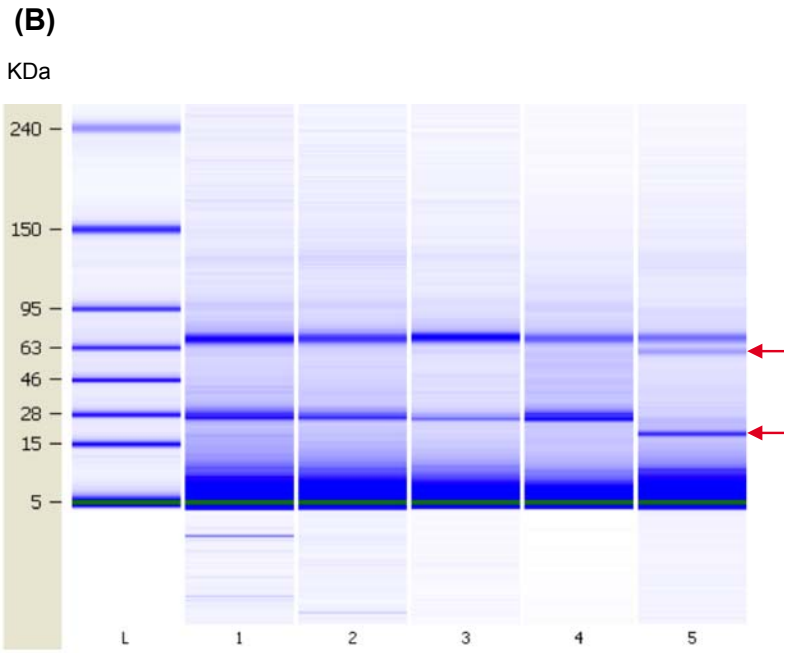
(B)
KDa
240 –
150 –
95 –
63 –
46 –
28 –
15 –
5 –
L
1
2
3
4
5

Figure 4.7. Analysis of the size and purity of synthetic antibodies. (A) The antibody size and purity was confirmed using electrophoresis under non–reductive and reductive conditions. Lane 2 represents anti–mIL3Rβ–1 antibody under non–reducing conditions. Lane 3 – 9 represent various antibodies under reducing condition; lane 3: anti–mIL3Rβ–1 antibody, lane 4: anti–mIL3Rβ–1*mut* antibody, lane 5: anti–mIL3Rβ–2 antibody, lane 6: anti–mIL3Rβ–2*mut* antibody, Lane 7: anti–mIL3Rα–1*mut* antibody; lane 8: anti–mIL3Rα–2 antibody; lane 9: anti–mIL3Rα–2*mut* antibody Heavy chain is detected at approximately 65 kDa and light chain at approximately 28 kDa. (B) Analysis of the size and purity of synthetic antibodies upon storage at 4°C. Antibodies were stored at 4°C for 1–2 months and tested for size and purity by electrophoresis under reductive conditions prior to use. Lane 1: anti–mIL3Rβ–1 antibody; Lane 2: anti–mIL3Rβ–1*mut* antibody; lane 3: anti–mIL3Rα–1*mut* antibody; Lane 4: anti–mIL3Rα–2*mut*; Lane 5 and 6: anti–mIL3Rα–2 antibody. Arrows indicate anti–mIL3Rα–2 antibody stored at 4ºC for over 2 months (Lane 5) versus fresh antibody (Lane 6). kDa: Kilo–Dalton. Antibody: monoclonal antibody. Lower marker is an internal standard used to align the ladder with data from sample wells.

4.3.2 Synthetic antibodies bind to IL3R with nanomolar affinity

The kinetic characterization of anti–mIL3Rα and anti–mIL3Rβ antibodies were carried out using the Octet RED384 (ForteBio) Biolayer Interferometer (BLI). The dissociation constant, K_D, was measured as the ratio of k_{off} / k_{on} from non–linear fitting of the data obtained by BLI. In the first kinetics experiment, antibodies were tested for binding using a concentration range of targets to generate multiple binding curves. Anti–Fab–CH1 biosensors were loaded with ~10 µg / mL purified antibody to an optical thickness of > 0.5 nm and < 1.0 nm. After a stable baseline, biosensors were moved in parallel into wells containing four concentrations of target (1000, 500, 250, and 125 nM) for association, and then moved to buffer–only wells to measure dissociation. Octet Data Analysis 7.1 software (ForteBio) was used to fit each curve individually to a 1:1 binding model based upon each target concentration tested. The kinetic profiling reported (Table 4.8) was taken from the concentration of target that yielded the tightest fit for each antibody interaction with lowest residual (based on the value of full R^2.) The K_D for anti–mIL3Rα–1 antibody was 1.00E–08 M ± 5.46E–10 and the K_D was not improved by affinity maturation selection (anti–mIL3Rα–1*mut* K_D = 1.49E–08M ± 3.77E–10). The K_D for anti–mIL3Rα–2 was 8.28E–09 M ± 5.74E–10 and the K_D was improved by affinity maturation selection for anti–mIL3Rα–2*mut* antibody to 4.82E–09 M ± 5.28E–11. The K_D for anti–IL3Rβ–1 was 5.04E–09 M ± 1.59E–10 and the K_D was not improved by affinity maturation selection for IL3Rβ–1*mut* antibody with K_D 7.04E–09 M ± 2.06E–10. Anti–IL3Rβ–2 antibody had a K_D of 2.90E–08 M ± 8.12E–10, while the mutated form of this antibody was not analyzed due to extremely low yield in the mammalian cell expression system.

Taken together, the level of antibody expression in mammalian cells, antibody stability during handling and storage, antibody affinity maturation, kinetics and receptor binding, and antibody inhibition of IL3 activity in preliminary *in vitro* functional assays (data not shown) were the inclusive criteria that established anti–mIL3Rα–2*mut* and anti–mIL3Rβ–1*mut* as compelling antibodies for further analyses (more details on selection criteria in section 4.3.3). Therefore, a more thorough kinetics analysis was performed for anti–mIL3Rα–2*mut* and anti–mIL3Rβ–1*mut* antibodies.

Using a similar approach as above, BLI was performed with a narrower range of target concentrations that yielded the best–fitting curves in preliminary experiments (above and data

not shown). In this case, data at three target concentrations between 400 nM and 1000 nM were used to produce the binding curves. This time, a 1:1 binding model was used for global curve–fitting to incorporate the data at all target concentrations (Figure 4.8), which resulted in the single kinetic values (Table 4.8).

Monoclonal Antibody	Binding Kinetics by BLI				
	k_{on} (M^{-1} S^{-1})	k_{off} (S^{-1})	KD (M)	KD Error	Full R^2
Anti–mIL3Rα–1	8.59E+03	8.59E–05	1.00E–08	5.46E–10	0.9994
Anti–mIL3Rα–1mut	4.36E+03	6.48E–05	1.49E–08	3.77E–10	0.9998
Anti–mIL3Rα–2	3.02E+03	2.50E–05	8.28E–09	5.74E–10	0.9998
Anti–mIL3Rα–2mut*	1.11E+05	5.36E–04	4.82E–09	5.28E–11	0.9949
Anti–mIL3Rβ–1	2.40E+04	1.21E–04	5.04E–09	1.59E–10	0.9896
Anti–mIL3Rβ–1mut*	7.31E+04	5.14E–04	7.04E–09	2.06E–10	0.9982
Anti–mIL3Rβ–2	1.73E+04	5.00E–04	2.90E–08	8.12E–10	0.9826
Anti–mIL3Rβ–2mut	N/A	N/A	N/A	N/A	N/A
Commercial Anti–hIL3Rα	N/A	N/A	N/A	N/A	N/A
Commercial Anti–mIL3Rβ	N/A	N/A	N/A	N/A	N/A

Table 4.8 Kinetic characterization of the synthetic Anti–mIL3Rα or –mIL3Rβ antibodies. To evaluate the binding of antibodies to the target protein**,** mouse IL3Rα or IL3Rβ target proteins were immobilized on the Fab–CH1 biosensors. The dissociation constants (K_D) of antibodies were measured using biolayer interferometry by measuring the rate of association of antibody to the target protein (k_{on}) and rate of dissociation of antibody (k_{off}) from the target protein. The kinetics are recorded based on concentration of target that yielded the tightest fit for each antibody interaction based on Full R^2. *The asterisks represent the antibodies that were selected for further analysis in this thesis. *The kinetic analysis and curve fitting was performed using 400, 800, and 1000 nM of the targets to produce the binding curves using 1:1 binding model and global curve–fitting to incorporate the data at all target concentrations.

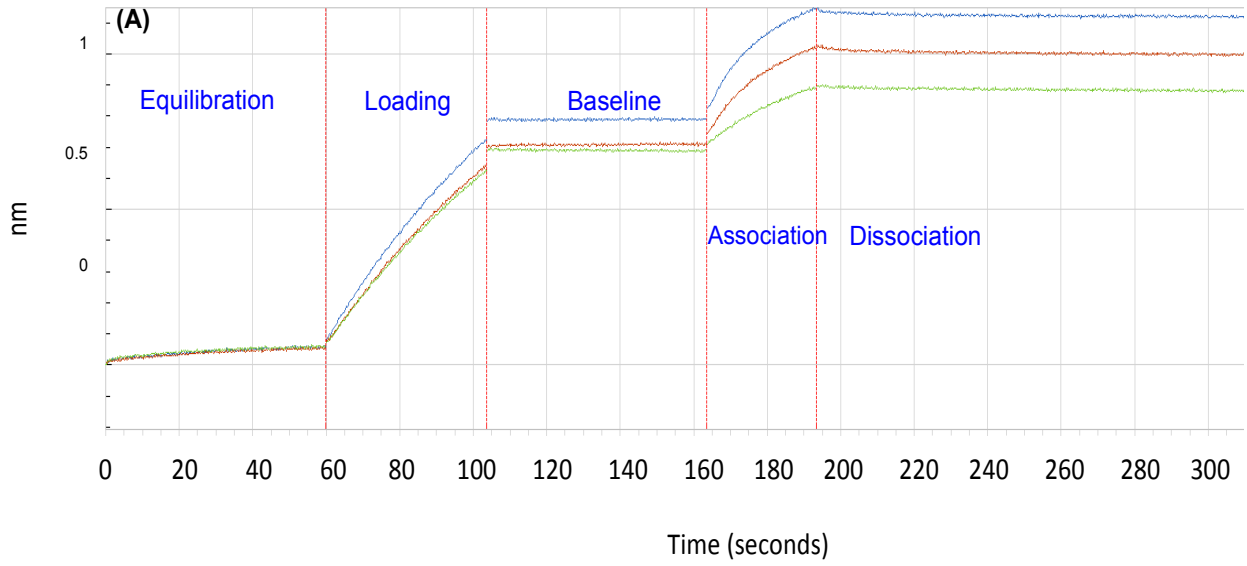
(A)
Equilibration
Loading
Baseline
Association
Dissociation
nm
1
0.5
0
0 20 40 60 80 100 120 140 160 180 200 220 240 260 280 300
Time (seconds)

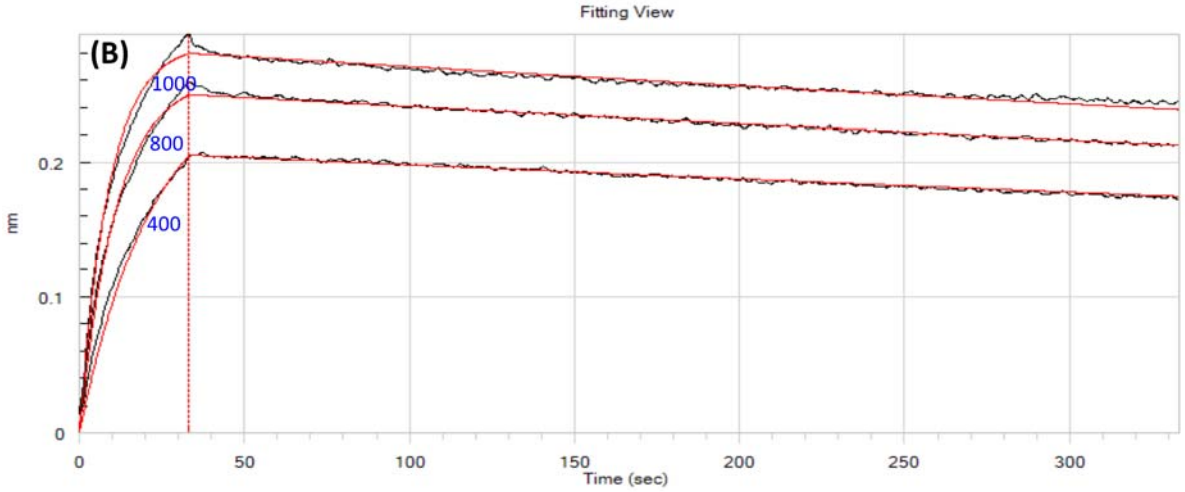
Fitting View
(B)
1000
800
400
nm
0.2
0.1
0
0 50 100 150 200 250 300
Time (sec)

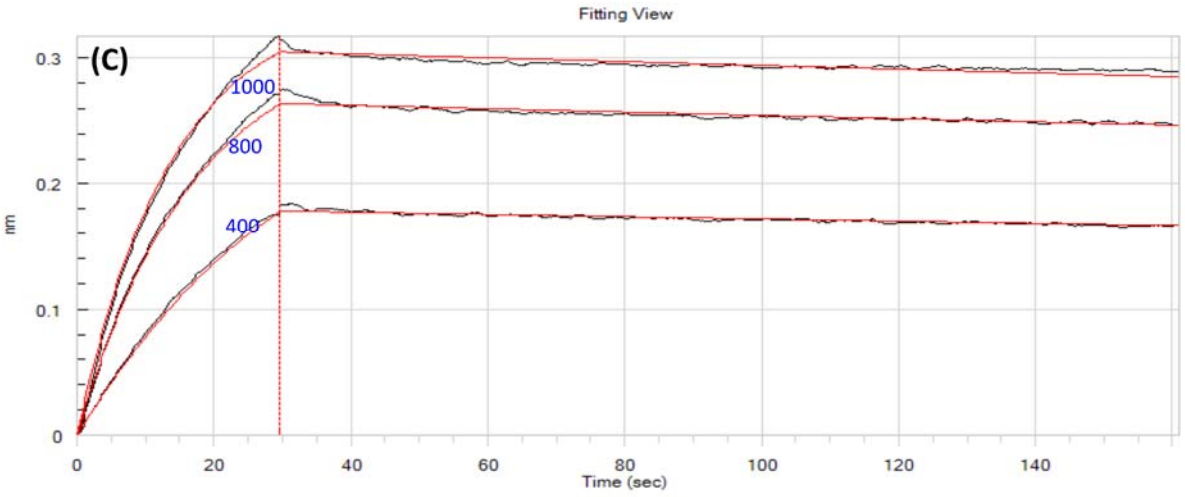
Fitting View
(C)
1000
800
400
nm
0.3
0.2
0.1
0
0 20 40 60 80 100 120 140
Time (sec)

Figure 4.8. Kinetic analysis of antibodies binding to Fc–fused cognate receptor. (A) Biolayer interferometry raw data to obtain kinetic constants. The panel was representative of raw data acquired by OctetREd 384. Anti–Fab–CH1 biosensors were equilibrated in buffer (0 – 60 second) and loaded with ~ 10 μg / mL purified antibody to an optical thickness of > 0.5 nm and < 1.0 nm. After a stable baseline, biosensors were moved in parallel into wells containing serial concentrations of target for association and then moved to buffer–only wells to measure dissociation. (B, C) Fitting view of full kinetic characterization: anti–mIL3Rα–2*mut* antibody to purified mouse IL3Rα–Fc target protein (B), and anti–mIL3Rβ–1*mut* antibody to purified mouse IL3Rβ–Fc target protein (C). Antibody was immobilized on anti–Fab–CH1 biosensors, which were then placed in parallel in the indicated 400–1000 nM receptor concentrations to yield association. Biosensors were transferred to buffer alone to yield dissociation curves (black traces). Global curve–fitting with a 1:1 binding model (red traces) was used to determine the statistical fitting of curves and measure kinetic values. Y–axis indicates optical thickness (nm). X–axis denotes time in seconds. nm: nanometer; sec: seconds.

4.3.3 Synthetic antibodies binding to IL3 receptor

4.3.3.1 Anti–mIL3Rα antibodies bind to IL3Rα cell surface receptor

In addition to BLI analysis, we tested the ability of anti–mIL3Rα antibodies to bind cell surface IL3R receptor. Antibodies were incubated with HEK293F cells transfected with a plasmid expressing human IL3α receptor and the affinity of antibodies for these cells was analyzed using flow cytometry.

Both unmutated and mutated anti–mIL3Rα–1 antibodies showed low binding to HEK293F expressing hIL3Rα and negligible binding to control HEK293F cells (Figure 4.9 A–D). Similarly, unmutated and mutated anti–mIL3Rα–2 antibodies rendered low binding to HEK293F expressing hIL3Rα and negligible binding to control HEK293F cells (Figure 4.9 E–H). The low binding of anti–mIL3Rα antibodies to human IL3Rα expressed on HEK293F in part due to the synthetic antibodies being raised against mouse IL3Rα target not hIL3Rα. Poor surface expression of human IL3Rα construct on HEK293F cells may be another reason for low binding of anti–mIL3Rα antibodies to HEK293F cells expressing hIL3Rα.

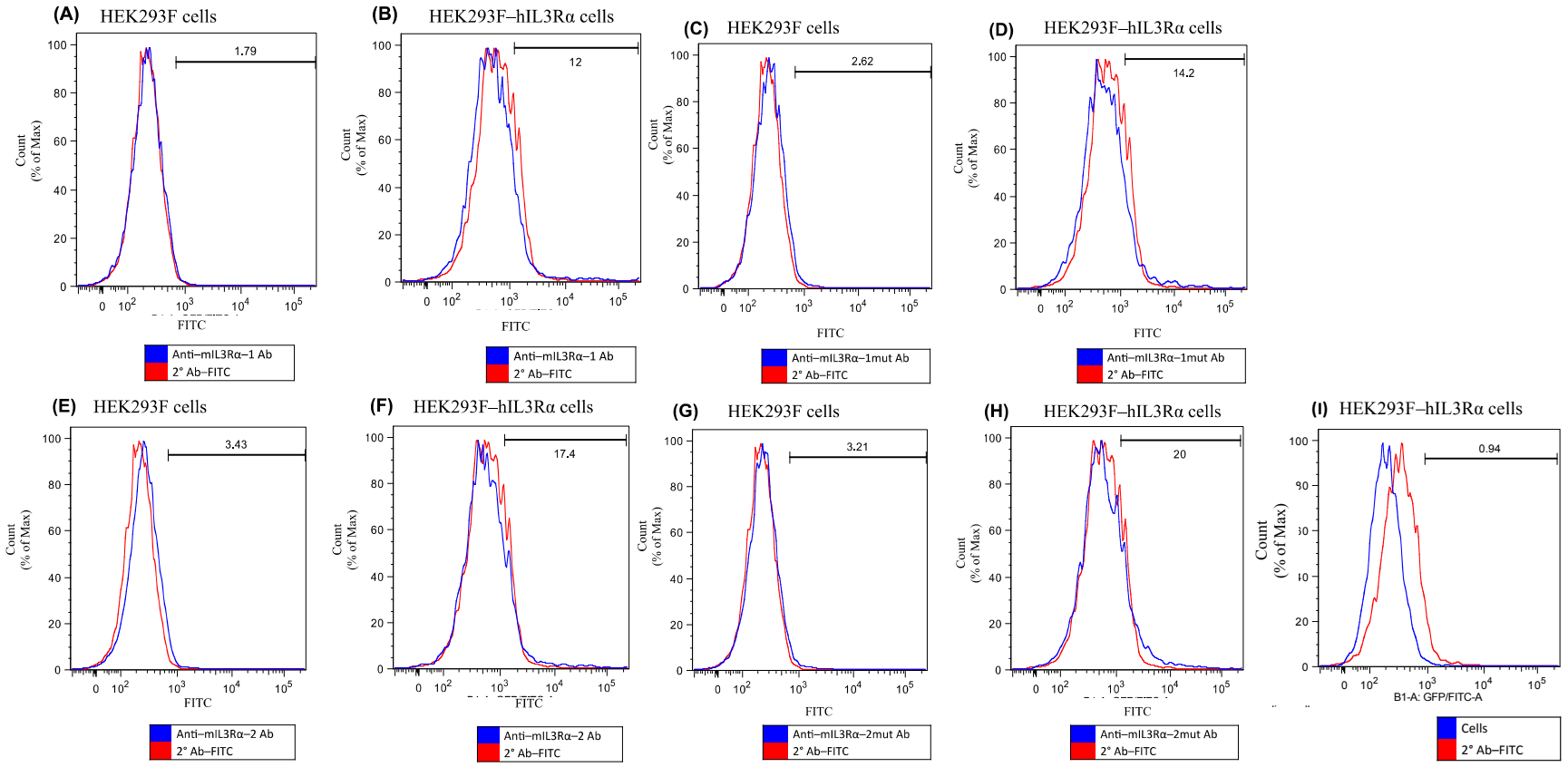
(A) HEK293F cells
1.79
(B) HEK293F–hIL3Rα cells
12
(C) HEK293F cells
2.62
(D) HEK293F–hIL3Rα cells
14.2
(E) HEK293F cells
3.43
(F) HEK293F–hIL3Rα cells
17.4
(G) HEK293F cells
3.21
(H) HEK293F–hIL3Rα cells
20
(I) HEK293F–hIL3Rα cells
0.94
Count (% of Max)
FITC
B1-A: GFP/FITC-A
Anti–mIL3Rα–1 Ab
Anti–mIL3Rα–1mut Ab
Anti–mIL3Rα–2 Ab
Anti–mIL3Rα–2mut Ab
2° Ab–FITC
Cells

Figure 4.9. Anti–mIL3Rα antibodies bind to HEK293F cells expressing human IL3Rα. HEK293F expressing hIL3Rα (1.0E06 cells) were incubated with 1 μg of each antibody at room temperature and flow cytometry analysis was performed to evaluate cell surface receptor binding. Flow cytometry analysis shown by representative histograms (red: secondary antibody; blue: synthetic antibodies). Left panels represent the control HEK293F cells. A–B) Anti–mIL3Rα–1 antibody; C–D) Anti–mIL3Rα–1*mut* antibody; E–F) Anti–mIL3Rα–2 antibody; G–H) Anti–mIL3Rα–2*mut* antibody. (I) Secondary antibody control**.** The data was normalized based on FITC conjugated secondary antibody. Gates are indicators of the percentage of cells bound to antibodies stained with the secondary anti–human IgG–FITC; 2° antibody: Secondary antibody (Goat anti–human IgG (H+L) FITC). FITC: Fluorescein Isothiocyanate. HEK293F: Human Embryonic Kidney 293F.

4.3.3.2 Anti–mIL3Rβ antibodies bind to mIL3Rβ cell surface receptor

Anti–mIL3Rβ antibodies were analyzed for binding to the cell surface mIL3Rβ by flow cytometry analysis. To test the ability of anti-IL3Rβ antibodies in binding IL3Rβ, we incubated antibodies with HEK293F cells transfected with a plasmid expressing human IL3β receptor and analyzed the affinity of antibodies to these cells using flow cytometry. Unmutated and mutated anti–mIL3Rβ–1 antibody bound to HEK293F expressing hIL3Rβ relative to control HEK293F cells (Figure 4.10 A–D). Similarly, anti–mIL3Rβ–2 antibody bound to HEK293F expressing hIL3Rβ relative to the nonspecific binding to control HEK293F cells (Figure 4.10 E–F). As described previously (section 4.2.5), anti–mIL3Rβ–2*mut* was not tested for binding to the cell surface receptor due to low yield in mammalian cell expression. In addition, commercial anti–mIL3Rβ antibody exhibited minor binding to HEK293F over–expressing hIL3Rβ (Figure 4.10 G–H). In summary, we confirmed the ability of anti–mIL3Rβ antibodies to bind HEK293F cells expressing IL3Rβ except for anti–mIL3Rβ–2mut antibody (Figure 4.10).

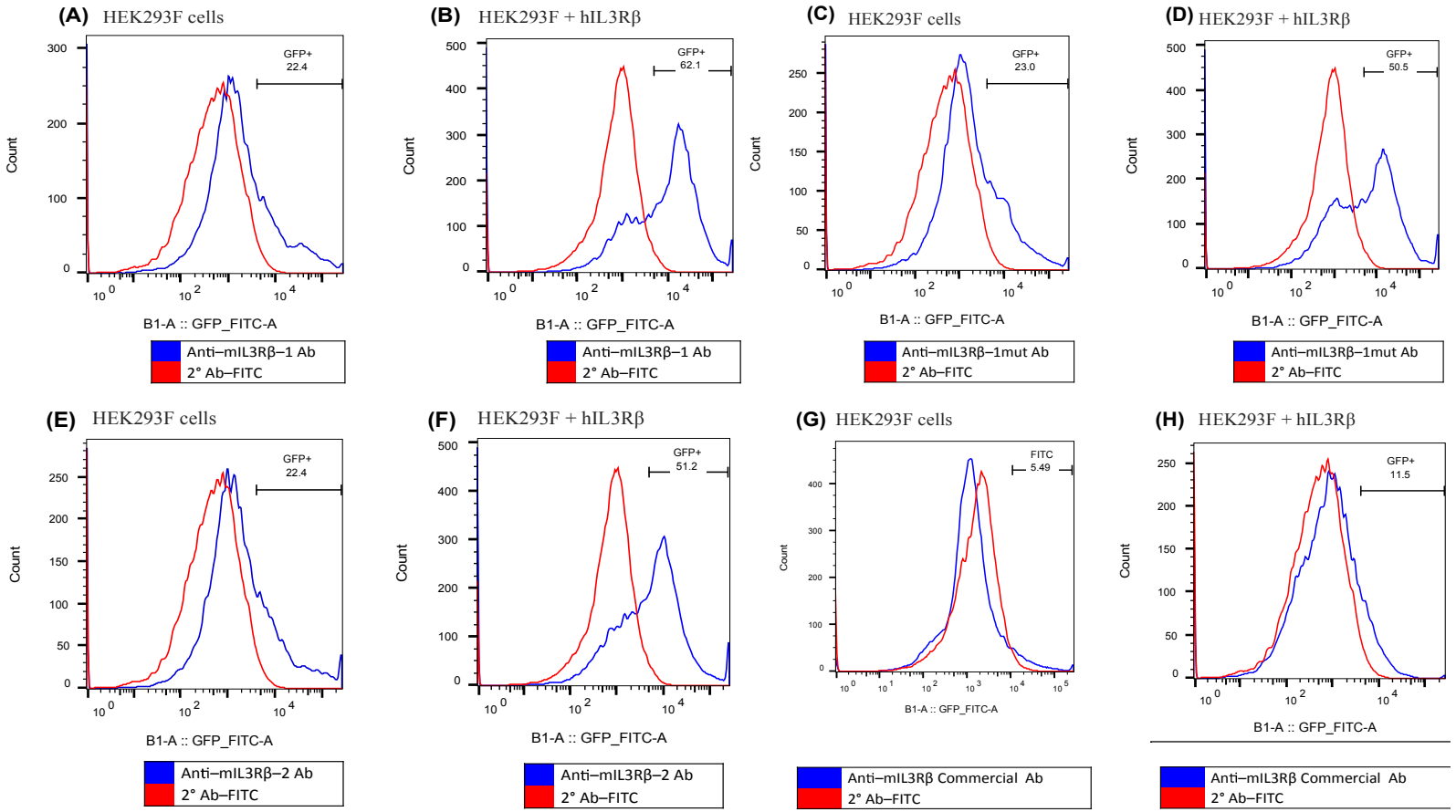

Figure 4.10. Anti–mIL3Rβ antibodies bind to HEK293F cells expressing human IL3β receptors. HEK293F–expressing hIL3Rβ (1.0E06 cells) were incubated with 1 µg of each antibody at room temperature and flow cytometry analysis was performed to evaluate cell surface receptor binding. A–B) Anti–mIL3Rβ–1 antibody; C–D) Anti–mIL3Rβ–1*mut* antibody; E–F) Anti–mIL3Rβ–2 antibody; G–H) Commercial Anti–mIL3Rβ antibody. Flow cytometry analysis shown by representative histograms; red: secondary antibody; blue: synthetic antibodies. Gates are indicators of the percentage of cells bind to the antibodies stained with the secondary anti–human IgG–FITC; 2° antibody: Secondary antibody (Goat anti–human IgG (H+L) FITC). FITC: Fluorescein Isothiocyanate. HEK293F: Human Embryonic Kidney 293F.

4.3.4 Antibodies bind to human and murine CML cell lines

4.3.4.1 Synthetic anti–mIL3Rα antibodies bind to human and murine CML cell lines

In order to show that antibodies bind to endogenously expressed IL3Rα on CML cell lines, we analyzed their interaction CML cell lines using flow cytometry. Anti–mIL3Rα–1 antibody and anti–mIL3Rα–1*mut* antibody bound multiple human CML cell lines, including JURL–MK1, K562, and KU–812. (Figures 4.11–14). Similarly, we confirmed binding of anti–mIL3Rα–2, and anti–mIL3Rα–2*mut* antibodies to JURL–MK1, K–562, and KU–812 human CML cell lines (Figure 4.11–14). We also analyzed the antibody binding to IL3R endogenously expressed on murine CML cell line, CJ cells (mouse HSCs retrovirally transfected with BCR-ABL and NUP98/HOAXA9; a kind gift from Dr. Craig Jordan). Anti–mIL3Rα–1*mut* and anti–mIL3Rα–2*mut* antibodies showed 80–90% binding to CJ cells, which was consistently higher binding than the parental anti-mIL3Rα–1 antibody and anti–mIL3Rα–2 antibody binding to CJ cells (Figure 4.15 C–E). Generally, the affinity–matured anti–mIL3Rα antibodies showed better binding to the human and murine CML cell lines than their parental antibodies.

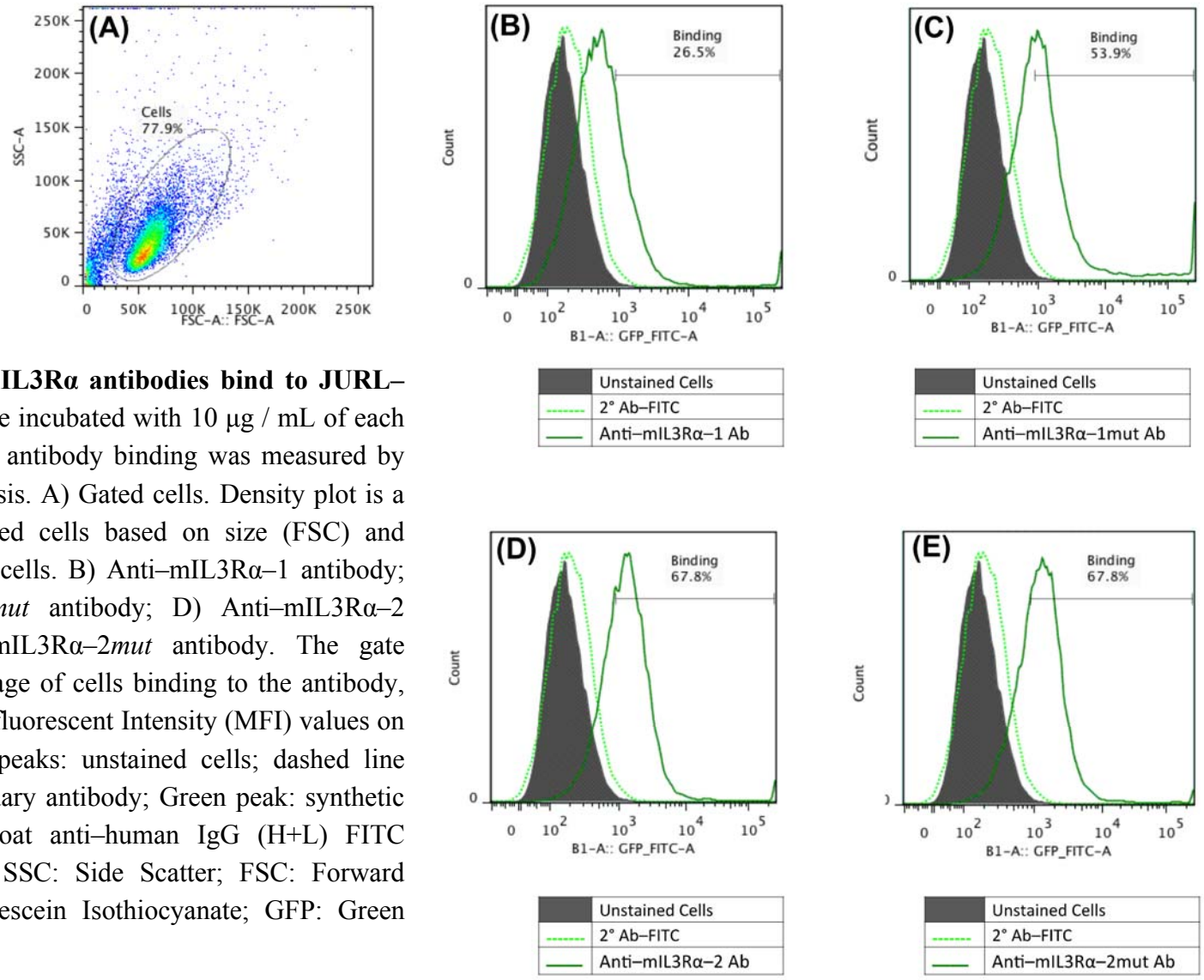

Figure 4.11. Anti–mIL3Rα antibodies bind to JURL–MK1 cells. Cells were incubated with 10 μg / mL of each antibody and relative antibody binding was measured by flow cytometry analysis. A) Gated cells. Density plot is a representative of gated cells based on size (FSC) and granularity (SSC) of cells. B) Anti–mIL3Rα–1 antibody; C) Anti–mIL3Rα–1*mut* antibody; D) Anti–mIL3Rα–2 antibody; E) Anti–mIL3Rα–2*mut* antibody. The gate indicated the percentage of cells binding to the antibody, based on the median fluorescent Intensity (MFI) values on each panel. Shaded peaks: unstained cells; dashed line peaks: control secondary antibody; Green peak: synthetic antibody. 2° Ab: Goat anti–human IgG (H+L) FITC secondary antibody. SSC: Side Scatter; FSC: Forward Scatter; FITC: Fluorescein Isothiocyanate; GFP: Green Fluorescent Protein.

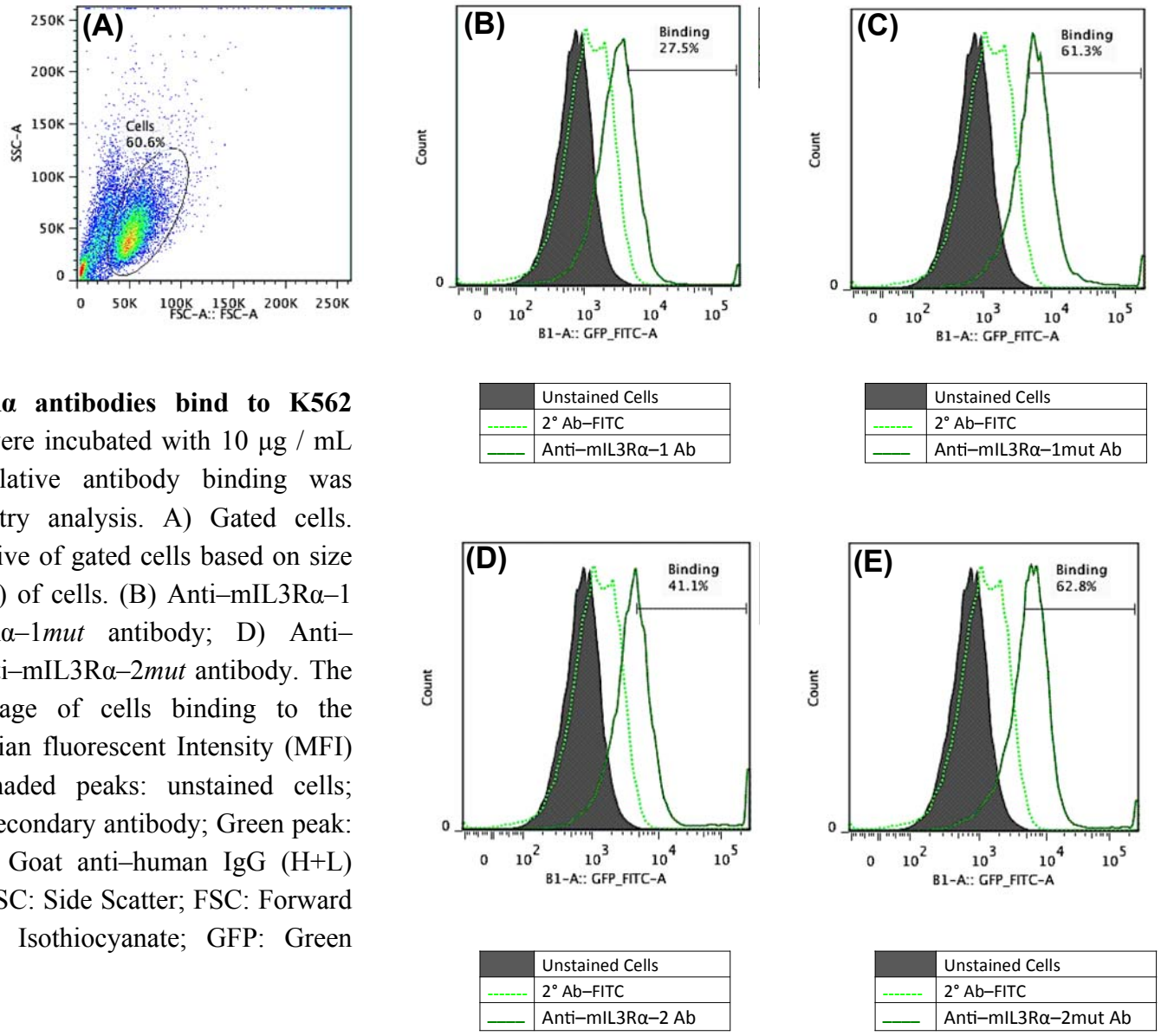

Figure 4.12. Anti–mIL3Rα antibodies bind to K562 human CML cells. Cells were incubated with 10 µg / mL of each antibody and relative antibody binding was measured by flow cytometry analysis. A) Gated cells. Density plot is a representative of gated cells based on size (FSC) and granularity (SSC) of cells. (B) Anti–mIL3Rα–1 antibody; C) Anti–mIL3Rα–1*mut* antibody; D) Anti–mIL3Rα–2 antibody; E) Anti–mIL3Rα–2*mut* antibody. The gate indicates the percentage of cells binding to the antibody, based on the median fluorescent Intensity (MFI) values on each panel. Shaded peaks: unstained cells; dashed–line peaks: control secondary antibody; Green peak: synthetic antibody. 2° Ab: Goat anti–human IgG (H+L) FITC secondary antibody. SSC: Side Scatter; FSC: Forward Scatter; FITC: Fluorescein Isothiocyanate; GFP: Green Fluorescent Protein.

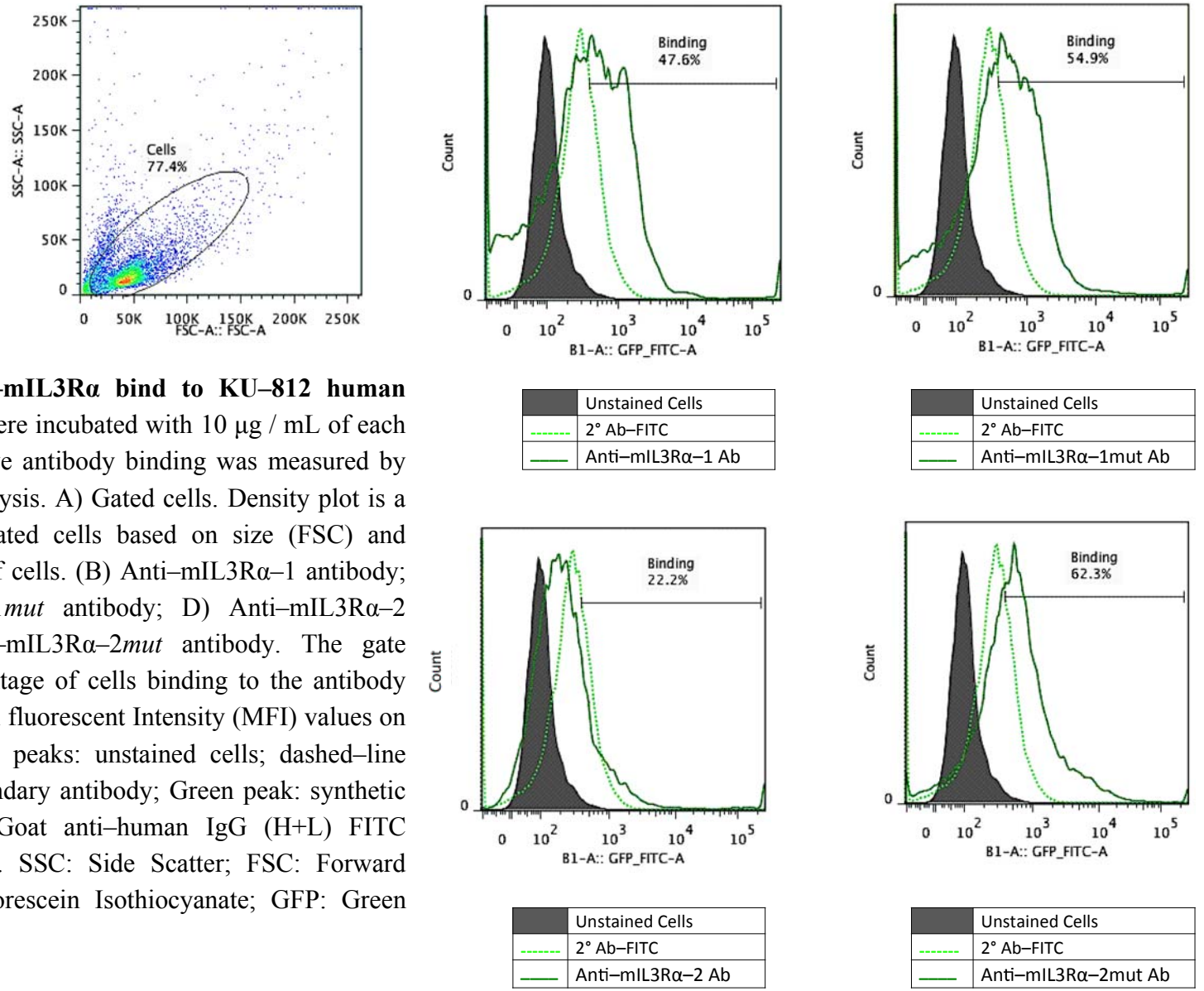

Figure 4.13. Anti–mIL3Rα bind to KU–812 human CML cells. Cells were incubated with 10 µg / mL of each antibody and relative antibody binding was measured by flow cytometry analysis. A) Gated cells. Density plot is a representative of gated cells based on size (FSC) and granularity (SSC) of cells. (B) Anti–mIL3Rα–1 antibody; C) Anti–mIL3Rα–1*mut* antibody; D) Anti–mIL3Rα–2 antibody; E) Anti–mIL3Rα–2*mut* antibody. The gate indicates the percentage of cells binding to the antibody based on the median fluorescent Intensity (MFI) values on each panel. Shaded peaks: unstained cells; dashed–line peaks: control secondary antibody; Green peak: synthetic antibody. 2° Ab: Goat anti–human IgG (H+L) FITC secondary antibody. SSC: Side Scatter; FSC: Forward Scatter; FITC: Fluorescein Isothiocyanate; GFP: Green Fluorescent Protein.

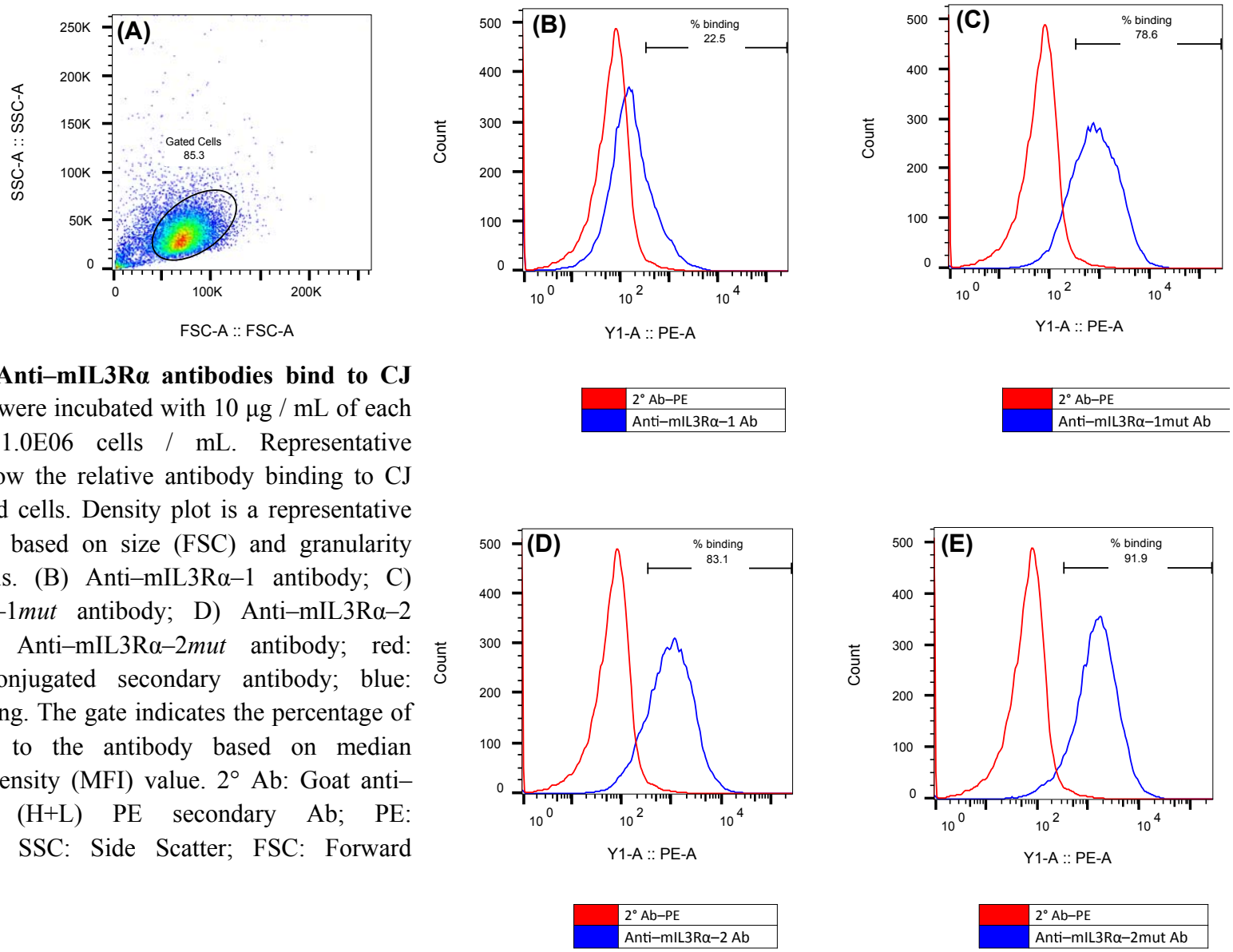

Figure 4.14. Anti–mIL3Rα antibodies bind to CJ cells. CJ cells were incubated with 10 µg / mL of each antibody at 1.0E06 cells / mL. Representative histograms show the relative antibody binding to CJ cells. A) Gated cells. Density plot is a representative of gated cells based on size (FSC) and granularity (SSC) of cells. (B) Anti–mIL3Rα–1 antibody; C) Anti–mIL3Rα–1*mut* antibody; D) Anti–mIL3Rα–2 antibody; E) Anti–mIL3Rα–2*mut* antibody; red: control PE–conjugated secondary antibody; blue: antibody binding. The gate indicates the percentage of cells binding to the antibody based on median fluorescent intensity (MFI) value. 2° Ab: Goat anti–human IgG (H+L) PE secondary Ab; PE: Phycoerythrin. SSC: Side Scatter; FSC: Forward Scatter.

4.3.4.2 Anti–mIL3Rβ antibodies bind to human and murine CML cell lines

In order to show that antibodies bind to endogenously expressed IL3Rα on CML cell lines, we analyzed their interaction with IL3R positive CML cell lines using flow cytometry. Anti–mIL3Rβ–1 antibody and anti–mIL3Rβ–1*mut* antibody bound to CJ cells (Figure 4.16). Similarly, we confirmed binding of anti–mIL3Rβ–1 antibody and anti–mIL3Rβ–1*mut* antibody to KU–812 human CML cells (Figures 4.17). As described previously, anti–mIL3Rβ–2 and –2*mut* antibodies rendered low yield in our mammalian cell expression system and therefore excluded from further analysis. Antibody binding constants, the level of binding to HEK293F / HEK293F–expressing IL3R (HEK293F–hIL3R), and binding to endogenously expressed IL3R on KU–812 or CJ cell lines are summarized in Table 4.9.

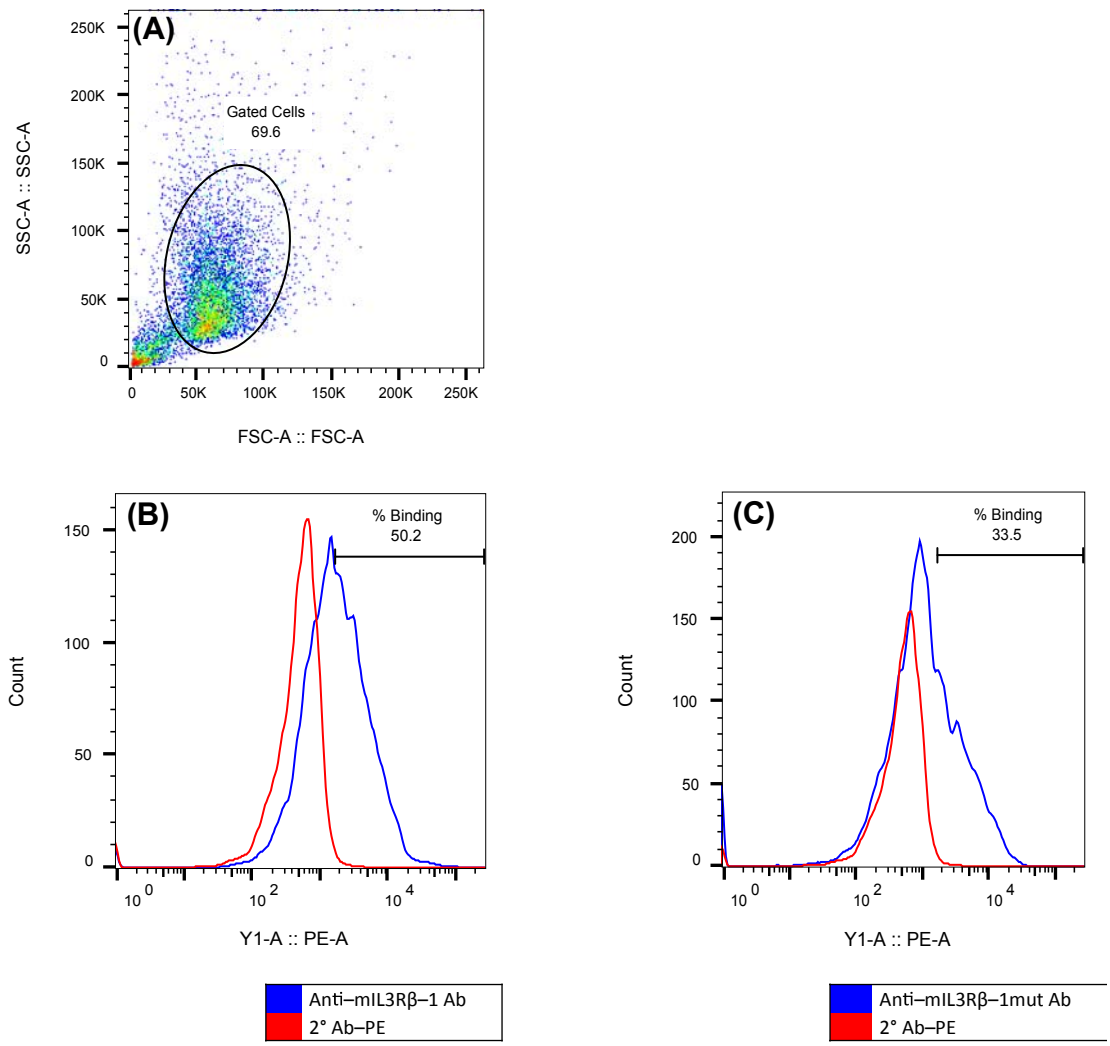

Figure 4.15. Anti–mIL3Rβ antibodies bind to CJ cells. CJ cells (1.0E06 cells) were incubated with 10 µg / mL of each antibody for 20 minutes at room temperature. The relative antibody binding to cells was tested by flow cytometry analysis. A) Gated CJ cells. Dot plot is a representative of gated cells, based on normal size (FSC) and granularity (SSC), analyzed for antibody binding analysis. B) Anti–mIL3Rβ–1 antibody, C) Anti–mIL3Rβ–1*mut* antibody. The median fluorescent intensity (MFI) value indicated by gates on each panel (% Binding) represents the percentage of cells binding to antibody. red peak: secondary PE–conjugated antibody; blue peak: antibody binding. 2° antibody: Goat anti–human IgG (H+L) PE secondary antibody; PE: Phycoerythrin. SSC: Side Scatter; FSC: Forward Scatter.

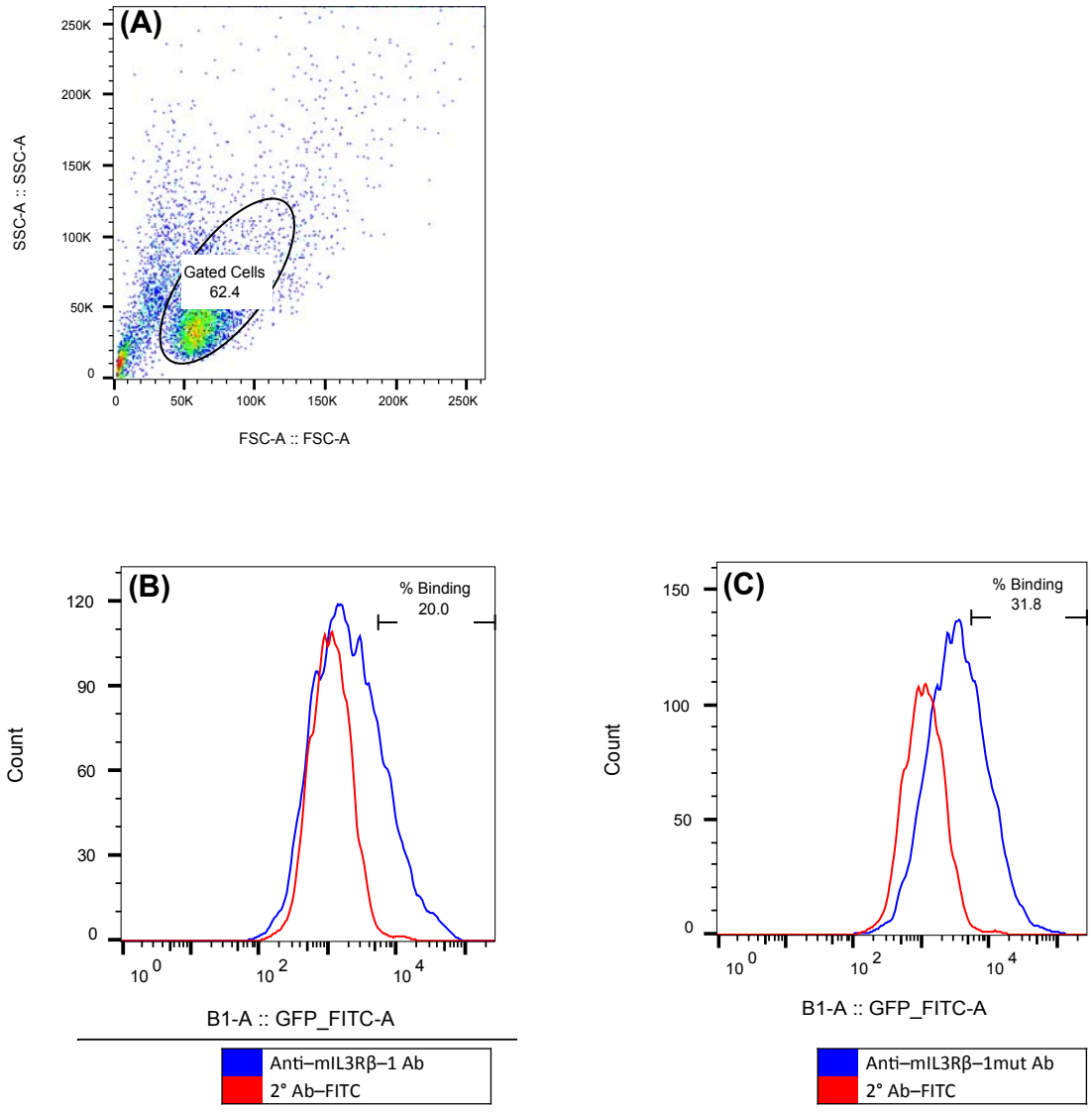

Figure 4.16. Anti–mIL3Rβ antibodies bind to KU–812 cells. KU–812 cells (1.0E06 cells) were incubated with 10 µg / mL of each antibody for 20 minutes at room temperature. The relative antibody binding to cells was tested by flow cytometry analysis. A) Gated KU–812 cells. Dot plot is a representative of gated cells, based on normal size (FSC) and granularity (SSC), analyzed for antibody binding analysis. (B) Anti–mIL3Rβ–1 antibody, C) Anti–mIL3Rβ–1*mut* **antibody.** The median fluorescent intensity (MFI) value indicated by gates on each panel (% Binding) represents the percentage of cells binding to the antibody; red peak: secondary antibody; blue peak: antibody binding. 2° antibody: Goat anti–human IgG (H+L) FITC secondary antibody; FITC: Fluorescein Isothiocyanate. SSC: Side Scatter; FSC: Forward Scatter.

Monoclonal Antibody		Relative Cell Binding (%)			
	KD (M)	HEK293F	HEK293F–R	CJ mouse CML cells	KU–812 CML cells
anti–mIL3Rα–1	1.00E–08	w+	+	+	++
anti–mIL3Rα–1mut	1.49E–08	w+	+	++++	+++
anti–mIL3Rα–2	8.28E–09	w+	+	++++	+
anti–mIL3Rα–2mut	4.82E–09	w+	+	+++++	+++
anti–mIL3Rβ–1	5.04E–09	+	+++	+++	+
anti–mIL3Rβ–1mut	7.04E–09	+	+++	++	++
anti–mIL3Rβ–2	2.90E–08	+	+++	N/A	N/A
anti–mIL3Rβ–2mut	N/A	N/A	N/A	N/A	N/A
Commercial anti–hIL3Rα	N/A	w+	+	w+	+
Commercial anti–mIL3Rβ	N/A	w+	+	+	++

0-10%	w+
10-29%	+
30-49%	++
50-69%	+++
70-90%	++++
90-100%	+++++

Table 4.9 Binding properties of anti–mIL3Rα and anti–mIL3Rβ antibodies generated in this project versus commercial anti–IL3Rα and anti–IL3Rβ antibodies. K_D (M) of generated antibodies was measured by BLI and relative comparison of antibody binding to the cell surface on HEK293F–R (HEK293F–overexpressing IL3R), CJ and KU–812 BC–CML cell lines assessed by flow cytometry analysis; K_D (M): Dissociation constant in Molar; HEK293F: Human embryonic kidney 293F; N/A: Not applicable.

4.3.5 Selection of antibodies for further study

Phage display selections yielded eight antibodies that were ultimately purified (Table 4.9). From the initial validation and characterization studies, we selected two antibodies for further study. Several guidelines were used to determine the best antibodies with which to proceed: (1) Antibodies should be easily expressed and purified. (2) Antibodies should be sufficiently stable during handling and storage. (3) Antibodies should be free of irrelevant phenotypes that do not directly address the core hypothesis such as direct cell killing (Appendix J; Appendix K). (4) Antibodies should bind the receptor with low nanomolar affinity and bind mouse and human CML cells. (5) Preference would be given to affinity-matured antibodies. (6) Antibodies should reverse IL3–mediated resistance to imatinib in preliminary assessments (data not shown).

Using these guidelines anti–mIL3Rα–1 antibody was eliminated due to poor expression and purification, and being unstable during handling. Anti–mIL3Rα–1*mut* antibody was successfully expressed and purified but exhibited direct cell killing phenotype and therefore was not used to test the hypothesis of the thesis (Appendix J; Appendix K). Anti–IL3Rβ–2 and anti–IL3Rβ–2*mut* antibodies were eliminated due to poor expression in mammalian cells and low purification yield.

Anti–mIL3Rα–2*mut* antibody was chosen over anti–mIL3Rα–2 antibody (Appendix G–I) as it had better binding to both purified receptor and CML cells *in vitro*. Both anti–IL3Rβ–1 (Appendix I) and anti–IL3Rβ–1*mut* antibodies showed similar properties in the validation and characterization experiments, therefore anti–IL3Rβ–1*mut* antibody was chosen because it was selected over anti–IL3Rβ–1 Fab in secondary phage selections. This may be due to better expression and / or display of anti–IL3Rβ–1*mut* Fab in phage display selections.

4.4 Imatinib IC_{50} and the minimum required dose of il3 for maximum imatinib suppression in murine cml cell lines

Preliminary experiments were performed to evaluate the half maximal inhibitory concentration (IC_{50}) of imatinib and the minimum concentration of IL3 cytokine required for imatinib suppression on CML cells. Imatinib IC_{50} was measured 0.916 μM for CJ murine CML cells (Figure 4.18A). The lowest concentration of recombinant mouse IL3 that showed maximum

suppression of imatinib was determined by titrating a range of IL3 concentrations (0 – 30 ng / mL) on imatinib treated cells. (Figure 4.18B). The IC_{50} concentration of imatinib (0.916 μM) and minimum IL3 concentration that showed maximum suppression of imatinib activity (10 ng / mL) were subsequently used to test the ability of anti–mIL3Rα–2*mut* antibody or anti–mIL3Rβ–1*mut* antibody to block innate imatinib resistance.

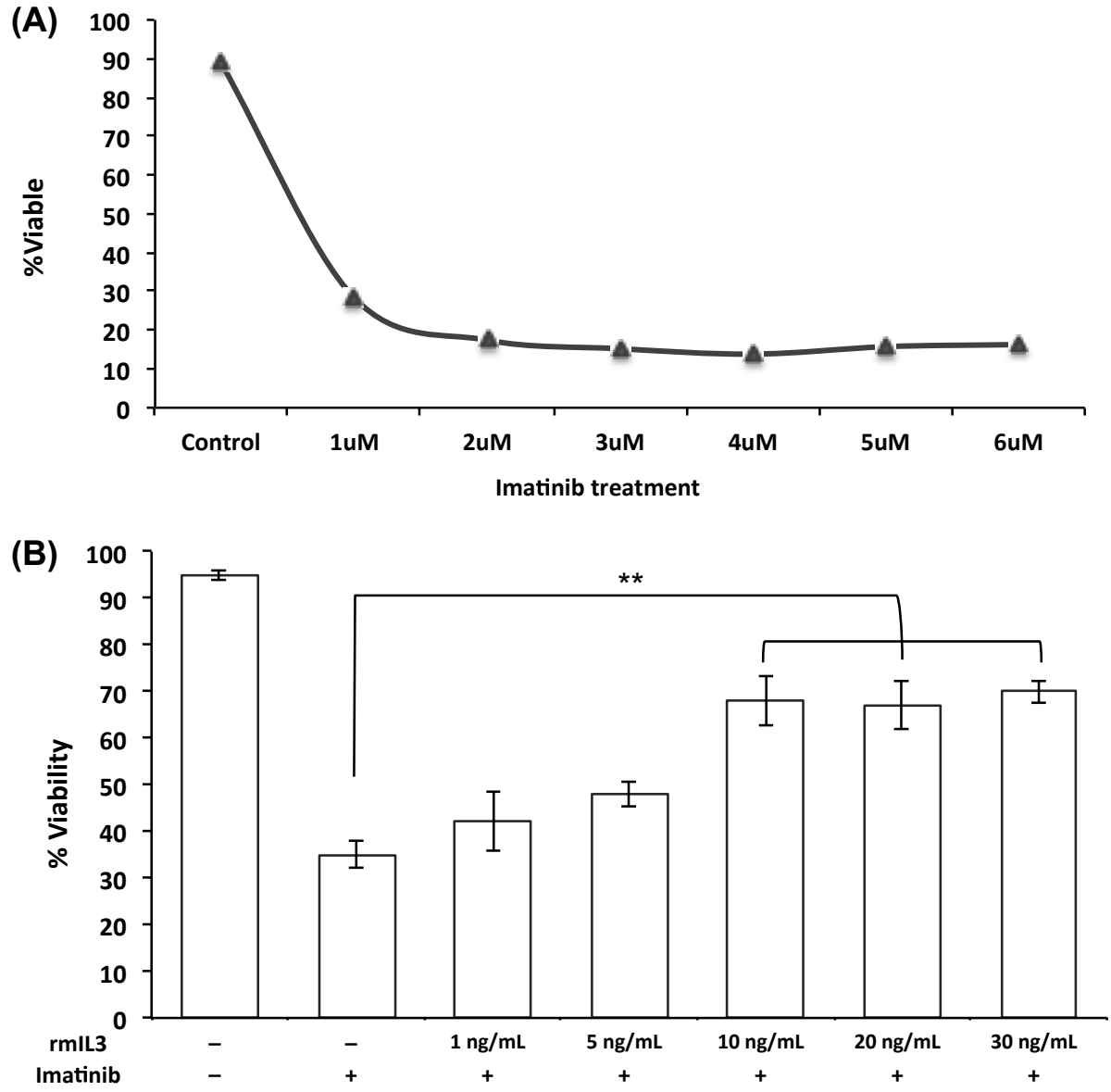

Figure 4.17. Imatinib IC_{50} and IL3 titration to suppress imatinib activity on CJ murine CML cells. (A) Imatinib treatment. CJ cells were treated with imatinib (ranging 0 – 6 μM) for 48 hours at 37ºC. Cell viability was assessed by trypan blue exclusion assay and imatinib IC_{50} was calculated by non–linear regression using CalcuSyn software. Untreated cells showed 90 – 100% viability and cell viability decreased by adding imatinib. (B) IL3 Titration. Cells were incubated with recombinant mouse IL3 (rmIL3) ranging 0 – 30 ng / mL in the presence of imatinib for 48 hours at 37ºC for 48 hours to calculate the minimum required dose of IL3 for suppression of imatinib activity. Bars represent the mean; error bars indicate Mean ± SD; $^{**}P = 0.0049$; Significance of difference was analyzed by one-way ANOVA followed by Tukey *post hoc* test. Y–axis: % cell viability; X–axis: treatments.

4.5 Analysis of the ability of mutated anti–mIL3Rα antibody and anti–mIL3R–β antibody to block IL3–mediated imatinib suppression

We characterized the ability of mutated anti–mIL3Rα antibody and anti–mIL3Rβ antibody to inhibit CML cell viability, induce apoptosis, and inhibit colony formation *in vitro*. We also tested whether engraftment *of* antibody–treated BC–CML cells prolonged disease latency in the CML C57BL/6 transplant mouse models.

We used CJ cells (a kind gift from Dr. **C**raig **J**ordan) as our murine CML cell model for the assays in this thesis. CJ cells co-express both BCR-ABL and Nup98 / HOXA9 translocation products that result in a distinct population of leukemic stem cells with aberrant immunotypes of lin^{-}, $Kit^{+/-}$, Sca^{+}, $CD34^{+}$, and $CD150^{-}$ (T. Ito et al., 2010; Neering et al., 2007). The green and yellow fluorescent protein labels on BCR–ABL and NUP98 / HOXA9, respectively, allows histological analysis, imaging, and detection of leukemic stem cells by flow cytometry. CJ cells are capable of initiating leukemogenesis, homing in the bone marrow, and development of blast crisis in recipient mice when injected intravenously (Neering et al., 2007).

For the *in vitro* or engraftment assays, CJ cells were incubated with antibody (total of 10 μg / mL of antibody for single or combination treatment) in the presence or absence of rmIL3 and imatinib for 48 hours at 37ºC. Specifically, the order of treatments was as follows: 1) antibody addition to cells followed by a three–hour incubation, 2) addition of IL3 followed by a three–hour incubation, and 3) addition of imatinib followed by a 48 hour incubation at 37ºC. Our preliminary *in vitro* results showed that anti–mIL3Rα–2*mut* antibody and anti–mIL3Rβ–1*mut* antibody blocked IL3–mediated imatinib suppression on CML cells at similar levels (data not shown).

4.5.1 Anti–mIL3Rα–2*mut* antibody and mIL3Rβ–1*mut* antibody inhibit IL3–mediated suppression of imatinib activity and reduce CML cell survival *in vitro*

In order to demonstrate the reversal of IL3–mediated imatinib suppression by the anti–mIL3Rα–2*mut* antibody and the anti–mIL3Rβ–1*mut* antibody, we incubated antibodies with CJ cells in the presence or absence of IL3 and imatinib. Anti–mIL3Rα–2*mut* and anti–mIL3Rβ–1*mut* antibodies were used individually or in pairs. IL3 suppression of imatinib activity was observed by a significant increase of approximately 30 – 40% in cell viability, as compared to imatinib treatment alone (Figure 4.18 A–C). Anti–mIL3Rα–2*mut* and anti–mIL3Rβ–1*mut* "antibody alone" treatments partially attenuated cell viability by approximately 20 – 25% as compared to control untreated cells (Figure 4.19 A–B). However, no additive effect of antibody co-treatment was found in viability assay. The combination of anti–mIL3Rα–2*mut* and anti–mIL3Rβ–1*mut* antibodies did not increase the direct cell killing effect of each antibody alone (Figure 4.18C).

Treatment of CJ cells with anti–mIL3Rα–2*mut* antibody in the presence of IL3 and imatinib significantly reduced cell viability by approximately 30% as compared to IL3 and imatinib treatment (Figure 4.18A). Similarly, anti–mIL3Rβ–1*mut* antibody significantly decreased the cell viability by about 25% in the presence of IL3 and imatinib (Figure 4.18B). These findings showed that both antibodies reversed the IL3 suppression of imatinib activity and significantly reduced CML cell survival. Furthermore, co–treatment of cells with both anti–mIL3Rα–2*mut* antibody and anti–mIL3Rβ–1*mut* antibody in the presence of IL3 and imatinib significantly decreased CJ cell viability by about 35% (Figure 4.18C). Despite the reversal of the IL3–induced imatinib suppression by antibody co–treatment, the overall reduction in cell viability was only 5 – 10% less than that of each antibody alone. Therefore, it is unlikely that antibody co-treatment enhanced the reversal of IL3–mediated suppression of imatinib.

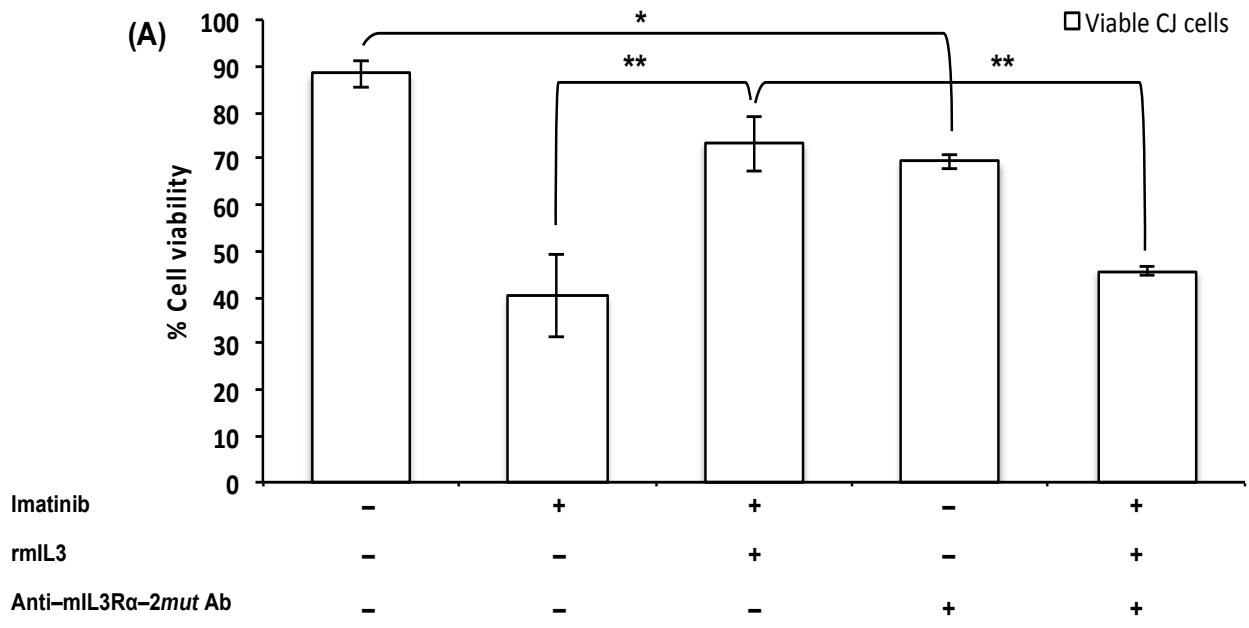
(A)
Viable CJ cells
% Cell viability
100
90
80
70
60
50
40
30
20
10
0
*
**
**
Imatinib – + + – +
rmIL3 – – + – +
Anti–mIL3Rα–2*mut* Ab – – – + +

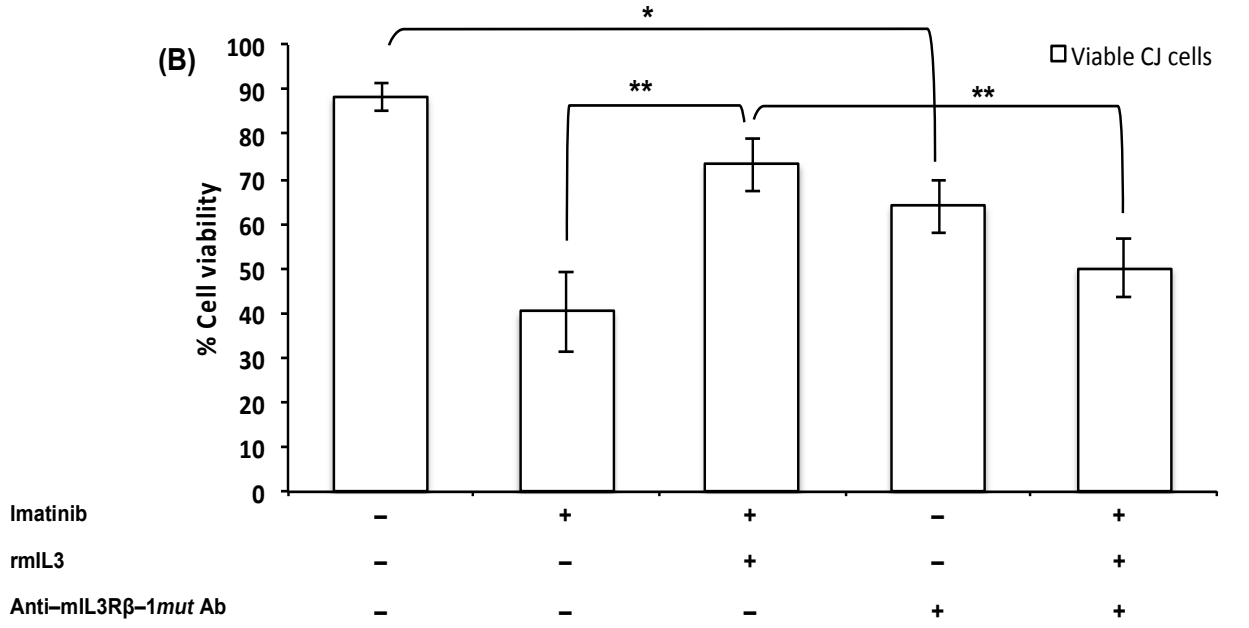
(B)
Viable CJ cells
% Cell viability
100
90
80
70
60
50
40
30
20
10
0
*
**
**
Imatinib – + + – +
rmIL3 – – + – +
Anti–mIL3Rβ–1*mut* Ab – – – + +

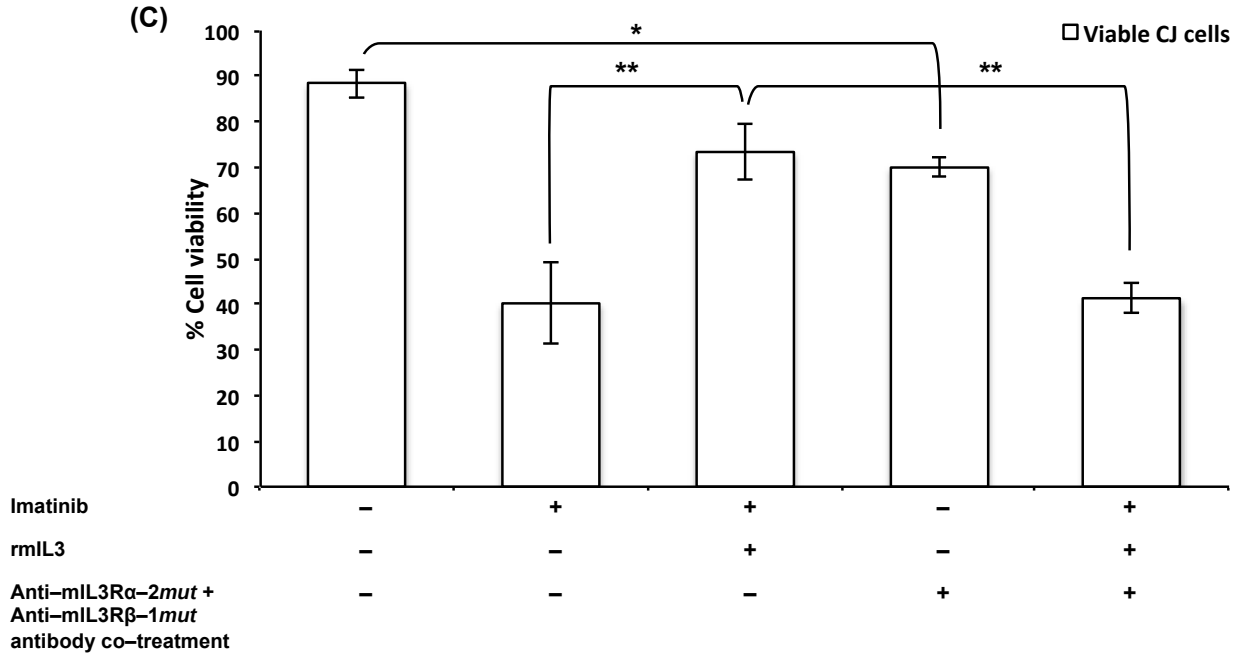

Figure 4.18. Anti–mIL3Rα–2*mut* and anti–mIL3Rβ–1*mut* antibodies inhibit *in vitro* IL3–induced suppression of Imatinib activity in CML cells individually or as co–treatment. CJ cells were incubated with 10 μg / mL antibody (single antibody or antibody co–treatment) for 3 hours at 37ºC followed by addition of rmIL3 and incubation for 3 hours and then imatinib. The cells were incubated with antibody in the presence or absence of rmIL3 and / or imatinib at 37ºC for 48 hours. Cell survival was analyzed using trypan blue exclusion assay. (A) Anti–mIL3Rα–2*mut* antibody; **P* = 0.0046; ***P* < 0.0001; (B) Anti–mIL3Rβ–1*mut* antibody; **P* = 0.003; ***P* = 0.0005; (C) Anti–mIL3Rα–2*mut* antibody + Anti–mIL3Rβ–1*mut* antibody co–treatment. **P* = 0.0065; ***P* < 0.0001; Bars represent the mean; error bars indicate Mean ± SD; Data analyzed with one-way ANOVA followed by Tukey *post hoc* test. Y–axis numbers denote the percentage of cell viability and X–axis shows multiple treatment combinations.

4.5.2 Anti–mIL3Rα–2*mut* antibody and anti–mIL3Rβ–1*mut* antibody reverse the IL3–mediated suppression of imatinib and promote apoptosis in CML cells *in vitro*

Levels of apoptosis and apoptotic cell death were quantified using flow cytometry analysis with Annexin V–APC and SYTOX^{TM} blue staining. One of the earlier events of apoptosis includes translocation of membrane phosphatidyl serine (PS) from the inner side of the plasma membrane to the outer surface. Annexin V, a Ca^{2+} dependent phospholipid–binding protein, has high affinity for PS, and APC–labeled Annexin V can be used for the detection of exposed PS using flow cytometry. Since CJ cells were GFP/YFP positive, we used SYTOX^{TM} Blue for dead cell staining to complement the Annexin V APC. SYTOX^{TM} Blue dead cell stain is a high–affinity nucleic acid stain that penetrates cells with compromised plasma membranes but does not cross uncompromised cell membranes. After brief incubation with SYTOX^{TM} Blue stain, nucleic acids of dead cells fluoresce blue when excited with a 405 nm violet laser. CJ cells were incubated with the antibody in the presence or absence of IL3 and imatinib, as previously described in section 4.5. We tested whether anti–mIL3Rα–2*mut* antibody and anti–mIL3Rβ–1*mut* antibody, as single or co-treatment, were associated with CML cell apoptosis due to reversal of IL3–mediated suppression of imatinib activity.

No significant increase in CJ cell apoptosis was observed for the single antibody treatment with anti–mIL3Rα–2*mut* antibody as compared to untreated cells or cell treated with control antibody (Figure 4.20A). However, anti–mIL3Rβ–1*mut* antibody showed a significant increase greater than 30% in apoptosis or apoptotic cell death in control CJ cells (Figure 4.20A). Co-treatment of CJ cells with both anti–mIL3Rα–2*mut* and anti–mIL3Rβ–1*mut* antibodies lead to a significant cell apoptosis and apoptotic cell death greater than 40%. However, no significant difference was observed beyond anti–mIL3Rβ–1*mut* antibody single treatment in a direct comparison (Figure 4.20A).

IL3 suppression of imatinib activity was confirmed by a significant decrease in the level of apoptosis in cells treated with IL3 and Imatinib (~30% less apoptosis) as compared with cells treated with imatinib alone (Figure 4.19D–E and 4.20 B–D).

Importantly, treatment of cells with anti–mIL3Rα–2*mut* antibody in the presence of IL3 and imatinib induced a significant increase of about 45% in cell apoptosis and apoptotic cell

death as compared to IL3 and imatinib treatment. This finding confirms that anti–mIL3Rα–2*mut* antibody inhibits IL3–mediated imatinib suppression and promotes CML cell apoptosis (Figure 4.20B). Similarly, anti–mIL3Rβ–1*mut* antibody showed reversal of IL3–mediated imatinib suppression that was confirmed by a significant increase of greater than 40% in cell apoptosis and apoptotic cell death as compared to IL3 and imatinib treatment (Figure 4.20C).

Anti–mIL3Rα–2*mut* antibody and anti–mIL3Rβ–1*mut* antibody co–treatment also increased the apoptosis and apoptotic cell death greater than 40% as compared to IL3 and imatinib treatment. However, we did not find an enhanced level of CML cells apoptosis induced by antibody co–treatment beyond that of each antibody separately (Figure 4.20D).

Together, our findings confirm the inhibitory effect of anti–mIL3Rα–2*mut* antibody and anti–mIL3Rβ–1*mut* antibody on IL3–induced suppression of imatinib activity leading to a significant increase in CML cell apoptosis. However, antibody co-treatment did not enhance CML cell apoptosis beyond single antibody treatments (Figure 4.19 and Figure 4.20).

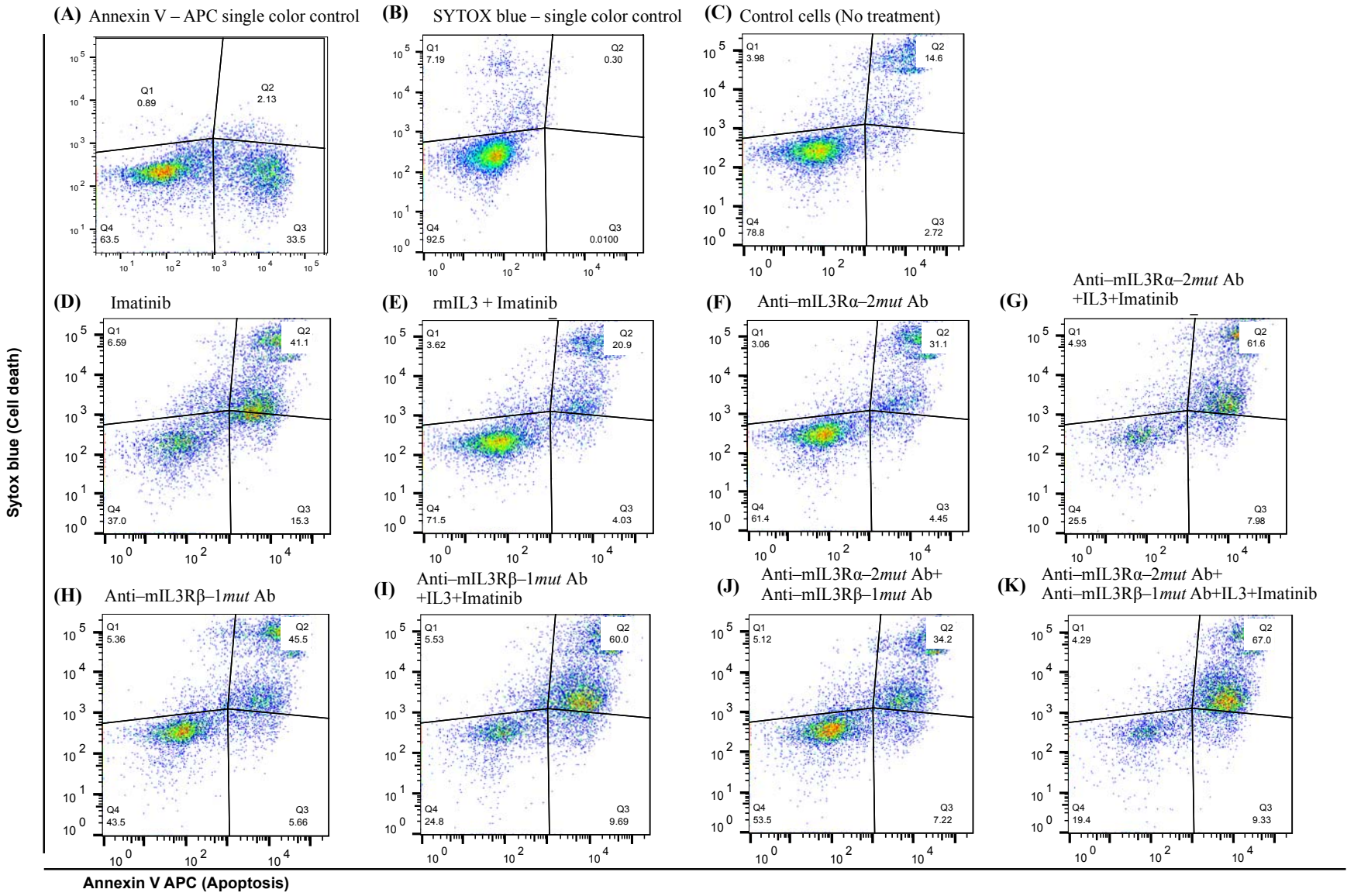
(A) Annexin V – APC single color control
Q1 0.89
Q2 2.13
Q4 63.5
Q3 33.5
(B) SYTOX blue – single color control
Q1 7.19
Q2 0.30
Q4 92.5
Q3 0.0100
(C) Control cells (No treatment)
Q1 3.98
Q2 14.6
Q4 78.8
Q3 2.72
(D) Imatinib
Q1 6.59
Q2 41.1
Q4 37.0
Q3 15.3
(E) rmIL3 + Imatinib
Q1 3.62
Q2 20.9
Q4 71.5
Q3 4.03
(F) Anti–mIL3Rα–2mut Ab
Q1 3.06
Q2 31.1
Q4 61.4
Q3 4.45
(G) Anti–mIL3Rα–2mut Ab +IL3+Imatinib
Q1 4.93
Q2 61.6
Q4 25.5
Q3 7.98
(H) Anti–mIL3Rβ–1mut Ab
Q1 5.36
Q2 45.5
Q4 43.5
Q3 5.66
(I) Anti–mIL3Rβ–1mut Ab +IL3+Imatinib
Q1 5.53
Q2 60.0
Q4 24.8
Q3 9.69
(J) Anti–mIL3Rα–2mut Ab+ Anti–mIL3Rβ–1mut Ab
Q1 5.12
Q2 34.2
Q4 53.5
Q3 7.22
(K) Anti–mIL3Rα–2mut Ab+ Anti–mIL3Rβ–1mut Ab+IL3+Imatinib
Q1 4.29
Q2 67.0
Q4 19.4
Q3 9.33
Sytox blue (Cell death)
Annexin V APC (Apoptosis)

Figure 4.19. Anti–mIL3Rα–2*mut* and anti–mIL3Rβ–1*mut* antibodies promote apoptosis and cell death in CJ cells: flow cytometry density plot analysis. In order to evaluate the impact of antibodies on apoptosis and cell death, CJ cells were incubated with 10 µg / mL antibody (single antibody or antibody co–treatment) in the presence or absence of imatinib or rmIL3 and imatinib at 37ºC for 48 hours. CJ cells were then washed and stained with Annexin V–APC / SYTOX blue as indicators of apoptosis and cell death and analyzed by flow cytometry. The density plot gates indicate Q1: SYTOX blue+|APC–, Q2: SYTOX blue+|APC+, Q3: SYTOX blue–|APC+, Q4: SYTOX blue–|APC–. (A, B) Single color control staining. To ensure the accuracy of the gating and data analysis, control groups (treated with control antibody) were stained with single color Annexin V–APC and SYTOX blue. Q2 indicates necrotic cell sub–population, and Q3 represents apoptotic cells. (C) Control Cells (No treatment); (D) Imatinib (E) rmIL3 and Imatinib treatment; (F) Anti–mIL3Rα–2*mut* antibody (G) Anti–mIL3Rα–2*mut* antibody and rmIL3 and Imatinib; (H) Anti–mIL3Rβ–1*mut* antibody; (I) Anti–mIL3Rβ–1*mut* antibody and rmIL3 and Imatinib; (J) Anti–mIL3Rα–2*mut* and β–1*mut* antibody co–treatment and rmIL3 and Imatinib. Y–axis shows cells stained with SYTOX blue indicating necrotic cells. X–axis indicates Annexin V APC staining for apoptotic cells. The density plots represent one set of data from three independent data collections. APC: Allophycocyanin. rmIL3: recombinant mouse Interleukin–3.

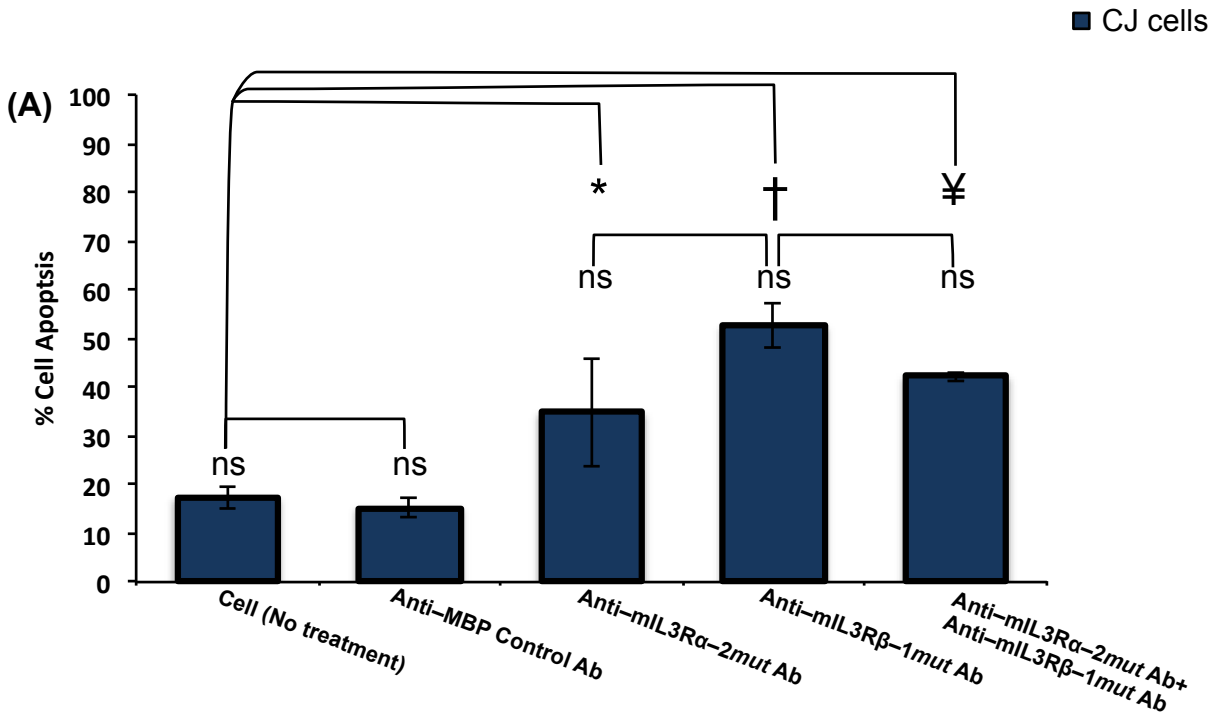
CJ cells
(A)
% Cell Apoptsis
100
90
80
70
60
50
40
30
20
10
0
*
†
¥
ns
ns
ns
ns
ns
Cell (No treatment)
Anti–MBP Control Ab
Anti–mIL3Rα–2mut Ab
Anti–mIL3Rβ–1mut Ab
Anti–mIL3Rα–2mut Ab+
Anti–mIL3Rβ–1mut Ab

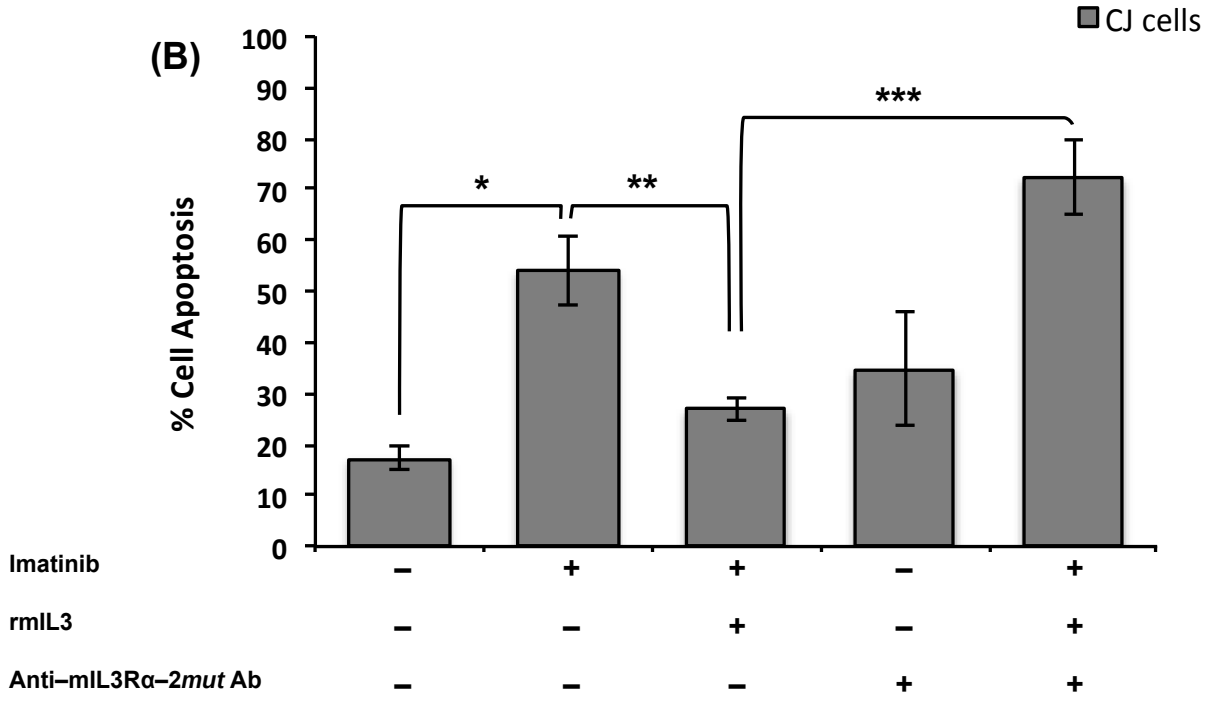
CJ cells
(B)
% Cell Apoptosis
100
90
80
70
60
50
40
30
20
10
0
*
**
***
Imatinib – + + – +
rmIL3 – – + – +
Anti–mIL3Rα–2mut Ab – – – + +

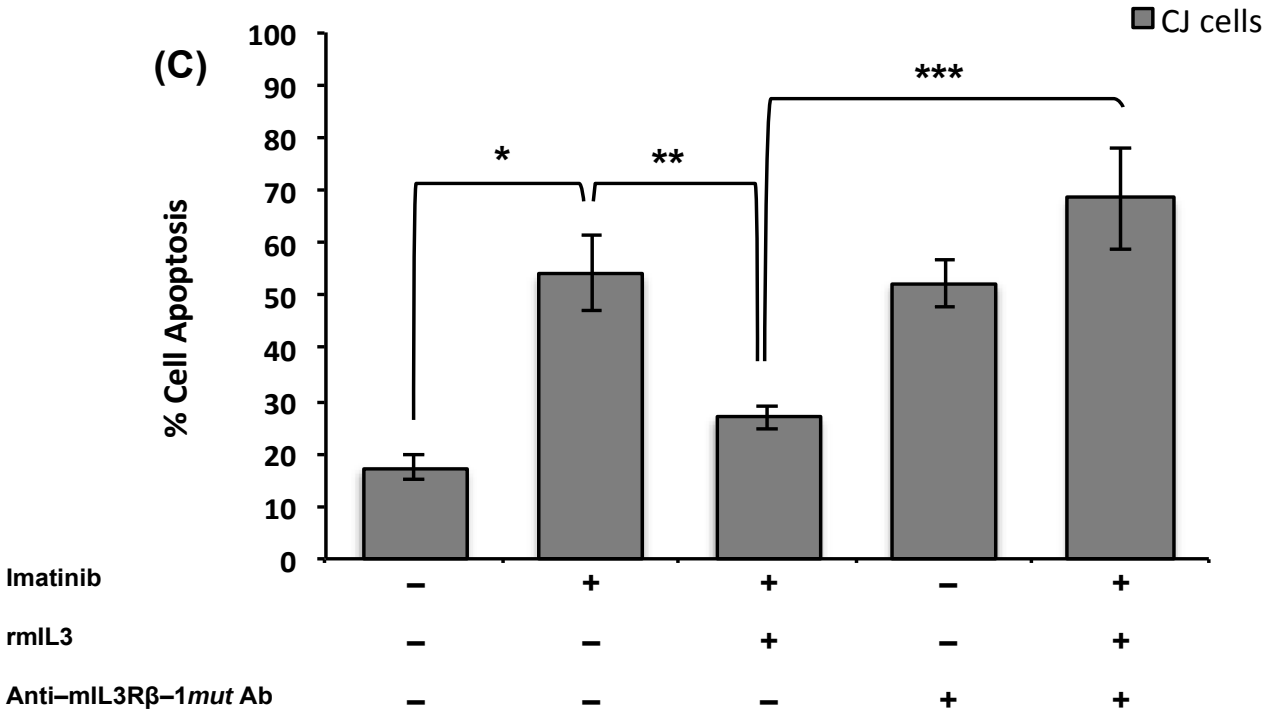
(C)
CJ cells
% Cell Apoptosis
100
90
80
70
60
50
40
30
20
10
0
*
**
***
Imatinib
rmIL3
Anti–mIL3Rβ–1*mut* Ab
– + + – +
– – + – +
– – – + +

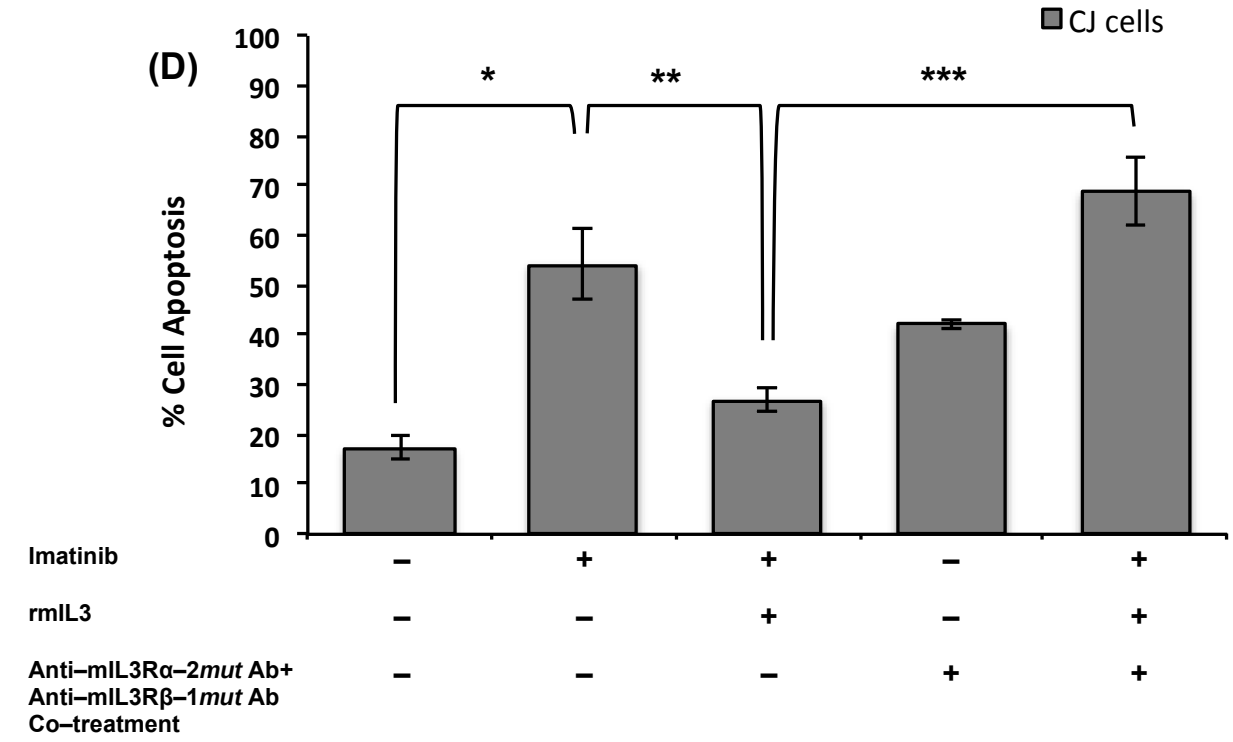
(D)
CJ cells
% Cell Apoptosis
100
90
80
70
60
50
40
30
20
10
0
*
**
***
Imatinib
rmIL3
Anti–mIL3Rα–2*mut* Ab+
Anti–mIL3Rβ–1*mut* Ab
Co–treatment
– + + – +
– – + – +
– – – + +

Figure 4.20. Anti–mIL3Rα–2*mut* antibody and anti–mIL3Rβ–1*mut* antibody promote apoptosis in CJ cells. CJ cells were treated with 10 μg / mL antibody (as single or co–treatment) in the presence or absence of IL3 and / or imatinib at 37ºC for 48 hours. Cells were then washed and stained with Annexin V–APC and SYTOX^{TM} blue as indicators of apoptosis and cell death, respectively. Flow cytometry analysis was performed on 15000 cells per treatment in three independent data collections. Bar graphs represent Annexin V positive apoptosis (Q2: SYTOX blue+|APC+ and Q3: SYTOX blue–|APC+). (A) Direct apoptosis. Direct cell apoptosis of antibody treatments alone. * $P = 0.068$; † $P < 0.0001$; ¥ $P < 0.0032$. (B) Anti–mIL3Rα–2*mut* antibody Treatment. CJ cells were treated with antibody in the presence or absence of imatinib and/or IL3 and imatinib. (C) Anti–mIL3Rβ–1*mut* antibody Treatment. CJ cells were treated with antibody in the presence or absence of imatinib and/or IL3 and imatinib. (D) Co–treatment with anti–mIL3Rα–2*mut* antibody and anti–mIL3Rβ–1*mut* antibody. CJ cells were treated with both antibodies in the presence or absence of imatinib and/or IL3 and imatinib. APC: Allophycocyanin; ns: not significant; rmIL3: recombinant mouse Interleukin-3; Ab: antibody. Y–axis represents the percentage of apoptotic Annexin V–APC+ cells. X–axis indicates various treatments. Bars represent the mean; error bars indicate Mean ± SD; Data analyzed with one-way ANOVA followed by Tukey *post hoc* test for multiple comparisons. * $P = 0.0012$; ** $P < 0.0001$; *** $P < 0.000.1$.

4.5.3 Anti–mIL3Rα–2*mut* antibody and anti–mIL3Rβ–1*mut* antibody impair IL3–induced colony formation capacity of CML cells in the presence of imatinib *in vitro*

The effect of anti–mIL3Rα–2*mut* and anti–mIL3Rβ–1*mut* antibodies on CML cell colony formation was tested using the colony forming unit (CFU) assay. CJ cells were incubated with anti–mIL3Rα–2*mut* and / or anti–mIL3Rβ–1*mut* antibody in the presence or absence of IL3 and imatinib (as previously described in section 4.5). Three hundred cells from each treatment group were seeded in MethoCult™ medium. MethoCult™ is a cytokine–enriched medium with Interleukin–3 (IL3), Interleukin –6 (IL6), Stem cell factor (SCF), and erythropoietin (EPO).

Single antibody treatments with anti–mIL3Rα–2*mut* or anti–mIL3Rβ–1*mut* antibody showed a significant decrease of 2.5– and 2.8–fold less CFU, respectively, as compared with untreated CJ cells (Figure 4.21A). Co–treatment of cells with both anti–mIL3Rα–2*mut* and anti–mIL3Rβ–1*mut* antibody significantly reduced colony formation to approximately 5.5–fold less CFUs than untreated CJ cells (Figure 4.21A). The direct suppression of clonogenicity in the absence of exogenously added IL3 suggests blocking of autocrine / paracrine IL3 pathways or other alternate pro–survival and self–renewal pathways in CJ cells.

CJ cells treated with imatinib and exogenously added IL3 showed approximately two fold increase in the number of CFUs of imatinib–treated cells (Figure 4.21B–D). Treatment of CJ cells with anti–mIL3Rα–2*mut* antibody in the presence of IL3 and imatinib lead to a significant reduction of 2–fold in colony formation as compared to IL3 and imatinib–treated cells. The number of colonies in this group was comparable to imatinib–treated cells (Figure 4.21B). Similarly, CJ cells treated with anti–mIL3Rβ–1*mut* antibody in the presence of IL3 and imatinib showed a significant decrease of 4.5–fold in colony formation as compared with IL3 and imatinib–treated cells (Figure 4.21C). Anti–mIL3Rα–2*mut* and anti–mIL3Rβ–1*mut* antibody co–treatment of CJ cells in the presence of IL3 and imatinib lead to 10–fold decrease in colony formation of cells as compared with IL3 and imatinib–treated cells (Figure 4.21B–D). This finding showed that inhibitory effects of anti–mIL3Rα–2*mut* and anti–mIL3Rβ–1*mut* antibodies on CML cell clonogenicity were enhanced when used in combination.

Together, colony formation analyses provided evidence of the effect of anti–mIL3Rα–2*mut* and anti–mIL3Rβ–1*mut* antibodies in disrupting IL3–induced colony formation of CML cells in

the presence of imatinib. In addition, the direct effect of antibodies on suppression of clonogenicity in the absence of exogenously added IL3 suggested the presence of autocrine / paracrine IL3 pathways or other alternate prosurvival and self–renewal pathways in CML cells. Furthermore, more detailed investigations are required to analyze the antibody–antibody interactions and optimize the dose–ratio of antibodies for potential combination therapy, in order to increase the potency and / or efficacy of antibody combination therapy.

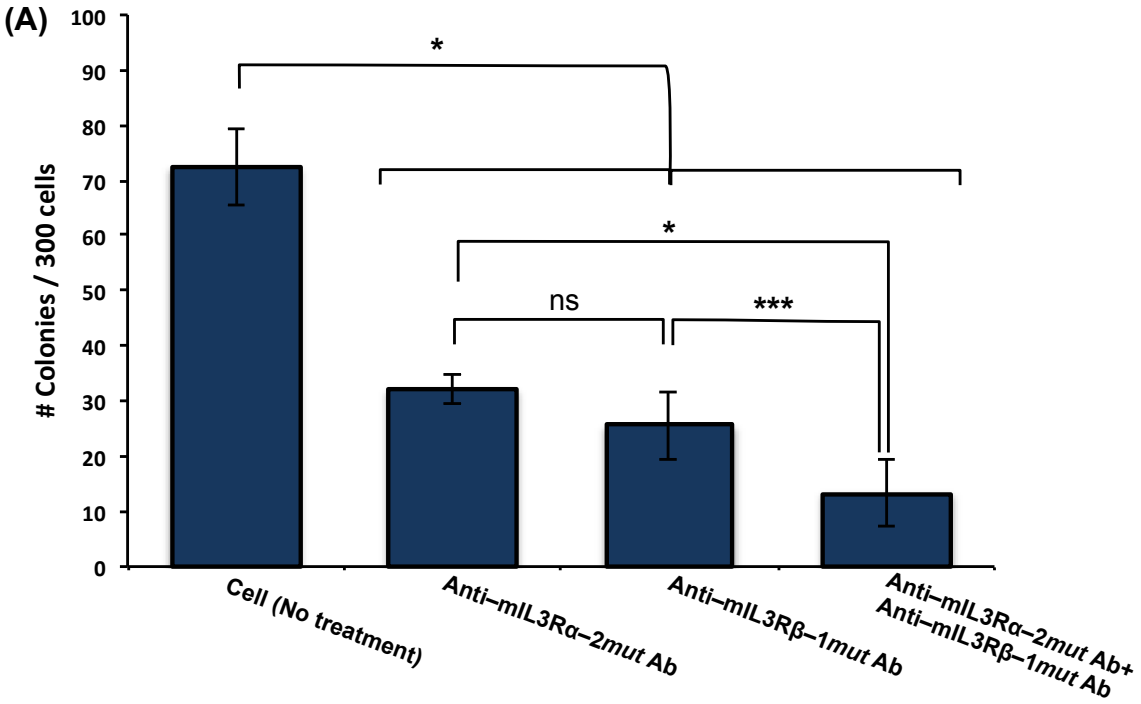
(A)
Colonies / 300 cells
100
90
80
70
60
50
40
30
20
10
0
*
*
ns
***
Cell (No treatment)
Anti–mIL3Rα–2mut Ab
Anti–mIL3Rβ–1mut Ab
Anti–mIL3Rα–2mut Ab+
Anti–mIL3Rβ–1mut Ab

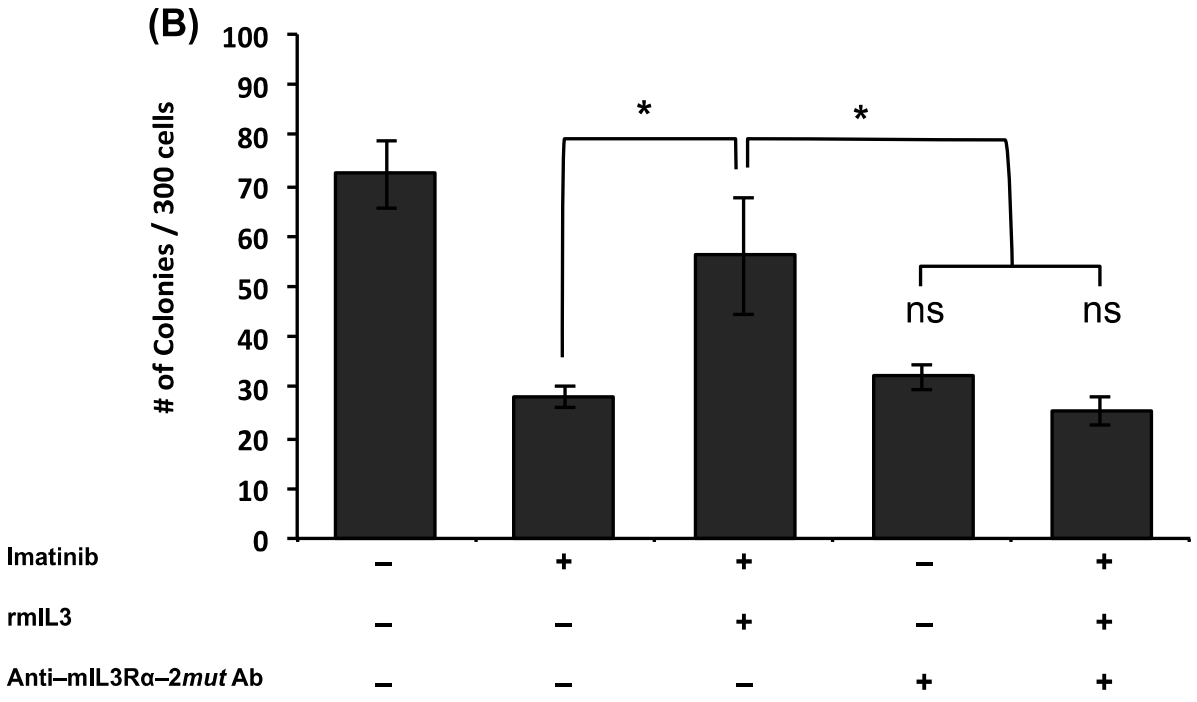
(B)
# of Colonies / 300 cells
100
90
80
70
60
50
40
30
20
10
0
*
*
ns
ns
Imatinib – + + – +
rmIL3 – – + – +
Anti–mIL3Rα–2mut Ab – – – + +

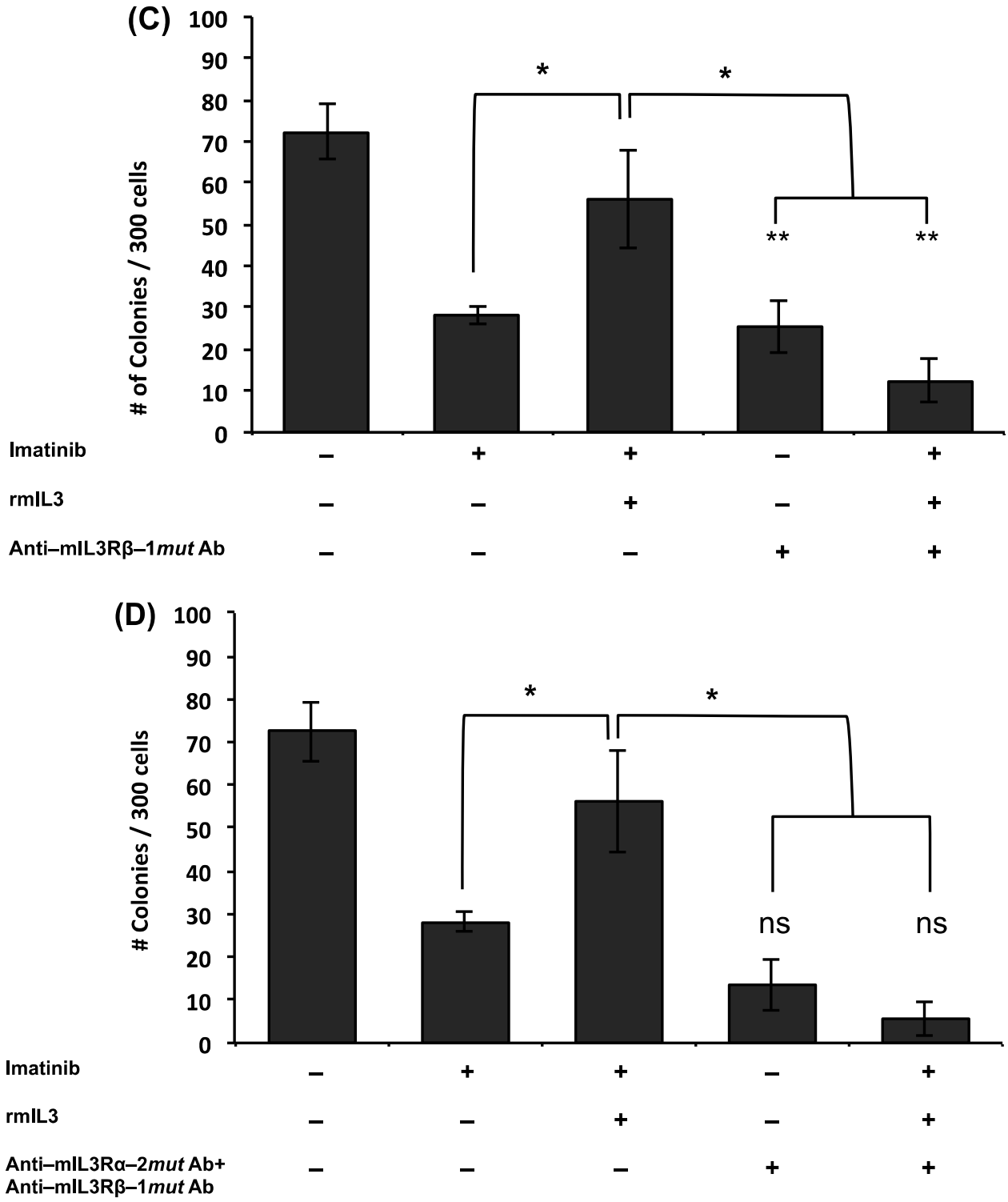
(C)
# of Colonies / 300 cells
100
90
80
70
60
50
40
30
20
10
0
*
*
**
**
Imatinib – + + – +
rmIL3 – – + – +
Anti–mIL3Rβ–1mut Ab – – – + +
(D)
Colonies / 300 cells
100
90
80
70
60
50
40
30
20
10
0
*
*
ns
ns
Imatinib – + + – +
rmIL3 – – + – +
Anti–mIL3Rα–2mut Ab+
Anti–mIL3Rβ–1mut Ab – – – + +

Figure 4.21. Anti–mIL3Rα–2*mut* antibody and anti–mIL3Rβ–1*mut* antibody impair the colony formation of CML cells individually and as co–treatment *in vitro.* CJ cells were incubated with antibodies individually or as co–treatment in the presence or absence of IL3 and imatinib at 37ºC for 48 hours. Three hundred cells were then washed and transferred to methylcellulose (in triplicates) and incubated at 37ºC for 10 – 14 days. (A) Direct inhibitory effect of antibodies on CML cell colony formation. CJ cells were treated with anti–mIL3Rα–2*mut* antibody, anti–mIL3Rβ–1*mut* antibody, or both antibodies as co-treatment in the absence of IL3 and imatinib $*P < 0.0001$; $***P = 0.0096$; (B) Anti–mIL3Rα–2*mut* antibody. CJ cells were treated with anti–mIL3Rα–2*mut* antibody in the presence or absence of IL3 and / or imatinib; $*P < 0.0001$; $**P = 0.0045$ (C) Anti–mIL3Rβ–1*mut* antibody. CJ cells were treated with anti–mIL3Rβ–1*mut* antibody in the presence or absence of IL3 and imatinib absence of IL3 and / or imatinib; $*P < 0.0001$; (D) Antibody Co–treatment. CJ cells were treated with anti–mIL3Rα–2*mut* antibody and anti–mIL3Rβ–1*mut* antibody co-treatment in the absence of IL3 and / or imatinib**;** $*P < 0.0001$; Y–axis represents the number of colonies per 300 cells. X–axis indicates various treatments. Bars represent the mean; error bars indicate Mean ± SD; Data analyzed with one-way ANOVA followed by Tukey *post hoc* test for multiple comparison; ns: not significant; Ab: antibody.

4.5.4 Anti–mIL3Rα–2*mut* antibody and mIL3Rβ–1*mut* antibody inhibit IL3–mediated signaling in CML cells

In order to test the ability of anti–mIL3Rα–2*mut* and anti–mIL3Rβ–1*mut* antibodies to block IL3 signaling in CML cells, we assessed tyrosine phosphorylation status of downstream STAT5 in response to IL3 and IL3 plus antibody treatment. STAT5 is one of the most specific readouts of IL3 downstream signaling cascade that indicates activation of JAK2 / STAT5 signaling pathways (Itoh et al., 1998). JAK2 is associated with multiple downstream signaling pathways activated in responses to IL3 stimulation and is required for mitogenesis. JAK / STAT pathway is mainly involved in anti-apoptotic events (O'Hare et al., 2011).To assess IL3–induced activation of STAT5, we serum–starved CJ cells and incubated them with 100 – 400 nM of anti–mIL3Rα–2*mut* and / or anti–mIL3Rβ–1*mut* antibody and then stimulated with 10 nM rmIL3 for 20 minutes at 37ºC. Western blot analysis showed a significant increase in tyrosine phosphorylation after exogenous IL3 stimulation alone (Figure 4.22A–B). However, treatment of CJ cells with anti–mIL3Rα–2*mut* antibody inhibited IL3–dependent STAT5 tyrosine phosphorylation (Figure 4.22A). There was only a slight decrease in STAT5 tyrosine phosphorylation when the dose of antibody was increased from 100 to 400 nM (Figure 4.22A). In addition, treatment of CJ cells with anti–mIL3Rβ–1*mut* antibody inhibited the IL3–dependent STAT5 tyrosine phosphorylation (Figure 4.22A) with no significant difference in the level of inhibition from 100 to 400 nM of anti–mIL3Rβ–1*mut* antibody (Figure 4.22A). This finding may suggest a threshold inhibition at the lowest dose tested.

Co–treatment of CJ cells with anti–mIL3Rα–2*mut* antibody and anti–mIL3Rβ–1*mut* antibody significantly inhibited the IL3–dependent STAT5 tyrosine phosphorylation in CJ cells (Figure 4.22B), and this inhibition was not further affected by escalating the dose of antibodies from 100 to 200 nM (Figure 4.22B). Furthermore, based on densitometry analysis, there was no difference in the degree of inhibition of STAT5 tyrosine phosphorylation when CJ cells treated with either of antibodies alone or in combination (data not shown). Together, our findings suggest that anti–mIL3Rα–2*mut* and anti–mIL3Rβ–1*mut* antibodies block IL3 signaling cascades, which was consistent with the observed effects on viability, apoptosis, and colony formation analyses that were mediated through blocking IL3-R and its downstream signaling pathways.

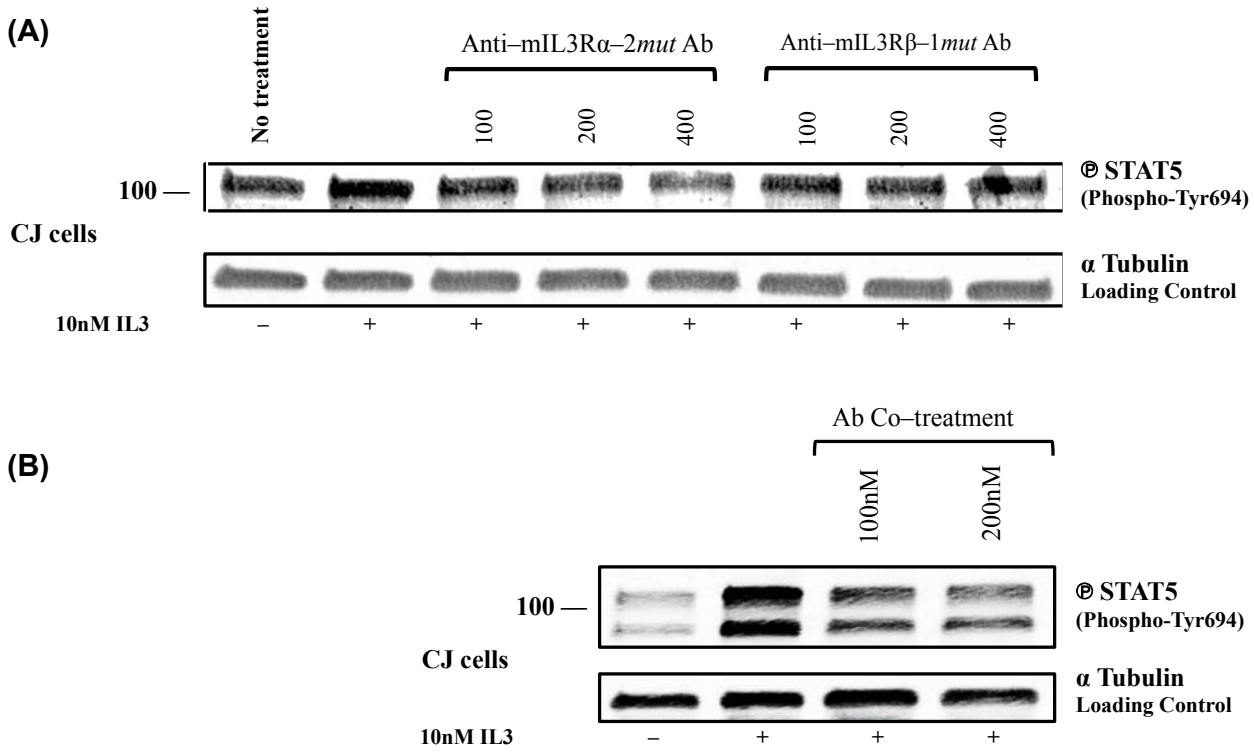

Figure 4.22. Anti–mIL3Rα–2*mut* and anti–mIL3Rβ–1*mut* antibodies inhibited IL3–induced phosphorylation of STAT5 in CJ cells individually or as co–treatment. CJ cells were serum starved for 5 hours and then incubated with anti–mIL3Rα–2*mut* or anti–mIL3Rβ–1*mut* antibody with 100, 200, and 400nM doses, or co–treated with both antibodies (100 and 200 nM) for 10 minutes on ice. Cells were then stimulated with 10 nM rmIL3 for 20 minutes at 37ºC, rinsed with cold PBS, and lysed. STAT5 tyrosine phosphorylation was assessed by Western blotting (A) Anti–mIL3Rα–2*mut* or anti–mIL3Rβ–1*mut* antibody as single treatment. (B) Co–treatment with Anti–mIL3Rα–2*mut* and anti–mIL3Rβ–1*mut* antibodies. The same blots were cut and used for loading control (α–Tubulin antibody). The blots were trimmed to remove irrelevant bands.

4.5.5 Engraftment of anti–mIL3Rα–2*mut* antibody and anti–mIL3Rβ–1*mut* antibody–treated BC–CML cells increases disease latency

In order to further assess the antibodyies, CJ cells were treated with antibodies (single or co–treatment) in the presence or absence of imatinib and engrafted into sub–lethally irradiated mice (6 Gy, 24 hours prior to transplantation) via intravenous injection. The number of cells transplanted per mouse was normalized based on 100,000 control (untreated) CJ cells per mouse. The final cell number transplanted per mouse is listed in Table 4.11.

Treatments	# Transplanted cells / Mouse
CJ Cells (No treatment)	**100000**
Imatinib	**18000**
Anti–mIL3Rα–2*mut* mAb	**90900**
Anti–mIL3Rα–2*mut* mAb + Imatinib	**18600**
Anti–mIL3Rβ–1*mut* mAb	**91600**
Anti–mIL3Rβ–1*mut* mAb + Imatinib	**14700**
Antibody co-treatment (Anti–mIL3Rα–2*mut* + Anti–mIL3Rβ–1*mut* mAb)	**89200**
Antibody co-treatment + Imatinib (Anti–mIL3Rα–2*mut* + Anti–mIL3Rβ–1*mut* mAb + Imatinib)	**18300**

Table 4.10 Number of cells transplanted into mice: engraftment of antibody–treated BC–CML cells. Following *in vitro* incubation of CJ cells with antibody (single or co–treatment) and / or imatinib at 37ºC for 48 hours, the number of cells was calculated based on the dilution ratio of control (untreated) cells at final number of 100,000 cells per mouse. The numbers represent the number of cells transplanted per mouse for each treatment; N = 5 mice per treatment group.

Anti–mIL3Rα–2*mut* antibody or anti–mIL3Rβ–1*mut* antibody, as single or combination treatments, to determine whether the antibodies can directly target BC–CMLs and inhibit their engraftment in bone marrow of C57BL/6 mice and / or alter the disease latency. Anti–mIL3Rα–2*mut* antibody–treated cells engrafted into mice caused significantly increased disease latency ($P = 0.0027$) with median mouse survival of 38 days compared to 16.5 days in mice that received control untreated cells (Figure 4.23A). Anti–mIL3Rβ–1*mut* antibody treatment and engraftment of CJ cells into mice also lead to a significantly increased mouse survival ($P = 0.0383$; Figure 4.23B); however, the mice did not survive beyond 32 days. Moreover, mouse survival in this group was significantly lower than anti–mIL3Rα–2*mut* antibody group ($P = 0.0056$; Figure 4.23D). Engraftment of CJ cells co–treated with anti–mIL3Rα–2*mut* and anti–mIL3Rβ–1*mut* antibodies showed an increase in disease latency ($P = 0.0294$; Figure 4.23C), while the median mouse survival was comparable to that of anti–mIL3Rβ–1*mut* antibody group (Figure 4.23D). This finding might be in part due to insufficient dose of antibodies in antibody co–treatment group since we used half the concentration of each antibody used for antibody co-treatment.

Engraftment CJ cells treated with imatinib revealed that imatinib does not improve mouse survival ($P = 0.0715$; Figure 4.24A). Interestingly, engraftment of CJ cells treated with anti–mIL3Rα–2*mut* antibody and imatinib caused a significant increase in mouse survival ($P = 0.0052$; Figure 4.24B). However, cells treated with imatinib in the presence of anti–mIL3Rβ–1*mut* antibodies or antibody co–treatment did not improve mouse survival upon engraftment ($P = 0.2499$ and $P = 0.0596$, respectively, data not shown).

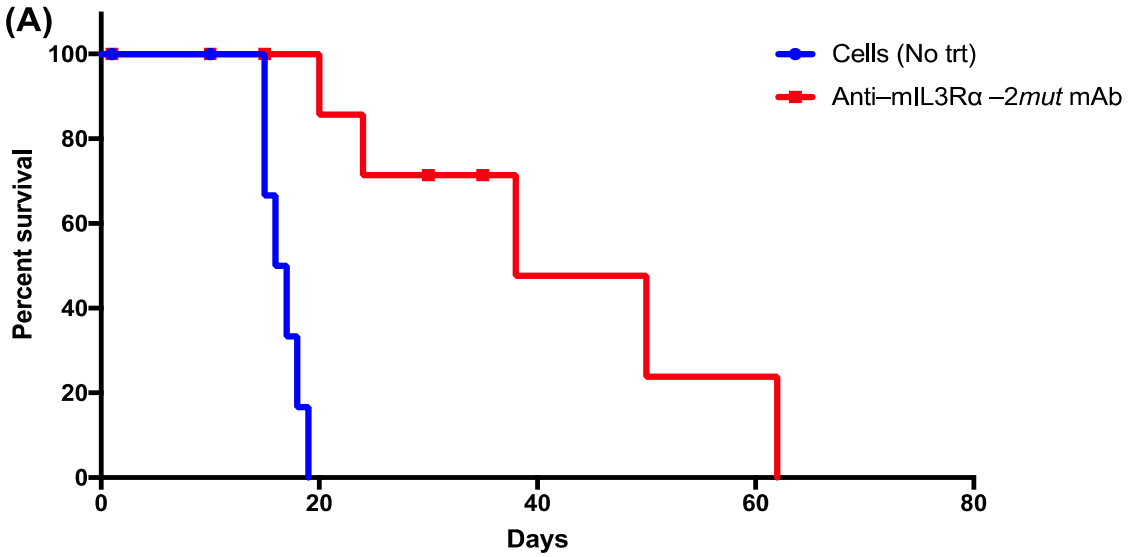
(A)
Percent survival
100
80
60
40
20
0
0
20
40
60
80
Days
Cells (No trt)
Anti–mIL3Rα –2*mut* mAb

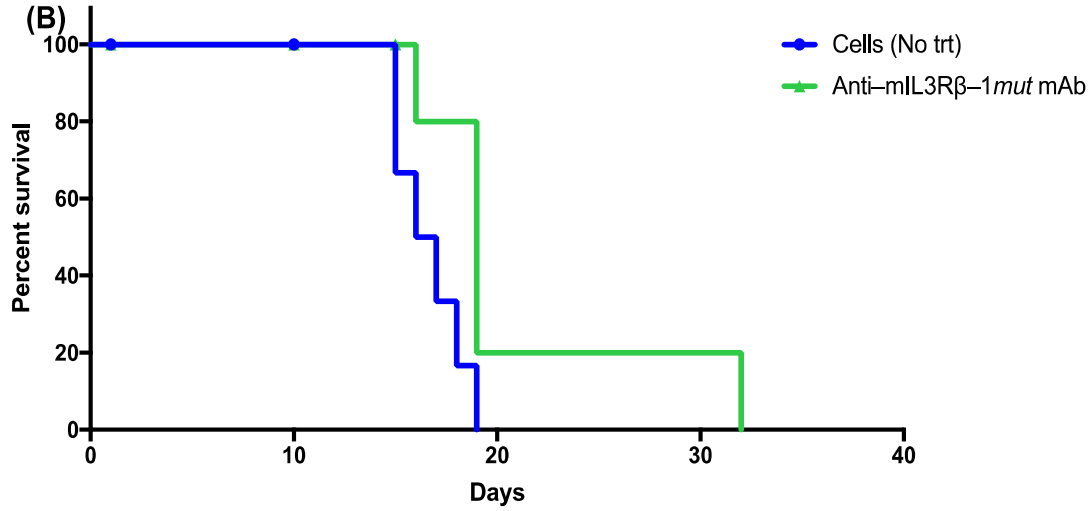
(B)
Percent survival
100
80
60
40
20
0
0
10
20
30
40
Days
Cells (No trt)
Anti–mIL3Rβ–1*mut* mAb

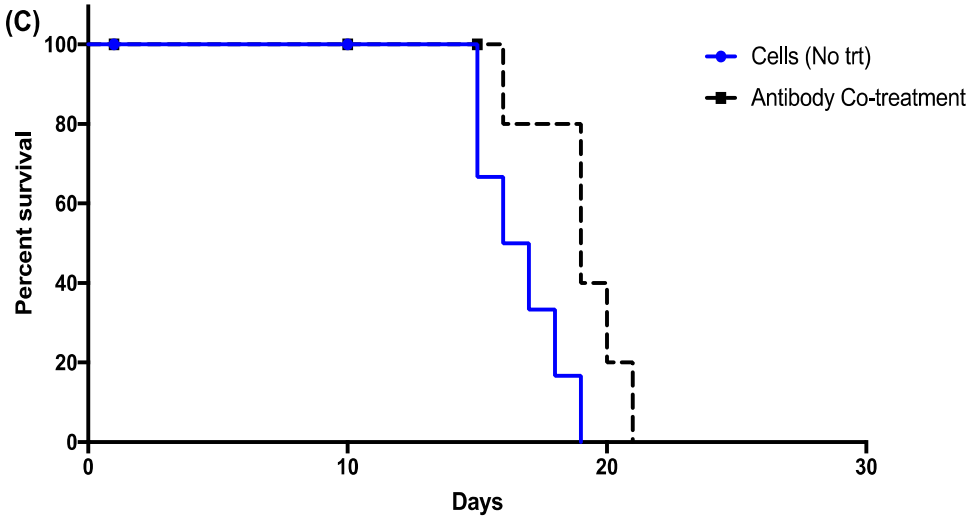
(C)
Percent survival
100
80
60
40
20
0
0
10
20
30
Days
Cells (No trt)
Antibody Co-treatment

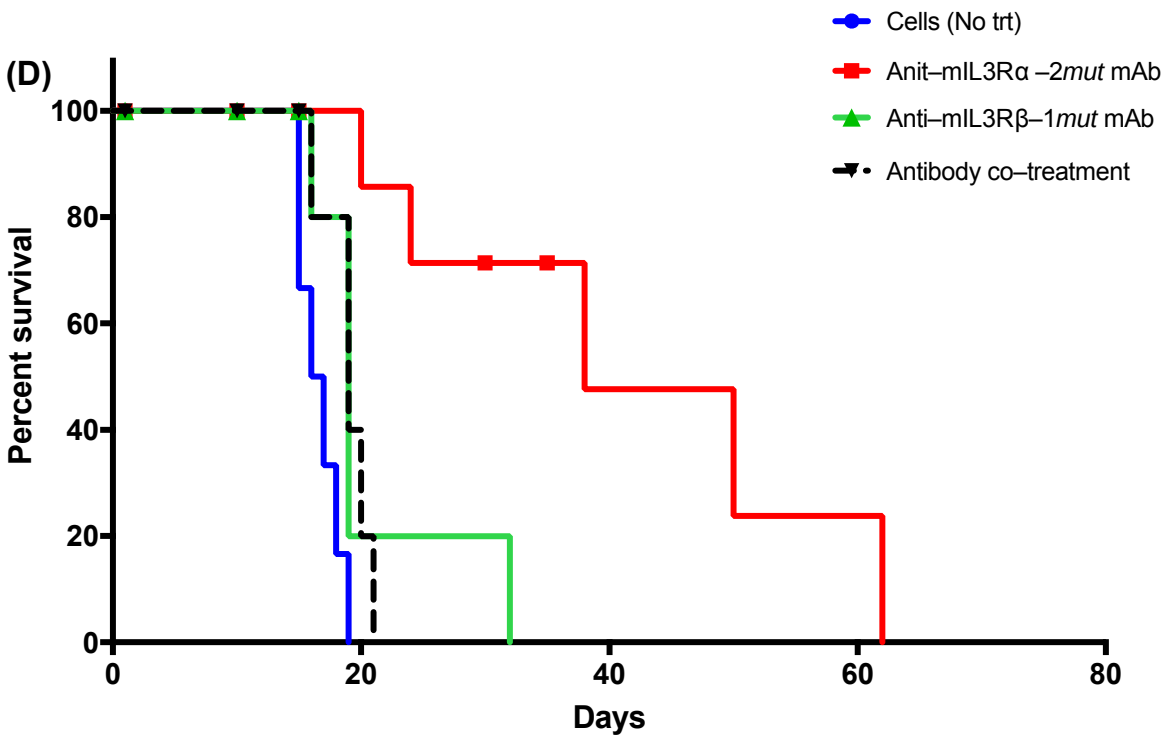

Figure 4.23. Kaplan–Meier survival curve of mice engrafted with antibody–treated BC–CML cells. CML cells were treated with antibody (single or co–treatment) at 37ºC for 48 hours and transplanted into sub–lethally irradiated C57BL/6 mice. Survival curves were compared by log rank test (N = 5 mice per treatment group). (A) Engraftment of anti–mIL3Rα–2*mut* antibody–treated cells. Median survival days of 16.5 in control group versus 38 days for antibody–treated mice; P = 0.0027; (B) Engraftment of anti–mIL3Rβ–1*mut* antibody–treated cells. Median survival of 19 days compared to 16.5 days in control (not treated); P = 0.0383; (C) Engraftment cells co–treated with anti–mIL3Rα–2*mut* antibody and anti–mIL3Rβ–1*mut* antibody. Median survival of 19 days compared to 16 days in control group; P 0.0294. (D) Engraftment of cells treated with single antibody versus antibody co–treatment. P = 0.0014; X–axis numbers denote the percentage of mouse survival. Y–axis indicates days of survival; N = 5 mice per treatment group; Significance of difference for Kaplan Meier graphs was evaluated by log–rank (Mantel–Cox) test. No trt: No treatment.

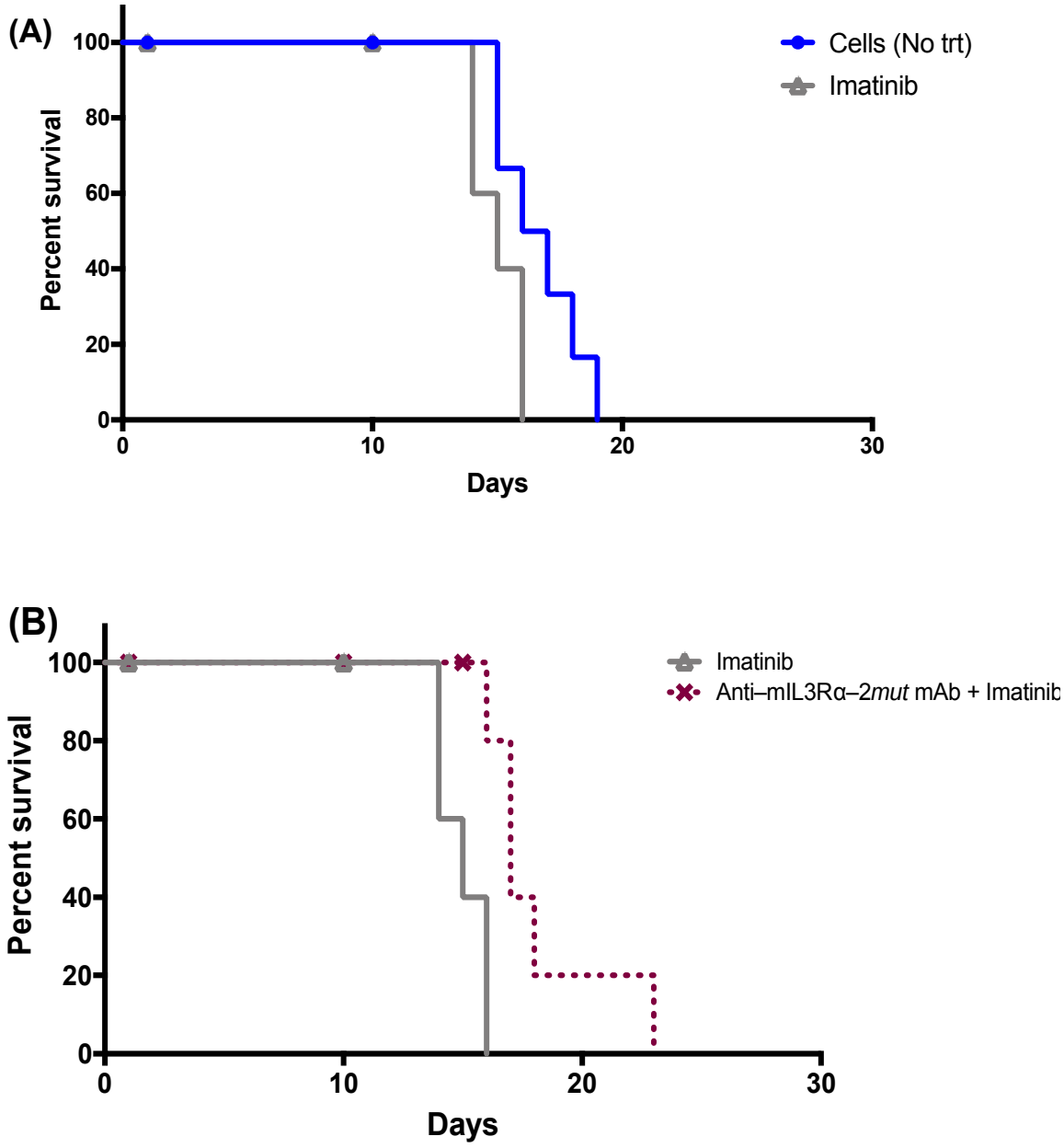

Figure 4.24. Kaplan–Meier survival curve of mice engrafted with BC–CML cells treated with imatinib in the presence or absence of anti–mIL3Rα–2*mut* antibody. (A) Engraftment of imatinib–treated cells. CJ cells were incubated with imatinib *in vitro* at 37ºC for 48 hours and transplanted intravenously into sub–lethally irradiated mice; $P = 0.0715$; Median survival of 16.5 days for imatinib and 16 days for control (No trt); (B) Engraftment of cells treated with anti–mIL3Rα–2*mut* antibody plus imatinib. Cells were incubated with imatinib in the presence or absence of anti–mIL3Rα–2*mut* antibody and engrafted intravenously into mice. $P = 0.0052$; X–axis numbers denote the percentage of mouse survival. Y–axis indicates days of survival; n = 5 mice per treatment group; Significance of difference for Kaplan Meier graphs was evaluated by log–rank (Mantel–Cox) test. No trt: No treatment.

In conclusion, our findings from multiple *in vitro* assays and engraftment tests suggested that anti–mIL3Rα–2*mut* antibody and anti–mIL3Rβ–1*mut* antibody generated in this project may potentially eliminate CML leukemic stem cells by targeting IL3R and inhibition of IL3 pathway. Clinically, IL3–overexpression is shown to be associated with greater blast cell count and poor diagnosis (Graf et al., 2004; U Testa et al., 2004), thus selective targeted therapy may provide clinical applications in AML and CML patients. Besides targeting IL3R, anti–mIL3Rα–2*mut* and anti–mIL3Rβ–1*mut* antibodies may offer innate immunity–activating properties for the host immune system and induction of CML or AML cell killing as single or combinatorial treatment with tyrosine kinase inhibitors (TKIs). Therefore, anti–mIL3Rα–2*mut* and anti–mIL3Rβ–1*mut* antibodies may be candidates for pre–clinical testing as therapeutics for selective targeting of CD123 and CD131 in AML and CML cells individually or as co–drugs.

4.6. Generation and characterization of novel anti–mIL3R–α and anti–mIL3R–β bivalent and bispecific antibody fragments (bi–FABs)

The success of anti–mIL3Rα–2*mut* and mIL3Rβ–1*mut* antibodies in blocking IL3–induced imatinib suppression encouraged us to use the antibodies to develop novel antibody fragments (Fabs) with dual specificity for IL3Rα and IL3Rβ subunits. Generation of a bispecific Fab by bridging antagonist–antagonist pairing (Mayes, Hance, & Hoos, 2018) of anti–mIL3Rα–2*mut* Fab and anti–mIL3Rβ–1*mut* Fab may lead to simultaneous engagement of both IL3R subunits and more potent blockade of IL3–mediated innate drug resistance. Moreover, despite the antagonistic phenotype of parental IgG, we recognize that bringing two distinct subunits of IL3R together may allow recruitment of more than one receptor monomer resulting more potent antagonist effect or co-stimulatory receptor heterodimerization activation and super cluster receptor formation (Mayes et al., 2018).

Furthermore, we also generated bivalent Fabs with two arms targeting either mIL3Rα or mIL3Rβ. Bivalent Fabs provide new avenues to study the efficacy of targeted therapy or diagnostics lacking the Fc region as the core effector function of antibodies. We investigated the *in vitro* function of a bispecific Fab and compared it to bivalent Fabs targeting IL3Rα or IL3Rβ subunits. In the clinical context, the dual specificity, smaller size compared to full size antibody, and lack of Fc portion might provide advantages to more effective / potent targeting of leukemic stem cells for therapeutic or diagnostic purposes.

4.6.1 Generation of bivalent and bispecific Fabs using SpyCatcher—SpyTag System

SpyCatcher—SpyTag system (Zakeri et al., 2012) was used to create a robust irreversible covalent bond between anti–mIL3Rα–2*mut* monovalent Fab and anti–mIL3Rβ–1*mut* monovalent Fab (mono–Fabs). In order to limit immunogenicity (Reddington & Howarth, 2015; Zakeri et al., 2012), we used a N–terminus truncated form of SpyCatcher herein referred as “SpyCatcherΔN”. The SpyTag or SpyCatcher were added to anti–mIL3Rα–2*mut* and anti–mIL3Rβ–1*mut* phage Fab clones (Figure 4.26A-C). SpyCatcherΔN / SpyTag–mono–Fabs were then expressed in *E. coli* and purified by protein L affinity chromatography. The reaction conditions for the SpyTag–mono–Fab and SpyCatcherΔN–mono–Fab were optimized under diverse pH, salt, and buffer types (Zakeri et al., 2012). Various protease inhibitors and considerable troubleshooting

was necessary to determine the precise conditions to avoid denaturation and / or aggregation (data now shown). The SpyTag–SpyCatcher reaction was optimal with a 2:1 ratio of mono–Fab–SpyTag to mono–Fab–SpyCatcherΔN. Optimal reaction conditions for attachment of mono–Fab–SpyTag to mono–Fab–SpyCatcher was citrate phosphate buffer pH 7.0 with incubation at 4°C overnight (Alam et al., 2017).

4.6.2 Purification and *in vitro* validation of bivalent and bispecific Fabs

Purified mono–Fabs were dialyzed and concentrated (Section 3.2.17). In order to facilitate bivalent and bispecific Fab purification, the SpyCatcherΔN was fused to a poly Histidine (6xHis) tag at its C–terminus. Following the SpyTag—SpyCatcher reaction, the resulting bivalent or bispecific Fabs was purified by immobilized metal affinity chromatography (IMAC) to capture the bi–Fabs via Histidine–tagged SpyCatcherΔN, allowing removal of excessive SpyTag–mono–Fab components (Figure 4.26F). Some degradation of the SpyCatcher–fused Fabs was observed. We used two approaches to remove these degradation products: (i) purification using His–Tag was performed to remove unfused mono–Fab and (ii) spin filter columns were used to remove low molecular weight unfused SpyCatcher.

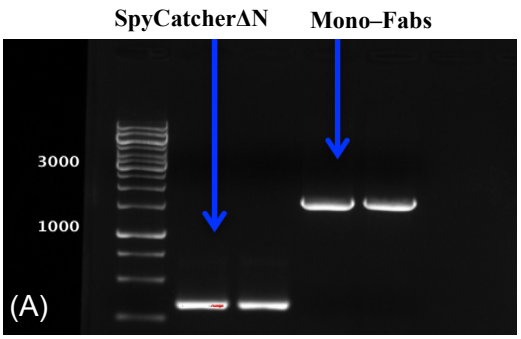

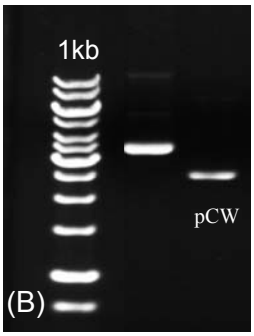

— SpyCatcherΔN–pCW

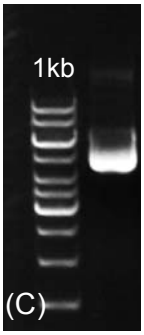

— Anti–mIL3Rα–2mut—SpyCatcherΔN–pCW

(D)

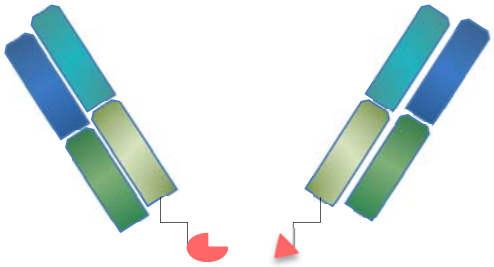

Monovalent Fab–SpyTag

Monovalent Fab–SpyCatcher

(E)

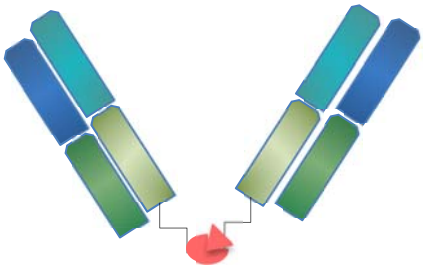

Bi-Fab

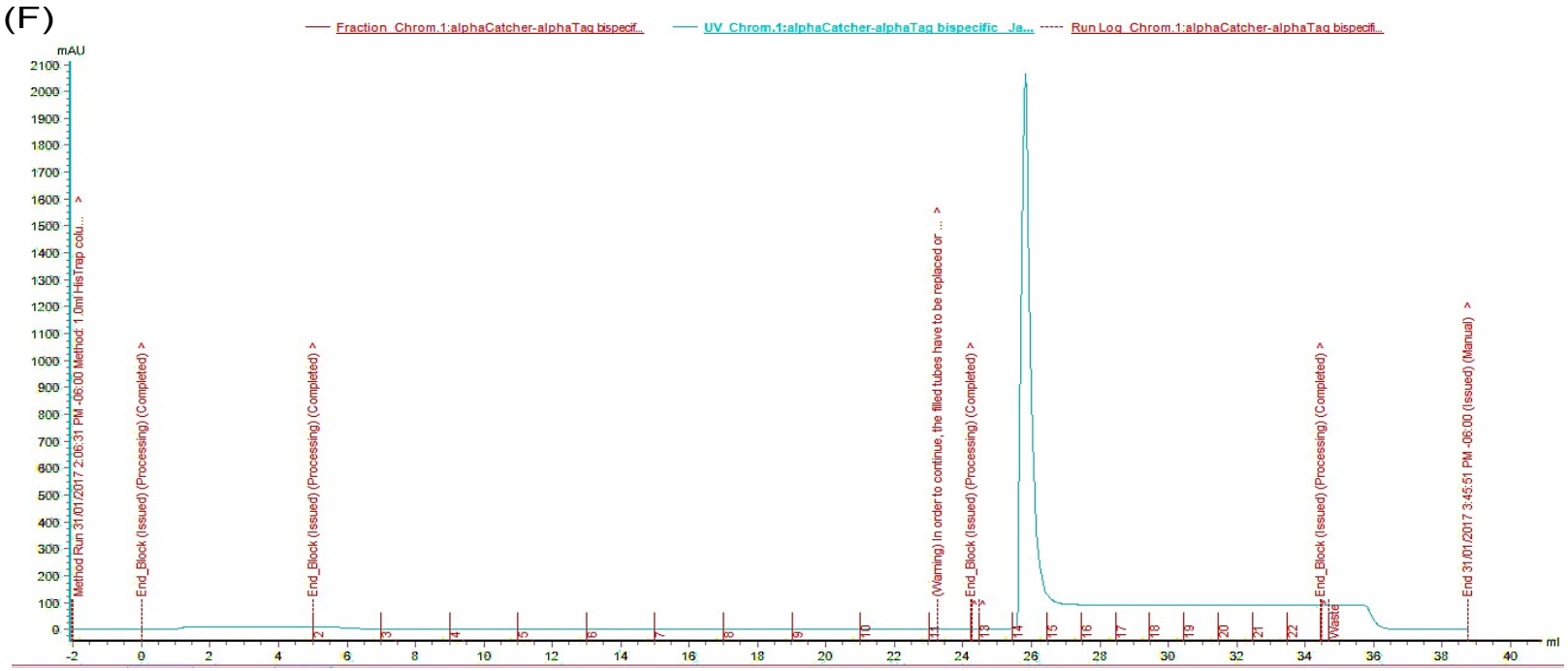

Figure 4.26. Generation of bivalent / bispecific Fab using SpyCatcher—SpyTag system. (A–C) Generation of mono–Fabs. SpyCatcherΔN and mono–Fabs were PCR–amplified (A). The amplified SpyCatcherΔN inserts were cloned into pCW expression vector by Gibson Assembly (B). Anti–mIL3Rα–2*mut* or mIL3Rβ–1*mut* mono–Fab were cloned into SpyCatcherΔN–pCW (C) or SpyTag–pCW backbone (not shown). The resulting mono–Fab–SpyCatcherΔN or mono–Fab–SpyTag were transformed into BL–21 cells and purified by protein L affinity chromatography. (D–F) Generation and purification of bi–Fabs. (D–E) A Schematic view of SpyCatcher—SpyTag covalent bond. The reaction was performed at the ratio of 2:1 mono–Fab–SpyTag to mono–Fab–SpyCatcher in citrate phosphate buffer pH 7.0, at 4°C overnight. (F) Bi–Fabs were purified by affinity chromatography using His–Tag purification to remove the excess SpyTag–mono–Fabs. Only a single eluted peak was observed and the corresponding fractions were collected to contain 95% pure bi–Fabs. X–axis represents the volume (mL) for the chromatography Run Log. Y–axis denotes the milli–absorbance unit (mAU) measured by UV–visible spectroscopy.

Altogether, we generated a bispecific Fab and two bivalent Fabs using SpyCatcher—SpyTag reaction:

i) Bispecific Fab: Anti–mIL3Rβ–1*mut*-SpyCatcherΔN–SpyTag-Anti–mIL3Rα–2*mut* herein labelled as "IL3RβΔN–α"
ii) Bivalent Fab: Anti–mIL3Rα–2*mut*-SpyCatcherΔN–SpyTag-Anti–mIL3Rα–2*mut* herein labelled as "IL3RαΔN–α"
iii) Bivalent Fab: Anti–mIL3Rβ–1mut-SpyCatcherΔN–SpyTag-Anti–mIL3Rβ–1*mut* herein labelled as "IL3RβΔN–β"

Mono, bivalent, and bispecific Fabs were validated for purity and size using an automated electrophoresis system with a High Sensitivity Protein–250 kit, as well as, SDS–PAGE protein gels under reducing conditions. The heavy chain connected to SpyCatcherΔN was ~ 63 kDa and the individual light chains were ~ 25 kDa (Figure 4.27A–B).

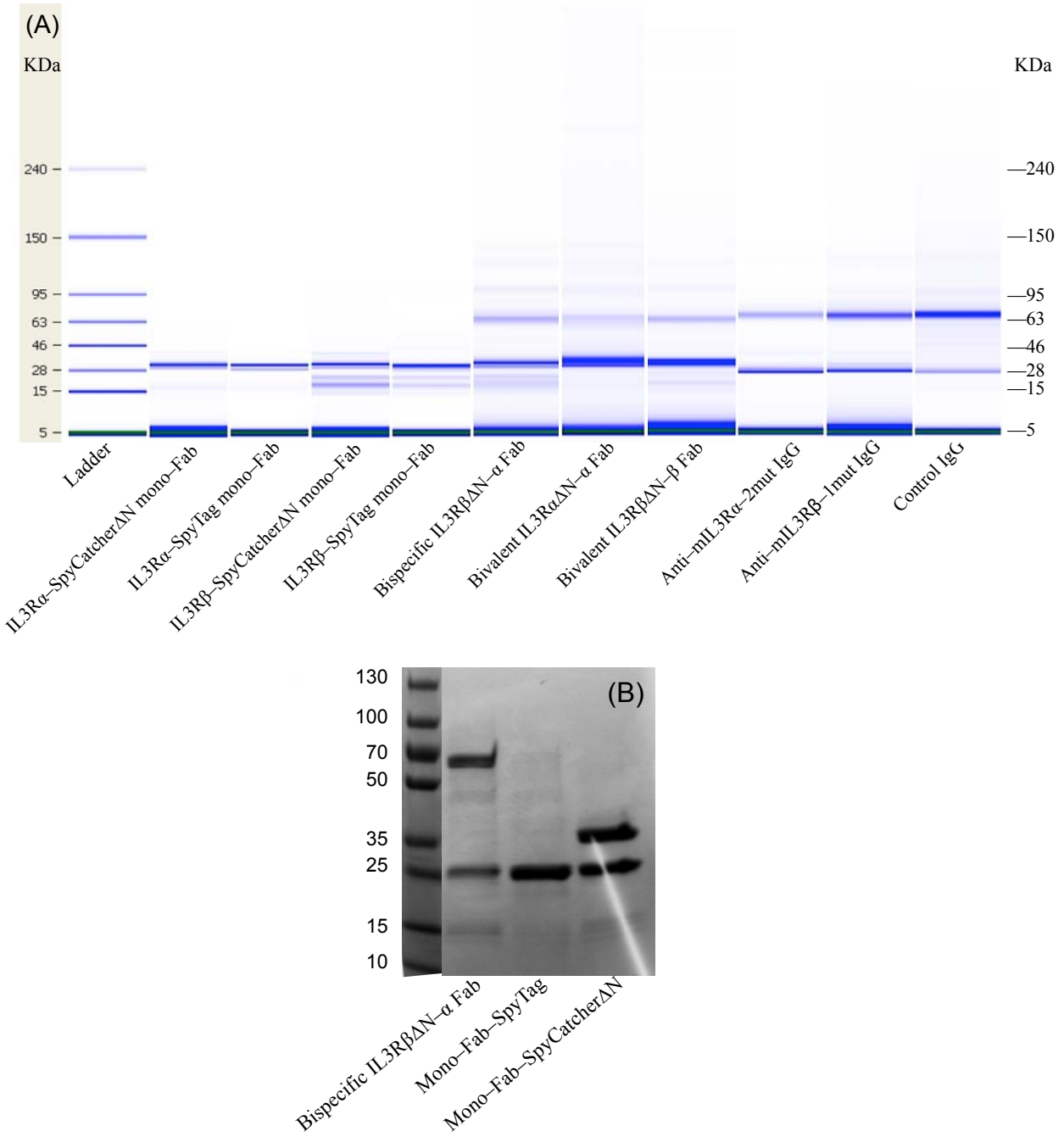

Figure 4.27. Testing the size and purity of mono, bivalent, and bispecific Fabs. (A) Size and purity was tested by automated electrophoresis under reducing condition with protein 250 high sensitivity kit. Lane 1 – 4: Mono–Fabs: ~25–30 kDa for light or heavy chains under reducing condition; Instability in the SpyCatcher–fused entities was observed in the mono–Fab (i.e. Lane 3: IL3Rβ–SpyCatcherΔN mono–Fab). Lane 5–7: Bi–Fabs: band size of ~25 kDa for individual light chains and ~63 kDa for heavy chains fused to SpyCatcherΔN–SpyTag. Lane 8–10: parental IgGs and control antibody (B) SDS protein gel also confirmed the size and purity of IL3RβΔN–α bispecific Fab and its corresponding SpyTag / SpyCatcher mono–Fabs under reducing conditions.

4.6.3 Bispecific and bivalent Fabs bind Fc–fused IL3Rα and IL3Rβ targets with nanomolar dissociation constant

Biolayer Interferometry (BLI) was used to determine kinetics for the Fab / target interaction. Fc–fused targets were immobilized on an anti–human IgG Fc Capture (AHC) biosensors and then dipped into mono–Fab or bi–Fab analyte ranging 0 – 200 nM in order to generate multiple association curves. Biosensors were then moved to buffer alone to allow dissociation to take place. The dissociation constant (K_D) of mono–Fabs was first measured in order to determine whether bivalent and bispecific Fabs have better affinity to the target.

K_{DS} of anti–mIL3Rα–2mut–SpyTag and anti–mIL3Rβ–SpyCatcherΔN mono–Fabs for Fc–fused IL3Rα or IL3Rβ target, respectively were 3.26E–09 M and 3.04E–09 M, (Table 4.11). However, anti–mIL3Rβ mono–Fab / target interaction did not yield a tight fit based on the value of full R^2 (Table 4.11). To determine the affinity of IL3RαΔN–α and IL3RβΔN–β bivalent Fabs to the target, the curve–fitting algorithm was adjusted for a 1:2 binding scenario (bivalent analyte) and the K_{DS} were calculated as 8.07E–10 M for IL3RαΔN–α bivalent Fab binding to IL3Rα, and 1.31E–09 M for IL3RβΔN–β bivalent Fab binding to IL3Rβ target. Furthermore, the binding affinity of the bispecific IL3RβΔN–α Fab was tested for binding to each cognate receptor using global curve–fitting algorithm adjusted to 1:1 binding and revealed nanomolar dissociation of 8.07E–10 M and 2.71E–09 M for Fc–fused mIL3Rα and mIL3Rβ target proteins, respectively.

Taken together, IL3RαΔN–α bivalent Fab showed enhanced binding affinity to the target with about 4-fold lower dissociation constant to IL3Rα target as compared with IL3Rα mono–Fab. IL3RβΔN–β showed K_D of approximately 2-fold higher than IL3Rβ mono–Fab, however, the data analysis demonstrated a better curve fitting for the bivalent Fab based on the value of full R^2 (Table 4.11; Figure 4.28). IL3RβΔN–α bispecific Fab demonstrated approximately 3–fold lower K_D to the IL3Rα target than IL3Rα mono–Fab and comparable affinity to IL3Rβ target as compared with IL3Rβ mono–Fab.

Antibody Fragments / Antibodies	Binding Kinetics by BLI				
	k_{on} (M^{-1} S^{-1})	k_{off} (S^{-1})	KD (nM)	Target Protein	Full R^2
IL3Rα mono–Fab	2.89E+05	9.42E-04	3.26	mIL3Rα–Fc	0.993544
IL3Rβ mono–Fab	8.19E+05	2.49E-03	3.04	mIL3Rβ –Fc	0.867258
IL3R αΔN–α bi–Fab	5.39E+05	4.35E-04	0.807	mIL3Rα–Fc	0.999052
IL3R βΔN–α bi–Fab	9.86E+05	7.96E-04	0.807	mIL3Rα–Fc	0.998733
IL3R βΔN–β bi–Fab	6.91E+05	9.03E-04	1.31	mIL3Rβ –Fc	0.997805
IL3R βΔN–α bi–Fab	3.84E+05	1.04E-03	2.71	mIL3Rβ –Fc	0.995462
Anti–mIL3Rα–2mut Ab	1.11E+05	5.36E–04	4.82	mIL3Rα–Fc	0.9949
Anti–mIL3Rβ–1mut Ab	7.31E+04	5.14E–04	7.04	mIL3Rβ –Fc	0.9982

Table 4.11 Kinetic characterization of mono–Fabs, bivalent and bispecific Fabs. Octet RED384 (ForteBio) was used for biolayer interferometry to determine the kinetics of binding between purified antibodies and targets. Octet Data Analysis 7.1 (ForteBio) software was used in order to perform global fitting model based upon multiple target concentrations ranging from 0 –200 nM. The dissociation constant, K_D, was measured as the ratio of k_{off}/ k_{on} from non–linear fitting. The curve fitting success was confirmed by the value of full R^2.

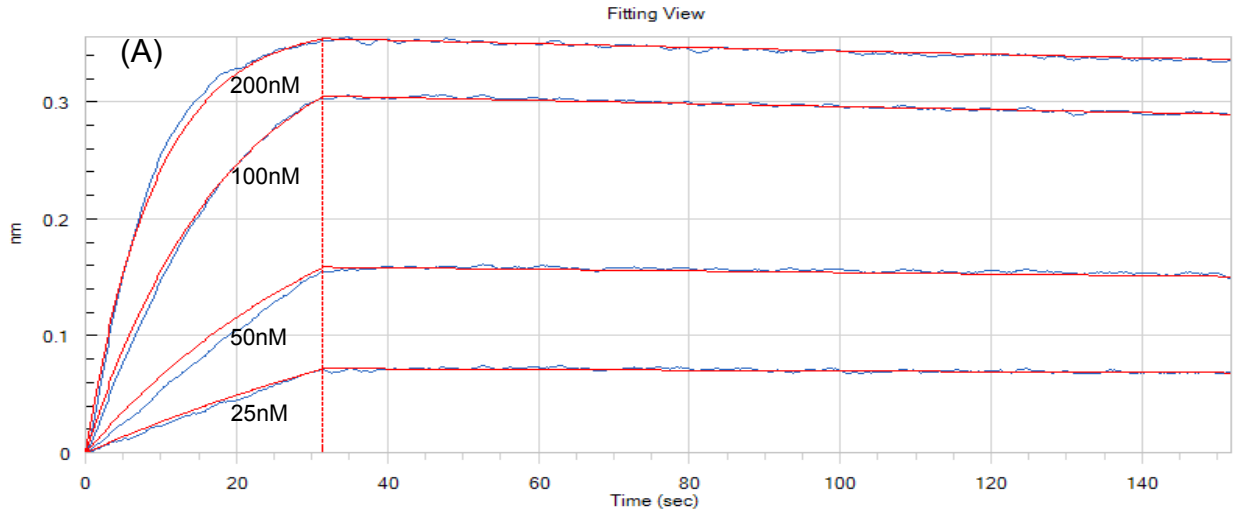
Fitting View
(A)
200nM
100nM
50nM
25nM
nm
0
0.1
0.2
0.3
0
20
40
60
80
100
120
140
Time (sec)

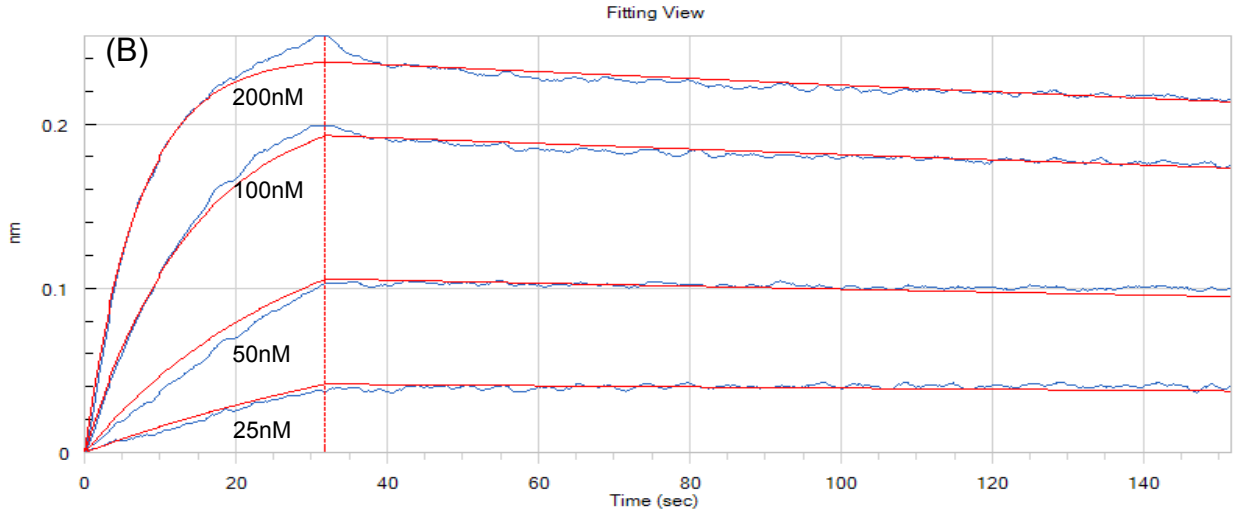
Fitting View
(B)
200nM
100nM
50nM
25nM
nm
0
0.1
0.2
0
20
40
60
80
100
120
140
Time (sec)

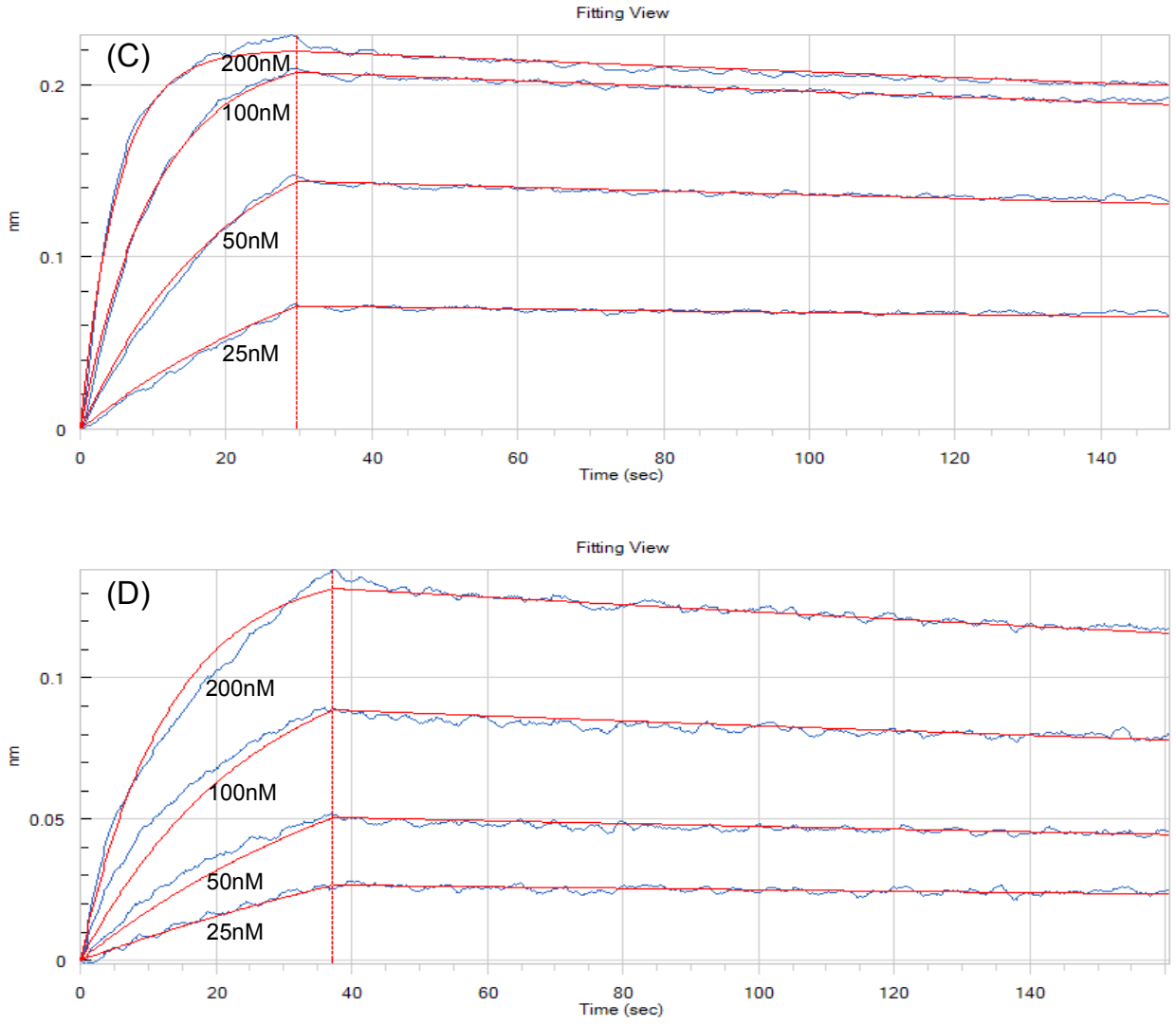

Figure 4.28. Kinetic analysis of bivalent and bispecific Fabs to cognitive receptors. Fc–fused IL3Rα and IL3Rβ targets were immobilized on anti–human IgG Fc Capture (AHC) biosensors. The biosensors were dipped into multiple concentrations of Fabs (0, 25, 50, 100, and 200 nM) to allow global curve–fitting of multiple curves with the lowest statistical residuals. The association of Fabs to the target was closely monitored to reach 0.15 – 0.35 optical thickness to prevent over–saturation of biosensors. Biosensors were then moved to buffer alone to allow dissociation to take place. (A, B) Bivalent Fabs. The binding affinity of IL3RαΔN–α (A) and IL3βΔN– β (B) was determined by global curve–fitting with a 1:2 bivalent analyte binding model (red traces). (C, D) Bispecific Fab. The binding affinity of IL3βΔN–α bispecific Fab to targets were analyzed by global curve–fitting with 1:1 binding model (red traces). The K_{DS} were measured for IL3Rα target (C) and IL3β target (D). Y–axis indicates optical thickness (nm). X–axis denotes time in seconds. nm: nanometer; sec: seconds.

4.6.4 Bivalent and bispecific Fabs bind murine CML cells *in vitro*

In order to show that bivalent or bispecific Fabs bind to endogenously expressed IL3R on CML cell lines, we analyzed their interaction with IL3R positive CML cell line (CJ cells) using flow cytometry. The mean fluorescence intensity (MFI) was analyzed on a 5–decade log scale (1–100000) relative to anti–MBP negative control antibody and secondary antibody. Bivalent IL3RαΔN–α and IL3RβΔN–β Fabs bound to CJ cells slightly lower than that of parental IgGs (Figure 4.29A–B). The MFI for IL3RαΔN–α bivalent Fab binding to CJ cells was approximately 5700 as compared to about 8000 for anti–IL3Rα IgG. The MFI for IL3RβΔN–β bivalent Fab binding to CJ was measured approximately 2100 as compared to the 3000 for parental anti–IL3Rβ IgG (Figure 4.29A–B). Interestingly, the bispecific IL3RβΔN–α Fab showed comparable or greater binding to the CJ cells than the corresponding anti–mIL3Rα–2*mut* or –mIL3Rβ–1*mut* IgGs, respectively (Figure 4.29C). The MFI for IL3RβΔN–α bispecific Fab binding to CJ cells was approximately 7300 as compared to 8000 for parental anti–IL3Rα–2*mut* IgG and approximately 3000 for the parental anti–IL3Rβ–1*mut* IgG. The MFI for IL3RβΔN–β bivalent Fab binding to CJ was measured approximately 2100 as compared to the 3000 for parental anti–IL3Rβ–1*mut* IgG (Figure 4.C). We next investigated the binding of IL3RβΔN–α bispecific Fab compared to each bivalent Fab. When analyzed at 100 nM, IL3RβΔN–α bispecific Fab showed higher binding to CJ cells than both IL3RαΔN–α and IL3RβΔN–β bivalent Fabs (Figure 4.29D), suggesting that engaging both IL3Rα and IL3Rβ subunits at once may be advantageous to bivalent binding to one or the other.

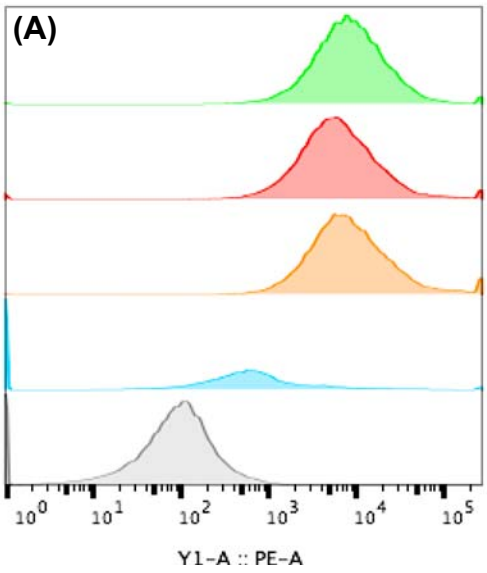

Treatment	M FI
mIL3R alpha-2mut Ab	8038
alpha-alpha Bifab	5767
alpha monoFab	7494
2nd Ab	444
Unstained cells	*83,6*

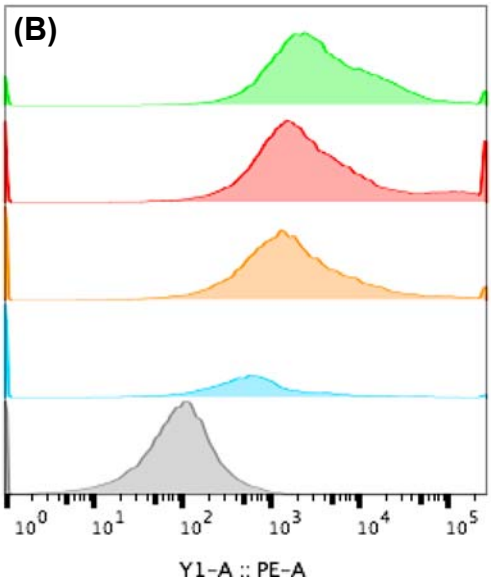

Treatment	M FI
mIL3R beta-1mut Ab	2996
beta-beta Bifab	2117
beta monoFab	1378
2nd Ab	444
Unstained cells	83,6

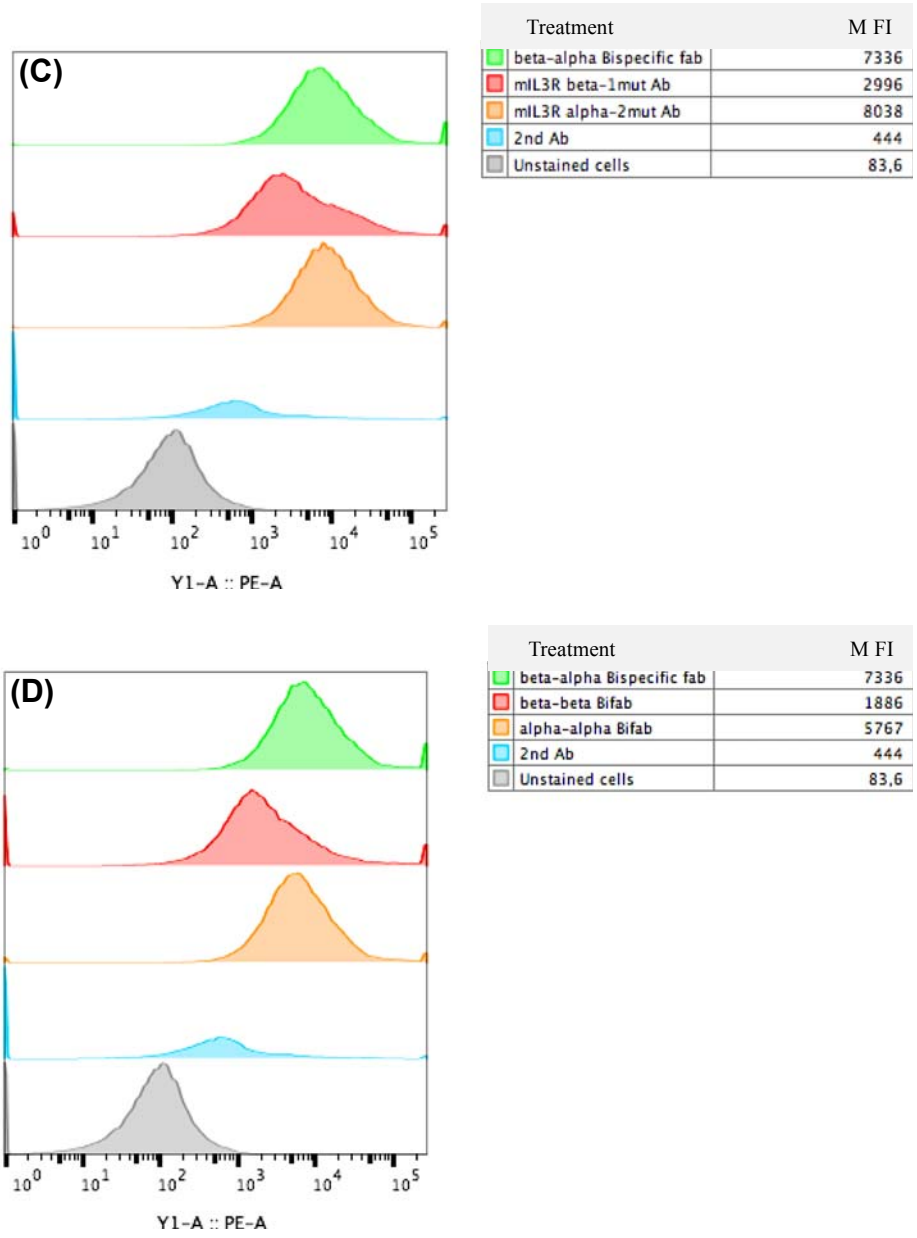

Figure 4.29. Mono–Fabs, bivalent Fabs, and bispecific Fabs bind to murine CML cells *in vitro*. (A–B) Bivalent Fabs. Each mono–Fab, bivalent, or bispecific Fab was incubated with CJ cells and cells were stained with anti–human IgG (H+L) Alexfluor546 secondary antibody to analyze by flow cytometry. IL3RαΔN–α and IL3RβΔN–β bivalent Fabs binding to CJ cells compared to parental IgGs (C–D) Bispecific Fab. IL3RβΔN–α bispecific Fab binding to CJ cells as compared with parental full–length IgGs (C) and compared to IL3RαΔN–α and IL3RβΔN–β bivalent Fabs (D). Mean Fluorescent Intensity (MFI) represented in histograms is presented in the figure legends. X–axis represents PE (Phycoerythrin) fluorescent staining.

4.7. *In vitro* functional analysis of bivalent and bispecific FABs

4.7.1 Dose–dependent CML cell killing effect of bivalent and bispecific Fabs *in vitro*

To evaluate the level of CML cell proliferation in response to bivalent / bispecific Fabs, CJ cells were treated with sequential concentrations of IL3RαΔN–α bivalent Fab, IL3RβΔN–β bivalent Fab, or IL3RβΔN–α bispecific Fab ranging from approximately 200 pM to 200 nM. All bi–Fabs showed inhibition of cell proliferation in a serial manner (Figure 4.30). In particular, the inhibitory effect of bivalent or bispecific Fab treatment was detectable in 400–800 picomolar concentrations and increased by escalating the dose to 200 nM (Figure 4.30A–C). The direct inhibitory effect of bivalent and bispecific Fab on CJ cell proliferation in the absence of exogenous IL3 suggested the possibility of autocrine or paracrine IL3 pathways or alternative prosurvival and proliferation mechanism that may be impaired by bivalent or bispecific Fabs targeting IL3R.

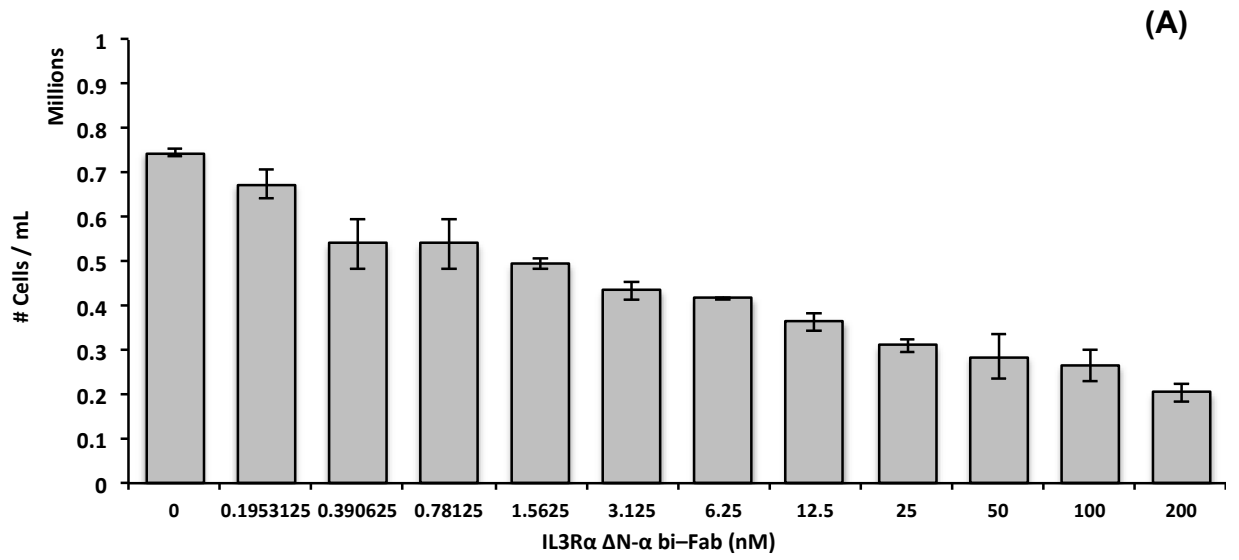
(A)
Millions
Cells / mL
1
0.9
0.8
0.7
0.6
0.5
0.4
0.3
0.2
0.1
0
0
0.1953125
0.390625
0.78125
1.5625
3.125
6.25
12.5
25
50
100
200
IL3Rα ΔN-α bi–Fab (nM)

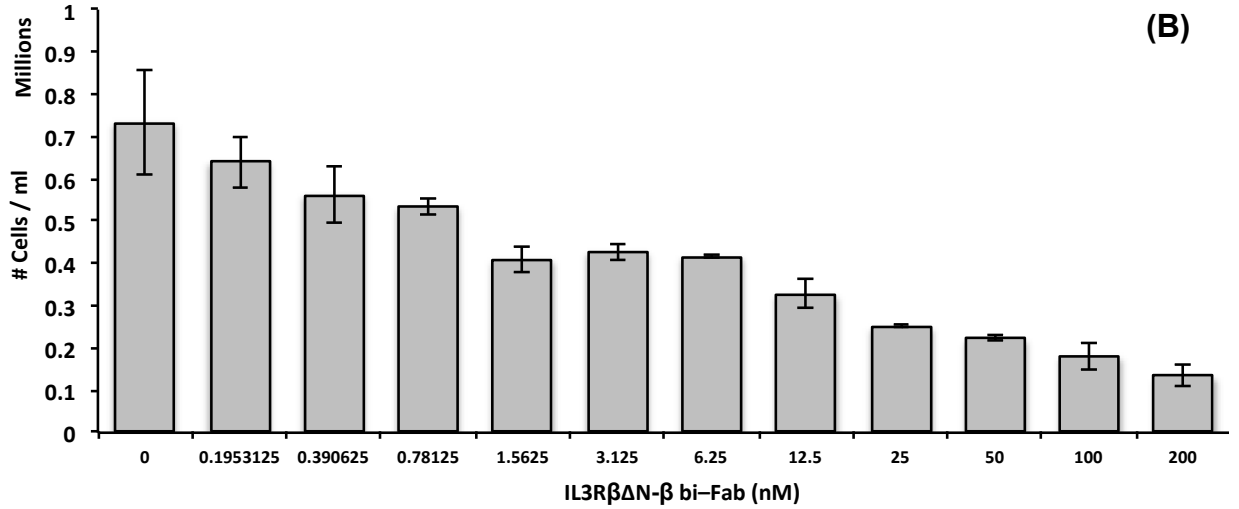
(B)
Millions
Cells / ml
1
0.9
0.8
0.7
0.6
0.5
0.4
0.3
0.2
0.1
0
0
0.1953125
0.390625
0.78125
1.5625
3.125
6.25
12.5
25
50
100
200
IL3RβΔN-β bi–Fab (nM)

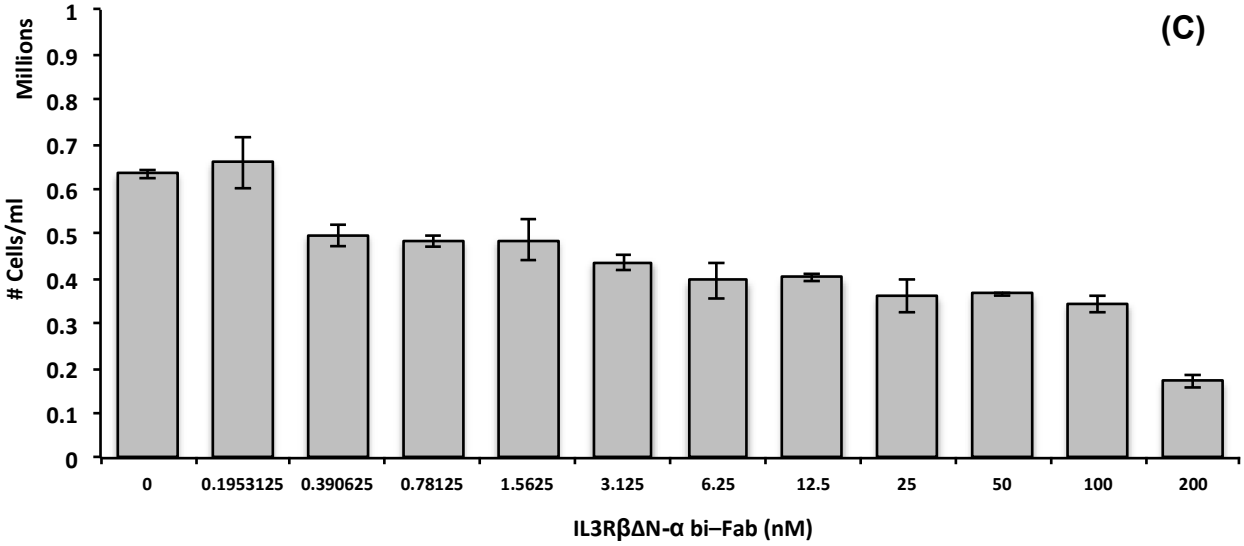
(C)
Millions
Cells/ml
1
0.9
0.8
0.7
0.6
0.5
0.4
0.3
0.2
0.1
0
0
0.1953125
0.390625
0.78125
1.5625
3.125
6.25
12.5
25
50
100
200
IL3RβΔN-α bi–Fab (nM)

Figure 4.30. Direct inhibition of CJ cell proliferation in response to bivalent and bispecific Fabs. Viability test was performed by treatment of CJ cells with sequential concentration of Bi–Fabs ranging from 200pM to 200nM for 48 hours at 37ºC. Cell survival was assessed by trypan blue exclusion viability assay. A) IL3RαΔN–α bivalent Fab. B) IL3RβΔN–β bivalent Fab C) IL3RβΔN–α bispecific Fab; Y–axis represents the number of viable CJ cells. X–axis indicates sequential treatments of CML cells with bi–Fabs. Bars represent Mean; Error bars are representative of mean ± SD. Significance of difference for dose–dependent cell killing effect of bi–Fabs was analyzed by one-way ANOVA followed by Tukey *post hoc* test for multiple comparison; $P < 0.0001$.

4.7.2 CML cell cytotoxicity of bivalent and bispecific Fabs: *in vitro* apoptosis assay

In order to gain further insight into the cytotoxicity of bivalent or bispecific Fabs on CML cells, Annexin V staining was performed to analyze the level of apoptosis. Additionally, SYTOX^{TM} Blue nucleic acid stain was used for dead cell staining to complement the Annexin V apoptosis assay. We compared the apoptotic cell killing effect of bi–Fabs versus imatinib cell killing on CJ cells.

A distinctive feature observed upon flow cytometry analysis was the presence of two discrete sub–population of Annexin V APC+ / SYTOX blue+ (double positive) cells. The double positive cells were especially detectable in CJ cells treated with bivalent or bispecific Fabs. These two sub–populations were gated and labeled as "early death" and "late death" (Figure 4.31). Further investigations in forward–scatter (FSC) and side–scatter (SSC) analysis for evaluation of cell size and granularity revealed that treatment with bivalent or bispecific Fab caused a substantial increase in cell size and granularity as compared to untreated or imatinib–treated cells (Figure 4.31C,E, G, I). Imatinib caused a significant increase in early cell death greater than 60% as compared with approximately 20% in untreated cells (Figure 4.32A). Bi–Fabs also induced a significant increase in early cell death ≥ 45% (Figure 32.A). Further, a more discreet late death cell population of about 25% was detected when CJ cells were treated with IL3RβΔN–α bi–Fab (Figure 4.31J). This proportion was significantly greater than that detected for untreated or bivalent Fabs-treated group (about 7% or 9-13% respectively; Figure 4.32B). Collectively, our findings suggest that bi–Fabs may trigger autocrine / paracrine IL3 pathways in CML cells and may offer potent therapeutic applications individually or as co–drugs with imatinib.

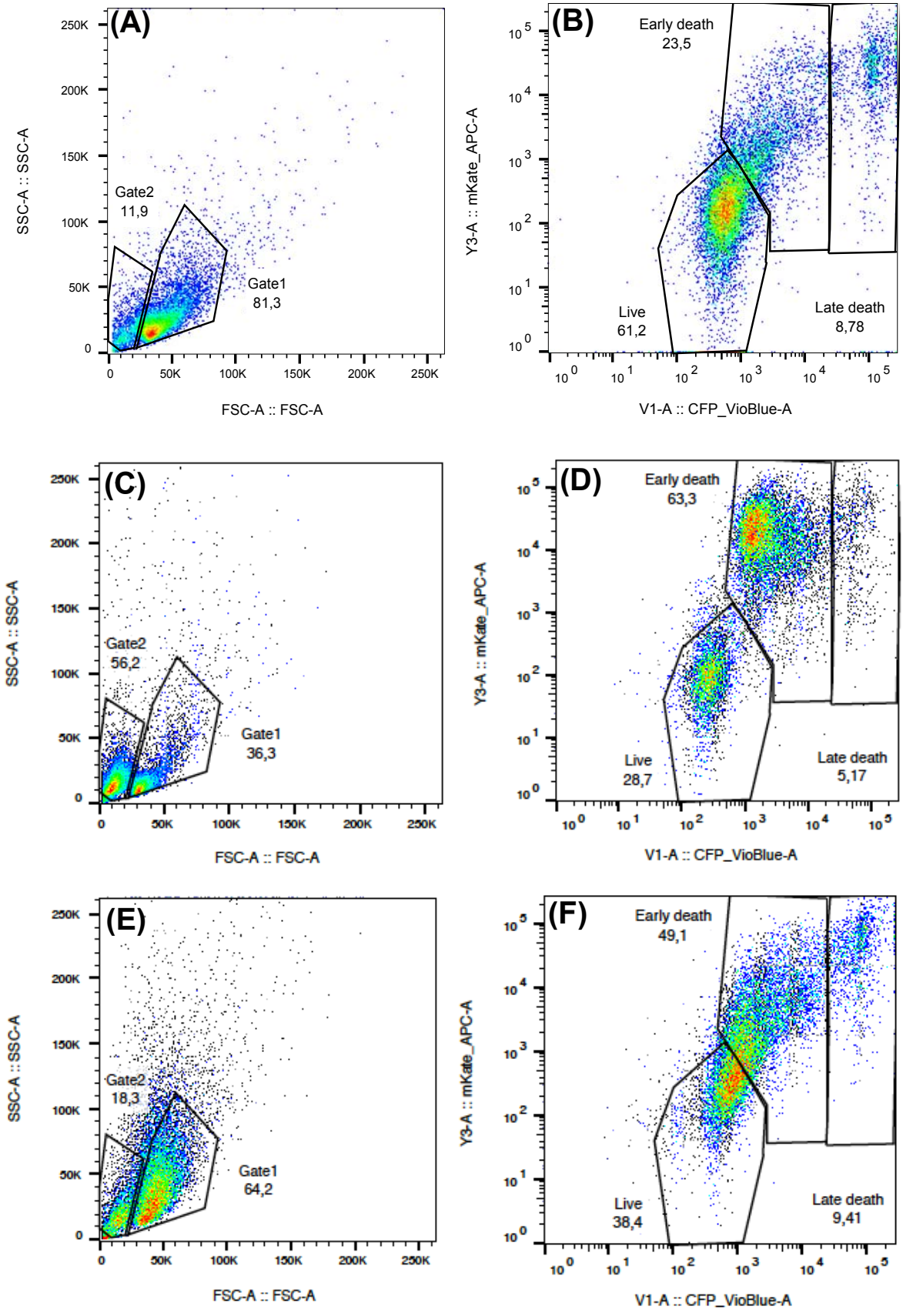
(A)
SSC-A :: SSC-A
FSC-A :: FSC-A
Gate2
11,9
Gate1
81,3
(B)
Y3-A :: mKate_APC-A
V1-A :: CFP_VioBlue-A
Early death
23,5
Live
61,2
Late death
8,78
(C)
SSC-A :: SSC-A
FSC-A :: FSC-A
Gate2
56,2
Gate1
36,3
(D)
Y3-A :: mKate_APC-A
V1-A :: CFP_VioBlue-A
Early death
63,3
Live
28,7
Late death
5,17
(E)
SSC-A :: SSC-A
FSC-A :: FSC-A
Gate2
18,3
Gate1
64,2
(F)
Y3-A :: mKate_APC-A
V1-A :: CFP_VioBlue-A
Early death
49,1
Live
38,4
Late death
9,41

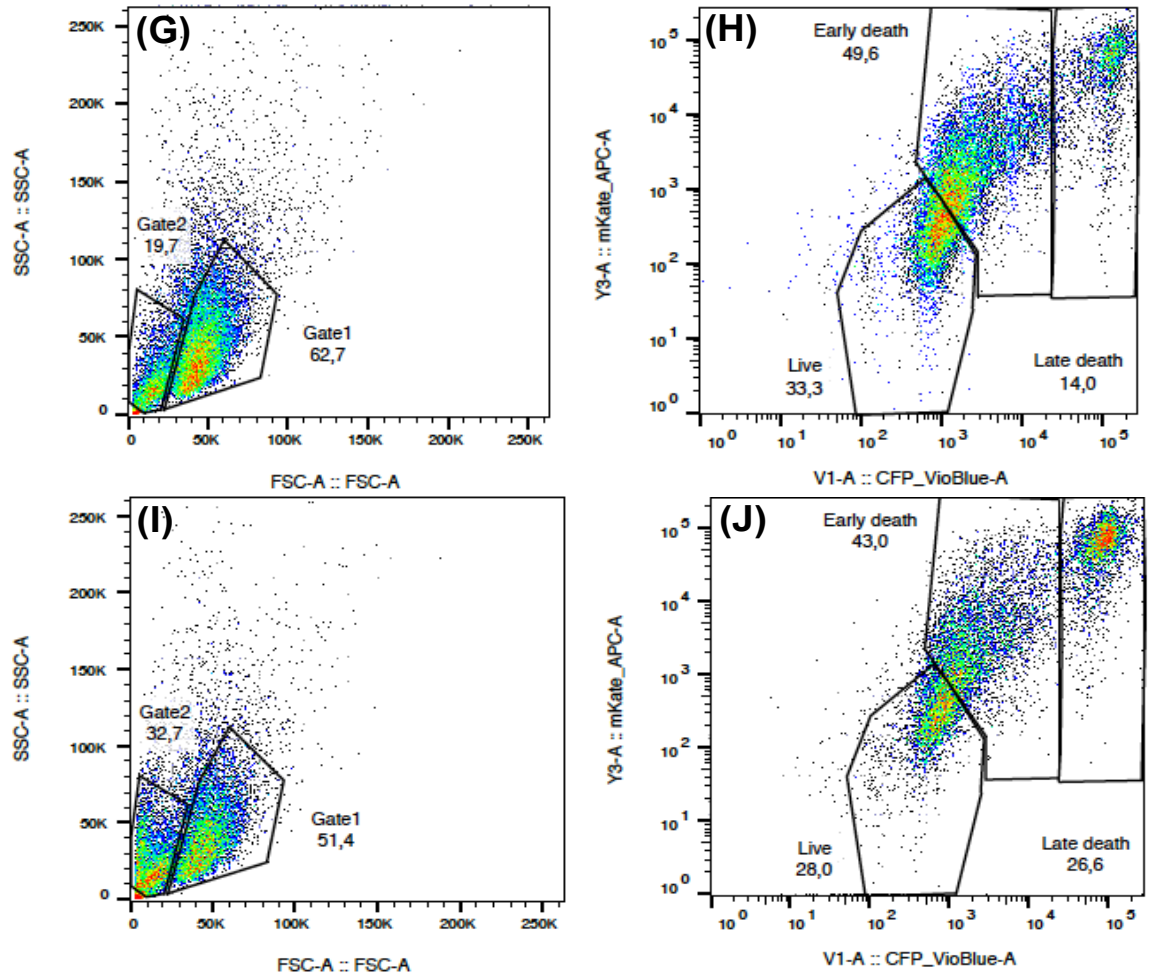

Figure 4.31. The effect of bivalent or bispecific Fabs on CML cell apoptosis and cell death. CJ cells were incubated with 50 nM antibody fragments or imatinib for 48 hours at 37ºC. Cells were analyzed for physical properties (diameter and granularity), apoptosis, and cell death by flow cytometry (MACSQuant VYB®**)** (A–B) Control anti–MBP antibody. (A) The homogenous cell population was found and gated based on size (X–axis: FSC) and granularity (Y–axis: SSC). (B) Control cells were gated to unstained (Live cells: gated live), early death and late death using Annexin V APC and SYTOX blue. (C–D) Imatinib treatment; (E–F) Treatment with L3RαΔN–α bivalent Fab. Increase in cell granularity (E) and early cell death (F). (G-H) Treatment with IL3RβΔN–β bivalent Fab treatment. Increase in cell granularity (G) early cell death (H) (I–J) Treatment withIL3RβΔN–α bispecific Fab treatment. Increase in cell granularity (I), early cell death and late cell death (J). Left Panels: size and granularity [X–axis: FSC (Forward Scatter); Y–axis: SSC (Side Scatter)]; Right Panels: early cell death and late cell death [X–axis: SYTOX blue; Y–axis: Annexin V–APC]. APC: Allophycocyanin.

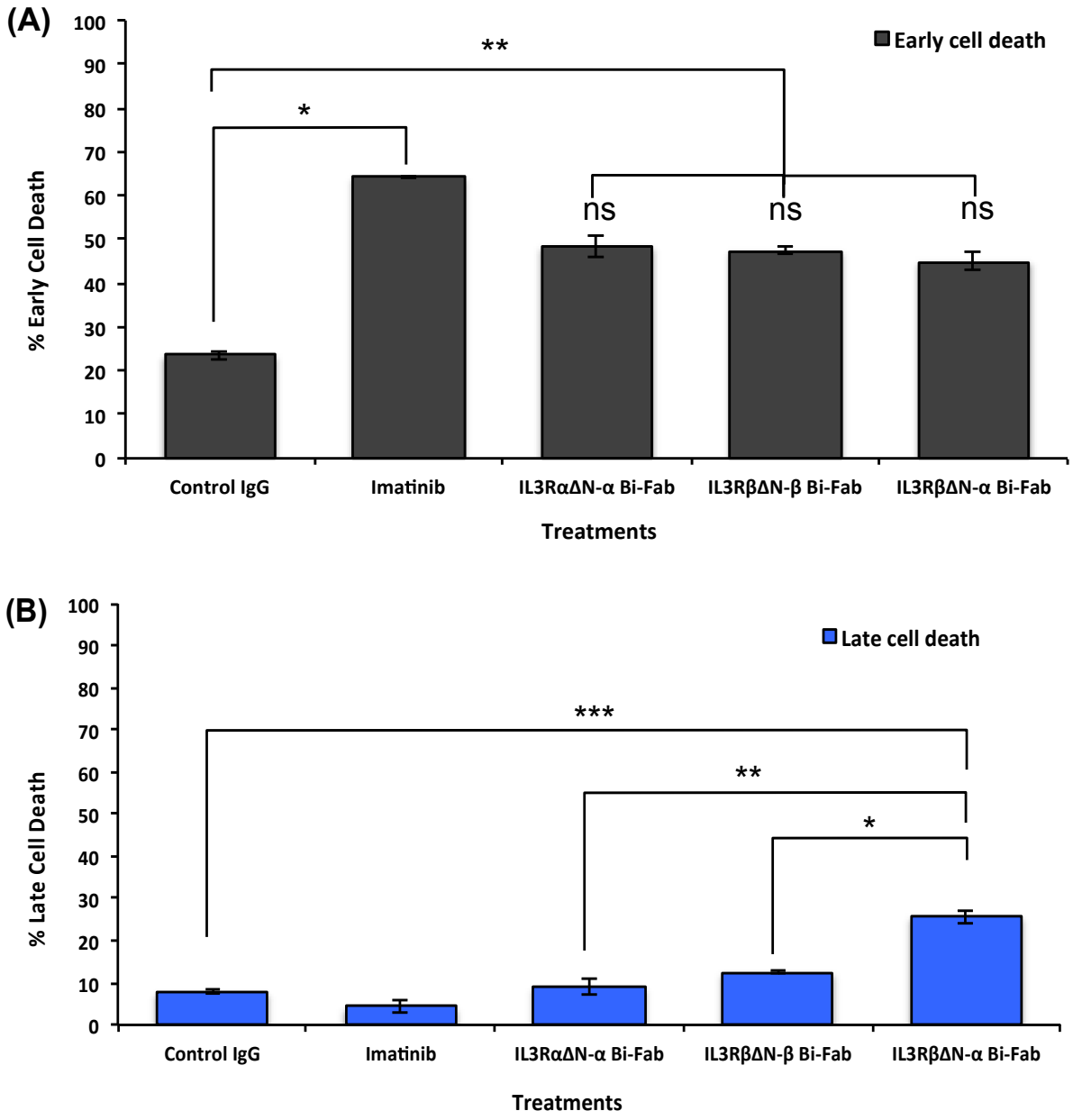

Figure 4.32. Bivalent and Bispecific Fabs induce early and late cell death in CJ cell. CJ cells were incubated with 50 nM bivalent Fab, bispecific Fab, or imatinib for 48 hours at 37ºC in triplicates. Cell apoptosis was then analyzed by flow cytometry (MACSQuant VYB®). (A) The effect of imatinib, bivalent, or bispecific Fab on early cell death. *$P < 0.0001$, ** $P < 0.0001$. (B) The effect of bispecific Fab on late cell death. *$P < 0.0001$, ** $P < 0.0001$, *** $P < 0.0001$. Bars represent Mean and error bars indicate Mean $\pm$ SD; Y–axis represents the percentage of apoptotic or dead cells. X–axis indicates various treatments. Data analyzed with one-way ANOVA followed by Tukey *post hoc* test for multiple comparison. ns: not significant.

4.7.3 IL3R βΔN–α bispecific Fab / IL3RβΔN–β bivalent Fab and imatinib kill CML cells in an additive manner

In order to investigate whether bivalent or bispecific Fabs have an additive cytotoxic effect with TKIs, Fabs were combined with imatinib at multiple concentrations. This assay allowed us to determine if a lower than typically required dose (suboptimal doses) of imatinib could be used for treatment. To test the potential additive effect, 0 – 100 nM mono–Fab / bi–Fab and 0 – 1 μM concentrations of imatinib were added alone or simultaneously to CJ cells. Cell viability assay was then used to measure the cytotoxic effect of Fab / imatinib combinations. Preliminary assays revealed an additive effect of 100 nM IL3RβΔN mono–Fab with 0.25 μM imatinib, 100 nM of βΔN–β bivalent Fab with 0.25 or 0.5 μM imatinib, and 50 – 100 nM βΔN–α bispecific Fab with 0.25 or 0.5 μM imatinib (Table 4.12A–C).

In contrast, IL3Rα mono–Fab or IL3RαΔN–α bivalent Fab did not show any additive killing effect with imatinib (Table 4.12D–E). To further confirm this finding, the assay was repeated in an independent experiment by incubating CJ cells with 10 μg / mL of bi–Fab (100 nM) or mono–Fab (200 nM) alone or in combination with imatinib (ranging 0 – 0.5 μM). Similar results were obtained in this assay, confirming that cell cytotoxicity was higher when IL3RβΔN–β bivalent Fab or IL3RβΔN–α bispecific Fab was combined with suboptimal doses of imatinib than either treatment alone. (Figure 4.33A–B). Collectively, our findings provide evidence that combination–therapy of IL3RβΔN–β bivalent Fab or IL3RβΔN–α bispecific Fab with tyrosine kinase inhibitors (TKIs) may present an opportunity for combination therapy in CML and eradication of CML–LSCs.

(A)

IL3Rβ mono–Fab	1uM Imatinib	0.5uM Imatinib	0.25uM Imatinib	0uM Imatinib
200 nM IL3Rβ mono-Fab	3.87E+05	6.16E+05	8.50E+05	1.50E+06
100 nM IL3Rβ mono-Fab	5.81E+05	7.92E+07	8.50E+05	1.50E+06
50 nM IL3Rβ mono-Fab	6.00E+05	8.56E+07	1.09E+06	1.83E+06
0 nM IL3Rβ mono-Fab	5.00E+05	7.00E+05	1.26E+06	1.82E+06

(B)

IL3RβΔN-β bivalent Fab	1 uM Imatinib	0.5 uM Imatinib	0.25 uM Imatinib	0 uM Imatinib
100 nM IL3RβΔN-β	4.00E+05	7.30E+05	1.32E+06	2.48E+06
50 nM IL3RβΔN-β	5.28E+05	1.13E+06	1.57E+06	2.33E+06
25 nM IL3RβΔN-β	4.99E+05	8.74E+05	1.47E+06	2.00E+06
0 nM IL3RβΔN-β	5.22E+05	1.04E+06	1.50E+06	2.40E+06

(C)

IL3RβΔN-α bispecific Fab	1 uM Imatinib	0.5 uM Imatinib	0.25 uM Imatinib	0 uM Imatinib
100 nM IL3RβΔN-α	6.16E+05	9.62E+05	7.21E+05	1.69E+06
50 nM IL3RβΔN-α	6.86E+05	8.50E+05	1.47E+06	1.92E+06
25 nM IL3RβΔN-α	6.22E+05	1.28E+06	1.33E+06	2.63E+06
0 nM IL3RβΔN-α	6.63E+05	1.20E+06	1.47E+06	2.80E+06

(D)

IL3Rα mono–Fab	1uM Imatinib	0.5uM Imatinib	0.25uM Imatinib	0uM Imatinib
200 nM IL3Rα mono-Fab	4.60E+05	8.15E+05	1.24E+06	1.50E+06
100 nM IL3Rα mono-Fab	6.45E+05	8.74E+07	1.08E+06	1.73E+06
50 nM IL3Rα mono-Fab	4.00E+05	6.92E+07	1.10E+06	1.78E+06
0 nM IL3Rα mono-Fab	4.00E+05	7.57E+05	1.03E+06	1.70E+06

(E)

IL3RαΔN-α bivalent Fab	1 uM Imatinib	0.5 uM Imatinib	0.25 uM Imatinib	0 uM Imatinib
100 nM IL3RαΔN-α	7.21E+05	1.21E+06	1.65E+06	2.41E+06
50 nM IL3RαΔN-α	6.63E+05	1.28E+06	1.57E+06	2.47E+06
25 nM IL3RαΔN-α	6.28E+05	9.74E+05	1.69E+06	2.33E+06
0 nM IL3RαΔN-α	4.34E+05	8.03E+05	1.34E+06	2.60E+06

Table 4.12 Additive effect of Fabs and Imatinib in CML cell killing. Mono–Fabs, bivalent or bispecific Fabs (ranging 0 – 100 nM) were co–administered with 0 – 1 μM of imatinib ($1x10^6$ cells / treatment). The cell proliferation was evaluated by viability assay. Treatment with **(A)** IL3RβΔN mono–Fab and imatinib; **(B)** IL3RβΔN–β bivalent Fab and imatinib, **(C)** IL3RβΔN–α bispecific Fab, **(D)** IL3Rα mono–Fab and imatinib **(E)** IL3RαΔN–α bivalent Fab and imatinib. The data is a representative of three assays on additive cytotoxicity. Highlighted values represent the additive cytotoxic effect of Fab and imatinib.

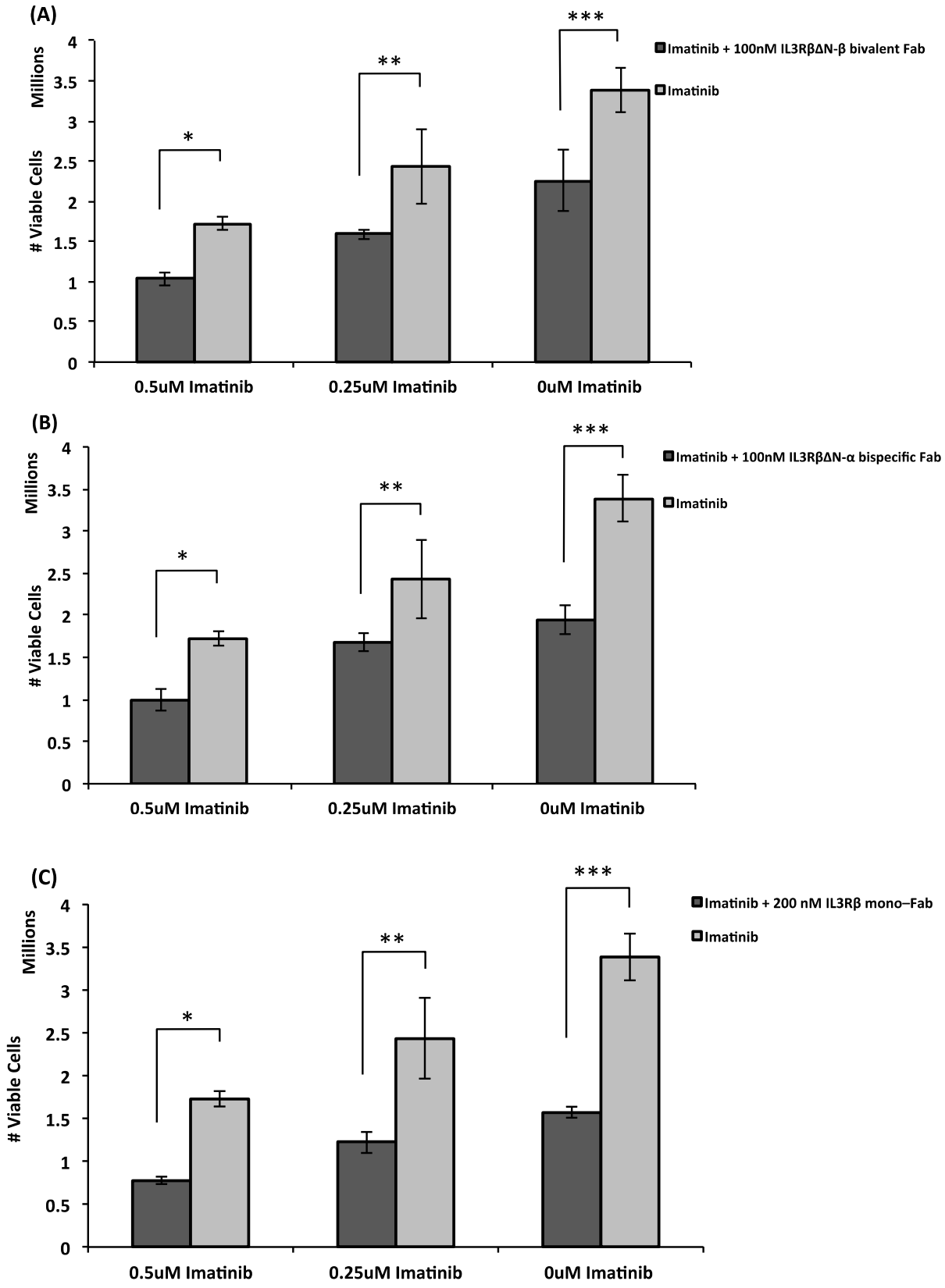
(A)
Millions
Viable Cells
4
3.5
3
2.5
2
1.5
1
0.5
0
*
**
***
Imatinib + 100nM IL3RβΔN-β bivalent Fab
Imatinib
0.5uM Imatinib
0.25uM Imatinib
0uM Imatinib
(B)
Millions
Viable Cells
*
**
***
Imatinib + 100nM IL3RβΔN-α bispecific Fab
Imatinib
0.5uM Imatinib
0.25uM Imatinib
0uM Imatinib
(C)
Millions
Viable Cells
*
**
***
Imatinib + 200 nM IL3Rβ mono–Fab
Imatinib
0.5uM Imatinib
0.25uM Imatinib
0uM Imatinib

Figure 4.33. Additive cytotoxic effect of IL3RβΔN–β bivalent Fab or IL3RβΔN–α bispecific Fab with suboptimal doses of imatinib on CML cells *in vitro*. CJ cells were incubated with 10 μg / mL of Fab (100nM and 200nM for bi–Fab or mono–Fab respectively) alone or in combination with suboptimal dose of imatinib (ranging 0 – 0.5 μM) for 48 hours at 37ºC. Cell viability was tested with trypan blue exclusion assay in triplicates. (A) Treatment with IL3RβΔN–β bivalent Fab and imatinib. **P* = 0.0288; ***P* = 0.0081; ****P* = 0.0009. (B) Treatment with IL3RβΔN–α bispecific Fab and imatinib. **P* = 0.01; ***P* = 0.0084; *** *P* < 0.0001. (C) Treatment with IL3RβΔN mono–Fab. **P* = 0.0195; ***P* < 0.0001; ****P* < 0.0001. Bar graphs are representative of mean viability; error bars indicate mean ± SD; Significance of difference between indicated groups was analyzed by two–way ANOVA followed by Sidak's multiple comparisons test.

4.7.4 Bi–Fabs block IL3–mediated signaling in CML cells

Bi–Fabs were tested for inhibition of downstream IL3R signaling by evaluating the tyrosine phosphorylation status of downstream JAK2 and STAT5 in response to Fab treatment. JAK2 / STAT5 pathway is one of the most specific readouts that indicates activation of IL3 signaling pathway (Itoh et al., 1998). JAK2 is associated with multiple downstream signaling pathways activated in responses to IL3 stimulation and is required for mitogenesis. JAK / STAT pathway is mainly involved in anti-apoptotic events (O'Hare et al., 2011).

To assay phosphorylation of JAK2 and STAT5, CJ cells were serum–starved prior to incubating with mono–Fab or bi–Fabs ranging from 100 to 400 nM or with 100 nM control anti–MBP (maltose–binding protein) antibody for 10 minutes on ice. Cells were then stimulated with 10 nM rmIL3 for 20 minutes at 37ºC and JAK2 and STAT5 tyrosine phosphorylation were analyzed by Western blotting. Both IL3Rα mono–Fab and IL3RαΔN–α bivalent Fab blocked the downstream JAK2 and STAT5 tyrosine phosphorylation at 100, 200, and 400 nM. Nevertheless, there was no dose–dependent phosphorylation inhibition at these concentrations (Figure 4.34A).

IL3Rβ mono–Fab and IL3RβΔN–β bivalent Fab inhibited JAK2 and STAT5 phosphorylation at 100 – 400 nM concentrations, and no dose–dependent phosphorylation inhibition was observed at these concentrations (Figure 4.34B). However, we found a slight increase in JAK2 and STAT5 signaling by escalating the dose of IL3RβΔN–β bivalent Fab, which may be due to receptor super-cluster formation and agonist activity of IL3RβΔN–β bivalent Fab in higher concentrations (Mayes et al., 2018) (Figure 4.34B).

Treatment of CJ cells with IL3RβΔN–α bispecific Fab also blocked the downstream phosphorylation of both JAK2 and STAT5 in CJ cells at 100 – 400 nM concentrations. Interestingly, antibody co–treatment (anti–mIL3Rα–2*mut* antibody and anti–mIL3Rβ–1*mut* antibody) of CJ cells at the same molar ratios showed comparable blocking of downstream JAK2 and STAT5 signaling (Figure 4.34C). Together, our findings support that bivalent and bispecific Fabs specifically impair IL3R. This finding may be highly relevant in various types of leukemia where IL3 over–expression is important.

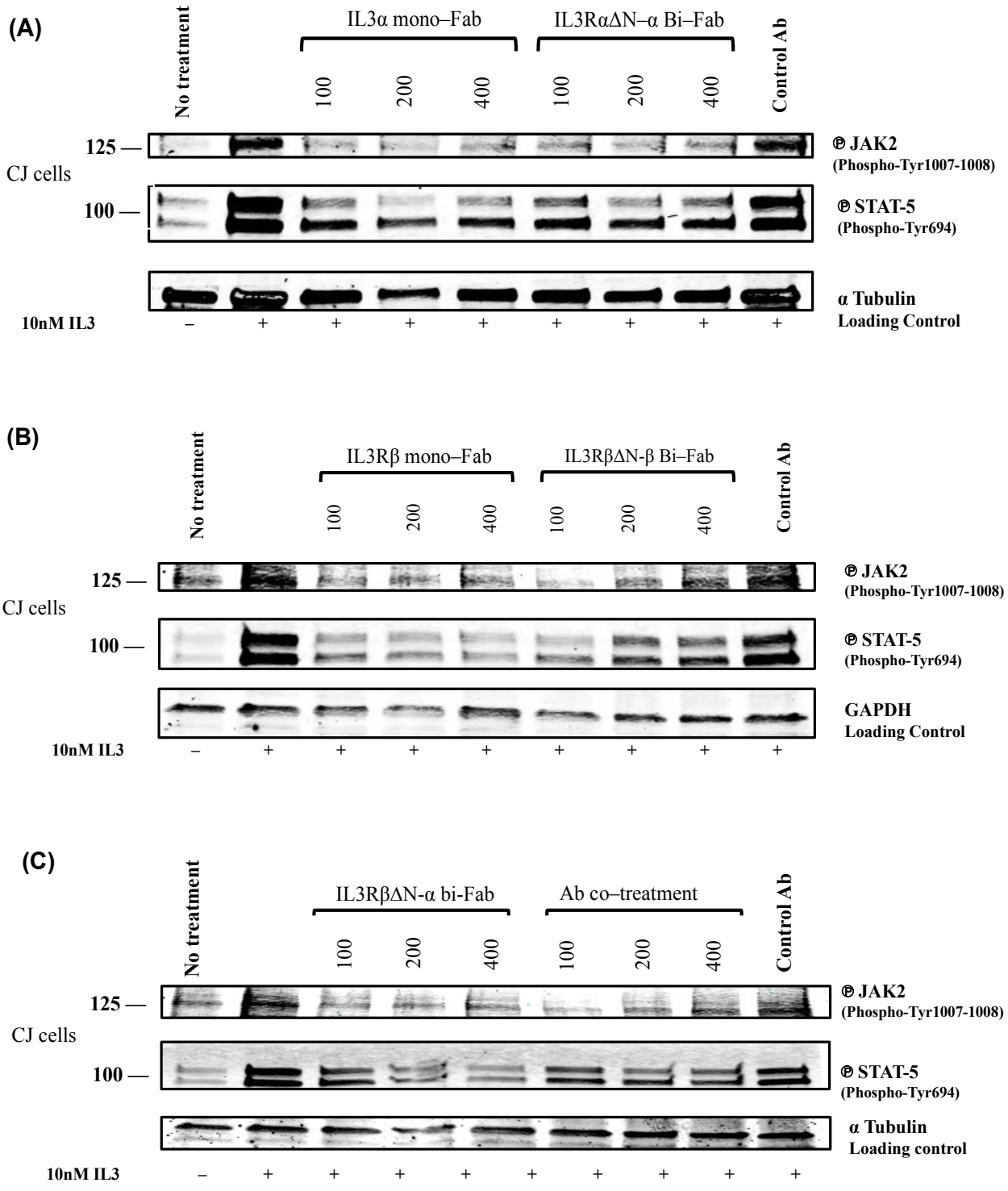
(A)
No treatment
IL3α mono–Fab
IL3RαΔN–α Bi–Fab
Control Ab
100
200
400
100
200
400
125 —
100 —
CJ cells
Ⓟ JAK2
(Phospho-Tyr1007-1008)
Ⓟ STAT-5
(Phospho-Tyr694)
α Tubulin
Loading Control
10nM IL3
– + + + + + + + +
(B)
No treatment
IL3Rβ mono–Fab
IL3RβΔN-β Bi–Fab
Control Ab
100
200
400
100
200
400
125 —
100 —
CJ cells
Ⓟ JAK2
(Phospho-Tyr1007-1008)
Ⓟ STAT-5
(Phospho-Tyr694)
GAPDH
Loading Control
10nM IL3
– + + + + + + + +
(C)
No treatment
IL3RβΔN-α bi-Fab
Ab co–treatment
Control Ab
100
200
400
100
200
400
125 —
100 —
CJ cells
Ⓟ JAK2
(Phospho-Tyr1007-1008)
Ⓟ STAT-5
(Phospho-Tyr694)
α Tubulin
Loading control
10nM IL3
– + + + + + + + +

Figure 4.34. Blocking IL3 signaling pathway by mono–Fabs, bivalent and bispecific Fabs. CJ cells were cultured in serum–free medium for 5 hours and then incubated with increasing concentrations of 100, 200, or 400 nM of mono– or bi–Fab, or control antibody for 10 minutes on ice. Cells were then stimulated with 10 nM of IL3 for 20 minutes at 37ºC. Cell lysates were assessed for the status of JAK2 and STAT5 tyrosine phosphorylation by Western blotting. (A) IL3Rα mono–Fab or IL3RαΔN–α bivalent Fab at 100, 200, and 400 nM; (B) IL3Rβ mono–Fab and IL3RβΔN–β bivalent Fab at 100, 200, and 400 nM; (C) IL3RβΔN–α bispecific Fab versus antibody co–treatment at 100, 200, and 400 nM; The densitometry data for each assay was normalized to loading control (data now shown) and no dose–dependence was observed for 100 – 400nM of antibody fragments. Assays were performed in triplicates. Blots were stripped and re–probed to evaluate tyrosine phosphorylation of JAK2. Same blots were cut and blotted to evaluate the loading control for each assay.

4.7.5 Anti–mIL3RβΔN–α bi–Fab impairs colony formation of CML cells *in vitro*

In order to investigate the impact of bispecific anti–IL3RβΔN–α Fab on *in vitro* colony formation capacity of CML cells, we performed colony forming unit (CFU) assay. CJ cells were incubated with imatinib or IL3RβΔN–α bispecific Fab and then seeded in cytokine–enriched methylcellulose. Colonies were counted by light microscopy after 10–14 days. We observed a dramatic reduction in the number of colonies from CJ cells treated with IL3RβΔN–α bispecific Fab (Figure 4.35A). In addition, it is noteworthy that we did not detect any large colonies from bispecific Fab–treated cells compared to control or imatinib–treated cells (Figure 4.35 B–D). This profound effect of IL3RβΔN–α bispecific Fab on colony formation may suggest blocking of autocrine / paracrine IL3 pathways or other alternate prosurvival and self–renewal pathways in CJ cells. Overall, colony formation results provided strong evidence that IL3RβΔN–α bispecific Fab inhibits the colony formation of CML cells.

In conclusion, the novel IL3RβΔN–α bispecific Fab generated in this project may offer a more potent alternative to full–size antibodies. Bispecificity, relatively small size (100 KDa), the ability in altering IL3 receptor function, disruption of CML cell colony formation, and strong additive cytotoxicity with imatinib are the advantages of IL3RβΔN–α bispecific Fab. These properties may offer novel therapeutic approaches for selective targeting and eradication of CML–LSCs in the bone marrow. Furthermore, bispecific and bivalent Fabs can be broadly applicable in preclinical diagnostic implications.

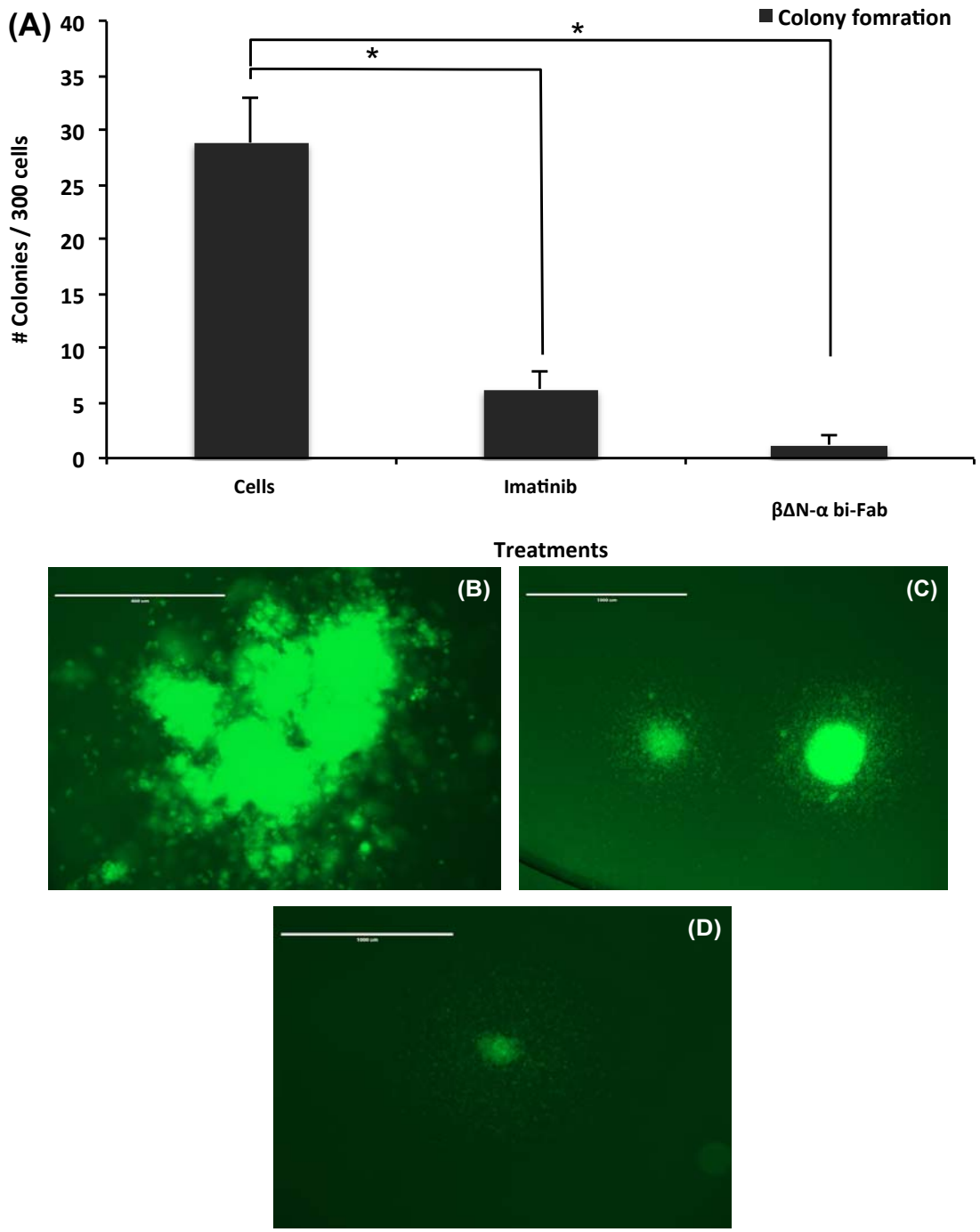

Figure 4.35 Bispecific IL3RβΔN–α Fab inhibits colony formation of CJ cells. **(A)** CJ cells treated with bispecific Fab for 48 at 37ºC were seeded in cytokine–enriched methylcellulose for 10–14 days. The colonies were counted by light microscopy. * $P <$ 0.0001; Significance of difference was analyzed by one way–ANOVA followed by Tukey *post hoc* test for multiple comparisons. Y–axis indicates the number of colonies and X–axis represents various treatments. **(B–D)** Fluorescent microscopy was used to evaluate the size of GFP+/YFP+ CJ cell colonies from βΔN–α bi–Fab–treated CJ cells (D) compared to the control (not treated) (B) or imatinib–treated (C) CJ cells.

5. CHAPTER 5. DISCUSSION

Tyrosine kinase inhibitors are the first–line therapy for CML treatment; however, eradication of CML has been elusive due to innate drug resistance in a subset of stem / progenitor cells that remain in a quiescent manner and escape the therapy (Corbin et al., 2011; Graham et al., 2002; Holyoake et al., 2001; M. Y. Konopleva & Jordan, 2011; Mahon et al., 2010). The key role of IL3 receptor in this subset of leukemic stem cells has been widely studied in AML (Jin et al., 2009; Jordan et al., 2000; U Testa et al., 2004; L. H. Xie et al., 2017). Additionally, higher expression levels of IL3Rα subunit (CD123) are correlated with NPM1 and FLT3–ITD mutations in AML (Rollins-Raval et al., 2013; L. H. Xie et al., 2017). A few studies have demonstrated high expression of IL3R in CML (Florian et al., 2006; Nievergall et al., 2014) and confirmed its association with disease progression from the chronic phase to the more aggressive blast crisis phase of CML (Nievergall et al., 2014; Radich et al., 2006). In this thesis, we evaluated effects of targeting CD123 (IL3Rα) and CD131 (IL3Rβ subunit) as a potential CML therapy. Although CD123 is the specific subunit for IL3R, CD131 is the signal–transducing subunit, and heterodimerization of IL3Rα– and IL3Rβ–subunits activates the downstream signalling of IL3 (T. R. Hercus et al., 2017). In a clinical context, CD131 may provide broad applications, since it is the common subunit for IL3R, GM-CSFR, and IL5R. We first analyzed CD123 and CD131 expression in various human and murine CML cell lines. In agreement with previous studies (Nievergall et al., 2014), we showed that CD123 and CD131 were highly expressed in several CML cell lines. Furthermore, we investigated targeting BC–CML cells with novel antibodies targeting CD123 or CD131 or co–targeting CD123 and CD131 with the goal of depleting CML cells (CML leukemic stem cells). Here, we showed that anti–IL3Rα and anti–IL3Rβ antibodies and antibody fragments efficiently reverted IL3–induced imatinib resistance in CML cells.

5.1. Generation of novel antibodies to block IL3–induced innate drug resistance in CML

We generated human anti–mouse IL3Rα and anti–mouse IL3Rβ antibodies using phage display selections against mouse IL3Rα or IL3Rβ target proteins. Anti–mIL3Rα and anti–mIL3Rβ antibodies had nanomolar dissociation for their target, and impaired IL3 receptor function, promoted apoptosis and cell death, impaired IL3 signalling (i.e. JAK2 / STAT5 signalling), and disrupted the colony formation of CML cells.

We used C57BL/6 mice as a CML animal model with a fully functional immune system for preclinical investigations of the activities of anti–IL3Rα and IL3Rβ antibodies. Engraftment of antibody–treated BC–CML cells revealed anti–leukemic effects of anti–mIL3Rα and anti–mIL3Rβ antibodies on the LSC population, leading to prolonged survival of C57BL/6 CML mouse model. These results showed that mice survived longer when engrafted of antibody–treated CML cells as compared with imatinib–treated cells. This finding may offer potential therapeutic approaches when imatinib fails to eradicate the quiescent LSCs that do not succumb to chemotherapies (i.e. imatinib). Altogether, we showed that antibodies targeting CD123 or CD131 impaired the IL3R function and inhibited IL3–induced proliferation and colony formation of CML cells *in vitro* and upon engraftment in the mouse model.

To date, few anti–IL3Rα antibodies and no IL3Rβ antibody are in preclinical or early phases of oncology clinical trials (Busfield et al., 2014; L. H. Xie et al., 2017). Anti–leukemic activity of anti–IL3Rα antibody was first reported in 1996 by development of 7G3 monoclonal antibody (Sun et al., 1996). 7G3 was categorized as a mouse IgG_{2a}, generated by immunization of mice with COS cell transfectants expressing IL3Rα and selection of Hybridoma cells producing 7G3 antibody (Sun et al., 1996). 7G3 antibody revealed specific antagonistic activity against IL3R (Sun et al., 1996) and targeted AML–LSCs by impairing LSCs homing to bone marrow, activating innate immunity, and reduced AML burden in bone marrow and peripheral blood of the AML mouse model (Jin et al., 2009). CSL360 was then developed as a second–generation recombinant, chimeric anti–IL3Rα IgG1, derived from 7G3 and was tested in a phase I study (S. Z. He et al., 2015). Although this report confirmed safety and tolerability of CSL360 antibody in AML patients, only one out of 27 patients showed durable complete response (S. Z. He et al., 2015). These findings lead to development of CSL362 anti–

IL3Rα antibody derived from 7G3. CSL362 is a humanized, affinity–matured and Fc–engineered antibody with two amino-acid mutations (S239D and I332E) for higher affinity to CD16 (FcγRIIIa) (Busfield et al., 2014; Nievergall et al., 2014). CSL362 elicited enhanced cytotoxicity by ADCC against primary AML blast cells and LSCs and efficiently depleted AML cells (Busfield et al., 2014). Various approaches of targeting IL3Rα with CSL362 antibody are being investigated in multiple Phase I and II clinical trials. Furthermore, anti–IL3Rα antibody treatment based on XmAb technology (XmAb14045 bispecific Fc) is under development for targeting CD123–expressing cells and T cell activation for the treatment of AML and systemic lupus erythematosus. IMGN-632 antibody is another novel monoclonal anti–IL3Rα antibody conjugated with potent DNA-alkylating payload as an antibody drug conjugate (ADC). IMGN-632 is currently being tested in clinical trials as second or third-line therapy in NK cell Lymphomas, ALL, or relapsed or refractory AMLs (Globaldata.com). IMGN-632 binds to CD123, undergoes internalization and is catabolized to release the payload. The payload induces DNA alkylation, cell cycle arrest S-phase, apoptosis and cell death in leukemic cells (Kovtun et al., 2018). Unlike 7G3 and its derivatives CSL360 and CSL362 bind to CD123 N–terminal domain, IMGN-632 binds to D2–D3 region and then a secondary binding to N–terminal domain of CD123 (J. Chen et al., 2009). SGN-CD123A was another ADC comprising an engineered cysteine antibody stably conjugated to a highly potent DNA binding agent (Pyrrolobenzodiazepine or PBD dimer) (Li et al., 2018) that discontinued for treatment of relapsed and refractory AML (Globaldata.com). Flotetuzumab (MGD006) is a CD123 x CD3 bispecific DART (dual-affinity re-targeting molecule) binding T lymphocytes and CD123–expressing cells (Chichili et al., 2015) is in an ongoing / recruiting phase I clinical trial as an orphan drug designation for myelodysplastic syndrome, refractory and relapsed AML (Globaldata.com). Diphtheria toxin–IL3 fusing protein (DT388 IL3 (Frankel, Liu, Rizzieri, & Hogge, 2008) and SL-401 / SL501 (Frolova et al., 2014)) are other CD123–targeted therapies under development for various leukemias (Globaldata.com). Other interventional studies for targeted anti-CD123 therapies are CD123–targeted CART (Chimeric antigen receptor-modified T cells) as first-line therapy in subjects with myeloid malignancies (Cummins & Gill, 2018; Kloss et al., 2017; Ruella et al., 2016, 2017; Tasian et al., 2017). CARTs elicit

their immunostimulant activity by binding to CD123 surface antigen and causing a cytotoxic T–lymphocyte response against cells expressing IL3R thereby inhibit cell proliferation (Cummins & Gill, 2018).

Our findings showed that the generated antibodies may provide candidates for immunotherapeutic intervention in CML-BC and AML. In particular, effective targeting of CD123 and / or CD131 with by anti–mIL3Rα and anti–mIL3Rβ antibodies may eliminate CD34+ / CD38– cells in both CP and BC phase, as well as CD34+ BC–CML cells (Nievergall et al., 2014). Clinically, this finding may be relevant since CD123 expression significantly increases by disease progression from chronic phase to blast crisis phase CML (Nievergall et al., 2014; Radich et al., 2006). Furthermore, long–term use of TKIs after remission is associated the risk of acquired TKI resistance in CML patients (Griswold et al., 2006; Mahon et al., 2010; Willis et al., 2005). Anti–IL3Rα and anti–IL3Rβ antibodies may provide new approaches to consolidate and maintain the TKI–induced complete molecular response (CMR) and complete cytogenetic response (CCyR) and minimize TKI therapies.

5.2.Why target the IL3 receptor?

IL3 is an attractive target for synthetic antibodies. IL3 plays a significant since role in innate drug resistance. Specifically, a subset of cells remains quiescent during the therapy without any previous exposure to the drug. This innate drug resistance in a small population of cells may be responsible for disease relapse and later on developing acquired drug resistance. Over–expression of CD123 in hematological malignancies and high level of serum IL3 are associated with higher leukemic burden and poor prognosis in leukemias (Ugo Testa et al., 2002).

Consistent with other reports (Corbin et al., 2011; Holyoake et al., 2001; Jiang et al., 1999), we demonstrated the key role of growth factors such as IL3 and GM–CSF in suppression of imatinib activity and innate imatinib resistance in CML cells. IL3R is being targeted in various hematological malignancies since CD123 (IL3R alpha–subunit) is preferentially expressed in AML blast cells and most AML cells irrespective of subgroup (Jordan et al., 2000; Munoz et al., 2001; L. H. Xie et al., 2017), CML blast cells

and CML cells (Florian et al., 2006; Nievergall et al., 2014), Hodgkin's lymphoma (Aldinucci et al., 2005), hairy cell leukemia (Munoz et al., 2001), myelodysplastic syndrome (Florian et al., 2006), B–cells acute lymphoblastic leukemia (De Waele et al., 2001), systemic mastocytosis (Florian et al., 2006), and plasmacytoid dendritic cells (pDC) leukemia (Oon et al., 2016), while normal HSCs have limited expression of CD123 required for differentiation and inhibition of apoptosis (De Waele et al., 2001; Djokic et al., 2009; Hassanein, Alcancia, Perkinson, Buckley, & Lagoo, 2009; Jordan et al., 2000; Munoz et al., 2001; Nievergall et al., 2014; Ugo Testa et al., 2002). Therefore, antibody–based targeted therapy and impairment of LSCs via IL3R with synthetic antibodies will have broad applicability in various types of leukemic malignancies.

Targeting the α–subunit of IL3R (CD123) has been investigated for depleting LSCs (S. Z. He et al., 2015; Jin et al., 2009; Nievergall et al., 2014; L. H. Xie et al., 2017), while targeting the β–subunit of IL3R (CD131) has not been reported. The development of novel anti–IL3Rα and anti–IL3Rβ antibodies provides an opportunity to evaluate targeting each subunit independently or co–targeting both subunits of IL3R. Anti–IL3Rβ antibodies that target the β–subunit of IL3R, which is the signal transducer subunit of the receptor, could potentially be more effective in inhibiting IL3 signalling and provide an alternative approach to more effectively block IL3–induced innate drug resistance.

Our present results were consistent with previous reports that document high expression of IL3 receptor–α (CD123) in various human or murine CML cells. Additionally, we confirmed high expression of IL3 receptor– β (CD131) in CML cells to underscore the importance of targeting or co–targeting of CD131 in hematological malignancies.

5.3. Direct cell killing of novel anti–IL3Rα antibodies

One of the key findings we found was the spontaneous inhibitory effect of anti–IL3Rα on CML cell proliferation and colony formation in the absence of exogenous IL3. One anti–IL3Rα antibody (anti–IL3Rα–1*mut* antibody) showed a direct cell killing effect in a dose–dependent manner and disrupted colony formation *in vitro.* Further investigations on the impact of this antibody on BC–CML programmed cell death

showed a trend towards non-apoptotic cell cytotoxicity. However, as described below, further studies are required to investigate mechanisms of direct CML cell killing of this antibody.

Besides the strong cell killing effect of anti–IL3Rα–1*mut* antibody, both the affinity–matured and the non–affinity matured anti–IL3Rα–2 antibodies (anti–mIL3Rα–2 and anti–IL3Rα–2*mut* IgG) showed a modest anti–leukemic effect on CML cells. These antibodies were able to attenuate CML cell proliferation, induce pro–apoptotic effects, and impair colony formation of CML cells in the absence of exogenous IL3 *in vitro*. The cell killing effect of an anti–IL3Rα antibody has been reported before (Jin et al., 2009). In this study, they reported that 7G3, a mouse anti–human IL3Rα antibody, inhibited AML cell proliferation by 50 – 75% (Jin et al., 2009). However, this group did not explore the mechanism of direct cell killing of this antibody.

Mechanisms of the cytotoxic activity of killer antibodies have been investigated in several studies. Some reports have shown evidence of direct apoptotic cell death by antibodies, while others reported non–apoptotic cell killing of antibodies. Kowlalczyk determined that anti–GD2 (Disialoganglioside) antibody is associated with apoptotic cell death in neuroblastoma cells by cleavage of Caspase 3 and elevated Caspase capacity. Furthermore, pro–apoptotic effect of the anti–ganglioside GM2 monoclonal antibody was shown on lymphoma, myeloma and small cell lung carcinoma cells *in vitro* (Retter et al., 2005). Likewise, other research groups showed the apoptotic cell killing of human monoclonal IgM antibody SAM–6 (S–Adenosylmethionine) by deadly intracellular accumulation of neutral lipids in cells leading to lipopoptosis (lipo–apoptosis) in gastric carcinoma cells and pancreatic carcinoma cells (Pohle, Brandlein, Ruoff, Muller-Hermelink, & Vollmers, 2004).

Other studies confirmed non–apoptotic mechanisms of cell killing for killer antibodies. Hernández found evidence of complement–independent cell killing of anti–NeuGcGM3 antibody in NSCLC (Non–small cell lung cancer) cells by cell swelling, cytoskeleton activation with no DNA fragmentation, and no Caspase activation (A. M. Hernandez et al., 2011). Similarly, another study by Roque–Navarro reported oncosis–like cytotoxicity of anti-NGcGM3 14F7 monoclonal antibody on lymphocytic leukemia cells. This group demonstrated that the antibody contributes to direct cell killing by loss

of membrane integrity accompanied by cell swelling and cytoskeleton activation with no indication of DNA fragmentation, no Caspase activation, or Fas mediation, suggesting an oncosis–like mechanism of action in tumor cells (Roque-Navarro et al., 2008). Although the underlying molecular mechanism for antibody–induced complement–independent cell death is not well understood, the role of cell membrane molecules such as gangliosides can be further studied (Roque-Navarro et al., 2008). Similarly, Loo showed that glycotope–specific RAV12 monoclonal antibody elicit direct cell killing by induction of oncosis on gastrointestinal adenocarcinoma cells through cytoskeletal rearrangement and membrane swelling. This finding by Loo *et al.* provided preclinical opportunities for Phase I/IIA clinical trials of RAV12 antibody on patients with metastatic or recurrent adenocarcinoma (Loo et al., 2007). There are multiple other reports of killer antibodies promoting non–apoptotic cell death in B–cell malignancies. Tositumomab–like type II anti–CD20 antibody, GA101, has shown programmed cell death through cytoskeleton actin reorganization, enlargement of lysosomal compartment and lysosome membrane permeabilization (LMP) resulting in cell death in B–cell malignancies (Alduaij et al., 2011; Ivanov et al., 2009). Likewise, non–apoptotic cell death by triggering actin reorganization was reported by monoclonal antibodies targeting HLA–DR (Mone et al., 2004), CD 47 (Mateo et al., 2002), CD 74 (Alinari et al., 2011), and CD99 (Cerisano et al., 2004). Moreover, Honeychurch et al., proposed that Obinutuzumab, a glycoengineered and humanized type II anti–CD20 antibody induces nonapoptotic cell death with generation of NADPH oxidase–derived ROS (reactive oxygen species) caused by actin reorganization, lysosomal membrane permeabilization, and cathepsin release (Honeychurch et al., 2012). Additionally, a very recent study by Gillissen reported that donor–derived B–cell antibodies produced by GVL (graft–versus–leukemia) immune response elicit an Fc–dependent nonapoptotic cell killing on AML blast cells in the absence of cytotoxic leukocytes or complement; while the mechanism of cell killing is not understood. Oncosis has been proposed to be associated with anti–tumor activity of killer antibodies. Conformational changes of integrin molecule, FAK (focal adhesion kinase) dephosphorylation and anoikis phenomenon was observed in small cell lung cancer cells treated with anti–GD2 monoclonal antibody (Aixinjueluo et al., 2005). Moreover, cell membrane excitation and cytoskeleton–dependent cell killing (Matsuoka

et al., 1995), as well as, complement–independent pore formation on cell plasma membrane have been confirmed to occur due to cytotoxic effect of killer antibodies (Bhat et al., 1997; C. Zhang, Xu, Gu, & Schlossman, 1998).

In order to further confirm the cell killing effect of the anti–IL3R α and anti–IL3Rβ antibodies, bivalent Fabs were generated using the novel parental anti–IL3Rα–2*mut* IgG or anti–IL3Rβ–1*mut* IgG. Bivalent Fabs resemble the parental IgG without the Fc domain on its activity. Remarkably, bivalent Fabs showed similar cell killing phenotype as the parental antibody. This finding supported the Fc–independent cell killing of the anti–IL3R α and anti–IL3Rβ antibodies.

5.4. Advantages of targeting CD131 with novel anti–IL3Rβ antibodies

In addition to targeting CD123 by anti–mIL3Rα antibodies, we targeted CD131 (IL3Rβ subunit) by anti–IL3Rβ antibodies. The rationale behind the development of anti–IL3Rβ antibodies was as follows: *First*, CD123 has emerged as a unique entity to target for a range of human hematological malignancies (De Waele et al., 2001; Djokic et al., 2009; Hassanein et al., 2009; Jordan et al., 2000; Munoz et al., 2001; Ugo Testa et al., 2002). In a clinical context, development of antibodies to target CD131, as the other subunit of IL3 receptor (Bagley, Woodcock, Stomski, & Lopez, 1997), can provide an alternative approach for various malignancies that elicit IL3 overexpression. *Second*, CD131 provides another component to target in order to inhibit the IL3R. This could be particularly important if anti–IL3Rα antibodies do not effectively or sufficiently impair IL3–mediated CML cell proliferation. As reported by He et al., CSL360, a humanized anti–IL3Rα antibody demonstrated no clinical responses in high risk relapsing / refractory AML (Clinical Trials.gov identifier: NCT0041739) (S. Z. He et al., 2015), suggesting that targeting CD123 alone is not sufficient in that case. *Third*, targeting IL3Rβ subunit plus α–subunit may provide a platform for combinatorial treatment that allows testing for additive or synergistic effects. *Fourth*, raising antibodies against both subunits of IL3R provides another opportunity to create bispecific antibodies to co–target the IL3 receptor. *Fifth*, we observed in our initial studies of innate resistance that GM–CSF also played a potential role in innate imatinib resistance in CML. The GM–CSF requires the IL3Rβ–subunit as it is the signal–transducing component for its activity.

Therefore, targeting CD131 could allow us to inhibit both IL3– and GM–CSF–mediated innate drug resistance in CML. Jin *et al.,* showed that the addition of exogenous GM–CSF enabled AML cells to overcome the inhibitory effect of anti–IL3Rα antibody (7G3) on AML cells (Jin et al., 2009). This finding brings two questions: (i) Is targeting CD131 a more effective approach to target both IL3R and GM–CSFR? (ii) Could novel anti–IL3Rβ antibodies complement the effect of anti–IL3Rα antibody to more effectively eliminate leukemic stem / progenitor cells *in vivo*?

Our findings revealed that anti–IL3Rβ antibodies blocked IL3Rβ–subunit thereby inhibiting IL3–mediated suppression of imatinib activity on mouse and human CML cells *in vitro*. In this context, anti–IL3Rβ–1 and anti–IL3Rβ–1*mut* antibodies were comparable. However, the affinity matured form of the anti–IL3Rβ antibody, anti–IL3Rβ–1*mut* antibody, but not the anti–IL3Rβ–1 antibody, induced direct apoptosis in mouse CML cells. Collectively, our data showed three key properties of affinity–matured anti–IL3Rβ antibody: (i) Anti–IL3Rβ–1*mut* antibody prevented IL3–dependent STAT5 phosphorylation and blocked IL3–mediated suppression of imatinib activity *in vitro.* (ii) Engraftment of antibody–treated CML cells into the mouse model prolonged the disease latency, suggesting that antibody may inhibit LSCs or interfere with CML cell engraftment in the bone marrow of C57BL/6 mice. (iii) Anti–mIL3Rβ–1*mut* showed modest cell killing effect, induced apoptosis, and disrupted CML cell colony formation in the absence of exogenous IL3 *in vitro*. This finding suggests the autocrine or paracrine secretion of IL3 in BC–CML cells (Guan et al., 2003; Jin et al., 2009). To our knowledge, this is the first report of a novel anti–IL3Rβ antibody with the potential to deliver anti–leukemic effects via blockade of IL3R signalling and inhibition of IL3–stimulated rescue of TKI–induced cell death in a hematological malignancy. This finding can be translated into preclinical *in vivo* treatments for CML or AML and offer new approaches to reverse the resistance.

The development of antibodies targeting CD131 may complement chemotherapies by specifically eliminating the small subset of quiescent cells that escape the therapy in hematological malignancies (Guan et al., 2003; Ishikawa et al., 2007; M. Y. Konopleva & Jordan, 2011). Anti–IL3Rβ antibodies may provide an avenue for treating CD34+ / D38– CD123+ CD45RA+ granulocyte macrophage progenitors (GMPs) with BC–CML

(Jamieson et al., 2004) by blocking the common β–subunit. In a broader clinical context, anti–IL3Rβ–1*mut* antibody may provide new clinical approaches for long–term management of CML, AML, or other hematological malignancies by blocking the signal-transducing β–subunit of IL3. Importantly, our findings underscore the potential to use anti–IL3Rβ and anti–IL3Rα antibodies as combinatorial treatment strategies with the aim to target the quiescent stem cells in post–stem cell transplants.

5.5.Antibody engineering to enhance anti–leukemic activity of antibodies

5.5.1 Antibody engineering to generate affinity–matured antibodies

With the rise of Immunoglobulins G (IgG) as the major modalities in cancer immunotherapy, the idea of fine–tuning the targeted therapy by co–engagement of target and immune system has been developed (Glassman & Balthasar, 2014; A. M. Scott, Wolchok, & Old, 2012). Antibody engineering provides the option to customize the variable fragment (Fv) or crystalizable fragment (Fc) components and modify the pharmacological effect of antibodies. These modifications may lead to improvements in the inhibitory function of antibodies through ligand–receptor interactions, induction of pro–apoptotic signalling, or triggering ADCC (antibody–dependent cell cytotoxicity), CDC (complement–dependent cytotoxicity), or ADCP (antibody–dependent cell phagocytosis) (Glassman & Balthasar, 2014; A. M. Scott et al., 2012).

Our first study was focused on generating anti–IL3Rα IgG and anti–IL3Rβ IgG with a functional Fv (variable fragment) for inhibition of IL3–IL3R interaction. The antibodies were derived from a library with completely synthetic CDRs on a single humanized framework 4D5 (Lee et al., 2004). This framework comes from a frequently used germline origin (V_k1–1 and V_H3–23 for light and heavy chain, respectively), which is successfully used for therapeutic purposes (Lee et al., 2004). We performed customized modulations on Fv component by soft–randomization of CDRL3, CDRH1, CDRH2, and CDRH3 with the goal of affinity maturation and improving the antibody inhibition of ligand–receptor binding. Additionally, we used the IgG1 isotype, which has high effector activity and affinity to induce ADCC and CDC. Hence, tailoring the antibody Fc component was not the focus of this project. Our findings supported the

concept that synthetic anti–mIL3Rα and anti–mIL3Rβ IgGs selectively engage CD123 and CD131, respectively. These IgGs elicit various phenotypes, including pro–apoptotic effects, direct cell cytotoxicity, blockade of IL3 receptor signalling, as well as targeting CML–LSCs and prolonging disease latency in the mouse model. In a clinical context, these properties provide new anti–mIL3Rα and anti–mIL3Rβ antibodies as potential alternative or combinatorial therapeutics for hematological malignancies.

Studies showed that blocking CD123 and impairing IL3 signalling in AML blast cells (either circulating or bone marrow blast cells) is an ineffective therapeutic approach for AML patients (Clinical Trials.gov identifier: NCT00401739) (S. Z. He et al., 2015; Jin et al., 2009). In a previous report, Busfield approached this problem by affinity–maturation of an anti–IL3Rα IgG (CSL360) and Fc modification to increase antibody affinity for human CD16 (FcγRIIIa) (Busfield et al., 2014). These modifications allowed them to enhance ADCC and antibody efficacy (Busfield et al., 2014). The resulting humanized Fc–engineered antibody was a derivative of CSL360, known as CSL362. As shown by various studies (Busfield et al., 2014; S. Z. He et al., 2015; Nievergall et al., 2014; Oon et al., 2016; L. H. Xie et al., 2017), incorporating Fc modifications enhances the efficacy of the antibody *in vivo* and further improves its cell killing. In particular, CSL362 depleted AML cells by activating NK (Natural killer) cells *in vitro* and *in vivo* (Busfield et al., 2014). Xie et al., also suggested that donor–derived NK cells provide sufficient effector function for CSL362 when used after allogeneic hematopoietic stem cell transplantation (allo-HSCT) in AML patients (L. H. Xie et al., 2017). Based on these reports, CSL362 elicits its highest efficacy in the presence of adequate number of NK cells. Clinically, this could be a challenge in AML or CML patients with low NK cell count. This can be especially problematic in relapsing patients at imatinib cessation (Rea et al., 2017), in cases of intrinsic resistance to autologous NK cells after bone marrow transplantations (L. H. Xie et al., 2017), or when donor–derived NK cells and allogeneic ADCC are compromised (L. H. Xie et al., 2017). Furthermore, AML patients with low affinity variant of FcγRIII that do not benefit from rituximab treatment (Cartron et al., 2002) would face a similar complication if treated with CSL362.

Collectively, we generated synthetic IgGs to CD123 or CD131. These anti–mIL3Rα IgG and anti–mIL3Rβ IgG were softly mutated in CDRH1, H2, H3, and L3 with

no modifications in Fc entity. IgGs were well–characterized for specificity, affinity, cytotoxicity and blockade of IL3–mediated imatinib suppression on CML cells. It could be inferred from our findings that anti–leukemic activity of anti–mIL3Rα IgG and anti–mIL3Rβ IgG was independent of Fc component. The antibody efficacy in engaging immune effector function, pharmacokinetics and toxicity are the next steps to be assessed using *in vivo* assays.

5.5.2 Construction of bivalent and bispecific anti–IL3R Fabs

Generation of antibodies *in vitro* provides the opportunity to use the DNA encoding sequences to engineer several antibody fragments (Fabs). Using the DNA encoding sequences of parental anti–mIL3Rα–2*mut* IgG and anti–mIL3Rβ–1*mut* IgG, we generated and developed anti–mIL3Rα and anti–mIL3Rβ monovalent Fabs, bivalent Fabs, and bispecific Fab. We generated anti–mIL3Rα–IL3Rα and anti–mIL3Rβ–IL3Rβ bivalent Fabs and an anti–mIL3Rβ–IL3Rα bispecific Fab by covalently linking mono–Fabs using a protein ligation system (SpyCatcher–SpyTag system (Alam et al., 2017; Zakeri et al., 2012)). As suggested by Zakeri et al., SpyCatcher was truncated at the N–terminus (ΔN) to minimize the immunogenicity of bivalent and bispecific Fabs *in vivo* (Zakeri et al., 2012).

Mono–Fabs were derivatives of the anti–IL3Rα–2*mut* IgG and anti–IL3Rβ–1*mut* IgG that previously showed effective blocking of IL3–mediated innate imatinib resistance and CML cell cytotoxicity. Thus, the resulting bivalent Fabs retain parental anti–mIL3Rα–2*mut* and anti–mIL3Rβ–1*mut* IgGs Fabs but lack the Fc domain. The bivalent IL3Rα–IL3Rα and IL3Rβ–IL3Rβ bi–Fabs showed a significant cytotoxic effect on CML cells *in vitro* at concentrations as low as 780 pM. *In vitro* CML cell cytotoxicity increased with escalating doses of bivalent Fabs. The higher potency of bivalent Fabs as compared to parental IgG1 may be due to better avidity and/or more suitable geometric properties as compared with IgG1, which has a relatively large span between antigen binding sites (about 150Å (Hadzhieva et al., 2017)). Related to this, the high density of IL3 receptors on CML cells may affect receptor occupancy and avidity effects of bivalent Fab / IgG resulting in an improved binding profile for bivalent Fabs (Hadzhieva et al., 2017). Similarly, the smaller molecular size of bivalent Fab might yield a propensity to more

efficiently bind and saturate the receptors in high antigen ratios (Rhoden, Dyas, & Wroblewski, 2016). Further investigations are needed to evaluate the conceptual and mathematical model of antibody or bivalent Fab binding to the antigen that was out of the scope of this study.

We also showed that IL3Rα–IL3Rα and IL3Rβ–IL3Rβ bivalent Fabs blocked IL3 signalling through impairment of JAK2 and STAT5 tyrosine phosphorylation *in vitro*. This finding highlights the potential of bivalent Fabs in targeting CML cells and underscore the advantage of bivalent Fabs in triggering the IL3 receptors compared to small molecule inhibitors of downstream signalling (Jin et al., 2009). In particular, JAK2 inhibitor was suggested as a potential candidate to block cytokine–mediated TKI resistance (Hiwase et al., 2010; Traer et al., 2012; Ying Wang et al., 2007). However, JAK2 lacks the capacity to discriminate between normal and leukemic stem/progenitor cells (Traer et al., 2012).

In addition to bivalent Fabs, another key finding of this thesis was the generation of a novel anti–IL3Rβ–IL3Rα bispecific Fab. Similar to bivalent Fabs, the SpyCatcher—SpyTag protein ligation system (Alam et al., 2017; Zakeri et al., 2012) was used to ligate anti–IL3Rα–2*mut* and anti–IL3Rβ–1*mut* mono–Fabs. Mono–Fabs were derivatives of parental anti–IL3Rα–2*mut* IgG and anti–IL3Rβ–1*mut* IgG that blocked IL3–mediated innate imatinib resistance and direct CML cell cytotoxicity *in vitro* and upon engraftment of antibody–treated CML cells in the mouse model. As described previously, SpyCatcher was truncated at the N–terminus (ΔN) to minimize the immunogenicity of bispecific Fab (i.e. IL3RβΔN–α bispecific Fab) *in vivo* (Zakeri et al., 2012).

The rationale for generating the IL3RβΔN–α bispecific Fab was (i) to investigate the dual specificity / affinity of a bispecific Fab derived from anti–IL3Rα and anti–IL3Rβ IgGs that successfully neutralize IL3 activity in CML cells, (ii) to evaluate the efficacy of IL3RβΔN–α bispecific Fab in blocking IL3–dependent innate drug resistance, and (iii) to further substantiate the potential clinical implications of bispecific Fabs in combinatorial therapies with TKIs for CML.

Our novel IL3RβΔN–α bispecific Fab showed nanomolar dissociation to IL3Rα and IL3Rβ targets and elicited comparable or greater binding to CML cells as compared with parental IgGs at equimolar concentrations. Moreover, IL3RβΔN–α bispecific Fab

induced direct cell cytotoxicity in CML cells with a significant reduction in CML cell colony formation *in vitro*. This finding agreed with our previous findings from parental anti–IL3Rα–2*mut* and anti–IL3Rβ–1*mut* IgGs and previous report by Jin et al., that found direct AML cell killing of mouse anti–IL3Rα antibody, 7G3 (Jin et al., 2009). IL3RβΔN–α bispecific Fab also blocked IL3 downstream signalling through impairment of JAK2 and STAT5 tyrosine phosphorylation. The blockade of IL3 signaling by IL3RβΔN–α bispecific Fab was as effective as parental anti–IL3Rα–2*mut* and anti–IL3Rβ–1*mut* IgGs combination treatment. Further studies within *in vivo* settings may reveal the advantages of dual specificity / affinity of IL3RβΔN–α bispecific Fab in depletion of CML–LSCs.

Owing to the smaller molecular size of ~110kDa, bivalent and bispecific Fabs will have a higher diffusion rate than IgGs, while retaining a hydrodynamic volume large enough to have a half–life longer than monovalent Fabs (Xenaki, Oliveira, & van Bergen En Henegouwen, 2017). An *in vivo* half–life of approximately 28 minutes has been reported for proteins of 50 kDa molecular weight, whereas larger molecules such as antibodies could exert serum half–life of 2–3 weeks, which is due in part to the larger size (Chapman et al., 1999; Kontermann, 2016; Schmidt & Wittrup, 2009). The smaller size of the bivalent and bispecific Fabs can be especially relevant in targeting the quiescent leukemic stem cells (LSCs) in the bone marrow niche, where the microenvironment can hinder the diffusion of IgGs (Xenaki et al., 2017). In addition to molecular size, affinity is another key parameter for *in vivo* half-life of bi–Fabs as compared with mono-Fabs. The high affinity of the bivalent Fab and high affinity / dual specificity of bispecific Fabs may enhance tumor retention and prevent fast dissemination back into the vasculature and subsequent serum clearance (Adams et al., 1998).

Altogether, our novel IL3Rα–IL3Rα, IL3Rβ–IL3Rβ bivalent Fab, and IL3Rβ–IL3Rα bispecific Fab possess several key properties, including low cost of generation in *E. coli*, no post–translational modifications, ~110 kDa molecular size, high target affinity, blockade of IL3R, and direct CML cytotoxic effect. Although further toxicity, pharmacokinetics and biodistribution assessments are essential, we have characterized desirable properties of bivalent and bispecific IL3R Fabs as potential candidates for drug development, therapeutic dosing, or diagnostic imaging for leukemias. Furthermore, SpyCatcher–SpyTag system can be used to as a platform to develop bispecific Fabs to

CD131 or CD123 and other biomarkers to enhance the specificity of potential therapeutic candidates for hematological malignancies.

5.6.Additive CML cell killing of bi–Fabs and imatinib

Anti–IL3Rβ–α bispecific Fab was additive with imatinib in CML cell killing. The combination treatment of IL3Rβ–α bispecific Fab with ½ or ¼ dose of imatinib IC_{50} showed a reduction in CML cell proliferation *in vitro*. Clinically, the combinatorial treatment of IL3β–α bispecific Fab with suboptimal doses of imatinib may reduce the chance of acquired TKI–resistance due to high / repeated doses of Imatinib treatment in CML patients (Griswold et al., 2006; Mahon et al., 2010; Willis et al., 2005). In addition, this additive cytotoxic effect of TKI and IL3β–α bispecific Fab targeting CD123 and CD131 on CML cells may offer a potential Fc–independent therapeutic approach. This approach provides the significant anti–leukemic effect of a combination therapy without engagement of immune system. The lack of Fc or T–cell engagement along with high specificity of IL3βΔN–α bispecific Fab may be especially beneficial for safety and tolerability of bispecific Fab as a potential therapeutic candidate for CML patients.

In addition, we demonstrated that IL3Rβ–β bivalent Fab was additive with imatinib in CML cell killing *in vitro*. However, imatinib and IL3Rα–α bivalent Fab did not show additive CML cell killing. Further studies are required to determine whether the additive effect of imatinib and bivalent IL3Rβ–β or bispecific IL3β–α Fabs is dependent on targeting CD131. To answer that question, we investigated the additive cytotoxic effect of imatinib with IL3Rα–mono–Fab or IL3Rβ–mono–Fab. Surprisingly, our results revealed the additive cytotoxic effect of imatinib and IL3Rβ–mono–Fab, but not IL3Rα–mono–Fab. This finding underscores the critical role of the IL3Rβ–subunit in CML cells and highlights the significance of targeting CD131. The additive effect of TKIs with CD131–dependent cell killing in CML cells may provide very relevant therapeutic implications for CML patients.

Furthermore, IL3Rβ–α bispecific Fab and IL3Rβ–β bivalent Fab may provide a new approach to eliminate CD123+ GMPs in BC–CML. BC–CML CD123+ GMPs have been suggested as the leukemic stem cell subset with self–renewal capacity that are expanded in BC–CML and imatinib–resistant CML patients (Jamieson et al., 2004).

Targeting CD131 with IL3Rβ–α bispecific Fab or IL3Rβ–β bivalent Fab may be especially advantageous since they trigger the common signal–transducing subunit of IL3R and GMCSFR, both of which are relevant to drug resistance in CML. Collectively, the IL3Rβ–α bispecific Fab and IL3Rβ–β bivalent Fab may provide a potential new therapeutic approaches to eradicate CML–LSCs, lower the dose of imatinib in CML patients, avoid repeated doses of imatinib or other TKIs in CML patients, and reduce the risk of imatinib resistance.

There are various preclinical developments and ongoing phase I, phase II, and phase III clinical studies evaluating bispecific platforms (Brinkmann & Kontermann, 2017; Thakur, Huang, & Lum, 2018). Bispecific antibodies (BsAbs) that are marketed or under development have been classified as IgG–like or non–IgG like antibodies (Thakur et al., 2018). The major difference between these antibody formats is in Fc–mediated effector functions, such as ADCC, ADCP, and CDC and the presence of physical properties associated with Fc component (Kontermann & Brinkmann, 2015; Thakur et al., 2018). The common feature of the majority of the bispecific antibody formats is co–targeting the immune system and a specific antigen–binding module. In particular, the majority of bispecific antibody formats either preferentially target Fc receptor via CD64 (FcγRI), CD32a (FcγRIIα), or CD16 (FcγRIII), or redirect the T cell killing through binding affinity to CD3 or with lower affinity to CD19 (Kontermann, 2016; Kontermann & Brinkmann, 2015; Thakur et al., 2018).

Most bispecific antibodies target hematological malignancies through simultaneous recruitment of an antigen and engaging T–cells. These bsAbs include BiTE (Bispecific T–cells engager), TandAb (Tetravalent bispecific tandem diabodies), DART (Dual–affinity re–targeting bispecific antibodies), BATs (BsAb armed T cells), TDB (T–cell-dependent BsAb), Xmab (Xencor's bsAb containing Fab x anti–CD3 scFv). Other bispecific antibodies such as TandAb, BiKE (Bispecific killer cell engager), TriKE (Trifunctional killer cell engager), TriFab (Trifunctional bsAb) and XmAbs (Xencor's bispecific Fc domain technology monoclonal antibodies) function by simultaneous binding to specific antigen, T cells, and accessory cells / FcR (Thakur et al., 2018).

Our bispecific Fab is different from the above–mentioned bsAbs as it was not designed to engage with immune cells and has a higher specificity for CML cells via

targeting both subunits of IL3R. The dual affinity of our novel CD123 x CD131 bispecific Fab could make it an excellent therapeutic candidate for targeting leukemic stem / progenitor cells over–expressing IL3R in bone marrow niche. The small size of approximately 110 kDa could be beneficial for effective diffusion in the bone marrow. Targeting CD123 and CD131 can be especially relevant since all other CD123 bispecific platforms, currently in preclinical phase I clinical trial, are contingent upon T–cell recruitment or T–cell and FcRn recruitment. The existing CD123 bispecific formats in phase I clinical trial for AML are CD123 x CD3 DARTs (MGD006 and Duvortuxizumab; Clinical Trials.gov identifier: NCT02152956 and NCT02454270, respectively) and CD123 x CD3 XmAb (XmAb14045; Clinical Trials.gov identifier: NCT02730312) (Cuesta-Mateos, Alcaraz-Serna, Somovilla-Crespo, & Muñoz-Calleja, 2018; Thakur et al., 2018). We argue that CD131 may enhance the specificity of bispecific Fab without engagement of the immune system. This may offer less toxicity related to off–target events and more tolerability in CML patients. More importantly, the additive cytotoxic effect of our CD123 x CD131 with imatinib, the front–line TKI therapy for CML, may provide a promising therapeutic platform to completely eradicate CML leukemic stem / progenitor cells.

Generation of engineered bispecific Fab by bridging antagonist–antagonist pairing (Mayes et al., 2018) of anti–mIL3Rα–2*mut* Fab and anti–mIL3Rβ–1*mut* Fab may lead to simultaneous engagement of both IL3R subunits and more potent blockade of IL3–mediated innate drug resistance. Despite this antagonistic phenotype, we also recognize that the bridging of two IL3R subunits may result instead, in the recruitment of multiple receptor complexes. This could lead to potent *agonist* effects, due to co-stimulatory receptor heterodimerization activation and supercluster receptor formation (Mayes et al., 2018).

6. CHAPTER 6. CONCLUSION AND FUTURE DIRECTIONS

6.1 CONCLUSION

This thesis was focused on development of novel antibodies as alternative or complementary therapeutic strategy to TKIs for CML. The incident cases (N) of CML were reported 11,418 diagnosed patients worldwide in 2017 with the prevalence of 0.01% (globaldata.com). Although many patients respond to the conventional chemotherapy, the majority relapse upon withdrawal of treatment (Ross et al., 2013). Therefore, there is an unmet need for safe, tolerable targeted therapies to maintain CML remission. The standard therapy for CML is a tyrosine kinase inhibitor, imatinib, that is effective in suppressing CP–CML, but it does not completely eliminate CML–LSCs, which can lead to relapse with CML drug resistance (Kreuzer et al., 2003). IL3 plays a crucial role in pro-survival and self-renewal of leukemic stem cells against TKI therapies (Nievergall et al., 2014). Since over–expression of IL3 receptor α–subunit has been confirmed in CML early progenitors and stem cells (Nievergall et al., 2014), this thesis was focused on blocking IL3–mediated imatinib suppression in CML cells. Anti–IL3R antibodies were generated to target CML–LSCs over–expressing IL3 receptor to explore the possibility of new potential therapeutic approaches for eradication of CML–LSCs.

In this work, novel synthetic IgGs were generated against mouse IL3 receptor–α and mouse IL3 receptor–β subunits using solid phase phage display selection. The purified phage displayed IgGs showed nanomolar dissociation for the cognitive target proteins and bound to IL3 cell surface receptor on multiple CML cell lines *in vitro*. Binding of synthetic novel anti–mIL3Rα and anti–mIL3R β IgGs was significantly higher than commercial IgGs available in the market.

The goal of the thesis was to test the hypothesis that targeting IL3R (α and β subunits) on CML cells would block the IL3–dependent survival of CML cells and deplete CML leukemic stem cells. Our novel anti–mIL3Rα IgG and anti–mIL3Rβ IgG showed significant blockade of downstream IL3 signalling in CML cells, and also reverted IL3–dependent imatinib activity *in vitro*. Reversal of IL3 suppression of imatinib

activity allowed sensitization of CML cells to imatinib, leading to inhibition of CML cell proliferation and colony formation *in vitro*. Further support for these findings was that engraftment of antibody–treated CML cells into the sub–lethally irradiated mouse model caused a prolonged survival of mice. Altogether, anti–mIL3Rα and anti–mIL3Rβ IgGs generated in this work may be especially relevant for targeted therapy of quiescent CML–LSCs that remain in bone marrow niche and escape the conventional chemotherapies (i.e. tyrosine kinase inhibitors). The anti–mIL3Rα and anti–mIL3Rβ IgGs may provide new therapeutics to eradicate CML–LSCs. As of June 2018, there is only a few interventional studies investigating anti–mIL3Rα IgG (Anti–CD123 monoclonal antibody or CSL362, Drug name JNJ–56022473 licensed to Johnson & Johnson) as therapeutic candidate for AML, systemic lupus erythmatosus, myelodysplastic syndrome, and myeloproliferative disorder patients (global data.com). Other CD123 bispecific formats in phase I clinical trial for AML are CD123 x CD3 DARTs (NCT02152956 and NCT02454270) and CD123 x CD3 XmAb (XmAb14045, NCT02730312) (Cuesta-Mateos et al., 2018; Thakur et al., 2018). However, there is no report of generation of anti–IL3Rβ antibody to target the β–subunit of IL3R (CD131) for novel therapeutic purposes in cancer patients. CSL311 is the only anti–IL3Rβ monoclonal antibody under development (phase I study) reported for targeting IL3Rβ in treatment of allergic asthma (globaldata.com).

The success of anti–mIL3Rα IgG and anti–mIL3Rβ IgG in suppression of IL3–mediated imatinib suppression encouraged us to pursue the project by co–targeting IL3Rα and IL3Rβ subunits. SpyCatcher—SpyTag system (Reddington & Howarth, 2015; Zakeri et al., 2012) was used to fuse IL3Rα mono–Fab and IL3Rβ mono–Fab and generate bispecific Fabs targeting both IL3Rα and IL3Rβ subunits. In addition to generation of IL3Rα–IL3Rβ bispecific Fab, we generated bivalent Fabs linking IL3Rα mono–Fabs or IL3Rβ mono–Fabs. Unlike full length IgGs, bivalent and bispecific Fabs have the advantage of not dictating Fab function by Fc portion. The purified IL3Rα–α / IL3Rβ–β bivalent and IL3Rβ–α bispecific Fabs were validated and characterized by size, purity, high target specificity and nanomolar affinity to the target *in vitro.* More importantly, we confirmed blocking of downstream IL3 signaling by bivalent and bispecific Fabs. In particular, bivalent and bispecific Fab blocked IL3 signaling with inhibition of JAK2 and STAT5 tyrosine phosphorylation. However, an increase in

signaling was observed when cells were treated with higher concentration of IL3Rβ–β bivalent Fab. This finding brought up the question whether bridging two IL3Rβ Fabs may cause agonistic activity of IL3Rβ–β bivalent Fab by co-stimulatory receptor heterodimerization activation and supercluster receptor formation. This question remains to be answered in future studies.

Interestingly, IL3Rα–α and IL3Rβ–β bivalent Fab and IL3Rβ–α bispecific Fab caused direct CML cell killing *in vitro*. In order to further investigate the therapeutic potential of bivalent and bispecific Fabs, we explored the additive effect of Fabs with imatinib. IL3Rβ–β bivalent Fab and IL3Rβ–α bispecific Fab showed a strong additive cytotoxic effect with imatinib on CML cells *in vitro*. However, IL3Rα–α bivalent Fab lacked the additive inhibitory effect with Imatinib on CML cells. Impairment of CML cell colony formation by IL3Rβ–α bispecific Fab was another evidence that confirmed targeting of CML–LSCs by our novel Fab. Collectively, IL3Rα–α and IL3Rβ–β bivalent Fab and IL3Rβ–α bispecific Fab may provide novel therapeutic approaches for targeting leukemic stem cells, possibility of administration as co–drugs with conventional chemotherapies, and new solutions to overcome recurrence and relapse in CML patients.

6.2. FUTURE DIRECTIONS

***In vivo* toxicity and pharmacokinetics of IgGs:** The novel synthetic anti–mIL3Rα IgG and anti–mIL3Rβ IgG generated in this thesis can be further investigated for *in vivo* toxicity and pharmacokinetics.

***In vivo* efficacy of anti–mIL3Rα and anti–mIL3Rβ IgGs in patient–derived xenograft models of leukemia:** Our anti–mIL3Rα and anti–mIL3Rβ antibodies can be further examined for *in vivo* therapeutic efficacy in patient–derived xenografts (PDX) mouse models.

Cellular immunotherapy to target CD123 / CD131 in various leukemias: Anti–mIL3Rα and anti–mIL3Rβ IgGs can be further investigated *in vitro* and *in vivo* for anti–leukemic effect on patient–derived hematological malignancies with IL3–overexpression.

Anti–IL3R antibodies as co–drugs with conventional chemotherapies: Anti–mIL3Rα and anti–mIL3Rβ IgG can be used for creating novel combinatorial treatment approaches, such as combination–therapy with potent TKIs to target CML or AML cells with more efficacy and potency and higher safety profile. This scenario may allow lowering the dose of chemotherapy in leukemia patients.

IL3R bivalent or bispecific Fabs as co–drugs with TKIs: The novel anti–IL3Rβ–α bispecific Fab can be further investigated individually or as co–drug with TKIs *in vivo* to explore potential therapeutic implications for anti–IL3R bispecific Fabs.

Personalized therapy with CD123 / CD131 redirected autologous T cells: Using the irreversible covalent bond between SpyCatcher and SpyTag allows fusion of any other antibody fragment of choice to our novel anti–mIL3Rα or anti–mIL3Rβ mono–Fabs to redirect target binding or increase specificity and selectivity. This method can be used to redirect chimeric antigen receptor T cells (CARTs) to enhance the specificity and selectivity of triggering cancer cells with CART–CD123, CART–CD131, or bispecific CART–CD123/CD131. This may provide novel bispecific Fabs with potential personalized therapeutics for multiple hematological malignancies.

Theranostics: Considering the specificity and high affinity of our anti–IL3Rα IgG and anti–IL3Rβ IgG, there is the possibility of repositioning the antibodies as companion diagnostic (CDx). Radio–labelled anti–IL3Rα or anti–IL3Rβ IgG may detect the quiescent leukemic stem cells or metastasis using PET (positron emission tomography) imaging. Moreover, our novel antibodies may be used for personalized theranostic strategies in pharmDx assays, as an aid in identifying patients with hematological malignancy and appropriate targeted therapy. Using our novel anti–IL3Rα and anti–mIL3Rβ IgGs as theranostics may provide novel new methods to reduce relapse in patients with any type of leukemia with IL3 expression.

REFERENCES

Abdel-Meguid, S. S., Shieh, H. S., Smith, W. W., Dayringer, H. E., Violand, B. N., & Bentle, L. A. (1987). Three-dimensional structure of a genetically engineered variant of porcine growth hormone. *Proceedings of the National Academy of Sciences of the United States of America*, *84*(18), 6434–6437.

Abelson, H. T., & Rabstein, L. S. (1970). Lymphosarcoma: virus-induced thymic-independent disease in mice. *Cancer Research*, *30*(8), 2213–2222.

Adams, G. P., Schier, R., Marshall, K., Wolf, E. J., McCall, A. M., Marks, J. D., & Weiner, L. M. (1998). Increased affinity leads to improved selective tumor delivery of single-chain Fv antibodies. *Cancer Research*, *58*(3), 485–490.

Advani, A. S., & Pendergast, A. M. (2002). Bcr-Abl variants: biological and clinical aspects. *Leukemia Research*, *26*(8), 713–720.

Ahmed, W., & Van Etten, R. A. (2013). Signal transduction in the chronic leukemias: implications for targeted therapies. *Current Hematologic Malignancy Reports*, *8*(1), 71–80. https://doi.org/10.1007/s11899-012-0150-1

Ahuja, H., Bar-Eli, M., Advani, S. H., Benchimol, S., & Cline, M. J. (1989). Alterations in the p53 gene and the clonal evolution of the blast crisis of chronic myelocytic leukemia. *Proceedings of the National Academy of Sciences of the United States of America*, *86*(17), 6783–6787.

Aixinjueluo, W., Furukawa, K. K., Zhang, Q., Hamamura, K., Tokuda, N., Yoshida, S., … Furukawa, K. K. (2005). Mechanisms for the apoptosis of small cell lung cancer cells induced by anti-GD2 monoclonal antibodies: roles of anoikis. *The Journal of Biological Chemistry*, *280*(33), 29828–29836. https://doi.org/10.1074/jbc.M414041200

Alam, M. K., Gonzalez, C., Hill, W., Fonge, H., Barreto, K., & Geyer, C. R. (2017). Synthetic Modular Antibody Construction Using the SpyTag/SpyCatcher Protein Ligase System. *Chembiochem : A European Journal of Chemical Biology*. https://doi.org/10.1002/cbic.201700411

Aldinucci, D., Olivo, K., Lorenzon, D., Poletto, D., Gloghini, A., Carbone, A., & Pinto, A. (2005). The role of interleukin-3 in classical Hodgkin's disease. *Leukemia & Lymphoma*,

46(3), 303–311. https://doi.org/10.1080/10428190400013712

Alduaij, W., Ivanov, A., Honeychurch, J., Cheadle, E. J., Potluri, S., Lim, S. H., … Illidge, T. M. (2011). Novel type II anti-CD20 monoclonal antibody (GA101) evokes homotypic adhesion and actin-dependent, lysosome-mediated cell death in B-cell malignancies. *Blood*, *117*(17), 4519–4529. https://doi.org/10.1182/blood-2010-07-296913

Alexander, W. S., & Nicola, N. A. (1998). Hemopoietic growth factor receptor abnormalities in leukemia. *Leukemia Research*, *22*(12), 1097–1111.

Alinari, L., Yu, B., Christian, B. A., Yan, F., Shin, J., Lapalombella, R., … Baiocchi, R. A. (2011). Combination anti-CD74 (milatuzumab) and anti-CD20 (rituximab) monoclonal antibody therapy has in vitro and in vivo activity in mantle cell lymphoma. *Blood*, *117*(17), 4530 LP-4541. Retrieved from http://www.bloodjournal.org/content/117/17/4530.abstract

Almagro, J. C., & Fransson, J. (2008). Humanization of antibodies. *Frontiers in Bioscience : A Journal and Virtual Library*, *13*, 1619–1633.

Andris-Widhopf, J., Steinberger, P., Fuller, R., Rader, C., & Barbas, C. F. 3rd. (2011). Generation of human scFv antibody libraries: PCR amplification and assembly of light- and heavy-chain coding sequences. *Cold Spring Harbor Protocols*, *2011*(9). https://doi.org/10.1101/pdb.prot065573

Arceci, R. J. (1993, May). Clinical significance of P-glycoprotein in multidrug resistance malignancies. *Blood*. United States.

Bagley, C. J., Woodcock, J. M., Stomski, F. C., & Lopez, A. F. (1997). The Structural and Functional Basis of Cytokine Receptor Activation: Lessons From the Common β Subunit of the Granulocyte-Macrophage Colony-Stimulating Factor, Interleukin-3 (IL-3), and IL-5 Receptors. *Blood*, *89*(5), 1471 LP-1482. Retrieved from http://www.bloodjournal.org/content/89/5/1471.abstract

Baig, N. A., Taylor, R. P., Lindorfer, M. A., Church, A. K., Laplant, B. R., Pavey, E. S., … Zent, C. S. (2012). Complement dependent cytotoxicity in chronic lymphocytic leukemia: ofatumumab enhances alemtuzumab complement dependent cytotoxicity and reveals cells resistant to activated complement. *Leukemia & Lymphoma*, *53*(11), 2218–2227. https://doi.org/10.3109/10428194.2012.681657

Ban, K., Gao, Y., Amin, H. M., Howard, A., Miller, C., Lin, Q., … Chandra, J. (2008). BCR-ABL1 mediates up-regulation of Fyn in chronic myelogenous leukemia. *Blood*,

111(5), 2904–2908. https://doi.org/10.1182/blood-2007-05-091769

Barbas, C. F. 3rd, Kang, A. S., Lerner, R. A., & Benkovic, S. J. (1991). Assembly of combinatorial antibody libraries on phage surfaces: the gene III site. *Proceedings of the National Academy of Sciences of the United States of America*, *88*(18), 7978–7982.

Barnes, D. J., Palaiologou, D., Panousopoulou, E., Schultheis, B., Yong, A. S. M., Wong, A., … Melo, J. V. (2005). Bcr-Abl expression levels determine the rate of development of resistance to imatinib mesylate in chronic myeloid leukemia. *Cancer Research*, *65*(19), 8912–8919. https://doi.org/10.1158/0008-5472.CAN-05-0076

Bartram, C. R., de Klein, A., Hagemeijer, A., van Agthoven, T., Geurts van Kessel, A., Bootsma, D., … Stone, M. (1983). Translocation of c-ab1 oncogene correlates with the presence of a Philadelphia chromosome in chronic myelocytic leukaemia. *Nature*, *306*(5940), 277–280.

Beerman, I., Bock, C., Garrison, B. S., Smith, Z. D., Gu, H., Meissner, A., & Rossi, D. J. (2013). Proliferation-dependent alterations of the DNA methylation landscape underlie hematopoietic stem cell aging. *Cell Stem Cell*, *12*(4), 413–425. https://doi.org/10.1016/j.stem.2013.01.017

Belloc, F., Airiau, K., Jeanneteau, M., Garcia, M., Guérin, E., Lippert, E., … Mahon, F.-X. (2009). The stem cell factor-c-KIT pathway must be inhibited to enable apoptosis induced by BCR-ABL inhibitors in chronic myelogenous leukemia cells. *Leukemia : Official Journal of the Leukemia Society of America, Leukemia Research Fund, U.K*, *23*(4), 679–685. https://doi.org/10.1038/leu.2008.364

Ben-Neriah, Y., Daley, G. Q., Mes-Masson, A. M., Witte, O. N., & Baltimore, D. (1986). The chronic myelogenous leukemia-specific P210 protein is the product of the bcr/abl hybrid gene. *Science (New York, N.Y.)*, *233*(4760), 212–214.

Beran, M., Cao, X., Estrov, Z., Jeha, S., Jin, G., O'Brien, S., … Kantarjian, H. (1998). Selective inhibition of cell proliferation and BCR-ABL phosphorylation in acute lymphoblastic leukemia cells expressing Mr 190,000 BCR-ABL protein by a tyrosine kinase inhibitor (CGP-57148). *Clinical Cancer Research : An Official Journal of the American Association for Cancer Research*, *4*(7), 1661–1672.

Besancon, F., Atfi, A., Gespach, C., Cayre, Y. E., & Bourgeade, M. F. (1998). Evidence for a role of NF-kappaB in the survival of hematopoietic cells mediated by interleukin 3 and

the oncogenic TEL/platelet-derived growth factor receptor beta fusion protein. *Proceedings of the National Academy of Sciences of the United States of America*, *95*(14), 8081–8086.

Bhat, N. M., Bieber, M. M., Hsu, F. J., Chapman, C. J., Spellerberg, M., Stevenson, F. K., & Teng, N. N. (1997). Rapid cytotoxicity of human B lymphocytes induced by VH4-34 (VH4.21) gene-encoded monoclonal antibodies, II. *Clinical and Experimental Immunology*, *108*(1), 151–159.

Birch, J. R., & Racher, A. J. (2006). Antibody production. *Advanced Drug Delivery Reviews*, *58*(5–6), 671–685. https://doi.org/10.1016/j.addr.2005.12.006

Blume-Jensen, P., & Hunter, T. (2001). Oncogenic kinase signalling. *Nature*, *411*(6835), 355–365. https://doi.org/10.1038/35077225

Bolin, R. W., Robinson, W. A., Sutherland, J., & Hamman, R. F. (1982). Busulfan versus hydroxyurea in long-term therapy of chronic myelogenous leukemia. *Cancer*, *50*(9), 1683–1686.

Bond, C. J., Wiesmann, C., Marsters, J. C. J., & Sidhu, S. S. (2005). A structure-based database of antibody variable domain diversity. *Journal of Molecular Biology*, *348*(3), 699–709. https://doi.org/10.1016/j.jmb.2005.02.063

Bone, H., & Welham, M. J. (2000). Shc associates with the IL-3 receptor beta subunit, SHIP and Gab2 following IL-3 stimulation. Contribution of Shc PTB and SH2 domains. *Cellular Signalling*, *12*(3), 183–194.

Bonnet, D., & Dick, J. E. (1997). Human acute myeloid leukemia is organized as a hierarchy that originates from a primitive hematopoietic cell. *Nature Medicine*, *3*(7), 730–737.

Borsellino, N., Bonavida, B., Ciliberto, G., Toniatti, C., Travali, S., & D'Alessandro, N. (1999). Blocking signaling through the Gp130 receptor chain by interleukin-6 and oncostatin M inhibits PC-3 cell growth and sensitizes the tumor cells to etoposide and cisplatin-mediated cytotoxicity. *Cancer*, *85*(1), 134–144.

Bowles, J. A., & Weiner, G. J. (2005). CD16 polymorphisms and NK activation induced by monoclonal antibody-coated target cells. *Journal of Immunological Methods*, *304*(1–2), 88–99. https://doi.org/10.1016/j.jim.2005.06.018

Bradbury, A. R. M., Sidhu, S., Dubel, S., & McCafferty, J. (2011). Beyond natural antibodies: the power of in vitro display technologies. *Nat Biotech*, *29*(3), 245–254. Retrieved from http://dx.doi.org/10.1038/nbt.1791

Bradley, T. R., & Metcalf, D. (1966). The growth of mouse bone marrow cells in vitro. *The Australian Journal of Experimental Biology and Medical Science*, *44*(3), 287–299.

Bradley, W. D., & Koleske, A. J. (2009). Regulation of cell migration and morphogenesis by Abl-family kinases: emerging mechanisms and physiological contexts. *Journal of Cell Science*, *122*(Pt 19), 3441–3454. https://doi.org/10.1242/jcs.039859

Branford, S., Rudzki, Z., Walsh, S., Parkinson, I., Grigg, A., Szer, J., … Hughes, T. (2003). Detection of BCR-ABL mutations in patients with CML treated with imatinib is virtually always accompanied by clinical resistance, and mutations in the ATP phosphate-binding loop (P-loop) are associated with a poor prognosis. *Blood*, *102*(1), 276–283. https://doi.org/10.1182/blood-2002-09-2896

Brasher, B. B., & Van Etten, R. A. (2000). c-Abl has high intrinsic tyrosine kinase activity that is stimulated by mutation of the Src homology 3 domain and by autophosphorylation at two distinct regulatory tyrosines. *The Journal of Biological Chemistry*, *275*(45), 35631–35637. https://doi.org/10.1074/jbc.M005401200

Brinkmann, U., & Kontermann, R. E. (2017). The making of bispecific antibodies. *MAbs*, *9*(2), 182–212. https://doi.org/10.1080/19420862.2016.1268307

Broughton, S. E., Dhagat, U., Hercus, T. R., Nero, T. L., Grimbaldeston, M. A., Bonder, C. S., … Parker, M. W. (2012). The GM- CSF/ IL-3/ IL-5 cytokine receptor family: from ligand recognition to initiation of signaling. *Immunological Reviews*, *250*(1), 277–302. Retrieved from 10.1111/j.1600-065X.2012.01164.x%5Cnhttps://ezproxy.library.astate.edu/login?url=http://search.ebscohost.com/login.aspx?direct=true&db=a9h&AN=82335818&site=ehost-live

Broughton, S. E., Hercus, T. R., Hardy, M. P., McClure, B. J., Nero, T. L., Dottore, M., … Lopez, A. F. (2014). Dual Mechanism of Interleukin-3 Receptor Blockade by an Anti-Cancer Antibody. *Cell Reports*, *8*(2), 410–419. https://doi.org/10.1016/j.celrep.2014.06.038

Broughton, S. E., Nero, T. L., Dhagat, U., Kan, W. L., Hercus, T. R., Tvorogov, D., … Parker, M. W. (2015). The betac receptor family - Structural insights and their functional implications. *Cytokine*, *74*(2), 247–258. https://doi.org/10.1016/j.cyto.2015.02.005

Bruggemann, M., Caskey, H. M., Teale, C., Waldmann, H., Williams, G. T., Surani, M. A., & Neuberger, M. S. (1989). A repertoire of monoclonal antibodies with human heavy chains from transgenic mice. *Proceedings of the National Academy of Sciences of the United States*

of America, *86*(17), 6709–6713.

Buchdunger, E., Zimmermann, J., Mett, H., Meyer, T., Muller, M., Druker, B. J., & Lydon, N. B. (1996). Inhibition of the Abl protein-tyrosine kinase in vitro and in vivo by a 2-phenylaminopyrimidine derivative. *Cancer Research*, *56*(1), 100–104.

Burke, B. a, & Carroll, M. (2010). BCR-ABL: a multi-faceted promoter of DNA mutation in chronic myelogeneous leukemia. *Leukemia : Official Journal of the Leukemia Society of America, Leukemia Research Fund, U.K*, *24*(6), 1105–1112. https://doi.org/10.1038/leu.2010.67

Busfield, S. J., Biondo, M., Wong, M., Ramshaw, H. S., Lee, E. M., Ghosh, S., … Nash, A. D. (2014). Targeting of acute myeloid leukemia in vitro and in vivo with an anti-CD123 mAb engineered for optimal ADCC. *Leukemia*, *28*(11), 2213–2221. https://doi.org/10.1038/leu.2014.128

Cahill, M. A., Janknecht, R., & Nordheim, A. (1996). Signalling pathways: jack of all cascades. *Current Biology : CB*, *6*(1), 16–19.

Calabretta, B., & Perrotti, D. (2004). The biology of CML blast crisis. *Blood*, *103*(11), 4010–4022. https://doi.org/10.1182/blood-2003-12-4111

Cao, X., Tanis, K. Q., Koleske, A. J., & Colicelli, J. (2008). Enhancement of ABL kinase catalytic efficiency by a direct binding regulator is independent of other regulatory mechanisms. *The Journal of Biological Chemistry*, *283*(46), 31401–31407. https://doi.org/10.1074/jbc.M804002200

Carella, A. M., Garuti, A., Cirmena, G., Catania, G., Rocco, I., Palermo, C., … Patrone, F. (2010). Kinase domain mutations of BCR-ABL identified at diagnosis before imatinib-based therapy are associated with progression in patients with high Sokal risk chronic phase chronic myeloid leukemia. *Leukemia & Lymphoma*, *51*(2), 275–278. https://doi.org/10.3109/10428190903503446

Carr, P. D., Gustin, S. E., Church, A. P., Murphy, J. M., Ford, S. C., Mann, D. A., … Young, I. G. (2001). Structure of the complete extracellular domain of the common ?? subunit of the human GM-CSF, IL-3, and IL-5 receptors reveals a novel dimer configuration. *Cell*, *104*(2), 291–300. https://doi.org/10.1016/S0092-8674(01)00213-6

Carroll, M., Ohno-Jones, S., Tamura, S., Buchdunger, E., Zimmermann, J., Lydon, N. B., … Druker, B. J. (1997). CGP 57148, a tyrosine kinase inhibitor, inhibits the growth of cells

expressing BCR-ABL, TEL-ABL, and TEL-PDGFR fusion proteins. *Blood*, *90*(12), 4947–4952.

Cartron, G., Dacheux, L., Salles, G., Solal-Celigny, P., Bardos, P., Colombat, P., & Watier, H. (2002). Therapeutic activity of humanized anti-CD20 monoclonal antibody and polymorphism in IgG Fc receptor FcgammaRIIIa gene. *Blood*, *99*(3), 754–758.

Catlett-Falcone, R., Landowski, T. H., Oshiro, M. M., Turkson, J., Levitzki, A., Savino, R., … Jove, R. (1999). Constitutive activation of Stat3 signaling confers resistance to apoptosis in human U266 myeloma cells. *Immunity*, *10*(1), 105–115.

Cerisano, V., Aalto, Y., Perdichizzi, S., Bernard, G., Manara, M. C., Benini, S., … Scotlandi, K. (2004). Molecular mechanisms of CD99-induced caspase-independent cell death and cell-cell adhesion in Ewing's sarcoma cells: actin and zyxin as key intracellular mediators. *Oncogene*, *23*(33), 5664–5674. https://doi.org/10.1038/sj.onc.1207741

Chames, P., Van Regenmortel, M., Weiss, E., & Baty, D. (2009). Therapeutic antibodies: successes, limitations and hopes for the future. *British Journal of Pharmacology*, *157*(2), 220–233. https://doi.org/10.1111/j.1476-5381.2009.00190.x

Chan, C. E. Z., Lim, A. P. C., MacAry, P. A., & Hanson, B. J. (2014). The role of phage display in therapeutic antibody discovery. *International Immunology*, *26*(12), 649–657. https://doi.org/10.1093/intimm/dxu082

Chang, F., & McCubrey, J. A. (2001). P21(Cip1) induced by Raf is associated with increased Cdk4 activity in hematopoietic cells. *Oncogene*, *20*(32), 4354–4364.

Chapman, A. P., Antoniw, P., Spitali, M., West, S., Stephens, S., & King, D. J. (1999). Therapeutic antibody fragments with prolonged in vivo half-lives. *Nature Biotechnology*, *17*(8), 780–783. https://doi.org/10.1038/11717

Chen, G; Sidhu, S. (2014). Design and Generation of Synthetic Antibody Libraries for Phage Display. In N. Ossipow, Vincent; Fischer (Ed.), *Monoclonal antibodies*. Totowa, NJ: Human Press.

Chen, J., Olsen, J., Ford, S., Mirza, S., Walker, A., Murphy, J. M., & Young, I. G. (2009). A new isoform of interleukin-3 receptor {alpha} with novel differentiation activity and high affinity binding mode. *The Journal of Biological Chemistry*, *284*(9), 5763–5773. https://doi.org/10.1074/jbc.M808197200

Chen, P.-H., Chien, F.-C., Lee, S.-P., Chan, W.-E., Lin, I.-H., Liu, C.-S., … Yen, J. J.-Y.

(2012). Identification of a novel function of the clathrin-coated structure at the plasma membrane in facilitating GM-CSF receptor-mediated activation of JAK2. *Cell Cycle (Georgetown, Tex.)*, *11*(19), 3611–3626. https://doi.org/10.4161/cc.21920

Chen, S., O'Reilly, L. P., Smithgall, T. E., & Engen, J. R. (2008). Tyrosine phosphorylation in the SH3 domain disrupts negative regulatory interactions within the c-Abl kinase core. *Journal of Molecular Biology*, *383*(2), 414–423. https://doi.org/10.1016/j.jmb.2008.08.040

Cheson, B. D., & Leonard, J. P. (2008). Monoclonal antibody therapy for B-cell non-Hodgkin's lymphoma. *The New England Journal of Medicine*, *359*(6), 613–626. https://doi.org/10.1056/NEJMra0708875

Chichili, G. R., Huang, L., Li, H., Burke, S., He, L., Tang, Q., … Bonvini, E. (2015). A CD3xCD123 bispecific DART for redirecting host T cells to myelogenous leukemia: preclinical activity and safety in nonhuman primates. *Science Translational Medicine*, *7*(289), 289ra82. https://doi.org/10.1126/scitranslmed.aaa5693

Chitnis, M. M., Yuen, J. S. P., Protheroe, A. S., Pollak, M., & Macaulay, V. M. (2008). The type 1 insulin-like growth factor receptor pathway. *Clinical Cancer Research : An Official Journal of the American Association for Cancer Research*, *14*(20), 6364–6370. https://doi.org/10.1158/1078-0432.CCR-07-4879

Chomel, J.-C., Bonnet, M.-L., Sorel, N., Bertrand, A., Meunier, M.-C., Fichelson, S., … Turhan, A. G. (2011). Leukemic stem cell persistence in chronic myeloid leukemia patients with sustained undetectable molecular residual disease. *Blood*, *118*(13), 3657–3660. https://doi.org/10.1182/blood-2011-02-335497

Chu, S., McDonald, T., Lin, A., Chakraborty, S., Huang, Q., Snyder, D. S., & Bhatia, R. (2011). Persistence of leukemia stem cells in chronic myelogenous leukemia patients in prolonged remission with imatinib treatment. *Blood*, *118*(20), 5565–5572. https://doi.org/10.1182/blood-2010-12-327437

Clackson, T., Hoogenboom, H. R., Griffiths, A. D., & Winter, G. (1991). Making antibody fragments using phage display libraries. *Nature*, *352*(6336), 624–628. https://doi.org/10.1038/352624a0

Colicelli, J. (2010). ABL tyrosine kinases: evolution of function, regulation, and specificity. *Science Signaling*, *3*(139), re6. https://doi.org/10.1126/scisignal.3139re6

Corbin, A. S., Agarwal, A., Loriaux, M., Cortes, J., Deininger, M. W., & Druker, B. J.

(2011). Human chronic myeloid leukemia stem cells are insensitive to imatinib despite inhibition of BCR-ABL activity. *The Journal of Clinical Investigation*, *121*(1), 396–409. https://doi.org/10.1172/JCI35721

Cortes, J., Jabbour, E., Kantarjian, H., Yin, C. C., Shan, J., O'Brien, S., … Jones, D. (2007). Dynamics of BCR-ABL kinase domain mutations in chronic myeloid leukemia after sequential treatment with multiple tyrosine kinase inhibitors. *Blood*, *110*(12), 4005–4011. https://doi.org/10.1182/blood-2007-03-080838

Cowan-Jacob, S. W., Guez, V., Fendrich, G., Griffin, J. D., Fabbro, D., Furet, P., … Manley, P. W. (2004). Imatinib (STI571) resistance in chronic myelogenous leukemia: molecular basis of the underlying mechanisms and potential strategies for treatment. *Mini Reviews in Medicinal Chemistry*, *4*(3), 285–299.

Crossman, L. C., Druker, B. J., Deininger, M. W. N., Pirmohamed, M., Wang, L., & Clark, R. E. (2005, August). hOCT 1 and resistance to imatinib. *Blood*. United States. https://doi.org/10.1182/blood-2005-02-0694

Cuenco, G. M., & Ren, R. (2001). Cooperation of BCR-ABL and AML1/MDS1/EVI1 in blocking myeloid differentiation and rapid induction of an acute myelogenous leukemia. *Oncogene*, *20*(57), 8236–8248. https://doi.org/10.1038/sj.onc.1205095

Cuesta-Mateos, C., Alcaraz-Serna, A., Somovilla-Crespo, B., & Muñoz-Calleja, C. (2018). Monoclonal Antibody Therapies for Hematological Malignancies: Not Just Lineage-Specific Targets . *Frontiers in Immunology* . Retrieved from https://www.frontiersin.org/article/10.3389/fimmu.2017.01936

Cullen, S. P., Brunet, M., & Martin, S. J. (2010). Granzymes in cancer and immunity. *Cell Death and Differentiation*, *17*(4), 616–623. https://doi.org/10.1038/cdd.2009.206

Cummins, K. D., & Gill, S. (2018). Anti-CD123 chimeric antigen receptor T-cells (CART): an evolving treatment strategy for hematological malignancies, and a potential ace-in-the-hole against antigen-negative relapse. *Leukemia & Lymphoma*, *59*(7), 1539–1553. https://doi.org/10.1080/10428194.2017.1375107

Dai, Y., Rahmani, M., Corey, S. J., Dent, P., & Grant, S. (2004). A Bcr/Abl-independent, Lyn-dependent form of imatinib mesylate (STI-571) resistance is associated with altered expression of Bcl-2. *The Journal of Biological Chemistry*, *279*(33), 34227–34239. https://doi.org/10.1074/jbc.M402290200

Daley, G. Q., Van Etten, R. A., & Baltimore, D. (1990). Induction of chronic myelogenous leukemia in mice by the P210bcr/abl gene of the Philadelphia chromosome. *Science (New York, N.Y.)*, *247*(4944), 824–830.

Damiano, J. S., Cress, A. E., Hazlehurst, L. A., Shtil, A. A., & Dalton, W. S. (1999). Cell adhesion mediated drug resistance (CAM-DR): role of integrins and resistance to apoptosis in human myeloma cell lines. *Blood*, *93*(5), 1658–1667.

Dan, S., Naito, M., & Tsuruo, T. (1998). Selective induction of apoptosis in Philadelphia chromosome-positive chronic myelogenous leukemia cells by an inhibitor of BCR - ABL tyrosine kinase, CGP 57148. *Cell Death and Differentiation*, *5*(8), 710–715. https://doi.org/10.1038/sj.cdd.4400400

Danhauser-Riedl, S., Warmuth, M., Druker, B. J., Emmerich, B., & Hallek, M. (1996). Activation of Src kinases p53/56lyn and p59hck by p210bcr/abl in myeloid cells. *Cancer Research*, *56*(15), 3589–3596.

Dash, A. B., Williams, I. R., Kutok, J. L., Tomasson, M. H., Anastasiadou, E., Lindahl, K., … Gilliland, D. G. (2002). A murine model of CML blast crisis induced by cooperation between BCR/ABL and NUP98/HOXA9. *Proceedings of the National Academy of Sciences of the United States of America*, *99*(11), 7622–7627. https://doi.org/10.1073/pnas.102583199

Davis, A. E. 3rd. (2004). Biological effects of C1 inhibitor. *Drug News & Perspectives*, *17*(7), 439–446.

De Keersmaecker, K., Graux, C., Odero, M. D., Mentens, N., Somers, R., Maertens, J., … Cools, J. (2005). Fusion of EML1 to ABL1 in T-cell acute lymphoblastic leukemia with cryptic t(9;14)(q34;q32). *Blood*, *105*(12), 4849–4852. https://doi.org/10.1182/blood-2004-12-4897

de la Fuente, M. T., Casanova, B., Moyano, J. V, Garcia-Gila, M., Sanz, L., Garcia-Marco, J., … Garcia-Pardo, A. (2002). Engagement of alpha4beta1 integrin by fibronectin induces in vitro resistance of B chronic lymphocytic leukemia cells to fludarabine. *Journal of Leukocyte Biology*, *71*(3), 495–502.

De Waele, M., Renmans, W., Vander Gucht, K., Jochmans, K., Schots, R., Otten, J., … Van Riet, I. (2001). Growth factor receptor profile of CD34+ cells in AML and B-lineage ALL and in their normal bone marrow counterparts. *European Journal of Haematology*, *66*(3),

178–187.

Deininger, M., Buchdunger, E., & Druker, B. J. (2005). Review in translational hematology The development of imatinib as a therapeutic agent for chronic myeloid leukemia. *Blood*, *105*(7), 2640–2653. https://doi.org/10.1182/blood-2004-08-3097

Deininger, M. W., Goldman, J. M., & Melo, J. V. (2000). The molecular biology of chronic myeloid leukemia. *Blood*, *96*(10), 3343–3356.

Deininger, M. W., Vieira, S. A., Parada, Y., Banerji, L., Lam, E. W., Peters, G., … Melo, J. V. (2001). Direct relation between BCR-ABL tyrosine kinase activity and cyclin D2 expression in lymphoblasts. *Cancer Research*, *61*(21), 8005–8013.

Desiderio, A., Franconi, R., Lopez, M., Villani, M. E., Viti, F., Chiaraluce, R., … Benvenuto, E. (2001). A semi-synthetic repertoire of intrinsically stable antibody fragments derived from a single-framework scaffold. *Journal of Molecular Biology*, *310*(3), 603–615. https://doi.org/10.1006/jmbi.2001.4756

Deutsch, E., Dugray, A., AbdulKarim, B., Marangoni, E., Maggiorella, L., Vaganay, S., … Bourhis, J. (2001). BCR-ABL down-regulates the DNA repair protein DNA-PKcs. *Blood*, *97*(7), 2084–2090.

Deutsch, E., Jarrousse, S., Buet, D., Dugray, A., Bonnet, M.-L., Vozenin-Brotons, M.-C., … Bourhis, J. (2003). Down-regulation of BRCA1 in BCR-ABL-expressing hematopoietic cells. *Blood*, *101*(11), 4583–4588. https://doi.org/10.1182/blood-2002-10-3011

Dhingra, K., Talpaz, M., Kantarjian, H., Ku, S., Rothberg, J., Gutterman, J. U., & Kurzrock, R. (1991). Appearance of acute leukemia-associated P190BCR-ABL in chronic myelogenous leukemia may correlate with disease progression. *Leukemia*, *5*(3), 191–195.

DiDonato, J. A., Hayakawa, M., Rothwarf, D. M., Zandi, E., & Karin, M. (1997). A cytokine-responsive IkappaB kinase that activates the transcription factor NF-kappaB. *Nature*, *388*(6642), 548–554. https://doi.org/10.1038/41493

Dierov, J., Dierova, R., & Carroll, M. (2004). BCR/ABL translocates to the nucleus and disrupts an ATR-dependent intra-S phase checkpoint. *Cancer Cell*, *5*(3), 275–285.

Ding, G., Chen, X., Zhu, J., & Cao, B. (2010). Identification of two aberrant transcripts derived from a hybridoma with amplification of functional immunoglobulin variable genes. *Cellular & Molecular Immunology*, *7*(5), 349–354. https://doi.org/10.1038/cmi.2010.33

Djokic, M., Bjorklund, E., Blennow, E., Mazur, J., Soderhall, S., & Porwit, A. (2009).

Overexpression of CD123 correlates with the hyperdiploid genotype in acute lymphoblastic leukemia. *Haematologica*, *94*(7), 1016–1019. https://doi.org/10.3324/haematol.2008.000299

Donato, N. J., Wu, J. Y., Stapley, J., Gallick, G., Lin, H., Arlinghaus, R., & Talpaz, M. (2003). BCR-ABL independence and LYN kinase overexpression in chronic myelogenous leukemia cells selected for resistance to STI571. *Blood*, *101*(2), 690–698. https://doi.org/10.1182/blood.V101.2.690

Donato, N. J., Wu, J. Y., Stapley, J., Lin, H., Arlinghaus, R., Aggarwal, B. B., … Talpaz, M. (2004). Imatinib mesylate resistance through BCR-ABL independence in chronic myelogenous leukemia. *Cancer Research*, *64*(2), 672–677.

Donehower, L. A., Harvey, M., Slagle, B. L., McArthur, M. J., Montgomery, C. A. J., Butel, J. S., & Bradley, A. (1992). Mice deficient for p53 are developmentally normal but susceptible to spontaneous tumours. *Nature*, *356*(6366), 215–221. https://doi.org/10.1038/356215a0

Dorey, K., Engen, J. R., Kretzschmar, J., Wilm, M., Neubauer, G., Schindler, T., & Superti-Furga, G. (2001). Phosphorylation and structure-based functional studies reveal a positive and a negative role for the activation loop of the c-Abl tyrosine kinase. *Oncogene*, *20*(56), 8075–8084. https://doi.org/10.1038/sj.onc.1205017

Druker, B. J., Tamura, S., Buchdunger, E., Ohno, S., Segal, G. M., Fanning, S., … Lydon, N. B. (1996). Effects of a selective inhibitor of the Abl tyrosine kinase on the growth of Bcr-Abl positive cells. *Nature Medicine*, *2*(5), 561–566.

Duan, Z., Foster, R., Bell, D. A., Mahoney, J., Wolak, K., Vaidya, A., … Seiden, M. V. (2006). Signal transducers and activators of transcription 3 pathway activation in drug-resistant ovarian cancer. *Clinical Cancer Research : An Official Journal of the American Association for Cancer Research*, *12*(17), 5055–5063. https://doi.org/10.1158/1078-0432.CCR-06-0861

Ebersbach, H; Proetzel, G. (2012). Methods in Molecular Biology. In *Antibody Methods and Protocols* (Vol. 901). Totowa, NJ: Human Press. https://doi.org/10.1007/978-1-61779-931-0

Echarri, A., & Pendergast, A. M. (2001). Activated c-Abl is degraded by the ubiquitin-dependent proteasome pathway. *Current Biology : CB*, *11*(22), 1759–1765.

Ecker, D. M., Jones, S. D., & Levine, H. L. (2015). The therapeutic monoclonal antibody market. *MAbs*, *7*(1), 9–14. https://doi.org/10.4161/19420862.2015.989042

Elbing, K., & Brent, R. (2002). Media preparation and bacteriological tools. *Current Protocols in Molecular Biology*, *Chapter 1*, Unit 1.1. https://doi.org/10.1002/0471142727.mb0101s59

Elrick, L. J., Jorgensen, H. G., Mountford, J. C., & Holyoake, T. L. (2005). Punish the parent not the progeny. *Blood*, *105*(5), 1862–1866. https://doi.org/10.1182/blood-2004-08-3373

Fellouse, F., & Sidhu, S. (2006). Making Antibodies in Bacteria. In *Making and Using Antibodies* (pp. 157–180). CRC Press. https://doi.org/doi:10.1201/9781420005196.ch8

Feng, Y., Klein, B. K., & McWherter, C. A. (1996). Three-dimensional solution structure and backbone dynamics of a variant of human interleukin-3. *Journal of Molecular Biology*, *259*(3), 524–541. https://doi.org/10.1006/jmbi.1996.0337

Finn, O. J. (2008). Cancer immunology. *The New England Journal of Medicine*, *358*(25), 2704–2715. https://doi.org/10.1056/NEJMra072739

Fioretos, T., Strombeck, B., Sandberg, T., Johansson, B., Billstrom, R., Borg, A., … Hoglund, M. (1999). Isochromosome 17q in blast crisis of chronic myeloid leukemia and in other hematologic malignancies is the result of clustered breakpoints in 17p11 and is not associated with coding TP53 mutations. *Blood*, *94*(1), 225–232.

Fleming, H. E., Janzen, V., Lo Celso, C., Guo, J., Leahy, K. M., Kronenberg, H. M., & Scadden, D. T. (2008). Wnt signaling in the niche enforces hematopoietic stem cell quiescence and is necessary to preserve self-renewal in vivo. *Cell Stem Cell*, *2*(3), 274–283. https://doi.org/10.1016/j.stem.2008.01.003

Florian, S., Sonneck, K., Hauswirth, A. W., Krauth, M.-T., Schernthaner, G.-H., Sperr, W. R., & Valent, P. (2006). Detection of molecular targets on the surface of CD34+/CD38-- stem cells in various myeloid malignancies. *Leukemia & Lymphoma*, *47*(2), 207–222. https://doi.org/10.1080/10428190500272507

Folgiero, V., Avetrani, P., Bon, G., Di Carlo, S. E., Fabi, A., Nistico, C., … Falcioni, R. (2008). Induction of ErbB-3 expression by alpha6beta4 integrin contributes to tamoxifen resistance in ERbeta1-negative breast carcinomas. *PloS One*, *3*(2), e1592. https://doi.org/10.1371/journal.pone.0001592

Foti, A., Bar-Eli, M., Ahuja, H. G., & Cline, M. J. (1990). A splicing mutation accounts for the lack of p53 gene expression in a CML blast crisis cell line: a novel mechanism of p53

gene inactivation. *British Journal of Haematology*, *76*(1), 143–145.

Frank, D. A., & Varticovski, L. (1996). BCR/abl leads to the constitutive activation of Stat proteins, and shares an epitope with tyrosine phosphorylated Stats. *Leukemia*, *10*(11), 1724–1730.

Frankel, A., Liu, J.-S., Rizzieri, D., & Hogge, D. (2008). Phase I clinical study of diphtheria toxin-interleukin 3 fusion protein in patients with acute myeloid leukemia and myelodysplasia. *Leukemia & Lymphoma*, *49*(3), 543–553. https://doi.org/10.1080/10428190701799035

Frassanito, M. A., Cusmai, A., Iodice, G., & Dammacco, F. (2001). Autocrine interleukin-6 production and highly malignant multiple myeloma: relation with resistance to drug-induced apoptosis. *Blood*, *97*(2), 483–489.

Frenzel, A., Schirrmann, T., & Hust, M. (2016). Phage display-derived human antibodies in clinical development and therapy. *MAbs*, *8*(7), 1177–1194. https://doi.org/10.1080/19420862.2016.1212149

Fricker, M., O'Prey, J., Tolkovsky, A. M., & Ryan, K. M. (2010). Phosphorylation of Puma modulates its apoptotic function by regulating protein stability. *Cell Death & Disease*, *1*, e59. https://doi.org/10.1038/cddis.2010.38

Frolova, O., Benito, J., Brooks, C., Wang, R.-Y., Korchin, B., Rowinsky, E. K., … Konopleva, M. (2014). SL-401 and SL-501, targeted therapeutics directed at the interleukin-3 receptor, inhibit the growth of leukaemic cells and stem cells in advanced phase chronic myeloid leukaemia. *British Journal of Haematology*, *166*(6), 862–874. https://doi.org/10.1111/bjh.12978

Gabriele, L., Phung, J., Fukumoto, J., Segal, D., Wang, I. M., Giannakakou, P., … Morse, H. C. 3rd. (1999). Regulation of apoptosis in myeloid cells by interferon consensus sequence-binding protein. *The Journal of Experimental Medicine*, *190*(3), 411–421.

Gaiger, A., Henn, T., Horth, E., Geissler, K., Mitterbauer, G., Maier-Dobersberger, T., … Lion, T. (1995). Increase of bcr-abl chimeric mRNA expression in tumor cells of patients with chronic myeloid leukemia precedes disease progression. *Blood*, *86*(6), 2371–2378.

Gambacorti-Passerini, C., le Coutre, P., Mologni, L., Fanelli, M., Bertazzoli, C., Marchesi, E., … Lydon, N. B. (1997). Inhibition of the ABL kinase activity blocks the proliferation of BCR/ABL+ leukemic cells and induces apoptosis. *Blood Cells, Molecules & Diseases*,

23(3), 380–394. https://doi.org/10.1006/bcmd.1997.0155

Gavilondo, J. V, & Larrick, J. W. (2000). Antibody engineering at the millennium. *BioTechniques*, *29*(1), 128–32, 134–6, 138 passim.

Geisberger, R., Lamers, M., & Achatz, G. (2006). The riddle of the dual expression of IgM and IgD. *Immunology*, *118*(4), 429–437. https://doi.org/10.1111/j.1365-2567.2006.02386.x

Gerdes, J., Schwab, U., Lemke, H., & Stein, H. (1983). Production of a mouse monoclonal antibody reactive with a human nuclear antigen associated with cell proliferation. *International Journal of Cancer*, *31*(1), 13–20.

Gesbert, F., & Griffin, J. D. (2000). Bcr/Abl activates transcription of the Bcl-X gene through STAT5. *Blood*, *96*(6), 2269–2276.

Ghetie, V., & Ward, E. S. (2000). Multiple roles for the major histocompatibility complex class I- related receptor FcRn. *Annual Review of Immunology*, *18*, 739–766. https://doi.org/10.1146/annurev.immunol.18.1.739

Glassman, P. M., & Balthasar, J. P. (2014). Mechanistic considerations for the use of monoclonal antibodies for cancer therapy. *Cancer Biology & Medicine*, *11*(1), 20–33. https://doi.org/10.7497/j.issn.2095-3941.2014.01.002

Goff, S. P., Gilboa, E., Witte, O. N., & Baltimore, D. (1980). Structure of the Abelson murine leukemia virus genome and the homologous cellular gene: studies with cloned viral DNA. *Cell*, *22*(3), 777–785.

Goldman, J. M. (1992). Bone marrow transplantation for chronic myeloid leukaemia. *Leukemia*, *6 Suppl 2*, 22–23.

Golub, T. R., Goga, A., Barker, G. F., Afar, D. E., McLaughlin, J., Bohlander, S. K., … Gilliland, D. G. (1996). Oligomerization of the ABL tyrosine kinase by the Ets protein TEL in human leukemia. *Molecular and Cellular Biology*, *16*(8), 4107–4116.

Gorham, J. D. (2005). Immunology, Infection, and Immunity. Edited by Gerald B Pier, Jeffrey B Lyczak, and Lee M Wetzler. *The Quarterly Review of Biology*, *80*(1), 147. https://doi.org/10.1086/431127

Gorre, M. E., Mohammed, M., Ellwood, K., Hsu, N., Paquette, R., Rao, P. N., & Sawyers, C. L. (2001). Clinical resistance to STI-571 cancer therapy caused by BCR-ABL gene mutation or amplification. *Science (New York, N.Y.)*, *293*(5531), 876–880. https://doi.org/10.1126/science.1062538

Graf, M., Hecht, K., Reif, S., Pelka-Fleischer, R., Pfister, K., & Schmetzer, H. (2004). Expression and prognostic value of hemopoietic cytokine receptors in acute myeloid leukemia (AML): implications for future therapeutical strategies. *European Journal of Haematology*, *72*(2), 89–106. https://doi.org/10.1046/j.0902-4441.2003.00184.x

Graf, M., Reif, S., Kroll, T., Hecht, K., Nuessler, V., & Schmetzer, H. (2006). Expression of MAC-1 (CD11b) in acute myeloid leukemia (AML) is associated with an unfavorable prognosis. *American Journal of Hematology*, *81*(4), 227–235. https://doi.org/10.1002/ajh.20526

Graham, S. M., Jørgensen, H. G., Allan, E., Pearson, C., Alcorn, M. J., Richmond, L., & Holyoake, T. L. (2002). Primitive, quiescent, Philadelphia-positive stem cells from patients with chronic myeloid leukemia are insensitive to STI571 in vitro. *Blood*, *99*(1), 319 LP-325. Retrieved from http://www.bloodjournal.org/content/99/1/319.abstract

Graux, C., Cools, J., Melotte, C., Quentmeier, H., Ferrando, A., Levine, R., … Hagemeijer, A. (2004). Fusion of NUP214 to ABL1 on amplified episomes in T-cell acute lymphoblastic leukemia. *Nature Genetics*, *36*(10), 1084–1089. https://doi.org/10.1038/ng1425

Grebien, F., Kerenyi, M. A., Kovacic, B., Kolbe, T., Becker, V., Dolznig, H., … Moriggl, R. (2008). Stat5 activation enables erythropoiesis in the absence of EpoR and Jak2. *Blood*, *111*(9), 4511–4522. https://doi.org/10.1182/blood-2007-07-102848

Greuber, E. K., Smith-Pearson, P., Wang, J., & Pendergast, A. M. (2013). Role of ABL family kinases in cancer: from leukaemia to solid tumours. *Nature Reviews. Cancer*, *13*(8), 559–571. https://doi.org/10.1038/nrc3563

Griffiths, A. D., Williams, S. C., Hartley, O., Tomlinson, I. M., Waterhouse, P., Crosby, W. L., … Allison, T. J. (1994). Isolation of high affinity human antibodies directly from large synthetic repertoires. *The EMBO Journal*, *13*(14), 3245–3260.

Griswold, I. J., MacPartlin, M., Bumm, T., Goss, V. L., O'Hare, T., Lee, K. A., … Deininger, M. W. (2006). Kinase domain mutants of Bcr-Abl exhibit altered transformation potency, kinase activity, and substrate utilization, irrespective of sensitivity to imatinib. *Molecular and Cellular Biology*, *26*(16), 6082–6093. https://doi.org/10.1128/MCB.02202-05

Groffen, J., Stephenson, J. R., Heisterkamp, N., de Klein, A., Bartram, C. R., & Grosveld, G. (1984). Philadelphia chromosomal breakpoints are clustered within a limited region, bcr,

on chromosome 22. *Cell*, *36*(1), 93–99.

Grover, A., Sanjuan-Pla, A., Thongjuea, S., Carrelha, J., Giustacchini, A., Gambardella, A., … Nerlov, C. (2016). Single-cell RNA sequencing reveals molecular and functional platelet bias of aged haematopoietic stem cells. *Nature Communications*, *7*, 11075. https://doi.org/10.1038/ncomms11075

Guan, Y., Gerhard, B., & Hogge, D. E. (2003). Detection, isolation, and stimulation of quiescent primitive leukemic progenitor cells from patients with acute myeloid leukemia (AML). *Blood*, *101*(8), 3142–3149. https://doi.org/10.1182/blood-2002-10-3062

Guo, J. Q., Wang, J. Y., & Arlinghaus, R. B. (1991). Detection of BCR-ABL proteins in blood cells of benign phase chronic myelogenous leukemia patients. *Cancer Research*, *51*(11), 3048–3051.

Guthridge, M. A., Barry, E. F., Felquer, F. A., McClure, B. J., Stomski, F. C., Ramshaw, H., & Lopez, A. F. (2004). The phosphoserine-585-dependent pathway of the GM-CSF/IL-3/IL-5 receptors mediates hematopoietic cell survival through activation of NF-kappaB and induction of bcl-2. *Blood*, *103*(3), 820–827. https://doi.org/10.1182/blood-2003-06-1999

Guthridge, M. A., Powell, J. A., Barry, E. F., Stomski, F. C., McClure, B. J., Ramshaw, H., … Lopez, A. F. (2006). Growth factor pleiotropy is controlled by a receptor Tyr/Ser motif that acts as a binary switch. *The EMBO Journal*, *25*(3), 479–489. https://doi.org/10.1038/sj.emboj.7600948

Guthridge, M. A., Stomski, F. C., Thomas, D., Woodcock, J. M., Bagley, C. J., Berndt, M. C., & Lopez, a F. (1998). Mechanism of activation of the GM-CSF, IL-3, and IL-5 family of receptors. *Stem Cells*, *16*, 301–313. https://doi.org/10.1002/stem.160301

Guzman, M. L., & Allan, J. N. (2014). Concise review: Leukemia stem cells in personalized medicine. *Stem Cells (Dayton, Ohio)*, *32*(4), 844–851. https://doi.org/10.1002/stem.1597

Guzman, M. L., Neering, S. J., Upchurch, D., Grimes, B., Howard, D. S., Rizzieri, D. A., … Jordan, C. T. (2001). Nuclear factor-kappaB is constitutively activated in primitive human acute myelogenous leukemia cells. *Blood*, *98*(8), 2301–2307.

Guzman, M. L., Swiderski, C. F., Howard, D. S., Grimes, B. A., Rossi, R. M., Szilvassy, S. J., & Jordan, C. T. (2002). Preferential induction of apoptosis for primary human leukemic stem cells. *Proceedings of the National Academy of Sciences of the United States of America*, *99*(25), 16220–16225. https://doi.org/10.1073/pnas.252462599

Hacker, H., & Karin, M. (2006). Regulation and function of IKK and IKK-related kinases. *Science's STKE : Signal Transduction Knowledge Environment*, *2006*(357), re13. https://doi.org/10.1126/stke.3572006re13

Hadzhieva, M., Pashov, A. D., Kaveri, S., Lacroix-Desmazes, S., Mouquet, H., & Dimitrov, J. D. (2017). Impact of Antigen Density on the Binding Mechanism of IgG Antibodies. *Scientific Reports*, *7*(1), 3767. https://doi.org/10.1038/s41598-017-03942-z

Hamad, A., Sahli, Z., El Sabban, M., Mouteirik, M., & Nasr, R. (2013). Emerging therapeutic strategies for targeting chronic myeloid leukemia stem cells. *Stem Cells International*, *2013*, 724360. https://doi.org/10.1155/2013/724360

Hantschel, O., Nagar, B., Guettler, S., Kretzschmar, J., Dorey, K., Kuriyan, J., & Superti-Furga, G. (2003). A myristoyl/phosphotyrosine switch regulates c-Abl. *Cell*, *112*(6), 845–857.

Hantschel, O., & Superti-Furga, G. (2004). Regulation of the c-Abl and Bcr-Abl tyrosine kinases. *Nature Reviews. Molecular Cell Biology*, *5*(1), 33–44. https://doi.org/10.1038/nrm1280

Hassanein, N. M., Alcancia, F., Perkinson, K. R., Buckley, P. J., & Lagoo, A. S. (2009). Distinct expression patterns of CD123 and CD34 on normal bone marrow B-cell precursors ("hematogones") and B lymphoblastic leukemia blasts. *American Journal of Clinical Pathology*, *132*(4), 573–580. https://doi.org/10.1309/AJCPO4DS0GTLSOEI

Hazlehurst, L. A., Damiano, J. S., Buyuksal, I., Pledger, W. J., & Dalton, W. S. (2000). Adhesion to fibronectin via beta1 integrins regulates p27kip1 levels and contributes to cell adhesion mediated drug resistance (CAM-DR). *Oncogene*, *19*(38), 4319–4327. https://doi.org/10.1038/sj.onc.1203782

He, S. Z., Busfield, S., Ritchie, D. S., Hertzberg, M. S., Durrant, S., Lewis, I. D., … Roberts, A. W. (2015). A Phase 1 study of the safety, pharmacokinetics and anti-leukemic activity of the anti-CD123 monoclonal antibody CSL360 in relapsed, refractory or high-risk acute myeloid leukemia. *Leukemia & Lymphoma*, *56*(5), 1406–1415. https://doi.org/10.3109/10428194.2014.956316

He, Y., Wertheim, J. A., Xu, L., Miller, J. P., Karnell, F. G., Choi, J. K., … Pear, W. S. (2002). The coiled-coil domain and Tyr177 of bcr are required to induce a murine chronic myelogenous leukemia-like disease by bcr/abl. *Blood*, *99*(8), 2957–2968.

Heinen, S., Hartmann, A., Lauer, N., Wiehl, U., Dahse, H.-M., Schirmer, S., … Skerka, C. (2009). Factor H-related protein 1 (CFHR-1) inhibits complement C5 convertase activity and terminal complex formation. *Blood*, *114*(12), 2439–2447. https://doi.org/10.1182/blood-2009-02-205641

Heinrich, M. C., Griffith, D. J., Druker, B. J., Wait, C. L., Ott, K. A., & Zigler, A. J. (2000). Inhibition of c-kit receptor tyrosine kinase activity by STI 571, a selective tyrosine kinase inhibitor. *Blood*, *96*(3), 925–932.

Heisterkamp, N., Stephenson, J. R., Groffen, J., Hansen, P. F., de Klein, A., Bartram, C. R., & Grosveld, G. (1983). Localization of the c-ab1 oncogene adjacent to a translocation break point in chronic myelocytic leukaemia. *Nature*, *306*(5940), 239–242.

Helgason, G. V., Karvela, M., & Holyoake, T. L. (2011). Kill one bird with two stones: Potential efficacy of BCR-ABL and autophagy inhibition in CML. *Blood*, *118*(8), 2035–2043. https://doi.org/10.1182/blood-2011-01-330621

Hercus, T. R., Dhagat, U., Kan, W. L. T., Broughton, S. E., Nero, T. L., Perugini, M., … Lopez, A. F. (2013). Signalling by the βc family of cytokines. *Cytokine and Growth Factor Reviews*, *24*(3), 189–201. https://doi.org/10.1016/j.cytogfr.2013.03.002

Hercus, T. R., Kan, W. L. T., Broughton, S. E., Tvorogov, D., Ramshaw, H. S., Sandow, J. J., … Lopez, A. F. (2017). Role of the beta Common (betac) Family of Cytokines in Health and Disease. *Cold Spring Harbor Perspectives in Biology*. https://doi.org/10.1101/cshperspect.a028514

Hercus, T., & Thomas, D. (2009). The granulocyte-macrophage colony-stimulating factor receptor: linking its structure to cell signaling and its role in disease. *Blood*, *114*(August), 1289–1298. https://doi.org/10.1182/blood-2008-12-164004.

Hernandez, A. M., Rodriguez, N., Gonzalez, J. E., Reyes, E., Rondon, T., Grinan, T., … Perez, R. (2011). Anti-NeuGcGM3 antibodies, actively elicited by idiotypic vaccination in nonsmall cell lung cancer patients, induce tumor cell death by an oncosis-like mechanism. *Journal of Immunology (Baltimore, Md.: 1950)*, *186*(6), 3735–3744. https://doi.org/10.4049/jimmunol.1000609

Hernandez, S. E., Krishnaswami, M., Miller, A. L., & Koleske, A. J. (2004). How do Abl family kinases regulate cell shape and movement? *Trends in Cell Biology*, *14*(1), 36–44.

Hiwase, D. K., White, D. L., Powell, J. a, Saunders, V. a, Zrim, S. A., Frede, A. K., …

Hughes, T. P. (2010). Blocking cytokine signaling along with intense Bcr-Abl kinase inhibition induces apoptosis in primary CML progenitors. *Leukemia*, *24*(4), 771–778. https://doi.org/10.1038/leu.2009.299

Hoelbl, A., Kovacic, B., Kerenyi, M. A., Simma, O., Warsch, W., Cui, Y., … Sexl, V. (2006). Clarifying the role of Stat5 in lymphoid development and Abelson-induced transformation. *Blood*, *107*(12), 4898–4906. https://doi.org/10.1182/blood-2005-09-3596

Holyoake, T. L., Jiang, X., Drummond, M. W., Eaves, A. C., & Eaves, C. J. (2002). Elucidating critical mechanisms of deregulated stem cell turnover in the chronic phase of chronic myeloid leukemia. *Leukemia*, *16*(4), 549–558. https://doi.org/10.1038/sj.leu.2402444

Holyoake, T. L., Jiang, X., Jorgensen, H. G., Graham, S., Alcorn, M. J., Laird, C., … Eaves, C. J. (2001). Primitive quiescent leukemic cells from patients with chronic myeloid leukemia spontaneously initiate factor-independent growth in vitro in association with up-regulation of expression of interleukin-3. *Blood*, *97*(3), 720–728.

Honda, H., Ushijima, T., Wakazono, K., Oda, H., Tanaka, Y., Aizawa, S. i, … Hirai, H. (2000). Acquired loss of p53 induces blastic transformation in p210(bcr/abl)-expressing hematopoietic cells: a transgenic study for blast crisis of human CML. *Blood*, *95*(4), 1144–1150.

Honeychurch, J., Alduaij, W., Azizyan, M., Cheadle, E. J., Pelicano, H., Ivanov, A., … Illidge, T. M. (2012). Antibody-induced nonapoptotic cell death in human lymphoma and leukemia cells is mediated through a novel reactive oxygen species-dependent pathway. *Blood*, *119*(15), 3523–3533. https://doi.org/10.1182/blood-2011-12-395541

Hongrong Cai, H. (2016). *Therapeutic Monoclonal Antibodies Approved by FDA in 2015*. *MOJ Immunology* (Vol. 3). https://doi.org/10.15406/moji.2016.03.00087

Hoogenboom, H. R., de Bruine, A. P., Hufton, S. E., Hoet, R. M., Arends, J. W., & Roovers, R. C. (1998). Antibody phage display technology and its applications. *Immunotechnology : An International Journal of Immunological Engineering*, *4*(1), 1–20.

Hoogenboom, H. R., Griffiths, A. D., Johnson, K. S., Chiswell, D. J., Hudson, P., & Winter, G. (1991). Multi-subunit proteins on the surface of filamentous phage: methodologies for displaying antibody (Fab) heavy and light chains. *Nucleic Acids Research*, *19*(15), 4133–4137.

Horita, M., Andreu, E. J., Benito, A., Arbona, C., Sanz, C., Benet, I., … Fernandez-Luna, J. L. (2000). Blockade of the Bcr-Abl kinase activity induces apoptosis of chronic myelogenous leukemia cells by suppressing signal transducer and activator of transcription 5-dependent expression of Bcl-xL. *The Journal of Experimental Medicine*, *191*(6), 977–984.

Hu, Y., Swerdlow, S., Duffy, T. M., Weinmann, R., Lee, F. Y., & Li, S. (2006). Targeting multiple kinase pathways in leukemic progenitors and stem cells is essential for improved treatment of Ph+ leukemia in mice. *Proceedings of the National Academy of Sciences of the United States of America*, *103*(45), 16870–16875. https://doi.org/10.1073/pnas.0606509103

Huang, W.-S., Metcalf, C. A., Sundaramoorthi, R., Wang, Y., Zou, D., Thomas, R. M., … Shakespeare, W. C. (2010). Discovery of 3-[2-(imidazo[1,2-b]pyridazin-3-yl)ethynyl]-4-methyl-N-{4-[(4-methylpiperazin-1-y l)methyl]-3-(trifluoromethyl)phenyl}benzamide (AP24534), a potent, orally active pan-inhibitor of breakpoint cluster region-abelson (BCR-ABL) kinase including t. *Journal of Medicinal Chemistry*, *53*(12), 4701–4719. https://doi.org/10.1021/jm100395q

Huang, Z.-L., Gao, M., Li, Q.-Y., Tao, K., Xiao, Q., Cao, W.-X., & Feng, W.-L. (2013). Induction of apoptosis by directing oncogenic Bcr-Abl into the nucleus. *Oncotarget*, *4*(12), 2249–2260. https://doi.org/10.18632/oncotarget.1339

Hubbard, S. R., & Till, J. H. (2000). Protein tyrosine kinase structure and function. *Annual Review of Biochemistry*, *69*, 373–398. https://doi.org/10.1146/annurev.biochem.69.1.373

Hughes, T., Deininger, M., Hochhaus, A., Branford, S., Radich, J., Kaeda, J., … Goldman, J. M. (2006). Monitoring CML patients responding to treatment with tyrosine kinase inhibitors: Review and recommendations for harmonizing current methodology for detecting BCR-ABL transcripts and kinase domain mutations and for expressing results. *Blood*, *108*(1), 28–37. https://doi.org/10.1182/blood-2006-01-0092

Hunter, T. (2000). Signaling--2000 and beyond. *Cell*, *100*(1), 113–127.

Huntly, B. J. P., & Gilliland, D. G. (2005, April). Leukaemia stem cells and the evolution of cancer-stem-cell research. *Nature Reviews. Cancer*. England. https://doi.org/10.1038/nrc1592

Idusogie, E. E., Presta, L. G., Gazzano-Santoro, H., Totpal, K., Wong, P. Y., Ultsch, M., … Mulkerrin, M. G. (2000). Mapping of the C1q binding site on rituxan, a chimeric antibody with a human IgG1 Fc. *Journal of Immunology (Baltimore, Md. : 1950)*, *164*(8), 4178–4184.

Ihle, J. N. (1992). Interleukin-3 and hematopoiesis. *Chemical Immunology*, *51*, 65–106.

Iijima, Y., Ito, T., Oikawa, T., Eguchi, M., Eguchi-Ishimae, M., Kamada, N., … Sato, Y. (2000). A new ETV6/TEL partner gene, ARG (ABL-related gene or ABL2), identified in an AML-M3 cell line with a t(1;12)(q25;p13) translocation. *Blood*, *95*(6), 2126–2131.

Ilaria, R. L. J., & Van Etten, R. A. (1996). P210 and P190(BCR/ABL) induce the tyrosine phosphorylation and DNA binding activity of multiple specific STAT family members. *The Journal of Biological Chemistry*, *271*(49), 31704–31710.

Ishikawa, F., Yoshida, S., Saito, Y., Hijikata, A., Kitamura, H., Tanaka, S., … Shultz, L. D. (2007). Chemotherapy-resistant human AML stem cells home to and engraft within the bone-marrow endosteal region. *Nature Biotechnology*, *25*(11), 1315–1321. https://doi.org/10.1038/nbt1350

Ito, K., Hirao, A., Arai, F., Matsuoka, S., Takubo, K., Hamaguchi, I., … Suda, T. (2004). Regulation of oxidative stress by ATM is required for self-renewal of haematopoietic stem cells. *Nature*, *431*(7011), 997–1002. https://doi.org/10.1038/nature02989

Ito, T., Kwon, H. Y., Zimdahl, B., Congdon, K. L., Blum, J., Lento, W. E., … Reya, T. (2010). Regulation of myeloid leukaemia by the cell-fate determinant Musashi. *Nature*, *466*(7307), 765–768. https://doi.org/10.1038/nature09171

Itoh, T., Liu, R., Yokota, T., Arai, K. I., & Watanabe, S. (1998). Definition of the role of tyrosine residues of the common beta subunit regulating multiple signaling pathways of granulocyte-macrophage colony-stimulating factor receptor. *Molecular and Cellular Biology*, *18*(2), 742–752.

Ivanov, A., Beers, S. A., Walshe, C. A., Honeychurch, J., Alduaij, W., Cox, K. L., … Cragg, M. S. (2009). Monoclonal antibodies directed to CD20 and HLA-DR can elicit homotypic adhesion followed by lysosome-mediated cell death in human lymphoma and leukemia cells. *The Journal of Clinical Investigation*, *119*(8), 2143–2159. https://doi.org/10.1172/JCI37884

Jabbour, E., Cortes, J. E., & Kantarjian, H. M. (2009). Suboptimal response to or failure of imatinib treatment for chronic myeloid leukemia: what is the optimal strategy? *Mayo Clinic Proceedings*, *84*(2), 161–169. https://doi.org/10.1016/S0025-6196(11)60824-0

Jabbour, E., Kantarjian, H., Jones, D., Breeden, M., Garcia-Manero, G., O'Brien, S., … Cortes, J. (2008). Characteristics and outcomes of patients with chronic myeloid leukemia

and T315I mutation following failure of imatinib mesylate therapy. *Blood*, *112*(1), 53–55. https://doi.org/10.1182/blood-2007-11-123950

Jabbour, E., Kantarjian, H., Jones, D., Talpaz, M., Bekele, N., O'Brien, S., … Cortes, J. (2006). Frequency and clinical significance of BCR-ABL mutations in patients with chronic myeloid leukemia treated with imatinib mesylate. *Leukemia*, *20*(10), 1767–1773. https://doi.org/10.1038/sj.leu.2404318

Jamieson, C. H. M., Ailles, L. E., Dylla, S. J., Muijtjens, M., Jones, C., Zehnder, J. L., … Weissman, I. L. (2004). Granulocyte-macrophage progenitors as candidate leukemic stem cells in blast-crisis CML. *The New England Journal of Medicine*, *351*(7), 657–667. https://doi.org/10.1056/NEJMoa040258

Janssen, J. W., Ridge, S. A., Papadopoulos, P., Cotter, F., Ludwig, W. D., Fonatsch, C., … Wiedemann, L. M. (1995). The fusion of TEL and ABL in human acute lymphoblastic leukaemia is a rare event. *British Journal of Haematology*, *90*(1), 222–224.

Jefferis, R., Lund, J., & Pound, J. D. (1998). IgG-Fc-mediated effector functions: molecular definition of interaction sites for effector ligands and the role of glycosylation. *Immunological Reviews*, *163*, 59–76.

Jiang, X., Lopez, A., Holyoake, T., Eaves, A., & Eaves, C. (1999). Autocrine production and action of IL-3 and granulocyte colony-stimulating factor in chronic myeloid leukemia. *Proceedings of the National Academy of Sciences of the United States of America*, *96*(22), 12804–12809.

Jiang, X., Zhao, Y., Smith, C., Gasparetto, M., Turhan, A., Eaves, A., & Eaves, C. (2007). Chronic myeloid leukemia stem cells possess multiple unique features of resistance to BCR-ABL targeted therapies. *Leukemia*, *21*(5), 926–935. https://doi.org/10.1038/sj.leu.2404609

Jin, L., Lee, E. M., Ramshaw, H. S., Busfield, S. J., Peoppl, A. G., Wilkinson, L., … Lock, R. B. (2009). Monoclonal Antibody-Mediated Targeting of CD123, IL-3 Receptor α Chain, Eliminates Human Acute Myeloid Leukemic Stem Cells. *Cell Stem Cell*, *5*(1), 31–42. https://doi.org/10.1016/j.stem.2009.04.018

Johansson, B., Fioretos, T., & Mitelman, F. (2002). Cytogenetic and molecular genetic evolution of chronic myeloid leukemia. *Acta Haematologica*, *107*(2), 76–94. https://doi.org/46636

Johnson, G., & Wu, T. T. (2000). Kabat database and its applications: 30 years after the first

variability plot. *Nucleic Acids Research*, *28*(1), 214–218.

Jones, M. L., Alfaleh, M. A., Kumble, S., Zhang, S., Osborne, G. W., Yeh, M., … Mahler, S. M. (2016). Targeting membrane proteins for antibody discovery using phage display. *Scientific Reports*, *6*, 26240. https://doi.org/10.1038/srep26240

Jordan, C., Upchurch, D., Szilvassy, S., Guzman, M., Howard, D., Pettigrew, A., … Phillips, G. (2000). The interleukin-3 receptor alpha chain is a unique marker for human acute myelogenous leukemia stem cells. *Leukemia*, *14*, 1777–1784. Retrieved from www.nature.com/leu

Jorgensen, H. G., & Holyoake, T. L. (2007). Characterization of cancer stem cells in chronic myeloid leukaemia. *Biochem Soc Trans*, *35*(Pt 5), 1347–1351. https://doi.org/10.1042/BST0351347

Kamizono, S., Hanada, T., Yasukawa, H., Minoguchi, S., Kato, R., Minoguchi, M., … Yoshimura, A. (2001). The SOCS box of SOCS-1 accelerates ubiquitin-dependent proteolysis of TEL-JAK2. *The Journal of Biological Chemistry*, *276*(16), 12530–12538. https://doi.org/10.1074/jbc.M010074200

Kantarjian, H., Giles, F., Wunderle, L., Bhalla, K., O'Brien, S., Wassmann, B., … Ottmann, O. G. (2006). Nilotinib in imatinib-resistant CML and Philadelphia chromosome-positive ALL. *The New England Journal of Medicine*, *354*(24), 2542–2551. https://doi.org/10.1056/NEJMoa055104

Kantarjian, H. M., Keating, M. J., Talpaz, M., Walters, R. S., Smith, T. L., Cork, A., … Freireich, E. J. (1987). Chronic myelogenous leukemia in blast crisis. Analysis of 242 patients. *The American Journal of Medicine*, *83*(3), 445–454.

Kantarjian, H. M., Smith, T. L., O'Brien, S., Beran, M., Pierce, S., & Talpaz, M. (1995). Prolonged survival in chronic myelogenous leukemia after cytogenetic response to interferon-alpha therapy. The Leukemia Service. *Annals of Internal Medicine*, *122*(4), 254–261.

Kim, J. K., Tsen, M. F., Ghetie, V., & Ward, E. S. (1994). Localization of the site of the murine IgG1 molecule that is involved in binding to the murine intestinal Fc receptor. *European Journal of Immunology*, *24*(10), 2429–2434. https://doi.org/10.1002/eji.1830241025

Kim, S., Prout, M., Ramshaw, H., Lopez, A. F., LeGros, G., & Min, B. (2010). Cutting

edge: basophils are transiently recruited into the draining lymph nodes during helminth infection via IL-3, but infection-induced Th2 immunity can develop without basophil lymph node recruitment or IL-3. *Journal of Immunology (Baltimore, Md. : 1950)*, *184*(3), 1143–1147. https://doi.org/10.4049/jimmunol.0902447

Kipriyanov, S. M., & Le Gall, F. (2004). Generation and production of engineered antibodies. *Molecular Biotechnology*, *26*(1), 39–60. https://doi.org/10.1385/MB:26:1:39

Klein, B. K., Feng, Y., McWherter, C. A., Hood, W. F., Paik, K., & McKearn, J. P. (1997). The receptor binding site of human interleukin-3 defined by mutagenesis and molecular modeling. *The Journal of Biological Chemistry*, *272*(36), 22630–22641.

Klejman, A., Schreiner, S. J., Nieborowska-Skorska, M., Slupianek, A., Wilson, M., Smithgall, T. E., & Skorski, T. (2002). The Src family kinase Hck couples BCR/ABL to STAT5 activation in myeloid leukemia cells. *The EMBO Journal*, *21*(21), 5766–5774.

Kloss, S., Oberschmidt, O., Morgan, M., Dahlke, J., Arseniev, L., Huppert, V., … Koehl, U. (2017). Optimization of Human NK Cell Manufacturing: Fully Automated Separation, Improved Ex Vivo Expansion Using IL-21 with Autologous Feeder Cells, and Generation of Anti-CD123-CAR-Expressing Effector Cells. *Human Gene Therapy*, *28*(10), 897–913. https://doi.org/10.1089/hum.2017.157

Knappik, A., Ge, L., Honegger, A., Pack, P., Fischer, M., Wellnhofer, G., … Virnekas, B. (2000). Fully synthetic human combinatorial antibody libraries (HuCAL) based on modular consensus frameworks and CDRs randomized with trinucleotides. *Journal of Molecular Biology*, *296*(1), 57–86. https://doi.org/10.1006/jmbi.1999.3444

Kohler, G., & Milstein, C. (1975). Continuous cultures of fused cells secreting antibody of predefined specificity. *Nature*, *256*(5517), 524–526.

Koide, S., & Sidhu, S. S. (2009). The importance of being tyrosine: lessons in molecular recognition from minimalist synthetic binding proteins. *ACS Chemical Biology*, *4*(5), 325–334. https://doi.org/10.1021/cb800314v

Konig, H., Copland, M., Chu, S., Jove, R., Holyoake, T. L., & Bhatia, R. (2008). Effects of dasatinib on Src kinase activity and downstream intracellular signaling in primitive chronic myelogenous leukemia hematopoietic cells. *Cancer Research*, *68*(23), 9624–9633. https://doi.org/10.1158/0008-5472.CAN-08-1131

Konig, H., Holtz, M., Modi, H., Manley, P., Holyoake, T., Forman, S., & Bhatia, R. (2008).

Enhanced BCR-ABL kinase inhibition does not result in increased inhibition of downstream signaling pathways or increased growth suppression in CML progenitors. *Leukemia*, *22*, 748–755. https://doi.org/10.1038/sj.leu.2405086

Konopleva, M., Contractor, R., Tsao, T., Samudio, I., Ruvolo, P. P., Kitada, S., … Andreeff, M. (2006). Mechanisms of apoptosis sensitivity and resistance to the BH3 mimetic ABT-737 in acute myeloid leukemia. *Cancer Cell*, *10*(5), 375–388. https://doi.org/10.1016/j.ccr.2006.10.006

Konopleva, M. Y., & Jordan, C. T. (2011). Leukemia stem cells and microenvironment: Biology and therapeutic targeting. *Journal of Clinical Oncology*, *29*(5), 591–599. https://doi.org/10.1200/JCO.2010.31.0904

Kontermann, R. E. (2016). Half-life extended biotherapeutics. *Expert Opinion on Biological Therapy*, *16*(7), 903–915. https://doi.org/10.1517/14712598.2016.1165661

Kontermann, R. E., & Brinkmann, U. (2015). Bispecific antibodies. *Drug Discovery Today*, *20*(7), 838–847. https://doi.org/10.1016/j.drudis.2015.02.008

Korfi, K., Mandal, A., Furney, S. J., Wiseman, D., Somervaille, T. C. P., & Marais, R. (2015). A personalised medicine approach for ponatinib-resistant chronic myeloid leukaemia. *Annals of Oncology : Official Journal of the European Society for Medical Oncology*, *26*(6), 1180–1187. https://doi.org/10.1093/annonc/mdv110

Kornblau, S. M., Womble, M., Qiu, Y. H., Jackson, C. E., Chen, W., Konopleva, M., … Andreeff, M. (2006). Simultaneous activation of multiple signal transduction pathways confers poor prognosis in acute myelogenous leukemia. *Blood*, *108*(7), 2358–2365. https://doi.org/10.1182/blood-2006-02-003475

Kovtun, Y., Jones, G. E., Adams, S., Harvey, L., Audette, C. A., Wilhelm, A., … Chittenden, T. (2018). A CD123-targeting antibody-drug conjugate, IMGN632, designed to eradicate AML while sparing normal bone marrow cells. *Blood Advances*, *2*(8), 848–858. https://doi.org/10.1182/bloodadvances.2018017517

Krause, D. S., & Van Etten, R. A. (2005). Tyrosine kinases as targets for cancer therapy. *The New England Journal of Medicine*, *353*(2), 172–187. https://doi.org/10.1056/NEJMra044389

Krause, D. S., & Van Etten, R. A. (2007). Right on target: eradicating leukemic stem cells. *Trends in Molecular Medicine*, *13*(11), 470–481.

https://doi.org/10.1016/j.molmed.2007.09.003

Krebber, A., Bornhauser, S., Burmester, J., Honegger, A., Willuda, J., Bosshard, H. R., & Pluckthun, A. (1997). Reliable cloning of functional antibody variable domains from hybridomas and spleen cell repertoires employing a reengineered phage display system. *Journal of Immunological Methods*, *201*(1), 35–55.

Kreuzer, K.-A., Le Coutre, P., Landt, O., Na, I.-K., Schwarz, M., Schultheis, K., … Dorken, B. (2003). Preexistence and evolution of imatinib mesylate-resistant clones in chronic myelogenous leukemia detected by a PNA-based PCR clamping technique. *Annals of Hematology*, *82*(5), 284–289. https://doi.org/10.1007/s00277-003-0644-y

Kroon, E., Thorsteinsdottir, U., Mayotte, N., Nakamura, T., & Sauvageau, G. (2001). NUP98-HOXA9 expression in hemopoietic stem cells induces chronic and acute myeloid leukemias in mice. *The EMBO Journal*, *20*(3), 350–361. https://doi.org/10.1093/emboj/20.3.350

Kunkel, T. A. (1985). Rapid and efficient site-specific mutagenesis without phenotypic selection. *Proceedings of the National Academy of Sciences of the United States of America*, *82*(2), 488–492.

Kunkel, T. A., Roberts, J. D., & Zakour, R. A. (1987). Rapid and efficient site-specific mutagenesis without phenotypic selection. *Methods in Enzymology*, *154*, 367–382.

Kurokawa, M., Mitani, K., Imai, Y., Ogawa, S., Yazaki, Y., & Hirai, H. (1998). The t(3;21) fusion product, AML1/Evi-1, interacts with Smad3 and blocks transforming growth factor-beta-mediated growth inhibition of myeloid cells. *Blood*, *92*(11), 4003–4012.

Kurokawa, M., Mitani, K., Irie, K., Matsuyama, T., Takahashi, T., Chiba, S., … Hirai, H. (1998). The oncoprotein Evi-1 represses TGF-beta signalling by inhibiting Smad3. *Nature*, *394*(6688), 92–96. https://doi.org/10.1038/27945

Kurzrock, R., Gutterman, J. U., & Talpaz, M. (1988). The molecular genetics of Philadelphia chromosome-positive leukemias. *The New England Journal of Medicine*, *319*(15), 990–998. https://doi.org/10.1056/NEJM198810133191506

Kuwazuru, Y., Yoshimura, A., Hanada, S., Utsunomiya, A., Makino, T., Ishibashi, K., … Akiyama, S. (1990). Expression of the multidrug transporter, P-glycoprotein, in acute leukemia cells and correlation to clinical drug resistance. *Cancer*, *66*(5), 868–873.

Lachmann, N., Ackermann, M., Frenzel, E., Happle, C., Klimenkova, O., Brennig, S., …

Moritz, T. (2014). IL-3 Specifies Early Hematopoietic Development from Human iPSCs and Synergizes with M-CSF and G-CSF on Myeloid Differentiation. *Blood*, *124*(21), 4308 LP-4308. Retrieved from http://www.bloodjournal.org/content/124/21/4308.abstract

Lagneaux, L., Delforge, A., Bron, D., De Bruyn, C., & Stryckmans, P. (1998). Chronic lymphocytic leukemic B cells but not normal B cells are rescued from apoptosis by contact with normal bone marrow stromal cells. *Blood*, *91*(7), 2387–2396.

Laneuville, P., Sun, G., Timm, M., & Vekemans, M. (1992). Clonal evolution in a myeloid cell line transformed to interleukin-3 independent growth by retroviral transduction and expression of p210bcr/abl. *Blood*, *80*(7), 1788–1797.

Lantz, C. S., Boesiger, J., Song, C. H., Mach, N., Kobayashi, T., Mulligan, R. C., … Galli, S. J. (1998). Role for interleukin-3 in mast-cell and basophil development and in immunity to parasites. *Nature*, *392*(6671), 90–93. https://doi.org/10.1038/32190

Larson, R. A., Hochhaus, A., Hughes, T. P., Clark, R. E., Etienne, G., Kim, D.-W., … Kantarjian, H. M. (2012). Nilotinib vs imatinib in patients with newly diagnosed Philadelphia chromosome-positive chronic myeloid leukemia in chronic phase: ENESTnd 3-year follow-up. *Leukemia*, *26*(10), 2197–2203. https://doi.org/10.1038/leu.2012.134

Lee, C. V, Liang, W.-C., Dennis, M. S., Eigenbrot, C., Sidhu, S. S., & Fuh, G. (2004). High-affinity human antibodies from phage-displayed synthetic Fab libraries with a single framework scaffold. *Journal of Molecular Biology*, *340*(5), 1073–1093. https://doi.org/10.1016/j.jmb.2004.05.051

Lei, J. T., Mazumdar, T., & Martinez-Moczygemba, M. (2011). Three lysine residues in the common beta chain of the interleukin-5 receptor are required for Janus kinase (JAK)-dependent receptor ubiquitination, endocytosis, and signaling. *The Journal of Biological Chemistry*, *286*(46), 40091–40103. https://doi.org/10.1074/jbc.M111.273482

Lei, K., & Davis, R. J. (2003). JNK phosphorylation of Bim-related members of the Bcl2 family induces Bax-dependent apoptosis. *Proceedings of the National Academy of Sciences of the United States of America*, *100*(5), 2432–2437. https://doi.org/10.1073/pnas.0438011100

Lemmon, M. A., & Schlessinger, J. (2010). Cell signaling by receptor tyrosine kinases. *Cell*, *141*(7), 1117–1134. https://doi.org/10.1016/j.cell.2010.06.011

Levinson, N. M., Kuchment, O., Shen, K., Young, M. A., Koldobskiy, M., Karplus, M., …

Kuriyan, J. (2006). A Src-like inactive conformation in the abl tyrosine kinase domain. *PLoS Biology*, *4*(5), e144. https://doi.org/10.1371/journal.pbio.0040144

Li, F., Sutherland, M. K., Yu, C., Walter, R. B., Westendorf, L., Valliere-Douglass, J., … Benjamin, D. R. (2018). Characterization of SGN-CD123A, A Potent CD123-Directed Antibody-Drug Conjugate for Acute Myeloid Leukemia. *Molecular Cancer Therapeutics*, *17*(2), 554–564. https://doi.org/10.1158/1535-7163.MCT-17-0742

Liesveld, J. L., Harbol, A. W., & Abboud, C. N. (1996). Stem cell factor and stromal cell co-culture prevent apoptosis in a subculture of the megakaryoblastic cell line, UT-7. *Leukemia Research*, *20*(7), 591–600.

Lin, J., Sun, T., Ji, L., Deng, W., Roth, J., Minna, J., & Arlinghaus, R. (2007). Oncogenic activation of c-Abl in non-small cell lung cancer cells lacking FUS1 expression: inhibition of c-Abl by the tumor suppressor gene product Fus1. *Oncogene*, *26*(49), 6989–6996. https://doi.org/10.1038/sj.onc.1210500

Liu, H., Saxena, A., Sidhu, S. S., & Wu, D. (2017). Fc Engineering for Developing Therapeutic Bispecific Antibodies and Novel Scaffolds. *Frontiers in Immunology*, *8*, 38. https://doi.org/10.3389/fimmu.2017.00038

Liu, J., Miwa, T., Hilliard, B., Chen, Y., Lambris, J. D., Wells, A. D., & Song, W.-C. (2005). The complement inhibitory protein DAF (CD55) suppresses T cell immunity in vivo. *The Journal of Experimental Medicine*, *201*(4), 567–577. https://doi.org/10.1084/jem.20040863

Lombardo, L. J., Lee, F. Y., Chen, P., Norris, D., Barrish, J. C., Behnia, K., … Borzilleri, R. M. (2004). Discovery of N-(2-chloro-6-methyl- phenyl)-2-(6-(4-(2-hydroxyethyl)-piperazin-1-yl)-2-methylpyrimidin-4- ylamino)thiazole-5-carboxamide (BMS-354825), a dual Src/Abl kinase inhibitor with potent antitumor activity in preclinical assays. *Journal of Medicinal Chemistry*, *47*(27), 6658–6661. https://doi.org/10.1021/jm049486a

Lonberg, N. (2005). Human antibodies from transgenic animals. *Nature Biotechnology*, *23*(9), 1117–1125. https://doi.org/10.1038/nbt1135

Loo, D., Pryer, N., Young, P., Liang, T., Coberly, S., King, K. L., … Mather, J. P. (2007). The glycotope-specific RAV12 monoclonal antibody induces oncosis in vitro and has antitumor activity against gastrointestinal adenocarcinoma tumor xenografts in vivo. *Molecular Cancer Therapeutics*, *6*(3), 856–865. https://doi.org/10.1158/1535-7163.MCT-

06-0581

Lopez, A. F., Hercus, T. R., Ekert, P., Littler, D. R., Guthridge, M., Thomas, D., … Parker, M. W. (2010). Critical Review Molecular Basis of Cytokine Receptor Activation. *IUBMB Life*, *62*(7), 509–518. https://doi.org/10.1002/iub.00350

Lopez, A. F., Hercus, T. R., Ekert, P., Littler, D. R., Guthridge, M., Thomas, D., … Parker, M. W. (2010). Molecular basis of cytokine receptor activation. *IUBMB Life*, *62*(7), 509–518. https://doi.org/10.1002/iub.350

Low, K. B. (1974). Experiments in Molecular Genetics. Jeffrey H. Miller . *The Quarterly Review of Biology*, *49*(2), 151. https://doi.org/10.1086/408025

Lund, J., Winter, G., Jones, P. T., Pound, J. D., Tanaka, T., Walker, M. R., … Jefferis, R. (1991). Human Fc gamma RI and Fc gamma RII interact with distinct but overlapping sites on human IgG. *Journal of Immunology (Baltimore, Md. : 1950)*, *147*(8), 2657–2662.

Mahon, F.-X., Belloc, F., Lagarde, V., Chollet, C., Moreau-Gaudry, F., Reiffers, J., … Melo, J. V. (2003). MDR1 gene overexpression confers resistance to imatinib mesylate in leukemia cell line models. *Blood*, *101*(6), 2368–2373. https://doi.org/10.1182/blood.V101.6.2368

Mahon, F.-X., Hayette, S., Lagarde, V., Belloc, F., Turcq, B., Nicolini, F., … Pasquet, J.-M. (2008). Evidence that resistance to nilotinib may be due to BCR-ABL, Pgp, or Src kinase overexpression. *Cancer Research*, *68*(23), 9809–9816. https://doi.org/10.1158/0008-5472.CAN-08-1008

Mahon, F.-X., Rea, D., Guilhot, J., Guilhot, F., Huguet, F., Nicolini, F., … Rousselot, P. (2010). Discontinuation of imatinib in patients with chronic myeloid leukaemia who have maintained complete molecular remission for at least 2 years: the prospective, multicentre Stop Imatinib (STIM) trial. *The Lancet. Oncology*, *11*(11), 1029–1035. https://doi.org/10.1016/S1470-2045(10)70233-3

Malumbres, M., Perez De Castro, I., Hernandez, M. I., Jimenez, M., Corral, T., & Pellicer, A. (2000). Cellular response to oncogenic ras involves induction of the Cdk4 and Cdk6 inhibitor p15(INK4b). *Molecular and Cellular Biology*, *20*(8), 2915–2925.

Manley, P. W., Cowan-Jacob, S. W., Buchdunger, E., Fabbro, D., Fendrich, G., Furet, P., … Zimmermann, J. (2002). Imatinib: a selective tyrosine kinase inhibitor. *European Journal of Cancer (Oxford, England : 1990)*, *38 Suppl 5*, S19-27.

Marais, R., Light, Y., Paterson, H. F., & Marshall, C. J. (1995). Ras recruits Raf-1 to the plasma membrane for activation by tyrosine phosphorylation. *The EMBO Journal*, *14*(13), 3136–3145.

Marks, J. D., Hoogenboom, H. R., Bonnert, T. P., McCafferty, J., Griffiths, A. D., & Winter, G. (1991). By-passing immunization. Human antibodies from V-gene libraries displayed on phage. *Journal of Molecular Biology*, *222*(3), 581–597.

Maru, Y. (2001). Molecular biology of chronic myeloid leukemia. *International Journal of Hematology*, *73*(3), 308–322.

Mashal, R., Shtalrid, M., Talpaz, M., Kantarjian, H., Smith, L., Beran, M., … Deisseroth, A. (1990). Rearrangement and expression of p53 in the chronic phase and blast crisis of chronic myelogenous leukemia. *Blood*, *75*(1), 180–189.

Mateo, V., Brown, E. J., Biron, G., Rubio, M., Fischer, A., Deist, F. Le, & Sarfati, M. (2002). Mechanisms of CD47-induced caspase-independent cell death in normal and leukemic cells: link between phosphatidylserine exposure and cytoskeleton organization. *Blood*, *100*(8), 2882 LP-2890. Retrieved from http://www.bloodjournal.org/content/100/8/2882.abstract

Matsunaga, T., Takemoto, N., Sato, T., Takimoto, R., Tanaka, I., Fujimi, A., … Niitsu, Y. (2003). Interaction between leukemic-cell VLA-4 and stromal fibronectin is a decisive factor for minimal residual disease of acute myelogenous leukemia. *Nature Medicine*, *9*(9), 1158–1165. https://doi.org/10.1038/nm909

Matsuoka, S., Asano, Y., Sano, K., Kishimoto, H., Yamashita, I., Yorifuji, H., … Tada, T. (1995). A novel type of cell death of lymphocytes induced by a monoclonal antibody without participation of complement. *The Journal of Experimental Medicine*, *181*(6), 2007–2015.

Mayes, P. A., Hance, K. W., & Hoos, A. (2018). The promise and challenges of immune agonist antibody development in cancer. *Nature Reviews. Drug Discovery*. https://doi.org/10.1038/nrd.2018.75

Mayotte, N., Roy, D.-C., Yao, J., Kroon, E., & Sauvageau, G. (2002). Oncogenic interaction between BCR-ABL and NUP98-HOXA9 demonstrated by the use of an in vitro purging culture system. *Blood*, *100*(12), 4177–4184. https://doi.org/10.1182/blood-2002-04-1244

Mazor, Y., Van Blarcom, T., Carroll, S., & Georgiou, G. (2010). Selection of full-length

IgGs by tandem display on filamentous phage particles and Escherichia coli fluorescence-activated cell sorting screening. *The FEBS Journal*, *277*(10), 2291–2303. https://doi.org/10.1111/j.1742-4658.2010.07645.x

McCafferty, J., Griffiths, A. D., Winter, G., & Chiswell, D. J. (1990). Phage antibodies: filamentous phage displaying antibody variable domains. *Nature*, *348*(6301), 552–554. https://doi.org/10.1038/348552a0

McCubrey, J. A., Steelman, L. S., Chappell, W. H., Abrams, S. L., Wong, E. W. T., Chang, F., … Franklin, R. A. (2007). Roles of the Raf/MEK/ERK pathway in cell growth, malignant transformation and drug resistance. *Biochimica et Biophysica Acta - Molecular Cell Research*, *1773*(8), 1263–1284. https://doi.org/10.1016/j.bbamcr.2006.10.001

McLaughlin, P., Grillo-Lopez, A. J., Link, B. K., Levy, R., Czuczman, M. S., Williams, M. E., … Dallaire, B. K. (1998). Rituximab chimeric anti-CD20 monoclonal antibody therapy for relapsed indolent lymphoma: half of patients respond to a four-dose treatment program. *Journal of Clinical Oncology : Official Journal of the American Society of Clinical Oncology*, *16*(8), 2825–2833. https://doi.org/10.1200/JCO.1998.16.8.2825

McWhirter, J. R., Galasso, D. L., & Wang, J. Y. (1993). A coiled-coil oligomerization domain of Bcr is essential for the transforming function of Bcr-Abl oncoproteins. *Molecular and Cellular Biology*, *13*(12), 7587–7595.

Meads, M. B., Gatenby, R. A., & Dalton, W. S. (2009). Environment-mediated drug resistance: a major contributor to minimal residual disease. *Nature Reviews. Cancer*, *9*(9), 665–674. https://doi.org/10.1038/nrc2714

Mellman, I., Coukos, G., & Dranoff, G. (2011). Cancer immunotherapy comes of age. *Nature*, *480*(7378), 480–489. https://doi.org/10.1038/nature10673

Melo, J. V., & Deininger, M. W. N. (2004). Biology of chronic myelogenous leukemia - Signaling pathways of initiation and transformation. *Hematology/Oncology Clinics of North America*, *18*(3), 545–568. https://doi.org/10.1016/j.hoc.2004.03.008

Melo, J. V, & Barnes, D. J. (2007). Chronic myeloid leukaemia as a model of disease evolution in human cancer. *Nature Reviews. Cancer*, *7*(6), 441–453. https://doi.org/10.1038/nrc2147

Meyn, M. A. 3rd, Wilson, M. B., Abdi, F. A., Fahey, N., Schiavone, A. P., Wu, J., … Smithgall, T. E. (2006). Src family kinases phosphorylate the Bcr-Abl SH3-SH2 region and

modulate Bcr-Abl transforming activity. *The Journal of Biological Chemistry*, *281*(41), 30907–30916. https://doi.org/10.1074/jbc.M605902200

Middleton, O., Cosimo, E., Dobbin, E., McCaig, A. M., Clarke, C., Brant, A. M., … Wheadon, H. (2015). Complement deficiencies limit CD20 monoclonal antibody treatment efficacy in CLL. *Leukemia*, *29*(1), 107–114. https://doi.org/10.1038/leu.2014.146

Miersch, S., & Sidhu, S. S. (2012). Synthetic antibodies: concepts, potential and practical considerations. *Methods (San Diego, Calif.)*, *57*(4), 486–498. https://doi.org/10.1016/j.ymeth.2012.06.012

Milojkovic, D., & Apperley, J. (2008). State-of-the-art in the treatment of chronic myeloid leukaemia. *Current Opinion in Oncology*, *20*(1), 112–121. https://doi.org/10.1097/CCO.0b013e3282f1fe8a

Milojkovic, D., & Apperley, J. (2009). Mechanisms of Resistance to Imatinib and Second-Generation Tyrosine Inhibitors in Chronic Myeloid Leukemia. *Clinical Cancer Research : An Official Journal of the American Association for Cancer Research*, *15*(24), 7519–7527. https://doi.org/10.1158/1078-0432.CCR-09-1068

Milstein, C. (1999). The hybridoma revolution: an offshoot of basic research. *BioEssays : News and Reviews in Molecular, Cellular and Developmental Biology*, *21*(11), 966–973. https://doi.org/10.1002/(SICI)1521-1878(199911)21:11<966::AID-BIES9>3.0.CO;2-Z

Mitani, K., Ogawa, S., Tanaka, T., Miyoshi, H., Kurokawa, M., Mano, H., … Hirai, H. (1994). Generation of the AML1-EVI-1 fusion gene in the t(3;21)(q26;q22) causes blastic crisis in chronic myelocytic leukemia. *The EMBO Journal*, *13*(3), 504–510.

Mizuchi, D., Kurosu, T., Kida, A., Jin, Z.-H., Jin, A., Arai, A., & Miura, O. (2005). BCR/ABL activates Rap1 and B-Raf to stimulate the MEK/Erk signaling pathway in hematopoietic cells. *Biochemical and Biophysical Research Communications*, *326*(3), 645–651. https://doi.org/10.1016/j.bbrc.2004.11.086

Mone, A. P., Huang, P., Pelicano, H., Cheney, C. M., Green, J. M., Tso, J. Y., … Byrd, J. C. (2004). Hu1D10 induces apoptosis concurrent with activation of the AKT survival pathway in human chronic lymphocytic leukemia cells. *Blood*, *103*(5), 1846 LP-1854. Retrieved from http://www.bloodjournal.org/content/103/5/1846.abstract

Moon, S. A., Ki, M. K., Lee, S., Hong, M.-L., Kim, M., Kim, S., … Shim, H. (2011). Antibodies against non-immunizing antigens derived from a large immune scFv library.

Molecules and Cells, *31*(6), 509–513. https://doi.org/10.1007/s10059-011-2268-8

Moore, M. A. S. (2005). Converging pathways in leukemogenesis and stem cell self-renewal. *Experimental Hematology*, *33*(7), 719–737. https://doi.org/10.1016/j.exphem.2005.04.011

Mott, H. R., & Campbell, I. D. (1995). Four-helix bundle growth factors and their receptors: protein-protein interactions. *Current Opinion in Structural Biology*, *5*(1), 114–121.

Muller, A. J., Young, J. C., Pendergast, A. M., Pondel, M., Landau, N. R., Littman, D. R., & Witte, O. N. (1991). BCR first exon sequences specifically activate the BCR/ABL tyrosine kinase oncogene of Philadelphia chromosome-positive human leukemias. *Molecular and Cellular Biology*, *11*(4), 1785–1792.

Munoz, L., Nomdedeu, J. F., Lopez, O., Carnicer, M. J., Bellido, M., Aventin, A., … Sierra, J. (2001). Interleukin-3 receptor alpha chain (CD123) is widely expressed in hematologic malignancies. *Haematologica*, *86*(12), 1261–1269.

Murphy, J. M., Ford, S. C., Olsen, J. E., Gustin, S. E., Jeffrey, P. D., Ollis, D. L., & Young, I. G. (2004). Interleukin-3 binding to the murine betaIL-3 and human betac receptors involves functional epitopes formed by domains 1 and 4 of different protein chains. *The Journal of Biological Chemistry*, *279*(25), 26500–26508. https://doi.org/10.1074/jbc.M402705200

Murphy, J. M., & Young, I. G. (2006). IL-3, IL-5, and GM-CSF Signaling: Crystal Structure of the Human Beta-Common Receptor. *Vitamins and Hormones*, *74*(06), 1–30. https://doi.org/10.1016/S0083-6729(06)74001-8

Nagar, B., Bornmann, W. G., Pellicena, P., Schindler, T., Veach, D. R., Miller, W. T., … Kuriyan, J. (2002). Crystal structures of the kinase domain of c-Abl in complex with the small molecule inhibitors PD173955 and imatinib (STI-571). *Cancer Research*, *62*(15), 4236–4243.

Nagar, B., Hantschel, O., Young, M. A., Scheffzek, K., Veach, D., Bornmann, W., … Kuriyan, J. (2003). Structural basis for the autoinhibition of c-Abl tyrosine kinase. *Cell*, *112*(6), 859–871.

Nakamura, T., Largaespada, D. A., Lee, M. P., Johnson, L. A., Ohyashiki, K., Toyama, K., … Shaughnessy, J. D. J. (1996). Fusion of the nucleoporin gene NUP98 to HOXA9 by the chromosome translocation t(7;11)(p15;p15) in human myeloid leukaemia. *Nature Genetics*,

12(2), 154–158. https://doi.org/10.1038/ng0296-154

Neering, S. J., Bushnell, T., Sozer, S., Ashton, J., Rossi, R. M., Wang, P.-Y., … Jordan, C. T. (2007). Leukemia stem cells in a genetically defined murine model of blast crisis CML. *Blood*, *110*(7), 2578–2585. https://doi.org/10.1182/blood-2007-02-073031

Nefedova, Y., Cheng, P., Alsina, M., Dalton, W. S., & Gabrilovich, D. I. (2004). Involvement of Notch-1 signaling in bone marrow stroma-mediated de novo drug resistance of myeloma and other malignant lymphoid cell lines. *Blood*, *103*(9), 3503–3510. https://doi.org/10.1182/blood-2003-07-2340

Nefedova, Y., Landowski, T. H., & Dalton, W. S. (n.d.). Bone marrow stromal-derived soluble factors and direct cell contact contribute to de novo drug resistance of myeloma cells by distinct mechanisms. *Leukemia*, *17*(6), 1175–1182.

Nelson, A. L., Dhimolea, E., & Reichert, J. M. (2010). Development trends for human monoclonal antibody therapeutics. *Nature Reviews. Drug Discovery*, *9*(10), 767–774. https://doi.org/10.1038/nrd3229

Nieborowska-Skorska, M., Wasik, M. A., Slupianek, A., Salomoni, P., Kitamura, T., Calabretta, B., & Skorski, T. (1999). Signal transducer and activator of transcription (STAT)5 activation by BCR/ABL is dependent on intact Src homology (SH)3 and SH2 domains of BCR/ABL and is required for leukemogenesis. *The Journal of Experimental Medicine*, *189*(8), 1229–1242.

Nievergall, E., Ramshaw, H. S., Yong, A. S. M., Biondo, M., Busfield, S. J., Vairo, G., … Hiwase, D. K. (2014). Monoclonal antibody targeting of IL-3 receptor alpha with CSL362 effectively depletes CML progenitor and stem cells. *Blood*, *123*(8), 1218–1228. https://doi.org/10.1182/blood-2012-12-475194

Nikkola, J., Vihinen, P., Vlaykova, T., Hahka-Kemppinen, M., Heino, J., & Pyrhonen, S. (2004). Integrin chains beta1 and alphav as prognostic factors in human metastatic melanoma. *Melanoma Research*, *14*(1), 29–37.

Nimmerjahn, F., & Ravetch, J. V. (2006). Fcgamma receptors: old friends and new family members. *Immunity*, *24*(1), 19–28. https://doi.org/10.1016/j.immuni.2005.11.010

Nishinakamura, R., Miyajima, A., Mee, P. J., Tybulewicz, V. L., & Murray, R. (1996). Hematopoiesis in mice lacking the entire granulocyte-macrophage colony-stimulating factor/interleukin-3/interleukin-5 functions. *Blood*, *88*(7), 2458–2464.

Nosaka, T., Kawashima, T., Misawa, K., Ikuta, K., Mui, A. L., & Kitamura, T. (1999). STAT5 as a molecular regulator of proliferation, differentiation and apoptosis in hematopoietic cells. *The EMBO Journal*, *18*(17), 4754–4765. https://doi.org/10.1093/emboj/18.17.4754

Notari, M., Neviani, P., Santhanam, R., Blaser, B. W., Chang, J.-S., Galietta, A., … Perrotti, D. (2006). A MAPK/HNRPK pathway controls BCR/ABL oncogenic potential by regulating MYC mRNA translation. *Blood*, *107*(6), 2507–2516. https://doi.org/10.1182/blood-2005-09-3732

Notta, F., Zandi, S., Takayama, N., Dobson, S., Gan, O. I., Wilson, G., … Dick, J. E. (2016). Distinct routes of lineage development reshape the human blood hierarchy across ontogeny. *Science (New York, N.Y.)*, *351*(6269), aab2116. https://doi.org/10.1126/science.aab2116

Nowell, P. C., & Hungerford, D. A. (1961). Chromosome studies in human leukemia. II. Chronic granulocytic leukemia. *Journal of the National Cancer Institute*, *27*, 1013–1035.

Nowicki, M. O., Falinski, R., Koptyra, M., Slupianek, A., Stoklosa, T., Gloc, E., … Skorski, T. (2004). BCR/ABL oncogenic kinase promotes unfaithful repair of the reactive oxygen species-dependent DNA double-strand breaks. *Blood*, *104*(12), 3746–3753. https://doi.org/10.1182/blood-2004-05-1941

O'Hare, T., Deininger, M. W. N., Eide, C. A., Clackson, T., & Druker, B. J. (2011). Targeting the BCR-ABL signaling pathway in therapy-resistant Philadelphia chromosome-positive leukemia. *Clinical Cancer Research*, *17*(2), 212–221. https://doi.org/10.1158/1078-0432.CCR-09-3314

O'Hare, T., Eide, C. A., & Deininger, M. W. N. (2007). Bcr-Abl kinase domain mutations, drug resistance, and the road to a cure for chronic myeloid leukemia. *Blood*, *110*(7), 2242–2249. https://doi.org/10.1182/blood-2007-03-066936

O'Hare, T., Walters, D. K., Stoffregen, E. P., Jia, T., Manley, P. W., Mestan, J., … Druker, B. J. (2005). In vitro activity of Bcr-Abl inhibitors AMN107 and BMS-354825 against clinically relevant imatinib-resistant Abl kinase domain mutants. *Cancer Research*, *65*(11), 4500–4505. https://doi.org/10.1158/0008-5472.CAN-05-0259

Olins, P. O., Bauer, S. C., Braford-Goldberg, S., Sterbenz, K., Polazzi, J. O., Caparon, M. H., … Klover, J. A. (1995). Saturation mutagenesis of human interleukin-3. *The Journal of Biological Chemistry*, *270*(40), 23754–23760.

Oliver Hantschel and Giulio Superti-Furga. (2000). Mechanisms of Activation of Abl Family Kinases. In *Madame Curie Bioscience Database [Internet]*. Austin (TX): Landes Bioscience. Retrieved from http://www.ncbi.nlm.nih.gov/books/NBK6477/

Oon, S., Huynh, H., Tai, T. Y., Ng, M., Monaghan, K., Biondo, M., … Wilson, N. J. (2016). A cytotoxic anti-IL-3Rα antibody targets key cells and cytokines implicated in systemic lupus erythematosus. *JCI Insight*, *1*(6), 1–15. https://doi.org/10.1172/jci.insight.86131

Orlandi, R., Gussow, D. H., Jones, P. T., & Winter, G. (1989). Cloning immunoglobulin variable domains for expression by the polymerase chain reaction. *Proceedings of the National Academy of Sciences of the United States of America*, *86*(10), 3833–3837.

Oshita, F., Kameda, Y., Ikehara, M., Tanaka, G., Yamada, K., Nomura, I., … Mitsuda, A. (2002). Increased expression of integrin beta1 is a poor prognostic factor in small-cell lung cancer. *Anticancer Research*, *22*(2B), 1065–1070.

Pane, F., Frigeri, F., Sindona, M., Luciano, L., Ferrara, F., Cimino, R., … Rotoli, B. (1996). Neutrophilic-chronic myeloid leukemia: a distinct disease with a specific molecular marker (BCR/ABL with C3/A2 junction). *Blood*, *88*(7), 2410–2414.

Patel, A. B., O'Hare, T., & Deininger, M. W. (2017). Mechanisms of Resistance to ABL Kinase Inhibition in Chronic Myeloid Leukemia and the Development of Next Generation ABL Kinase Inhibitors. *Hematology/Oncology Clinics of North America*, *31*(4), 589–612. https://doi.org/10.1016/j.hoc.2017.04.007

Pawson, T., & Nash, P. (2000). Protein-protein interactions define specificity in signal transduction. *Genes & Development*, *14*(9), 1027–1047.

Pear, W. S., Miller, J. P., Xu, L., Pui, J. C., Soffer, B., Quackenbush, R. C., … Baltimore, D. (1998). Efficient and rapid induction of a chronic myelogenous leukemia-like myeloproliferative disease in mice receiving P210 bcr/abl-transduced bone marrow. *Blood*, *92*(10), 3780–3792.

Pendergast, A. M. (2002). The Abl family kinases: mechanisms of regulation and signaling. *Advances in Cancer Research*, *85*, 51–100.

Pendergast, A. M., Quilliam, L. A., Cripe, L. D., Bassing, C. H., Dai, Z., Li, N., … Schlessinger, J. (1993). BCR-ABL-induced oncogenesis is mediated by direct interaction with the SH2 domain of the GRB-2 adaptor protein. *Cell*, *75*(1), 175–185.

Perez, L. E., Parquet, N., Shain, K., Nimmanapalli, R., Alsina, M., Anasetti, C., & Dalton,

W. (2008). Bone marrow stroma confers resistance to Apo2 ligand/TRAIL in multiple myeloma in part by regulating c-FLIP. *Journal of Immunology (Baltimore, Md. : 1950)*, *180*(3), 1545–1555.

Persson, H., Ye, W., Wernimont, A., Adams, J. J., Koide, A., Koide, S., … Sidhu, S. S. (2013). CDR-H3 Diversity is Not Required For Antigen Recognition by Synthetic Antibodies. *Journal of Molecular Biology*, *425*(4), 803–811. https://doi.org/10.1016/j.jmb.2012.11.037

Plattner, R., Koleske, A. J., Kazlauskas, A., & Pendergast, A. M. (2004). Bidirectional signaling links the Abelson kinases to the platelet-derived growth factor receptor. *Molecular and Cellular Biology*, *24*(6), 2573–2583.

Pohle, T., Brandlein, S., Ruoff, N., Muller-Hermelink, H. K., & Vollmers, H. P. (2004). Lipoptosis: tumor-specific cell death by antibody-induced intracellular lipid accumulation. *Cancer Research*, *64*(11), 3900–3906. https://doi.org/10.1158/0008-5472.CAN-03-3149

Presta, L. G. (2002). Engineering antibodies for therapy. *Current Pharmaceutical Biotechnology*, *3*(3), 237–256.

Puil, L., Liu, J., Gish, G., Mbamalu, G., Bowtell, D., Pelicci, P. G., … Pawson, T. (1994). Bcr-Abl oncoproteins bind directly to activators of the Ras signalling pathway. *The EMBO Journal*, *13*(4), 764–773.

Putcha, G. V, Le, S., Frank, S., Besirli, C. G., Clark, K., Chu, B., … Johnson, E. M. J. (2003). JNK-mediated BIM phosphorylation potentiates BAX-dependent apoptosis. *Neuron*, *38*(6), 899–914.

Puttini, M., Coluccia, A. M. L., Boschelli, F., Cleris, L., Marchesi, E., Donella-Deana, A., … Gambacorti-Passerini, C. (2006). In vitro and in vivo activity of SKI-606, a novel Src-Abl inhibitor, against imatinib-resistant Bcr-Abl+ neoplastic cells. *Cancer Research*, *66*(23), 11314–11322. https://doi.org/10.1158/0008-5472.CAN-06-1199

Quackenbush, R. C., Reuther, G. W., Miller, J. P., Courtney, K. D., Pear, W. S., & Pendergast, A. M. (2000). Analysis of the biologic properties of p230 Bcr-Abl reveals unique and overlapping properties with the oncogenic p185 and p210 Bcr-Abl tyrosine kinases. *Blood*, *95*(9), 2913–2921.

Quintás-Cardama, A., & Cortes, J. (2009). Molecular biology of bcr-abl1-positive chronic myeloid leukemia. *Blood*, *113*(8), 1619–1630. https://doi.org/10.1182/blood-2008-03-

144790

Quintas-Cardama, A., Kantarjian, H. M., & Cortes, J. E. (2009). Mechanisms of primary and secondary resistance to imatinib in chronic myeloid leukemia. *Cancer Control : Journal of the Moffitt Cancer Center*, *16*(2), 122–131.

Quotti Tubi, L., Canovas Nunes, S., Brancalion, A., Doriguzzi Breatta, E., Manni, S., Mandato, E., … Piazza, F. (2017). Protein kinase CK2 regulates AKT, NF-kappaB and STAT3 activation, stem cell viability and proliferation in acute myeloid leukemia. *Leukemia*, *31*(2), 292–300. https://doi.org/10.1038/leu.2016.209

Radich, J. P. (2007). The Biology of CML blast crisis. *Hematology / the Education Program of the American Society of Hematology. American Society of Hematology. Education Program*, (Cml), 384–391. https://doi.org/10.1182/asheducation-2007.1.384

Radich, J. P., Dai, H., Mao, M., Oehler, V., Schelter, J., Druker, B., … Linsley, P. S. (2006). Gene expression changes associated with progression and response in chronic myeloid leukemia. *Proceedings of the National Academy of Sciences of the United States of America*, *103*(8), 2794–2799. https://doi.org/10.1073/pnas.0510423103

Rajan, S., & Sidhu, S. S. (2012). Simplified synthetic antibody libraries. *Methods in Enzymology*, *502*, 3–23. https://doi.org/10.1016/B978-0-12-416039-2.00001-X

Rakonjac, J., Bennett, N. J., Spagnuolo, J., Gagic, D., & Russel, M. (2011). Filamentous bacteriophage: biology, phage display and nanotechnology applications. *Current Issues in Molecular Biology*, *13*(2), 51–76.

Rea, D., Henry, G., Khaznadar, Z., Etienne, G., Guilhot, F., Nicolini, F., … Toubert, A. (2017). Natural killer-cell counts are associated with molecular relapse-free survival after imatinib discontinuation in chronic myeloid leukemia: the IMMUNOSTIM study. *Haematologica*, *102*(8), 1368 LP-1377. Retrieved from http://www.haematologica.org/content/102/8/1368.abstract

Reddington, S. C., & Howarth, M. (2015). Secrets of a covalent interaction for biomaterials and biotechnology: SpyTag and SpyCatcher. *Current Opinion in Chemical Biology*, *29*, 94–99. https://doi.org/10.1016/j.cbpa.2015.10.002

Reichert, J. M. (2017). Antibodies to watch in 2017. *MAbs*, *9*(2), 167–181. https://doi.org/10.1080/19420862.2016.1269580

Reis, E. S., Mastellos, D. C., Ricklin, D., Mantovani, A., & Lambris, J. D. (2017).

Complement in cancer: untangling an intricate relationship. *Nature Reviews. Immunology*. https://doi.org/10.1038/nri.2017.97

Ren, R. (2005). Mechanisms of BCR-ABL in the pathogenesis of chronic myelogenous leukaemia. *Nature Reviews. Cancer*, *5*(3), 172–183. https://doi.org/10.1038/nrc1567

Retter, M. W., Johnson, J. C., Peckham, D. W., Bannink, J. E., Bangur, C. S., Dresser, K., … Rock, K. L. (2005). Characterization of a proapoptotic antiganglioside GM2 monoclonal antibody and evaluation of its therapeutic effect on melanoma and small cell lung carcinoma xenografts. *Cancer Research*, *65*(14), 6425–6434. https://doi.org/10.1158/0008-5472.CAN-05-0300

Rhoden, J. J., Dyas, G. L., & Wroblewski, V. J. (2016). A Modeling and Experimental Investigation of the Effects of Antigen Density, Binding Affinity, and Antigen Expression Ratio on Bispecific Antibody Binding to Cell Surface Targets. *The Journal of Biological Chemistry*, *291*(21), 11337–11347. https://doi.org/10.1074/jbc.M116.714287

Riechmann, L., Clark, M., Waldmann, H., & Winter, G. (1988). Reshaping human antibodies for therapy. *Nature*, *332*(6162), 323–327. https://doi.org/10.1038/332323a0

Risch, H. A., McLaughlin, J. R., Cole, D. E. C., Rosen, B., Bradley, L., Fan, I., … Narod, S. A. (2006). Population BRCA1 and BRCA2 mutation frequencies and cancer penetrances: a kin-cohort study in Ontario, Canada. *Journal of the National Cancer Institute*, *98*(23), 1694–1706. https://doi.org/10.1093/jnci/djj465

Roche-Lestienne, C., Soenen-Cornu, V., Grardel-Duflos, N., Lai, J.-L., Philippe, N., Facon, T., … Preudhomme, C. (2002). Several types of mutations of the Abl gene can be found in chronic myeloid leukemia patients resistant to STI571, and they can pre-exist to the onset of treatment. *Blood*, *100*(3), 1014–1018.

Rodon, J., DeSantos, V., Ferry, R. J. J., & Kurzrock, R. (2008). Early drug development of inhibitors of the insulin-like growth factor-I receptor pathway: lessons from the first clinical trials. *Molecular Cancer Therapeutics*, *7*(9), 2575–2588. https://doi.org/10.1158/1535-7163.MCT-08-0265

Rogers, L. M., Veeramani, S., & Weiner, G. J. (2014). Complement in monoclonal antibody therapy of cancer. *Immunologic Research*, *59*(1–3), 203–210. https://doi.org/10.1007/s12026-014-8542-z

Rollins-Raval, M., Pillai, R., Warita, K., Mitsuhashi-Warita, T., Mehta, R., Boyiadzis, M.,

… Roth, C. G. (2013). CD123 immunohistochemical expression in acute myeloid leukemia is associated with underlying FLT3-ITD and NPM1 mutations. *Applied Immunohistochemistry & Molecular Morphology : AIMM*, *21*(3), 212–217. https://doi.org/10.1097/PAI.0b013e318261a342

Roque-Navarro, L., Chakrabandhu, K., de Leon, J., Rodriguez, S., Toledo, C., Carr, A., … Perez, R. (2008). Anti-ganglioside antibody-induced tumor cell death by loss of membrane integrity. *Molecular Cancer Therapeutics*, *7*(7), 2033–2041. https://doi.org/10.1158/1535-7163.MCT-08-0222

Ross, D. M., Branford, S., Seymour, J. F., Schwarer, A. P., Arthur, C., Yeung, D. T., … Hughes, T. P. (2013). Safety and efficacy of imatinib cessation for CML patients with stable undetectable minimal residual disease: results from the TWISTER study. *Blood*, *122*(4), 515–522. https://doi.org/10.1182/blood-2013-02-483750

Rossi, D. J., Bryder, D., Zahn, J. M., Ahlenius, H., Sonu, R., Wagers, A. J., & Weissman, I. L. (2005). Cell intrinsic alterations underlie hematopoietic stem cell aging. *Proceedings of the National Academy of Sciences of the United States of America*, *102*(26), 9194–9199. https://doi.org/10.1073/pnas.0503280102

Rothenberg, M. E., Owen, W. F. J., Silberstein, D. S., Woods, J., Soberman, R. J., Austen, K. F., & Stevens, R. L. (1988). Human eosinophils have prolonged survival, enhanced functional properties, and become hypodense when exposed to human interleukin 3. *The Journal of Clinical Investigation*, *81*(6), 1986–1992. https://doi.org/10.1172/JCI113547

Rowley, J. D. (1973). Letter: A new consistent chromosomal abnormality in chronic myelogenous leukaemia identified by quinacrine fluorescence and Giemsa staining. *Nature*, *243*(5405), 290–293.

Ruella, M., Barrett, D. M., Kenderian, S. S., Shestova, O., Hofmann, T. J., Perazzelli, J., … Gill, S. (2016). Dual CD19 and CD123 targeting prevents antigen-loss relapses after CD19-directed immunotherapies. *The Journal of Clinical Investigation*, *126*(10), 3814–3826. https://doi.org/10.1172/JCI87366

Ruella, M., Klichinsky, M., Kenderian, S. S., Shestova, O., Ziober, A., Kraft, D. O., … Gill, S. (2017). Overcoming the Immunosuppressive Tumor Microenvironment of Hodgkin Lymphoma Using Chimeric Antigen Receptor T Cells. *Cancer Discovery*, *7*(10), 1154–1167. https://doi.org/10.1158/2159-8290.CD-16-0850

Sakata, T., Anzai, N., Shin, H. J., Noshiro, R., Hirata, T., Yokoyama, H., … Endou, H. (2004). Novel single nucleotide polymorphisms of organic cation transporter 1 (SLC22A1) affecting transport functions. *Biochemical and Biophysical Research Communications*, *313*(3), 789–793.

Sandow, J. J., Jabbour, A. M., Condina, M. R., Daunt, C. P., Stomski, F. C., Green, B. D., … Ekert, P. G. (2012). Cytokine receptor signaling activates an IKK-dependent phosphorylation of PUMA to prevent cell death. *Cell Death and Differentiation*, *19*(4), 633–641. https://doi.org/10.1038/cdd.2011.131

Sattler, M., Mohi, M. G., Pride, Y. B., Quinnan, L. R., Malouf, N. A., Podar, K., … Neel, B. G. (2002). Critical role for Gab2 in transformation by BCR/ABL. *Cancer Cell*, *1*(5), 479–492.

Schindler, T., Bornmann, W., Pellicena, P., Miller, W. T., Clarkson, B., & Kuriyan, J. (2000). Structural mechanism for STI-571 inhibition of abelson tyrosine kinase. *Science (New York, N.Y.)*, *289*(5486), 1938–1942.

Schlessinger, J. (2000). Cell signaling by receptor tyrosine kinases. *Cell*, *103*(2), 211–225.

Schmidt, M. M., & Wittrup, K. D. (2009). A modeling analysis of the effects of molecular size and binding affinity on tumor targeting. *Molecular Cancer Therapeutics*, *8*(10), 2861–2871. https://doi.org/10.1158/1535-7163.MCT-09-0195

Schorpp-Kistner, M., Wang, Z. Q., Angel, P., & Wagner, E. F. (1999). JunB is essential for mammalian placentation. *The EMBO Journal*, *18*(4), 934–948. https://doi.org/10.1093/emboj/18.4.934

Schroeder, H. W. J., & Cavacini, L. (2010). Structure and function of immunoglobulins. *The Journal of Allergy and Clinical Immunology*, *125*(2 Suppl 2), S41-52. https://doi.org/10.1016/j.jaci.2009.09.046

Scott, A. M., Wolchok, J. D., & Old, L. J. (2012). Antibody therapy of cancer. *Nature Reviews. Cancer*, *12*(4), 278–287. https://doi.org/10.1038/nrc3236

Scott, G., Cassidy, L., & Busacco, A. (1997). Fibronectin suppresses apoptosis in normal human melanocytes through an integrin-dependent mechanism. *The Journal of Investigative Dermatology*, *108*(2), 147–153.

Serra, A., Gottardi, E., Della Ragione, F., Saglio, G., & Iolascon, A. (1995). Involvement of the cyclin-dependent kinase-4 inhibitor (CDKN2) gene in the pathogenesis of lymphoid

blast crisis of chronic myelogenous leukaemia. *British Journal of Haematology*, *91*(3), 625–629.

Sexl, V., Piekorz, R., Moriggl, R., Rohrer, J., Brown, M. P., Bunting, K. D., … Ihle, J. N. (2000). Stat5a/b contribute to interleukin 7-induced B-cell precursor expansion, but abl- and bcr/abl-induced transformation are independent of stat5. *Blood*, *96*(6), 2277–2283.

Shah, N. P., Rousselot, P., Schiffer, C., Rea, D., Cortes, J. E., Milone, J., … Saglio, G. (2016). Dasatinib in imatinib-resistant or -intolerant chronic-phase, chronic myeloid leukemia patients: 7-year follow-up of study CA180-034. *American Journal of Hematology*, *91*(9), 869–874. https://doi.org/10.1002/ajh.24423

Shah, N. P., Tran, C., Lee, F. Y., Chen, P., Norris, D., & Sawyers, C. L. (2004). Overriding imatinib resistance with a novel ABL kinase inhibitor. *Science (New York, N.Y.)*, *305*(5682), 399–401. https://doi.org/10.1126/science.1099480

Shain, K. H., Landowski, T. H., & Dalton, W. S. (2002). Adhesion-mediated intracellular redistribution of c-Fas-associated death domain-like IL-1-converting enzyme-like inhibitory protein-long confers resistance to CD95-induced apoptosis in hematopoietic cancer cell lines. *Journal of Immunology (Baltimore, Md. : 1950)*, *168*(5), 2544–2553.

Shawver, L. K., Slamon, D., & Ullrich, A. (2002). Smart drugs: tyrosine kinase inhibitors in cancer therapy. *Cancer Cell*, *1*(2), 117–123.

Shet, A. S., Jahagirdar, B. N., & Verfaillie, C. M. (2002). Chronic myelogenous leukemia: mechanisms underlying disease progression. *Leukemia*, *16*(8), 1402–1411. https://doi.org/10.1038/sj.leu.2402577

Shinohara, A., & Ogawa, T. (1995). Homologous recombination and the roles of double-strand breaks. *Trends in Biochemical Sciences*, *20*(10), 387–391.

Shtivelman, E., Lifshitz, B., Gale, R. P., Roe, B. A., & Canaani, E. (1986). Alternative splicing of RNAs transcribed from the human abl gene and from the bcr-abl fused gene. *Cell*, *47*(2), 277–284.

Sidhu, S. S., & Fellouse, F. A. (2006). Synthetic therapeutic antibodies. *Nature Chemical Biology*, *2*(12), 682–688. https://doi.org/10.1038/nchembio843

Sidhu, S. S., Li, B., Chen, Y., Fellouse, F. A., Eigenbrot, C., & Fuh, G. (2004). Phage-displayed antibody libraries of synthetic heavy chain complementarity determining regions. *Journal of Molecular Biology*, *338*(2), 299–310. https://doi.org/10.1016/j.jmb.2004.02.050

Sidhu, S. S., Lowman, H. B., Cunningham, B. C., & Wells, J. A. (2000). Phage display for selection of novel binding peptides. *Methods in Enzymology*, *328*, 333–363.

Sill, H., Goldman, J. M., & Cross, N. C. (1995). Homozygous deletions of the p16 tumor-suppressor gene are associated with lymphoid transformation of chronic myeloid leukemia. *Blood*, *85*(8), 2013–2016.

Silvestri, I., & Taniuchi, H. (1988). A study of fine specificity of monoclonal antibodies to yeast iso-1-cytochrome c. *The Journal of Biological Chemistry*, *263*(35), 18702–18715.

Skerka, C., Chen, Q., Fremeaux-Bacchi, V., & Roumenina, L. T. (2013). Complement factor H related proteins (CFHRs). *Molecular Immunology*, *56*(3), 170–180. https://doi.org/10.1016/j.molimm.2013.06.001

Skorski, T., Bellacosa, A., Nieborowska-Skorska, M., Majewski, M., Martinez, R., Choi, J. K., … Calabretta, B. (1997). Transformation of hematopoietic cells by BCR/ABL requires activation of a PI-3k/Akt-dependent pathway. *The EMBO Journal*, *16*(20), 6151–6161. https://doi.org/10.1093/emboj/16.20.6151

Skorski, T., Nieborowska-Skorska, M., Wlodarski, P., Perrotti, D., Martinez, R., Wasik, M. A., & Calabretta, B. (1996). Blastic transformation of p53-deficient bone marrow cells by p210bcr/abl tyrosine kinase. *Proceedings of the National Academy of Sciences of the United States of America*, *93*(23), 13137–13142.

Slupianek, A., Nowicki, M. O., Koptyra, M., & Skorski, T. (2006). BCR/ABL modifies the kinetics and fidelity of DNA double-strand breaks repair in hematopoietic cells. *DNA Repair*, *5*(2), 243–250. https://doi.org/10.1016/j.dnarep.2005.10.005

Slupianek, A., Schmutte, C., Tombline, G., Nieborowska-Skorska, M., Hoser, G., Nowicki, M. O., … Skorski, T. (2001). BCR/ABL regulates mammalian RecA homologs, resulting in drug resistance. *Molecular Cell*, *8*(4), 795–806.

Smith, G. P. (1985). Filamentous fusion phage: novel expression vectors that display cloned antigens on the virion surface. *Science (New York, N.Y.)*, *228*(4705), 1315–1317.

Smith, K. A., Nelson, P. N., Warren, P., Astley, S. J., Murray, P. G., & Greenman, J. (2004). Demystified...recombinant antibodies. *Journal of Clinical Pathology*, *57*(9), 912–917. https://doi.org/10.1136/jcp.2003.014407

Smith, K. M., & Van Etten, R. A. (2001). Activation of c-Abl kinase activity and transformation by a chemical inducer of dimerization. *The Journal of Biological Chemistry*,

276(26), 24372–24379. https://doi.org/10.1074/jbc.M100786200

Smith, K. M., Yacobi, R., & Van Etten, R. A. (2003). Autoinhibition of Bcr-Abl through its SH3 domain. *Molecular Cell*, *12*(1), 27–37.

Sobacchi, C., Palagano, E., Villa, A., & Menale, C. (2017). Soluble Factors on Stage to Direct Mesenchymal Stem Cells Fate. *Frontiers in Bioengineering and Biotechnology*, *5*, 32. https://doi.org/10.3389/fbioe.2017.00032

Soderlind, E., Strandberg, L., Jirholt, P., Kobayashi, N., Alexeiva, V., Aberg, A. M., … Borrebaeck, C. A. (2000). Recombining germline-derived CDR sequences for creating diverse single-framework antibody libraries. *Nature Biotechnology*, *18*(8), 852–856. https://doi.org/10.1038/78458

Soverini, S., Martinelli, G., Rosti, G., Bassi, S., Amabile, M., Poerio, A., … Baccarani, M. (2005). ABL mutations in late chronic phase chronic myeloid leukemia patients with up-front cytogenetic resistance to imatinib are associated with a greater likelihood of progression to blast crisis and shorter survival: a study by the GIMEMA Working Party on Chr. *Journal of Clinical Oncology : Official Journal of the American Society of Clinical Oncology*, *23*(18), 4100–4109. https://doi.org/10.1200/JCO.2005.05.531

Steelman, L. S., Pohnert, S. C., Shelton, J. G., Franklin, R. A., Bertrand, F. E., & McCubrey, J. A. (2004). JAK/STAT, Raf/MEK/ERK, PI3K/Akt and BCR-ABL in cell cycle progression and leukemogenesis. *Leukemia*, *18*(2), 189–218. https://doi.org/10.1038/sj.leu.2403241

Strebhardt, K., & Ullrich, A. (2008, June). Paul Ehrlich's magic bullet concept: 100 years of progress. *Nature Reviews. Cancer*. England. https://doi.org/10.1038/nrc2394

Stuppia, L., Calabrese, G., Peila, R., Guanciali-Franchi, P., Morizio, E., Spadano, A., & Palka, G. (1997). p53 loss and point mutations are associated with suppression of apoptosis and progression of CML into myeloid blastic crisis. *Cancer Genetics and Cytogenetics*, *98*(1), 28–35.

Sun, Q., Woodcock, J. M., Rapoport, A., Stomski, F. C., Korpelainen, E. I., Bagley, C. J., … Lopez, A. F. (1996). Monoclonal antibody 7G3 recognizes the N-terminal domain of the human interleukin-3 (IL-3) receptor alpha-chain and functions as a specific IL-3 receptor antagonist. *Blood*, *87*(1), 83–92.

Taagepera, S., McDonald, D., Loeb, J. E., Whitaker, L. L., McElroy, A. K., Wang, J. Y., &

Hope, T. J. (1998). Nuclear-cytoplasmic shuttling of C-ABL tyrosine kinase. *Proceedings of the National Academy of Sciences of the United States of America*, *95*(13), 7457–7462.

Talpaz, M., Shah, N. P., Kantarjian, H., Donato, N., Nicoll, J., Paquette, R., … Sawyers, C. L. (2006). Dasatinib in imatinib-resistant Philadelphia chromosome-positive leukemias. *The New England Journal of Medicine*, *354*(24), 2531–2541. https://doi.org/10.1056/NEJMoa055229

Tanis, K. Q., Veach, D., Duewel, H. S., Bornmann, W. G., & Koleske, A. J. (2003). Two distinct phosphorylation pathways have additive effects on Abl family kinase activation. *Molecular and Cellular Biology*, *23*(11), 3884–3896.

Tasian, S. K., Kenderian, S. S., Shen, F., Ruella, M., Shestova, O., Kozlowski, M., … Gill, S. (2017). Optimized depletion of chimeric antigen receptor T cells in murine xenograft models of human acute myeloid leukemia. *Blood*, *129*(17), 2395–2407. https://doi.org/10.1182/blood-2016-08-736041

Taylor, R. P., & Lindorfer, M. A. (2016). Cytotoxic mechanisms of immunotherapy: Harnessing complement in the action of anti-tumor monoclonal antibodies. *Seminars in Immunology*, *28*(3), 309–316. https://doi.org/10.1016/j.smim.2016.03.003

Tempescul, A., Bagacean, C., Riou, C., Bendaoud, B., Hillion, S., Debant, M., … Renaudineau, Y. (2016). Ofatumumab capacity to deplete B cells from chronic lymphocytic leukaemia is affected by C4 complement exhaustion. *European Journal of Haematology*, *96*(3), 229–235. https://doi.org/10.1111/ejh.12573

Testa, U., Riccioni, R., Diverio, D., Rossini, A., Coco, F. Lo, & Peschle, C. (2004). Interleukin-3 receptor in acute leukemia. *Leukemia*, *18*, 219–226. https://doi.org/10.1038/sj.leu.2403224

Testa, U., Riccioni, R., Militi, S., Coccia, E., Stellacci, E., Samoggia, P., … Peschle, C. (2002). Elevated expression of IL-3Ralpha in acute myelogenous leukemia is associated with enhanced blast proliferation, increased cellularity, and poor prognosis. *Blood*, *100*(8), 2980–2988. https://doi.org/10.1182/blood-2002-03-0852

Thakur, A., Huang, M., & Lum, L. G. (2018). Bispecific antibody based therapeutics: Strengths and challenges. *Blood Reviews*. https://doi.org/10.1016/j.blre.2018.02.004

Thielens, N. M., Tedesco, F., Bohlson, S. S., Gaboriaud, C., & Tenner, A. J. (2017). C1q: A fresh look upon an old molecule. *Molecular Immunology*, *89*, 73–83.

https://doi.org/10.1016/j.molimm.2017.05.025

Thomas, J., Wang, L., Clark, R. E., & Pirmohamed, M. (2004). Active transport of imatinib into and out of cells: implications for drug resistance. *Blood*, *104*(12), 3739–3745. https://doi.org/10.1182/blood-2003-12-4276

Tiller, T., Schuster, I., Deppe, D., Siegers, K., Strohner, R., Herrmann, T., … Urlinger, S. (2013). A fully synthetic human Fab antibody library based on fixed VH/VL framework pairings with favorable biophysical properties. *MAbs*, *5*(3), 445–470. https://doi.org/10.4161/mabs.24218

Tlsty, T. D., & Coussens, L. M. (2006). Tumor stroma and regulation of cancer development. *Annual Review of Pathology*, *1*, 119–150. https://doi.org/10.1146/annurev.pathol.1.110304.100224

Tonikian, R., Zhang, Y., Boone, C., & Sidhu, S. S. (2007). Identifying specificity profiles for peptide recognition modules from phage-displayed peptide libraries. *Nature Protocols*, *2*(6), 1368–1386. https://doi.org/10.1038/nprot.2007.151

Torres, M., & Casadevall, A. (2008). The immunoglobulin constant region contributes to affinity and specificity. *Trends in Immunology*, *29*(2), 91–97. https://doi.org/10.1016/j.it.2007.11.004

Traer, E., MacKenzie, R., Snead, J., Agarwal, A., Eiring, A. M., O'Hare, T., … Deininger, M. W. (2012, May). Blockade of JAK2-mediated extrinsic survival signals restores sensitivity of CML cells to ABL inhibitors. *Leukemia*. England. https://doi.org/10.1038/leu.2011.325

Trapani, J. A. (1995). Target cell apoptosis induced by cytotoxic T cells and natural killer cells involves synergy between the pore-forming protein, perforin, and the serine protease, granzyme B. *Australian and New Zealand Journal of Medicine*, *25*(6), 793–799.

Traxler, P., Bold, G., Buchdunger, E., Caravatti, G., Furet, P., Manley, P., … Zimmermann, J. (2001). Tyrosine kinase inhibitors: from rational design to clinical trials. *Medicinal Research Reviews*, *21*(6), 499–512.

Underdown, B. J., & Schiff, J. M. (1986). Immunoglobulin A: Strategic Defense Initiative at the Mucosal Surface. *Annual Review of Immunology*, *4*(1), 389–417. https://doi.org/10.1146/annurev.iy.04.040186.002133

Ungureanu, D., Saharinen, P., Junttila, I., Hilton, D. J., & Silvennoinen, O. (2002).

Regulation of Jak2 through the ubiquitin-proteasome pathway involves phosphorylation of Jak2 on Y1007 and interaction with SOCS-1. *Molecular and Cellular Biology*, *22*(10), 3316–3326.

Ungureanu, D., Wu, J., Pekkala, T., Niranjan, Y., Young, C., Jensen, O. N., … Silvennoinen, O. (2011). The pseudokinase domain of JAK2 is a dual-specificity protein kinase that negatively regulates cytokine signaling. *Nature Structural & Molecular Biology*, *18*(9), 971–976. https://doi.org/10.1038/nsmb.2099

Van Etten, R. A., Jackson, P., & Baltimore, D. (1989). The mouse type IV c-abl gene product is a nuclear protein, and activation of transforming ability is associated with cytoplasmic localization. *Cell*, *58*(4), 669–678.

Van Etten, R. A., Jackson, P. K., Baltimore, D., Sanders, M. C., Matsudaira, P. T., & Janmey, P. A. (1994). The COOH terminus of the c-Abl tyrosine kinase contains distinct F- and G-actin binding domains with bundling activity. *The Journal of Cell Biology*, *124*(3), 325–340.

Varela, J. C., Imai, M., Atkinson, C., Ohta, R., Rapisardo, M., & Tomlinson, S. (2008). Modulation of protective T cell immunity by complement inhibitor expression on tumor cells. *Cancer Research*, *68*(16), 6734–6742. https://doi.org/10.1158/0008-5472.CAN-08-0502

Vigneri, P., & Wang, J. Y. (2001). Induction of apoptosis in chronic myelogenous leukemia cells through nuclear entrapment of BCR-ABL tyrosine kinase. *Nature Medicine*, *7*(2), 228–234. https://doi.org/10.1038/84683

Virnekas, B., Ge, L., Pluckthun, A., Schneider, K. C., Wellnhofer, G., & Moroney, S. E. (1994). Trinucleotide phosphoramidites: ideal reagents for the synthesis of mixed oligonucleotides for random mutagenesis. *Nucleic Acids Research*, *22*(25), 5600–5607.

Vuoristo, M., Vihinen, P., Vlaykova, T., Nylund, C., Heino, J., & Pyrhonen, S. (2007). Increased gene expression levels of collagen receptor integrins are associated with decreased survival parameters in patients with advanced melanoma. *Melanoma Research*, *17*(4), 215–223. https://doi.org/10.1097/CMR.0b013e328270b935

Wang, S.-Y., & Weiner, G. (2008). Complement and cellular cytotoxicity in antibody therapy of cancer. *Expert Opinion on Biological Therapy*, *8*(6), 759–768. https://doi.org/10.1517/14712598.8.6.759

Wang, W., Erbe, A. K., Hank, J. A., Morris, Z. S., & Sondel, P. M. (2015). NK Cell-Mediated Antibody-Dependent Cellular Cytotoxicity in Cancer Immunotherapy. *Frontiers in Immunology*, *6*, 368. https://doi.org/10.3389/fimmu.2015.00368

Wang, W., Xu, R., & Li, J. (2010). Production of native bispecific antibodies in rabbits. *PloS One*, *5*(6), e10879. https://doi.org/10.1371/journal.pone.0010879

Wang, Y., Cai, D., Brendel, C., Barett, C., Erben, P., Manley, P. W., … Burchert, A. (2007). Adaptive secretion of granulocyte-macrophage colony-stimulating factor (GM-CSF) mediates imatinib and nilotinib resistance in BCR/ABL+ progenitors via JAK-2/STAT-5 pathway activation. *Blood*, *109*(5), 2147–2155. https://doi.org/10.1182/blood-2006-08-040022

Wang, Y., Krivtsov, A. V, Sinha, A. U., North, T. E., Goessling, W., Feng, Z., … Armstrong, S. A. (2010). The Wnt/beta-catenin pathway is required for the development of leukemia stem cells in AML. *Science (New York, N.Y.)*, *327*(5973), 1650–1653. https://doi.org/10.1126/science.1186624

Weiner, G. J. (2015). Building better monoclonal antibody-based therapeutics. *Nature Reviews. Cancer*, *15*(6), 361–370. https://doi.org/10.1038/nrc3930

Weiner, L. M. (2006). Fully human therapeutic monoclonal antibodies. *Journal of Immunotherapy (Hagerstown, Md. : 1997)*, *29*(1), 1–9.

Weisberg, E., Manley, P. W., Breitenstein, W., Bruggen, J., Cowan-Jacob, S. W., Ray, A., … Griffin, J. D. (2005). Characterization of AMN107, a selective inhibitor of native and mutant Bcr-Abl. *Cancer Cell*, *7*(2), 129–141. https://doi.org/10.1016/j.ccr.2005.01.007

Weisberg, E., Manley, P. W., Cowan-Jacob, S. W., Hochhaus, A., & Griffin, J. D. (2007). Second generation inhibitors of BCR-ABL for the treatment of imatinib-resistant chronic myeloid leukaemia. *Nature Reviews. Cancer*, *7*(5), 345–356. https://doi.org/10.1038/nrc2126

Weisberg, E., Wright, R. D., McMillin, D. W., Mitsiades, C., Ray, A., Barrett, R., … Griffin, J. D. (2008). Stromal-mediated protection of tyrosine kinase inhibitor-treated BCR-ABL-expressing leukemia cells. *Molecular Cancer Therapeutics*, *7*(5), 1121–1129. https://doi.org/10.1158/1535-7163.MCT-07-2331

Wen, S. T., & Van Etten, R. A. (1997). The PAG gene product, a stress-induced protein with antioxidant properties, is an Abl SH3-binding protein and a physiological inhibitor of c-Abl

tyrosine kinase activity. *Genes & Development*, *11*(19), 2456–2467.

White, D. L., Saunders, V. A., Dang, P., Engler, J., Venables, A., Zrim, S., … Hughes, T. (2007). Most CML patients who have a suboptimal response to imatinib have low OCT-1 activity: higher doses of imatinib may overcome the negative impact of low OCT-1 activity. *Blood*, *110*(12), 4064–4072. https://doi.org/10.1182/blood-2007-06-093617

Williams, A. F., & Barclay, A. N. (1988). The immunoglobulin superfamily--domains for cell surface recognition. *Annual Review of Immunology*, *6*, 381–405. https://doi.org/10.1146/annurev.iy.06.040188.002121

Willis, S. G., Lange, T., Demehri, S., Otto, S., Crossman, L., Niederwieser, D., … Deininger, M. W. (2005). High-sensitivity detection of BCR-ABL kinase domain mutations in imatinib-naive patients: correlation with clonal cytogenetic evolution but not response to therapy. *Blood*, *106*(6), 2128–2137. https://doi.org/10.1182/blood-2005-03-1036

Wlodarski, P., Wasik, M., Ratajczak, M. Z., Sevignani, C., Hoser, G., Kawiak, J., … Skorski, T. (1998). Role of p53 in hematopoietic recovery after cytotoxic treatment. *Blood*, *91*(8), 2998–3006.

Wolff, N. C., & Ilaria, R. L. J. (2001). Establishment of a murine model for therapy-treated chronic myelogenous leukemia using the tyrosine kinase inhibitor STI571. *Blood*, *98*(9), 2808–2816.

Wong, S., McLaughlin, J., Cheng, D., Shannon, K., Robb, L., & Witte, O. N. (2003). IL-3 receptor signaling is dispensable for BCR-ABL-induced myeloproliferative disease. *Proceedings of the National Academy of Sciences of the United States of America*, *100*(20), 11630–11635. https://doi.org/10.1073/pnas.2035020100

Woodring, P. J., Hunter, T., & Wang, J. Y. (2001). Inhibition of c-Abl tyrosine kinase activity by filamentous actin. *The Journal of Biological Chemistry*, *276*(29), 27104–27110. https://doi.org/10.1074/jbc.M100559200

Woof, J. M., & Burton, D. R. (2004). Human antibody-Fc receptor interactions illuminated by crystal structures. *Nature Reviews. Immunology*, *4*(2), 89–99. https://doi.org/10.1038/nri1266

Xenaki, K. T., Oliveira, S., & van Bergen En Henegouwen, P. M. P. (2017). Antibody or Antibody Fragments: Implications for Molecular Imaging and Targeted Therapy of Solid Tumors. *Frontiers in Immunology*, *8*, 1287. https://doi.org/10.3389/fimmu.2017.01287

Xie, L. H., Biondo, M., Busfield, S. J., Arruda, A., Yang, X., Vairo, G., & Minden, M. D. (2017). CD123 target validation and preclinical evaluation of ADCC activity of anti-CD123 antibody CSL362 in combination with NKs from AML patients in remission. *Blood Cancer Journal*, *7*(6), e567. https://doi.org/10.1038/bcj.2017.52

Xie, S., Wang, Y., Liu, J., Sun, T., Wilson, M. B., Smithgall, T. E., & Arlinghaus, R. B. (2001). Involvement of Jak2 tyrosine phosphorylation in Bcr-Abl transformation. *Oncogene*, *20*(43), 6188–6195. https://doi.org/10.1038/sj.onc.1204834

Xu, J. L., & Davis, M. M. (2000). Diversity in the CDR3 region of V(H) is sufficient for most antibody specificities. *Immunity*, *13*(1), 37–45.

Yamaoka, S., Courtois, G., Bessia, C., Whiteside, S. T., Weil, R., Agou, F., … Israel, A. (1998). Complementation cloning of NEMO, a component of the IkappaB kinase complex essential for NF-kappaB activation. *Cell*, *93*(7), 1231–1240.

Yao, E. S., Zhang, H., Chen, Y.-Y., Lee, B., Chew, K., Moore, D., & Park, C. (2007). Increased beta1 integrin is associated with decreased survival in invasive breast cancer. *Cancer Research*, *67*(2), 659–664. https://doi.org/10.1158/0008-5472.CAN-06-2768

Yao, Z., Cui, Y., Watford, W. T., Bream, J. H., Yamaoka, K., Hissong, B. D., … O'Shea, J. J. (2006). Stat5a/b are essential for normal lymphoid development and differentiation. *Proceedings of the National Academy of Sciences of the United States of America*, *103*(4), 1000–1005. https://doi.org/10.1073/pnas.0507350103

Yokoyama, W. M. (2001). Production of monoclonal antibodies. *Current Protocols in Cell Biology*, *Chapter 16*, Unit 16.1. https://doi.org/10.1002/0471143030.cb1601s03

Zakeri, B., Fierer, J. O., Celik, E., Chittock, E. C., Schwarz-Linek, U., Moy, V. T., & Howarth, M. (2012). Peptide tag forming a rapid covalent bond to a protein, through engineering a bacterial adhesin. *Proceedings of the National Academy of Sciences of the United States of America*, *109*(12), E690-7. https://doi.org/10.1073/pnas.1115485109

Zandi, E., Rothwarf, D. M., Delhase, M., Hayakawa, M., & Karin, M. (1997). The IkappaB kinase complex (IKK) contains two kinase subunits, IKKalpha and IKKbeta, necessary for IkappaB phosphorylation and NF-kappaB activation. *Cell*, *91*(2), 243–252.

Zhang, C., Xu, Y., Gu, J., & Schlossman, S. F. (1998). A cell surface receptor defined by a mAb mediates a unique type of cell death similar to oncosis. *Proceedings of the National Academy of Sciences of the United States of America*, *95*(11), 6290–6295.

Zhang, J., Adrian, F. J., Jahnke, W., Cowan-Jacob, S. W., Li, A. G., Iacob, R. E., … Gray, N. S. (2010). Targeting Bcr-Abl by combining allosteric with ATP-binding-site inhibitors. *Nature*, *463*(7280), 501–506. https://doi.org/10.1038/nature08675

Zhang, X., & Ren, R. (1998). Bcr-Abl efficiently induces a myeloproliferative disease and production of excess interleukin-3 and granulocyte-macrophage colony-stimulating factor in mice: a novel model for chronic myelogenous leukemia. *Blood*, *92*(10), 3829–3840.

Zhang, X., Subrahmanyam, R., Wong, R., Gross, A. W., & Ren, R. (2001). The NH(2)-terminal coiled-coil domain and tyrosine 177 play important roles in induction of a myeloproliferative disease in mice by Bcr-Abl. *Molecular and Cellular Biology*, *21*(3), 840–853. https://doi.org/10.1128/MCB.21.3.840-853.2001

Zhao, X., Ghaffari, S., Lodish, H., Malashkevich, V. N., & Kim, P. S. (2002). Structure of the Bcr-Abl oncoprotein oligomerization domain. *Nature Structural Biology*, *9*(2), 117–120. https://doi.org/10.1038/nsb747

Zhu, J., & Emerson, S. G. (2002). Hematopoietic cytokines, transcription factors and lineage commitment. *Oncogene*, *21*(21), 3295–3313. https://doi.org/10.1038/sj.onc.1205318

Zimmermann, J., Caravatti, G., Mett, H., Meyer, T., Muller, M., Lydon, N. B., & Fabbro, D. (1996). Phenylamino-pyrimidine (PAP) derivatives: a new class of potent and selective inhibitors of protein kinase C (PKC). *Archiv Der Pharmazie*, *329*(7), 371–376.

APPENDECIS

Appendix A. Soft randomiztion of oligonucleotides and barcodes used for NGS . Oligonucleotides were selected for CDRH3, CDRH2, CDRH1, CDRL3 diversification based on conservative randomiztion of any amino acid at frequency of 76% wild type – 8% – 8% – 8% randomiztion to other amino acids . N1, N2, N3, and N4 identify various diversification ratios (as defindedin the blue table). O oligonuceotides were designed to contain the diversified CDR region and the 5'– and 3'– overlapping primer to ensure PCR primer binding .

N1 = 76080808	N2 = 08760808	N3 = 08087608	N4 = 08080876

Name	Sequence	Product	Purification	Services
mIL3Rα–1_H3_*mut*	ct gcc gtc tat tat tgt gct cgc (N4:08080876)(N1:76080808)(N2:08760808)(N4)(N2)(N4)(N3:08087608)(N2)(N4)(N4)(N1)(N2)(N4)(N1)(N2)(N3)(N3)(N4)(N3)(N2)(N4)(N3)(N4)(N4)(N3)(N2)(N4)(N4)(N4)(N3)gac tac tgg ggt caa gga acc c	100 nmole DNA oligo	Standard Desalting	Hand Mix Fee
mIL3Rα–1_H2_*mut*	gt aag ggc ctg gaa tgg gtt gca(N4:08080876)(N2:08760808)(N4)(N1:76080808)(N4)(N4)(N4)(N1)(N4)(N2)(N2)(N4)(N4)(N2)(N4)(N4)(N1)(N4)(N3:08087608)(N3)(N2)(N4)(N1)(N4)(N1)(N2)(N4)(N4)(N1)(N4)tat gcc gat agc gtc aag ggc c	100 nmole DNA oligo	Standard Desalting	Hand Mix Fee
mIL3Rα–1_H1_*mut*	cc tgt gca gct tct ggc ttc aac (N1:76080808)(N4:08080876)(N2:08760808)(N4)(N2)(N4)(N4)(N1)(N4)(N4)(N2)(N4)(N4)(N2)(N4)(N1)(N4)(N3:08087608)cac tgg gtg cgt cag gcc	100 nmole DNA oligo	Standard Desalting	Hand Mix Fee
mIL3Rα–1_L3_*mut*	gaa gac ttc gca act tat tac tgt cag caa (N4:08080876)(N2:08760808)(N4)(N3:08087608)(N2)(N4)(N3)(N3)(N4)(N2)(N4)(N3)(N1:76080808)(N4)(N2)acg ttc gga cag ggt acc aag g	100 nmole DNA oligo	Standard Desalting	Hand Mix Fee

Name	Sequence	Product	Purification	Services
mIL3Rα–2_H3_*mut*	ct gcc gtc tat tat tgt gct cgc (N3:08087608)(N3)(N4:08080876)(N3)(N4)(N4)(N4)(N3)(N3)(N4)(N2:08760808)(N4)(N4)(N1:76080808)(N2)(N3)(N2)(N4)(N3)(N3)(N4)(N4)(N3)(N3)(N4)(N2)(N4)(N4)(N2)(N4)(N3)(N2)(N4)(N3)(N4)(N4)(N3)(N3)(N4)(N4)(N4)(N4) gac tac tgg ggt caa gga acc c	100 nmole DNA oligo	Standard Desalting	Hand Mix Fee
mIL3Rα–2_H2_*mut*	gt aag ggc ctg gaa tgg gtt gca(N4:08080876)(N2:08760808)(N4)(N1:76080808)(N4)(N4)(N4)(N1)(N4)(N2)(N2)(N4)(N4)(N1)(N4)(N4)(N1)(N4)(N3:08087608)(N3)(N2)(N4)(N2)(N4)(N1)(N2)(N4)(N4)(N1)(N4)tat gcc gat agc gtc aag ggc c	100 nmole DNA oligo	Standard Desalting	Hand Mix Fee
mIL3Rα–2_H1_*mut*	cc tgt gca gct tct ggc ttc aac (N1:76080808)(N4:08080876)(N2:08760808)(N4)(N2)(N4)(N4)(N2)(N4)(N4)(N1)(N4)(N4)(N1)(N4)(N1)(N4)(N3:08087608)cac tgg gtg cgt cag gcc	100 nmole DNA oligo	Standard Desalting	Hand Mix Fee
mIL3Rα–2_L3_*mut*	gaa gac ttc gca act tat tac tgt cag caa (N4:08080876)(N3:08087608)(N3)(N2:08760808)(N1:76080808)(N4)(N4)(N2)(N4)(N4)(N2)(N4)(N2)(N1)(N4)(N2)(N2)(N3)(N1)(N4)(N2)acg ttc gga cag ggt acc aag g	100 nmole DNA oligo	Standard Desalting	Hand Mix Fee

Appendix B. NGS analysis of CDRL3, CDRH1, CDRH2, and CDRH3 encoding sequences of anti–mIL3Rα Fab phage pool. Phage display selection 1: Round 4 panning against Fc–fused mIL3Rα. The abundance of the CDRH3 sequence reads was rank–ordered. The sequences highlighted *red* represent the top most abundant CDRH3 discovered by NGS analysis. The corresponding CDRL3, H1, and H2 encoding sequence was identified by single clone sequencing (highlighted *red*). The CDRH3 encoding sequences highlighted *purple* represent the second most abundant CDRH3 based on NGS analysis, although its corresponding CDRL3, H1, and H2 that were identified by single clone sequencing was not frequently found in NGS analysis. The clone selection for affinity maturation was exclusively based on the frequency of occurrence of CDRH3. The most abundant CDRH3 (TVRGSKKPYFSGWAMDYWGQG) was identified as the original library framework and excluded from analyses.

CDRL3	% Frequency	CDRH1	% Frequency	CDRH2	% Frequency	CDRH3	% Frequency
QQSAGRITFGQGT	38.2%	FNISYSSMHWVRQ	20.7%	VASMYTSFGYTYYADSV	13.1%	ARTVRGSKKPYFSGWAMDYWGQG	19.2%
QQSAGLITFGQGT	14.2%	FNLTSSIHWVRQ	9.5%	VASIYPSYGSTYYADSV	12.9%	ARYSAYYGAVALDYWGQG	16.0%
QQSAGLLTFGQGT	10.5%	FNVSHSSMHWVRQ	9.4%	VATIYPTYVYTYYADSV	8.4%	ARYWWYGLDYWGQG	15.1%
QQSAGVITFGQGT	6.9%	FNIGYSSMHWVRQ	8.8%	VASIYPSYGYTYYADSV	4.1%	ARGVWSYAGWSSAVGFDYWGQG	11.2%
QQSAGMITFGQGT	5.0%	FNIAYSSMHWVRQ	3.5%	VASIYTSYGYTYYADSV	2.9%	ARYYYSYSVSWSFSGLDYWGQG	8.6%
QQSAGPITFGQGT	3.0%	FNISYSSIHWVRQ	2.7%	VASNYPDYGYSYYADSV	2.6%	ARGVYYYYWSGYYSGVYGLDYWGQG	4.6%
QQSAGHITFGQGT	2.6%	FNVSYSSMHWVRQ	2.0%	VASIYPSYAFTYYADSV	1.9%	ARHPWPWYGLDYWGQG	3.7%
QQSGGPITFGQGT	2.3%	FNIYYSSMHWVRQ	1.7%	VATYPSYGYVYYADSV	1.7%	ARYWYPGSYSYVWAIDYWGQG	3.1%
QQSAGQITFGQGT	2.1%	FNISYSSLHWVRQ	1.5%	VASIIPSFAYTYYADSV	1.6%	ARAPYSWSHGPYWYGYYSGLDYWGQG	1.8%
QQSAGKITFGQGT	1.9%	FNMSYSSMHWVRQ	1.5%	VASLYTSYGYTYYADSV	1.4%	ARYAPGYYWYGLDYWGQG	1.8%
QQSGGRITFGQGT	1.3%	FNISHSSMHWVRQ	1.4%	VASIYPSYALTYYADSV	1.1%	ARSYPGPWAGAWYGAMDYWGQG	1.5%
QQSAGRVTFGQGT	1.2%	FNISSSSMHWVRQ	1.4%	VASIYPTYSYTYYADSV	1.1%	ARGWYYPYPGSSSVSGAMDYWGQG	1.4%
QQSAGRLTFGQGT	1.1%	FNLSYSSVHWVRQ	1.4%	VASIYASYGWTYYADSV	1.0%	ARSSYWGSWSSYPAYVSGGLDYWGQG	1.3%
QQSAGRMTFGQGT	1.0%	FNIPYSSMHWVRQ	1.3%	VASTYHSYGFTYYADSV	0.9%	ARWWSFGYWWHAFDYWGQG	1.3%
QQSAGLVTFGQGT	0.9%	FNIRYSSMHWVRQ	1.2%	VASIYHSYTWSYYADSV	0.8%	ARGWFYWSFVAPSGGGAIDYWGQG	1.1%
QQSGGLITFGQGT	0.7%	FNISYASMHWVRQ	1.2%	VASIYHSHGYTYYADSV	0.7%	ARHHHAFDYWGQG	1.0%
QQSSGRITFGQGT	0.6%	FNISHSSLHWVRQ	1.0%	VATVYPSYGYIYYADSV	0.6%	ARYWSWSGAGGSSGMDYWGQG	0.8%
QQAAGRITFGQGT	0.4%	FNLSYSSMHWVRQ	0.9%	VASIYAPYGYIYYADSV	0.6%	ARFWWPGMDYWGQG	0.6%
QQAAGLITFGQGT	0.4%	FNVGLSSMHWVRQ	0.8%	VASIYHSYGFAYYADSV	0.6%	ARGGGGYYWYSGLDYWGQG	0.6%
QQVAGRITFGQGT	0.3%	FNVSYSSLHWVRQ	0.8%	VASTYLSGGYSYYADSV	0.5%	ARYHYGYGLDYWGQG	0.6%
QQSTGRITFGQGT	0.2%	FNISSSIHWVRQ	0.7%	VASSYPSYGYTYYADSV	0.5%	ARAWWGPAPGSAVGHVYGAMDYWGQG	0.5%
QQSAGRTTFGQGT	0.2%	FNISNSSMHWVRQ	0.6%	VALIYPSYGYAYYADSV	0.5%	ARAPSYSGAGGFDYWGQG	0.3%
QQSSGLITFGQGT	0.2%	FNITYSSMHWVRQ	0.6%	VASIYPSYRYTYYADSV	0.4%	ARGVYVYGSSYSFVGLDYWGQG	0.3%
QQSGGMITFGQGT	0.2%	FNFSYSSMHWVRQ	0.5%	VASMYPSYGYTYYADSV	0.4%	ARGYYYGASYGYYYVASAGMDYWGQG	0.3%
QQSAGRSTFGQGT	0.2%	FNISSSSLHWVRQ	0.5%	VASSYLSYRYTYYADSV	0.4%	ARGSSYSYYSVPYAWPPFHALDYWGQG	0.2%
QQSAGTITFGQGT	0.2%	FNISYSSTHWVRQ	0.5%	VASIYHSYGYTYYADSV	0.4%	ARYSAYYGAVVLDYWGQG	0.2%
QQSAGLMTFGQGT	0.1%	FNISYTSMHWVRQ	0.5%	VATSYNPYGHNYYADSV	0.4%	ARYWYSGWYGLDYWGQG	0.2%
QQSAARITFGQGT	0.1%	FNFYYSSMHWVRQ	0.4%	VASIYPSYGYSYYADSV	0.4%	ARFFVYSSVYGSHWVVGGGGMDYWGQG	0.1%
QQSAGGITFGQGT	0.1%	FNIAYASMHWVRQ	0.4%	VATTYPSYGSTYYADSV	0.4%	ARGFYYYYHGHHGVAYGMDYWGQG	0.1%
QQSAGIITFGQGT	0.1%	FNIDYSSMHWVRQ	0.4%	VASTYPSYGYSYYADSV	0.4%	ARGHYGVYSYPHGFSVYSALDYWGQG	0.1%
QQAAGPITFGQGT	0.1%	FNISNASMHWVRQ	0.4%	VASIYPAYGYTYYADSV	0.4%	ARGVWSYAGWSSAVSFDYWGQG	0.1%
QQSAAPITFGQGT	0.1%	FNIWRSSMHWVRQ	0.4%	VASIYPSYGFTYYADSV	0.3%	ARGVYYYYWSGYYSVLIGLDYWGQG	0.1%
QQGAGRITFGQGT	0.1%	FNFSYSSLHWVRQ	0.3%	VASIYPSYAYTYYADSV	0.3%	ARHSYVYYWSYYPVAFDYWGQG	0.1%
QQAAGVITFGQGT	0.1%	FNIASSIHWVRQ	0.3%	VASIYPYYGHLYYADSV	0.3%	ARSHSYSSGAYSYGFDYWGQG	0.1%
QQSAGRFTFGQGT	0.1%	FNIASSMHWVRQ	0.3%	VASTSTSYGYSYYADSV	0.3%	ARSLTGFLVFLPGLRFWWLDYWGQG	0.1%
QQAAGQITFGQGT	0.1%	FNIAYSSIHWVRQ	0.3%	VASIYLPYGYTYYADSV	0.2%	ARTVRGSKKPYFSVGLLDYWGQG	0.1%
QQSASRITFGQGT	0.1%	FNISHASMHWVRQ	0.3%	VASMYPSYAYTYYADSV	0.2%	ARTVRGSKNRTSSGWAMDYWGQG	0.1%
QQSAGMTTFGQGT	0.1%	FNISHSSIHWVRQ	0.3%	VASIYASYGYTYYADSV	0.2%	ARVPYWGSYHAGFYWHALDYWGQG	0.1%
QQSAGPVTFGQGT	0.1%	FNISISSMHWVRQ	0.3%	VASIYPSYGHTYYADSV	0.2%	ARWPFGWAYALDYWGQG	0.1%
QQSAGPTTFGQGT	0.1%	FNISNSSLHWVRQ	0.3%	VASMYPPFGYTYYADSV	0.2%	ARWSAWGPPYAGWSSAVGFDYWGQG	0.1%
QQSAGQVTFGQGT	0.1%	FNISYASLHWVRQ	0.3%	VATIYPSYGYTYYADSV	0.2%	ARWSAWGPPYGGWYWYSAAMDYWGQG	0.1%
QQSAGVMTFGQGT	0.1%	FNISYSSVHWVRQ	0.3%	VASIYPSYGYNYYADSV	0.2%	ARWSFGGMDYWGQG	0.1%
QQAGGRITFGQGT	0.1%	FNIWYSSMHWVRQ	0.3%	VASVYPAYDYTYYADSV	0.2%	ARYGFYWFSGFDYWGQG	0.1%
QQSAGMLTFGQGT	0.1%	FNLAYSSMHWVRQ	0.3%	VASLYPSYGYAYYADSV	0.2%	ARYGGVGPYPGGPWWGHSAMDYWGQG	0.1%
QQSAGPMTFGQGT	0.1%	FNLIYSSIHWVRQ	0.3%	VASMYHSYGYTYYADSV	0.2%	ARYIHSYSVSWSFSGLDYWGQG	0.1%
QQSAGSITFGQGT	0.1%	FNLNYSSMHWVRQ	0.3%	VASIYPTYGYTYYADSV	0.2%	ARYWWYAMDYWGQG	0.1%
QQSGGVITFGQGT	0.1%	FNMYYSSMHWVRQ	0.3%	VASTYPSYGYTYYADSV	0.2%	ARYWYSGCDGLDYWGQG	0.1%
QQSLGPITFGQGT	0.1%	FNFSYASMHWVRQ	0.2%	VATTYPSYGYTYYADSV	0.2%	ARYYYSYVVSWSFSGLDYWGQG	0.1%
QQSVGRITFGQGT	0.1%	FNIAYSSVHWVRQ	0.2%	VASIYPSYGYTYADSV	0.1%	VRTVRGSKKPYFSGWAMDYWGQG	0.1%
QQSAGLTTFGQGT	0.1%	FNIGYSSIHWVRQ	0.2%	VASIYTPYGYTYYADSV	0.1%		
QQSAGPFTFGQGT	0.1%	FNIIYSSIHWVRQ	0.2%	VASIYPSYVYTYYADSV	0.1%		
QQSAGPLTFGQGT	0.1%	FNILYSSMHWVRQ	0.2%	VASIYPSYSYTYYADSV	0.1%		
QQAAARITFGQGT	0.0%	FNINYSSIHWVRQ	0.2%	VASIYPSYGYAYYADSV	0.1%		
QQAAGQVTFGQGT	0.0%	FNIQNGSMHWVRQ	0.2%	VATSYHAFGYTYYADSV	0.1%		
QQSAGAITFGQGT	0.0%	FNISFASMHWVRQ	0.2%	VASIYPSHGYTYYADSV	0.1%		
QQSAGRNTFGQGT	0.0%	FNISPTSMHWVRQ	0.2%	VASMYTSYGYTYYADSV	0.1%		
QQSAGVLTFGQGT	0.0%	FNISRSSMHWVRQ	0.2%	VATIYPSYGSTYYADSV	0.1%		
QQSASRLTFGQGT	0.0%	FNISSSMHWVRQ	0.2%	VASIYTSYGFTYYADSV	0.1%		
QQSASVTTFGQGT	0.0%	FNISYASIHWVRQ	0.2%	VASMYPSHGFTYYADSV	0.1%		
QQSGGQITFGQGT	0.0%	FNISYSAMHWVRQ	0.2%	VATIYPYYDYTYYADSV	0.1%		
QQSGGRVTFGQGT	0.0%	FNISYSNMHWVRQ	0.2%	VASTYHVYGYTYYADSV	0.1%		
QQSTGLITFGQGT	0.0%	FNITNSSMHWVRQ	0.2%	VASVYTSYGMTYYADSV	0.1%		
QQAGGLITFGQGT	0.0%	FNIYHSSMHWVRQ	0.2%	VASLYPSYGYTYYADSV	0.1%		
QQSAGMVTFGQGT	0.0%	FNIYYSSIHWVRQ	0.2%	VASYPSYGYTYYADSV	0.1%		
QQSAGQLTFGQGT	0.0%	FNIYYSSLHWVRQ	0.2%	VASIYPSYGHTYADSV	0.1%		
QQSAGRPTFGQGT	0.0%	FNLADSSMHWVRQ	0.2%	VASIYPYGYTYYADSV	0.1%		
QQSAGVTTFGQGT	0.0%	FNLAYASMHWVRQ	0.2%	VASIYSSYGFTYYADSV	0.1%		
QQSGARITFGQGT	0.0%	FNLSDSSMHWVRQ	0.2%	VASIYTTYGYTYYADSV	0.1%		
QQGAGLITFGQGT	0.0%	FNLSRSSTHWVRQ	0.2%	VASMYHSYGYSYYADSV	0.1%		
QQSAALITFGQGT	0.0%	FNLSYSSIHWVRQ	0.2%	VASSYPSYGYSYYADSV	0.1%		
QQSASPITFGQGT	0.0%	FNMAYASMHWVRQ	0.2%	VASIYSSYGYTYYADSV	0.1%		
QQSGGGITFGQGT	0.0%	FNMFFTSLHWVRQ	0.2%	VASIYTNYGYTYYADSV	0.1%		
QQYAGRITFGQGT	0.0%	FNVRFSSVHWVRQ	0.2%	VATMYPSYGYTYYADSV	0.1%		
QQSAAMITFGQGT	0.0%	FNVSYASIHWVRQ	0.2%	VASIYHSYGHSYYADSV	0.1%		
QQSASQITFGQGT	0.0%	FNVSYSSIHWVRQ	0.2%	VASIYPLYGYSYYADSV	0.1%		

Appendix C. NGS analysis of CDRL3, CDRH1, CDRH2, and CDRH3 encoding sequences in anti–mIL3Rβ Fab phage pool. <u>Phage display selection 1: Round 4 panning against Fc–fused mIL3Rβ</u>. CDRH3 sequence reads were rank–ordered based on abundance. The top most abundant CDRH3, highlighted *red,* was discovered by NGS analysis and the corresponding CDRL3, H1 and H2 sequence were identified by single clone sequencing (highlighted *red*). The corresponding CDRH1 sequence was not frequently found in NGS analysis. The sequences highlighted *purple* represent second most abundant CDRH3 based on NGS analysis.

CDRL3	% Frequency	CDRH1	% Frequency	CDRH2	% Frequency	CDRH3	% Frequency
QQYSFSRYNPITFGQGT	6.1%	FNLSSSFMHWVRQ	6.4%	VASIYSYYGYRSYADSV	7.1%	ARSSSGWYGFDYWGQG	49.5%
QQYSYSYYYPITFGQGT	5.5%	FNLSSSFVHWVRQ	3.2%	VASIYSYYSYTSYADSV	4.3%	ARSSWGYYYPYGLDYWGQG	23.6%
QQYSYSYYSPITFGQGT	3.2%	FNLASSYTHWVRQ	2.7%	VASRLSYYSYTSYADSV	3.3%	ARSGSPSAYSFGALDYWGQG	11.2%
QQYSYDYYAPITFGQGT	1.4%	FNLSSSFIHWVRQ	2.7%	VASIYSHYSYTSYADSV	1.2%	ARTVRGSKKPYFSGWAMDYWGQG	4.7%
QQYSYSNYSPITFGQGT	1.3%	FNHLLLRHWVRQ	2.3%	VASIYSNYSYTSYADSV	1.0%	ARYGLDYWGQG	1.8%
QQYSLSYYYPITFGQGT	1.1%	FNLSSSFLHWVRQ	2.3%	VASVHTYYSYTSYADSV	1.0%	ARSSSWLYGFDYWGQG	1.1%
QQYSYSQYYPITFGQGT	1.0%	FNISSYLMHWVRQ	1.8%	VASIYSYYRYTSYADSV	0.8%	ARSSYFGHAIDYWGQG	0.9%
QQYSYSHYYPITFGQGT	0.8%	FNLASSYMHWVRQ	1.8%	VASMYSYYSYTSYADSV	0.8%	ARWPGAYWYSFGMDYWGQG	0.8%
QQYSFSYHSPITFGQGT	0.8%	FNLSSSYMHWVRQ	1.8%	VASIYSSYSYTSYADSV	0.7%	ARYSYYYAHYGWGYFAGAYALDYWGQG	0.7%
QQYSYSYYTPITFGQGT	0.8%	FNLTSSYMHWVRQ	1.8%	VASIYSYYGYTSYADSV	0.7%	ARSHYWHGMDYWGQG	0.6%
QQYSYSYYSAITFGQGT	0.7%	FNYLLLIHWVRQ	1.8%	VASIYAYYSYTSYADSV	0.6%	ARSWYYVVGLDYWGQG	0.5%
QQYSYLLLPITFGQGT	0.7%	FNFSSSFMHWVRQ	1.4%	VASIYSYYSYSSYADSV	0.6%	ARWYGGPYHAGMDYWGQG	0.5%
QQYSYSYHSPITFGQGT	0.7%	FNLSSFFMHWVRQ	1.4%	VASVYSYYSYTSYADSV	0.6%	ARAHASWYWPWVGYHVWYGMDYWGQG	0.4%
QQYSYSYSYPITFGQGT	0.7%	FNLSSSYIHWVRQ	1.4%	VASIYANYSYTSYADSV	0.5%	ARYGYHSFWAMDYWGQG	0.4%
QQYSYSSSSSPITFGQGT	0.7%	FNLTTSFMHWVRQ	1.4%	VASIHSYYGYTSYADSV	0.5%	ARGYYSSGYWYYYGLDYWGQG	0.3%
QQYTYSYYHPITFGQGT	0.7%	FNFSSSFIHWVRQ	0.9%	VASIYSYSYTSYADSV	0.5%	ARSWPWFGGSYAMDYWGQG	0.3%
QQYSYSSYSPVTFGQGT	0.6%	FNLASFMHWVRQ	0.9%	VASIYYHYSYTSYADSV	0.4%	ARYSYHYVGGGSYHYWYVYGFDYWGQG	0.3%
QQYSYSFYYPITFGQGT	0.6%	FNLASSFNHWVRQ	0.9%	VASSYSYYSYTSYADSV	0.4%	ARFWSYSYSYYSYSSYAMDYWGQG	0.2%
QQYSYSHRNAITFGQGT	0.6%	FNLASYIHWVRQ	0.9%	VASTYSYYSYTSYADSV	0.4%	ARHGGAYAMDYWGQG	0.2%
QQYTYSYHFPMTFGQGT	0.6%	FNLNSSFMHWVRQ	0.9%	VATTYSAYSYTSYADSV	0.4%	ARSWYGGAYVGWSSPAYVAFDYWGQG	0.2%
QQYSYSSYYPVTFGQGT	0.6%	FNLSNSFLHWVRQ	0.9%	VASIYSHYGYTSYADSV	0.4%	ARYGMDYWGQG	0.2%
QQYSYSYYHPITFGQGT	0.6%	FNLSSAYMHWVRQ	0.9%	VASIYSGYSYTSYADSV	0.4%	ARYSYGYYFVSGFASSYAFDYWGQG	0.2%
QQYSYYYYSPITFGQGT	0.5%	FNLSSSLMHWVRQ	0.9%	VATIYSYYSYTSYADSV	0.4%	AHSSSGWYGFDYWGQG	0.1%
QQYSYSYYYAITFGQGT	0.5%	FNLSYSFMHWVRQ	0.9%	VASIYSEYSYTSYADSV	0.4%	ARAHASWYWPWVGYHVWYDMDYWGQG	0.1%
QQYTYSYYYPITFGQGT	0.5%	FNLTYSYMHWVRQ	0.9%	VASIYPYYSYTSYADSV	0.4%	ARAPWYSAIDYWGQG	0.1%
QQYSYSNYDTVTFGQGT	0.5%	FNPSSSFMHWVRQ	0.9%	VASLYSHYSYTSYADSV	0.3%	ARSCFWLYGFDYWGQG	0.1%
QQYTYSSYYPVTFGQGT	0.5%	FNVSSSYMHWVRQ	0.9%	VASIYYYSYTSYADSV	0.3%	ARSFYYHAFDYWGQG	0.1%
QQYSYSYYKPITFGQGT	0.5%	FNYLTFMHWVRQ	0.9%	VASIYSYYSYASYADSV	0.3%	ARSGSPSALLFRCLDYWGQG	0.1%
QQYSYSNYHAITFGQGT	0.5%	FNDASTFMHWVRQ	0.5%	VASLYSYYSYTSYADSV	0.3%	ARSGSPSAYSFGASDYWGQG	0.1%
QQYSYSYHYPITFGQGT	0.5%	FNDSSWFMHWVRQ	0.5%	VASHYPYYSYTTYADSV	0.3%	ARSGSPSDLLFRCLDYWGQG	0.1%
QQYSYSYNYPITFGQGT	0.5%	FNFHSSFIHWVRQ	0.5%	VASIYSYYTYTSYADSV	0.3%	ARSHYSYHSWAWYYWSGAMDYWGQG	0.1%
QQYSYSYYGPITFGQGT	0.5%	FNFSSSFLHWVRQ	0.5%	VASIYSDYSYTSYADSV	0.3%	ARSSCGWYGFDYWGQG	0.1%
QQYSYSYYSPVTFGQGT	0.5%	FNFSSSLIHWVRQ	0.5%	VASSYSYYRYTSYADSV	0.3%	ARSSSDWYGFDYWGQG	0.1%
QQYSYSNNNPITFGQGT	0.4%	FNFSTSFMHWVRQ	0.5%	VASVYSYYSYSSYADSV	0.3%	ARSSSGWYGLDYWGQG	0.1%
QQYSYSNYQPITFGQGT	0.4%	FNGASSFLHWVRQ	0.5%	VATIYSYMYNSYADSV	0.3%	ARSVRGWYGFDYWGQG	0.1%
QQYSYSYYVPITFGQGT	0.4%	FNGSSSFMHWVRQ	0.5%	VASIYSYYSYTAYADSV	0.3%	ARTVRGSKNRTSRGWAMDYWGQG	0.1%
QQYSYSFYSPITFGQGT	0.4%	FNHSSGLHWVRQ	0.5%	VASIYSYYSYTTYADSV	0.3%	ARWGMDYWGQG	0.1%
QQYSYSLPPITFGQGT	0.4%	FNHSSSFLHWVRQ	0.5%	VASIYSNYRYTSYADSV	0.3%	ARWYRCPYHAGMDYWGQG	0.1%
QQYSYSNFYSITFGQGT	0.4%	FNHSSSFVHWVRQ	0.5%	VASIYTYYSYTSYADSV	0.3%		
QQYSYSNHHAITFGQGT	0.4%	FNIASSFLHWVRQ	0.5%	VASIYSDYSYSSYADSV	0.3%		
QQYSYSTHLPITFGQGT	0.4%	FNIDSFIHWVRQ	0.5%	VASIYSYYSYNSYADSV	0.3%		
QQYSYSSYYPITFGQGT	0.4%	FNINSSFLHWVRQ	0.5%	VASTYSNYSYTSYADSV	0.3%		
QQYSYSYYDPITFGQGT	0.4%	FNIRSSYIHWVRQ	0.5%	VASVYPYYSYASYADSV	0.3%		
QQYSYSYYHAITFGQGT	0.4%	FNISAVVHWVRQ	0.5%	VASGYSYYRYTSYADSV	0.3%		
QQYSYAYRYPITFGQGT	0.4%	FNISSAFMHWVRQ	0.5%	VATIYHSPRYTSYADSV	0.3%		
QQYSYAYYSTITFGQGT	0.4%	FNISSFFMHWVRQ	0.5%	VASIYGYYSYTSYADSV	0.3%		
QQYSYSNYYAITFGQGT	0.4%	FNISSSFLHWVRQ	0.5%	VASIYSSYRYTSYADSV	0.3%		
QQYSYSNYYPITFGQGT	0.4%	FNISSSFMHWVRQ	0.5%	VASTYSSYSYTSYADSV	0.3%		
QQYSYSWYSAATFGQGT	0.3%	FNISSSYTHWVRQ	0.5%	VASVYSAYSYSSYADSV	0.3%		
QQYSYSYYSEITFGQGT	0.3%	FNISSTFMHWVRQ	0.5%	VASVYSYTSYNSYADSV	0.3%		
QQYSYSYYWPITFGQGT	0.3%	FNISTSFIHWVRQ	0.5%	VASSYSYHSYTSYADSV	0.3%		
QQYSYSYYYPVTFGQGT	0.3%	FNISTSYIHWVRQ	0.5%	VASVYSSYSYTSYADSV	0.2%		
QQYYYSYYSPVTFGQGT	0.3%	FNISYSFVHWVRQ	0.5%	VASSYSASRYTSYADSV	0.2%		
QQYSYAYNSAITFGQGT	0.3%	FNITSPFMHWVRQ	0.5%	VASVFPNHSYASYADSV	0.2%		
QQYSYSFNYAITFGQGT	0.3%	FNITSSFLHWVRQ	0.5%	VASIYPYYSYTAYADSV	0.2%		
QQYSYSLQNAITFGQGT	0.3%	FNIYASCLHWVRQ	0.5%	VASIYSLYSYTSYADSV	0.2%		
QQYSYSSYHPITFGQGT	0.3%	FNIYSAFMHWVRQ	0.5%	VASYSYYSYTSYADSV	0.2%		
QQYSYSYHYPVTFGQGT	0.3%	FNIYSSFMHWVRQ	0.5%	VASIYTVWGYTSYADSV	0.2%		
QQYAYSYSLRTTFGQGT	0.3%	FNLASSFMHWVRQ	0.5%	VASNYYYYSYTSYADSV	0.2%		
QQYSYAYYYPITFGQGT	0.3%	FNLASTYMHWVRQ	0.5%	VASYSNYSFTAYADSV	0.2%		
QQYSYSYSAPITFGQGT	0.3%	FNLAYSYIHWVRQ	0.5%	VASINYSYSYTAYADSV	0.2%		
QQYTYSHSYAITFGQGT	0.3%	FNLCIILMHWVRQ	0.5%	VASIYAYYRYNSYADSV	0.2%		
QQYAYSFYYPITFGQGT	0.3%	FNLDSFLHWVRQ	0.5%	VASTSYSYTSYADSV	0.2%		
QQYSYGYDSPITFGQGT	0.3%	FNLDTYYIHWVRQ	0.5%	VATIYSYHSYTSYADSV	0.2%		
QQYSYSYYFPITFGQGT	0.3%	FNLDYPFFHWVRQ	0.5%	VAATYSSYRYTSYADSV	0.2%		
QQYTYSYYSPITFGQGT	0.3%	FNLFDFFIHWVRQ	0.5%	VASMFSYHSYTSYADSV	0.2%		
QQYSYSAYVPITFGQGT	0.3%	FNLFSSMHWVRQ	0.5%	VASIYSHYLYTGYADSV	0.2%		
QQYSYSYESAITFGQGT	0.3%	FNLFSSYIHWVRQ	0.5%	VASNYSYYRYTSYADSV	0.2%		
QQYSYSYYRPVTFGQGT	0.3%	FNLILLIHWVRQ	0.5%	VASIYPQYSFSSYADSV	0.2%		
QQYRYSYYHPITFGQGT	0.3%	FNLLGSYNHWVRQ	0.5%	VASIYPYHTYSSYADSV	0.2%		
QQYSYSHYSPITFGQGT	0.3%	FNLLILIHWVRQ	0.5%	VASMYTHYGYTSYADSV	0.2%		
QQYSYSYYNAITFGQGT	0.3%	FNLLLLMHWVRQ	0.5%	VASSYSYYRYSSYADSV	0.2%		
QQYSYSYYNPITFGQGT	0.3%	FNLLPPFLHWVRQ	0.5%	VASIYSYHSYTSYADSV	0.2%		
QQYSFSQSNAITFGQGT	0.2%	FNLNLSYMHWVRQ	0.5%	VASMLSDYSYTSYADSV	0.2%		
QQYSYSYHNPVTFGQGT	0.2%	FNLNTVFSHWVRQ	0.5%	VASNYSYYSYTSYADSV	0.2%		
QQYSYSYNKPITFGQGT	0.2%	FNLPSAYLHWVRQ	0.5%	VATIYSSYSYTSYADSV	0.2%		
QQYSYSYSEPITFGQGT	0.2%	FNLPSSFMHWVRQ	0.5%	VASAYSYHSYTPYADSV	0.2%		
QQYSYSYYYPNTFGQGT	0.2%	FNLPSYFLHWVRQ	0.5%	VASIHSDYSYTTYADSV	0.2%		
QQYLFELLPITFGQGT	0.2%	FNLRSTFIHWVRQ	0.5%	VASIYSHYSYSSYADSV	0.2%		
QQYSYSHYRPITFGQGT	0.2%	FNLSASFMHWVRQ	0.5%	VASIYSYHSYASYADSV	0.2%		
QQYSYSRYSPITFGQGT	0.2%	FNLSASYLHWVRQ	0.5%	VASIYSYYSYQSYADSV	0.2%		
QQYSYSYNSPITFGQGT	0.2%	FNLSFDFLHWVRQ	0.5%	VASMYSSYLYTSYADSV	0.2%		
QQYSYSYYTPVTFGQGT	0.2%	FNLSFLFIHWVRQ	0.5%	VASYSYYSYKSYADSV	0.2%		
QQYSYTHYAAITFGQGT	0.2%	FNLSHSYRHWVRQ	0.5%	VASIFSYYSYTSYADSV	0.2%		

Appendix D. NGS analysis of CDRL3, CDRH1, CDRH2, and CDRH3 anti–mIL3Rα–1mut Fab phage pool. Phage display selection 2: Round 3 panning against Fc–fused mIL3Rα. The most abundant CDRH1, H2, H3, and L3 sequences were identified by NGS. The clone containing the top most frequent CDRH1, H2, H3, and L3 sequences (bold and highlighted in yellow) was obtained by conventional single clone sequencing. This clone was labeled as mIL3Rα–1mut clone and used for generation of affinity–matured mIL3Rα–1mut antibody and further in vitro and in vivo analysis. The sequences highlighted red represent the original unmutated clone from the first round of phage display selections based on NGS analysis.

mIL3Rα–1mut phage pool
(Secetion 2: Round3 pool)

CDRL3		CDRH1		CDRH2		CDRH3	
	%Frequency		% Frequency		% Frequency		% Frequency
QQSAGRIPITFGQGT	33.0%	FNVSHSSMHWVRQ	17.1%	VASIYPSYGSTYYADSV	16.1%	YTAYYGAVALDYWGQG	14.8%
QQSAGLIPITFGQGT	13.0%	FNIGYSSMHWVRQ	13.9%	VASMYTSFGYTYYADSV	14.8%	YAAYFGPVTLDYWGQG	10.3%
QQSAGLLPITFGQGT	9.3%	FNISYSSMHWVRQ	9.6%	VASIYPSYGYTYYADSV	5.1%	YTAYYGTVALDYWGQG	8.1%
QQSAGQIPITFGQGT	6.9%	FNITFASMHWVRQ	5.4%	VASIYTSYGYTYYADSV	3.4%	YSAYYGAVALDYWGQG	7.4%
QQSAGVIPITFGQGT	6.1%	FNVSYSSMHWVRQ	3.9%	VASNYPDYWGQGGYSYYADSV	3.0%	YSAYYGSVALDYWGQG	4.5%
QQTAGRIPITFGQGT	4.8%	FNISYSSIHWVRQ	3.6%	VASIYPSYAFTYYADSV	2.2%	HSSYYGAVALDYWGQG	1.8%
QQSAGMIPITFGQGT	4.2%	FNLSYSSVHWVRQ	2.5%	VASIIPSFAYTYYADSV	1.8%	YSAYYGAVSLDYWGQG	1.8%
QQSAGPIPITFGQGT	3.1%	FNISYSSLHWVRQ	2.4%	VASIYASYGWTYYADSV	1.5%	HSAYYGAVAFDYWGQG	1.6%
QQSAGHIPITFGQGT	2.3%	FNLSYSSMHWVRQ	2.1%	VATTYPAYGLTYYADSV	1.2%	YSAYYGSIALDYWGQG	1.6%
QQSGGPIPITFGQGT	2.0%	FNLTFSSIHWVRQ	1.8%	VASIYPTYSYTYYADSV	1.1%	YSGYYGAVALDYWGQG	1.6%
QQSAGKIPITFGQGT	1.6%	FNISFSSMHWVRQ	1.6%	VASTYHSYGFTYYADSV	1.0%	YTAYYGPVSLDYWGQG	1.6%
QQSAGRVPITFGQGT	1.1%	FNVSYSSLHWVRQ	1.3%	VATVYPSYGYIYYADSV	0.9%	YAAYYGAVALDYWGQG	1.3%
QQSGGRIPITFGQGT	1.1%	FNISHSSLHWVRQ	1.2%	VASIYHSYTWSYYADSV	0.9%	YSDYWGQGYGAVALDYWGQG	1.3%
QQSAGRLPITFGQGT	1.0%	FNIFYSSMHWVRQ	1.1%	VASIYAPYGYIYYADSV	0.8%	HSAYYGAVDLDYWGQG	1.1%
QQSAGLVPITFGQGT	0.9%	FNVGLSSMHWVRQ	0.9%	VASIYHSHGYTYYADSV	0.8%	YSAYYGPVALDYWGQG	1.1%
QQSAGRMPITFGQGT	0.8%	FNISFSSIHWVRQ	0.7%	VASSYPSYGYTYYADSV	0.6%	HSAYYGTVSLDYWGQG	0.9%
QQTAGLIPITFGQGT	0.7%	FNISHSSMHWVRQ	0.7%	VASIYHSYGFAYYADSV	0.6%	HSVYYGSVALDYWGQG	0.9%
QQSGGLIPITFGQGT	0.6%	FNIAYSSMHWVRQ	0.7%	VASTYLSGGYSYYADSV	0.6%	YSAFYGAAYLDYWGQG	0.9%
QQSSGRIPITFGQGT	0.5%	FNFSYSSMHWVRQ	0.6%	VASIYHSYGYTYYADSV	0.5%	YSAYYGVVALDYWGQG	0.9%
QQAAGRIPITFGQGT	0.4%	FNMSYSSMHWVRQ	0.5%	VASSYLSYRYTYYADSV	0.5%	HSAYYGAVSLDYWGQG	0.7%
QQAAGLIPITFGQGT	0.3%	FNIAYSSLHWVRQ	0.5%	VATTYPSYGSTYYADSV	0.5%	HSAYYGSVSLDYWGQG	0.7%
QQVAGRIPITFGQGT	0.2%	FNISYSSVHWVRQ	0.5%	VASIYPAYGYTYYADSV	0.5%	HSTYYGSVALDYWGQG	0.7%
QQTAGVIPITFGQGT	0.2%	FNISYASMHWVRQ	0.4%	VASIYPSYRYTYYADSV	0.4%	YSAFYGFVALDYWGQG	0.7%
QQSTGRIPITFGQGT	0.2%	FNIPYSSMHWVRQ	0.4%	VASIYPSYGYSYYADSV	0.4%	YSAYFGAVALDYWGQG	0.7%
QQSAGRTPITFGQGT	0.2%	FNFSYSSLHWVRQ	0.4%	VASTYPSYGYSYYADSV	0.4%	YSAYYGAVSFDYWGQG	0.7%
QQSSGLIPITFGQGT	0.2%	FNIYYSSMHWVRQ	0.4%	VASIYTSYGFTYYADSV	0.4%	YSAYYGAVVLDYWGQG	0.7%
QQSAGLMPITFGQGT	0.1%	FNITYSSMHWVRQ	0.3%	VASIYPSYGFTYYADSV	0.3%	YSGYYGFVAFDYWGQG	0.7%
QQSAGRSPITFGQGT	0.1%	FNISNSSMHWVRQ	0.3%	VASIYPSYGYTFYADSV	0.3%	HSAFYGPIALDYWGQG	0.4%
QQSGGMIPITFGQGT	0.1%	FNISVSSMHWVRQ	0.3%	VASTSTSYGYSYYADSV	0.3%	HSAYYGAVALDYWGQG	0.4%
QQSASQIPITFGQGT	0.1%	FNISNASMHWVRQ	0.3%	VASIYPSYAYTYYADSV	0.3%	HSAYYGAVTLDYWGQG	0.4%
QQSAARIPITFGQGT	0.1%	FNIRYSSMHWVRQ	0.3%	VASIYPSYGYNYYADSV	0.3%	WSAYYGSVALDYWGQG	0.4%
QQSAGTIPITFGQGT	0.1%	FNLSYSSLHWVRQ	0.2%	VASLYPSYGYAYYADSV	0.3%	YSAYYGAIALDYWGQG	0.4%
QQTAGRMPITFGQGT	0.1%	FNTSYSSMHWVRQ	0.2%	VASIYLPYGYTYYADSV	0.2%	YSAYYGSVFLDYWGQG	0.4%
QQAAGPIPITFGQGT	0.1%	FNISHSSIHWVRQ	0.2%	VASIYPTYGYTYYADSV	0.2%	YSAYYGSVSLDYWGQG	0.4%
QQSAGIIPITFGQGT	0.1%	FNISNSSLHWVRQ	0.2%	VASMYPSYAYTYYADSV	0.2%	YSAYYGTVALDYWGQG	0.4%
QQSAGGIPITFGQGT	0.1%	FNITYSSLHWVRQ	0.2%	VASIYPSHGYSYYADSV	0.2%	YSAYYGTVSLDYWGQG	0.4%
QQSAAPIPITFGQGT	0.1%	FNIYYSSLHWVRQ	0.2%	VASMYPPFGYTYYADSV	0.2%	YSDYWGQGYGNVALDYWGQG	0.4%
QQSAGRFPITFGQGT	0.1%	FNIFHSSMHWVRQ	0.2%	VASVYPAYDYWGQGTYYADSV	0.2%	YSDYWGQGYGSVALDYWGQG	0.4%
QQSASRIPITFGQGT	0.1%	FNISSSSLHWVRQ	0.2%	VATTYPSYGYTYYADSV	0.2%	YSSYYGSVSFDYWGQG	0.4%
QQAAGQIPITFGQGT	0.1%	FNISSSSMHWVRQ	0.2%	VASIYASYGYTYYADSV	0.2%	YTAYYGAVAFDYWGQG	0.4%
QQAAGVIPITFGQGT	0.1%	FNLSHSSMHWVRQ	0.2%	VATIYPSYGYTYYADSV	0.2%	YTAYYGPVALDYWGQG	0.4%
QQSAGPLPITFGQGT	0.1%	FNVFHSSMHWVRQ	0.2%	VASIYPSYVYTYYADSV	0.2%	YTSYYGAVALDYWGQG	0.4%
QQSAGPMPITFGQGT	0.1%	FNVSYSSIHWVRQ	0.2%	VASIYPSYGHTYYADSV	0.2%	FAAYYGSVALDYWGQG	0.2%
QQSAGPVPITFGQGT	0.1%	FNIFYSSIHWVRQ	0.2%	VATSYHAFGYTYYADSV	0.2%	FSAYYGAVALDYWGQG	0.2%
QQSAGMTPITFGQGT	0.1%	FNLYYSSMHWVRQ	0.2%	VASTYPSYGYTYYADSV	0.2%	FSAYYGGVALDYWGQG	0.2%
QQSAGPTPITFGQGT	0.1%	FNIWRSSMHWVRQ	0.2%	VASIYPSYSYTYYADSV	0.2%	FSAYYGSVTLDYWGQG	0.2%
QQGAGRIPITFGQGT	0.1%	FNIAYASMHWVRQ	0.2%	VASMYPSHGFTYYADSV	0.2%	FSGYYGAVSLDYWGQG	0.2%
QQSAGQVPITFGQGT	0.1%	FNIAYSSIHWVRQ	0.2%	VASMYPSYGYTYYADSV	0.2%	FSPYYGAVSFDYWGQG	0.2%
QQSGGVIPITFGQGT	0.1%	FNISKSSMHWVRQ	0.2%	VATIYPSYGSTYYADSV	0.2%	FSSYYGTVAFDYWGQG	0.2%
QQSAGVMPITFGQGT	0.1%	FNLAYSSMHWVRQ	0.2%	VASIYPSHGYTYYADSV	0.2%	FTAYYGAVALDYWGQG	0.2%
QQSLGPIPITFGQGT	0.1%	FNISDSSLHWVRQ	0.2%	VASIYTPYGYTYYADSV	0.2%	HAAYYGSVALDYWGQG	0.2%
QQTAGQIPITFGQGT	0.1%	FNISFSSLHWVRQ	0.2%	VASLYPSYGYTYYADSV	0.2%	HGAYYGSVALDYWGQG	0.2%
QQSGGQIPITFGQGT	0.1%	FNVSHSSIHWVRQ	0.2%	VASTYHVYGYTYYADSV	0.2%	HSAFYGHVALDYWGQG	0.2%
QQAGGRIPITFGQGT	0.0%	FNIADRSLHWVRQ	0.2%	VASNYPSYGYTYYADSV	0.1%	HSAYFGTVALDYWGQG	0.2%
QQSAGLTPITFGQGT	0.0%	FNLSNSSMHWVRQ	0.2%	VASFYPSYGYTYYADSV	0.1%	HSAYYGHVTLDYWGQG	0.2%
QQSAGMLPITFGQGT	0.0%	FNLNYSSMHWVRQ	0.2%	VASIYPSYGYAYYADSV	0.1%	HSAYYGPVALDYWGQG	0.2%
QQSAGPFPITFGQGT	0.0%	FNMSYSSLHWVRQ	0.2%	VATIYPYYDYWGQGTYYADSV	0.1%	HSAYYGSVGLDYWGQG	0.2%
QQSAGSIPITFGQGT	0.0%	FNVSYSAMHWVRQ	0.2%	VASIYHSYGHSYYADSV	0.1%	HSAYYGSVILDYWGQG	0.2%
QQSAGVTPITFGQGT	0.0%	FNIGYSSIHWVRQ	0.2%	VASIYSSYGFTYYADSV	0.1%	HSAYYGSVYFDYWGQG	0.2%
QQSASVTPITFGQGT	0.0%	FNISDSSMHWVRQ	0.2%	VATSYPSYGYTYYADSV	0.1%	HSAYYGTVTLDYWGQG	0.2%
QQSVGRIPITFGQGT	0.0%	FNLAYASMHWVRQ	0.2%	VASIYPFYGYTYYADSV	0.1%	HSAYYVLSCTLDYWGQG	0.2%
QQTAGPIPITFGQGT	0.0%	FNISFASMHWVRQ	0.1%	VASIYPSYGYKYYADSV	0.1%	HSFYYGAVALDYWGQG	0.2%
QQAAGQVPITFGQGT	0.0%	FNITFSSMHWVRQ	0.1%	VASIYTSYGFTYYADSV	0.1%	HSRYYGTVVFDYWGQG	0.2%
QQSAGAIPITFGQGT	0.0%	FNVSHSSLHWVRQ	0.1%	VASVYTSYGMTYYADSV	0.1%	HSSYYGSVALDYWGQG	0.2%
QQSAGRPPITFGQGT	0.0%	FNVTLSSMHWVRQ	0.1%	VASLYPAYGYTYYADSV	0.1%	HTAYFGNIALDYWGQG	0.2%
QQSAGVLPITFGQGT	0.0%	FNIFYSSLHWVRQ	0.1%	VASIYPLYGYSYYADSV	0.1%	HTAYYGAVALDYWGQG	0.2%
QQSASPIPITFGQGT	0.0%	FNISYTSMHWVRQ	0.1%	VASIYPSYSYKYYADSV	0.1%	HTAYYGAVTMDYWGQG	0.2%
QQSTGLIPITFGQGT	0.0%	FNLSYSSIHWVRQ	0.1%	VASIYPSFGYTYYADSV	0.1%	HTAYYGTVALDYWGQG	0.2%
QQSAGRNPITFGQGT	0.0%	FNTTYSSMHWVRQ	0.1%	VATIYPTYVYTYYADSV	0.1%	SAALYGAVAFDYWGQG	0.2%
QQSASRLPITFGQGT	0.0%	FNVSSSSMHWVRQ	0.1%	VATMYPSYGYTYYADSV	0.1%	WSSYYGSVFLDYWGQG	0.2%
QQSGGRVPITFGQGT	0.0%	FNIPYSSLHWVRQ	0.1%	VATSYPSYGYNFYADSV	0.1%	YAAYYAAVALDYWGQG	0.2%
QQTAGMIPITFGQGT	0.0%	FNISFASIHWVRQ	0.1%	VASIYPAYRYTYYADSV	0.1%	YGAYYGSVALDYWGQG	0.2%
QQYAGRIPITFGQGT	0.0%	FNVSYASIHWVRQ	0.1%	VASIYPNYGYTYYADSV	0.1%	YLAYYGSIVFDYWGQG	0.2%
QQAAARIPITFGQGT	0.0%	FNFYYSSMHWVRQ	0.1%	VASIYPSHGYVYYADSV	0.1%	YPLTTVLLVDDYWGQG	0.2%
QQAGGLIPITFGQGT	0.0%	FNISYASIHWVRQ	0.1%	VASIYPYHGYTFYADSV	0.1%	YSAFYGAAALDYWGQG	0.2%
QQGAGLIPITFGQGT	0.0%	FNIYHSSMHWVRQ	0.1%	VASNYPDYWGQGGYTYYADSV	0.1%	YSAFYGAVALDYWGQG	0.2%

Appendix E. NGS analysis of CDRL3, CDRH1, CDRH2, and CDRH3 mIL3Rα–2*mut* phage pool: Phage display <u>selection 2 – Round 3</u> panning against Fc–fused mIL3Rα protein. The most abundant CDRH1, H2, H3, and L3 sequences were identified by NGS. The clone containing the top most frequent CDRH1, H2, H3, and L3 sequences (bold and highlighted in yellow) was obtained by conventional single clone sequencing. This clone was labeled as mIL3Rα–2*mut* clone and used for generation of affinity–matured mIL3Rα–2*mut* antibody and further *in vitro* and *in vivo* analysis. The sequences highlighted *purple* represent the original unmutated clone from the first round of phage display selections based on NGS analysis.

CDRL3	% Frequency	CDRH1	% Frequency	CDRH2	% Frequency	CDRH3	% Frequency
QQWYSYHPITFGQGT	20.86%	**FNISSYYLHWVRQ**	25.76%	**VAFTYPYYDSSQYADSV**	28.17%	**ARGVWAYSAWSSKIGFDYWGQG**	24.26%
QQWHSSQPVTFGQGT	12.96%	FNVSGFYMHWVRQ	14.17%	VAWIYPHYGTTYYADSV	19.18%	ARGIWYNAGLSSTVGFDYWGQG	16.97%
QQWRSSYPITFGQGT	12.63%	FNISSYYVHWVRQ	11.68%	VASNYPYYGSSFYADSV	6.71%	ARGVWSYAGWSSAVGFDYWGQG	13.78%
QQWYSSHPITFGQGT	8.64%	FNISSYYMHWVRQ	11.60%	VASIYPHYGSTYYADSV	6.62%	ARGFWYLAGRSSAVGFDYWGQG	6.95%
QQWRASTPITFGQGT	5.47%	FNLSFSYLHWVRQ	7.93%	VASTYSYYGSTYYADSV	4.61%	ARGFWSYDGWSSAVGFDYWGQG	6.26%
QQWRSSKPITFGQGT	5.33%	FNISYNYMHWVRQ	4.18%	VASNYLYYGSTYYADSV	4.01%	ARGFWSYQGWSLAAGFDYWGQG	3.64%
QQWHASHPITFGQGT	4.66%	FNISSSYMHWVRQ	3.23%	VASTYPYYASNRYADSV	3.77%	ARGVWSYADRSPFVGFDYWGQG	2.05%
QQWHASSAITFGQGT	3.17%	FNSYGYYMHWVRQ	2.53%	VASIYPYYDSSYYADSV	2.35%	ARGVWSYAVWSSAVGFDYWGQG	2.05%
QQWHAANPITFGQGT	2.09%	FNIFSYYTHWVRQ	2.48%	VASIYPYYGSTYYADSV	2.35%	ARGVWYYSGWTPTVGFDYWGQG	1.71%
QQWYSSHRITFGQGT	1.96%	FNISSGYIHWVRQ	2.18%	VASIYRYYSKTDYADSV	1.86%	ARGFWSYAGWSSAVGFDYWGQG	1.37%
QQWHAAHPITFGQGT	1.89%	FNISASYMHWVRQ	1.79%	VAWIYPHYGSTYYADSV	1.51%	ARGFWYYTGWTSAVGFDYWGQG	1.03%
QQWKASHPITFGQGT	1.49%	FNIAAYYMHWVRQ	1.26%	VAYIYPVYGSSYYADSV	1.28%	ARGIWSYAGLSSVVGFDYWGQG	1.03%
QQWQSSHPITFGQGT	1.22%	FNTSLYYMHWVRQ	1.09%	VASIFPYYDSTYYADSV	1.22%	ARGVWSYLDGSSAVGFDYWGQG	0.91%
QQWVSSQAITFGQGT	1.22%	FNISSSYLHWVRQ	0.96%	VASTYPYYGSMYYADSV	1.11%	ARGVWSYSGWSSAVGFDYWGQG	0.91%
QQWHSSHPITFGQGT	0.95%	FNISPSYMHWVRQ	0.87%	VAWIYPYYSATNYADSV	0.64%	ARGVWSSRAISFLVGFDYWGQG	0.80%
QQLHATHPVTFGQGT	0.81%	FNISFYYMHWVRQ	0.70%	VARIYPYYGSIYYADSV	0.60%	ARGFWSYAGWSPAAGLDYWGQG	0.68%
QQWHPSHPITFGQGT	0.81%	FNFSSYYMHWVRQ	0.52%	VASSYPYYDSISYADSV	0.60%	ARGVWFAYAWSFAVGFDYWGQG	0.68%
QQWKSSHQITFGQGT	0.81%	FNIASYYMHWVRQ	0.52%	VASFYTYYGSSNYADSV	0.58%	ARGVWYYAAWAPAVGFDYWGQG	0.68%
QQWRSSHPITFGQGT	0.81%	FNISGYYMHWVRQ	0.48%	VASTYPYYDSSQYADSV	0.49%	ARGIWSYDGWSYAVGFDYWGQG	0.57%
QQWHSFHPITFGQGT	0.74%	FNMPSYYMHWVRQ	0.39%	VAFLYPYYGLTFYADSV	0.47%	ARGVWSFAGWASAVGFDYWGQG	0.57%
QQLHATHPITFGQGT	0.68%	FNISSYYIHWVRQ	0.31%	VASNYPYYDSSQYADSV	0.42%	ARGVWYLAGRSSAVGFDYWGQG	0.57%
QQWHSAHRITFGQGT	0.68%	FNIFSGYMHWVRQ	0.26%	VADIYPYYGSTFYADSV	0.40%	ARGVWYYTGWSSAIGFDYWGQG	0.46%
QQWHSSNPITFGQGT	0.54%	FNISNAFTHWVRQ	0.22%	VASIYPHYGTTYYADSV	0.38%	ARGIWFYSSWSSAVGFDYWGQG	0.34%
QQWRSSQPITFGQGT	0.47%	FNISSFYMHWVRQ	0.22%	VASIYPYYGSNYYADSV	0.38%	ARGIWSYTGWSFAVGFDYWGQG	0.34%
QQWRSSSPITFGQGT	0.47%	FNISSWYMHWVRQ	0.22%	VASIYSYYGSRYYADSV	0.33%	ARGVWNHGRWYSAVSFDYWGQG	0.34%
QQWHWSHPVTFGQGT	0.41%	FNISSYYSHWVRQ	0.22%	VASIFTYYGSTYYADSV	0.31%	ARGVWSYSGRASAVGFDYWGQG	0.34%
QQWHSSHAITFGQGT	0.34%	FNISSYYTHWVRQ	0.22%	VASIYPNYRSTNYADSV	0.27%	ARGVWSYVGSSSAVGFDYWGQG	0.34%
QQWKPSGPITFGQGT	0.34%	FNLSSYYMHWVRQ	0.22%	VASIYPYYDSSQYADSV	0.27%	ARGFGIWLVGLLQSVLDYWGQG	0.23%
QQWHSSYQITFGQGT	0.27%	FNTSFYYIHWVRQ	0.22%	VAYIYPYYGSDYYADSV	0.27%	ARGFWSYQGWSSAVGFDYWGQG	0.23%
QQWHSWHPITFGQGT	0.27%	FNISYYYLHWVRQ	0.17%	VAAIYPYYGATGYADSV	0.24%	ARGIWYNAGWSSAVGFDYWGQG	0.23%
QQWHTAHAITFGQGT	0.27%	FNSTSYYMHWVRQ	0.17%	VASIYPYYGLIGYADSV	0.24%	ARGLWFNWGWSSAVGFDYWGQG	0.23%
QQWRASQPITFGQGT	0.27%	FNVSSYYVHWVRQ	0.17%	VASLYPNYGSTSYADSV	0.24%	ARGVWRLSLWSSAVGFDYWGQG	0.23%
QQWHSSDSITFGQGT	0.20%	FNFSYYYMHWVRQ	0.13%	VAAIYPYYGFSYYADSV	0.22%	ARGVWSYAGWTFSIGFDYWGQG	0.23%
QQWHSSYPITFGQGT	0.20%	FNMSLYYVHWVRQ	0.13%	VASIYPYYGFTSYADSV	0.20%	ARGVWSYDGWSSAVGFDYWGQG	0.23%
QQWHSTQPLTFGQGT	0.20%	FNMSSYYMHWVRQ	0.13%	VASIYPYYGTFSYADSV	0.20%	ARGVWSYDPWSSRIGFDYWGQG	0.23%
QQWHSYHPITFGQGT	0.20%	FNPNTYYMHWVRQ	0.13%	VASTYPYYGETDYADSV	0.20%	ARGVWSYQGWSLAAGFDYWGQG	0.23%
QQWHTSRPLTFGQGT	0.20%	FNASSYYMHWVRQ	0.09%	VASIYPKYASNSYADSV	0.18%	ARGVWYSAGWSSFIGFDYWGQG	0.23%
QQWHWSHQVTFGQGT	0.20%	FNIPSYYIHWVRQ	0.09%	VAWIYPYHGSTYYADSV	0.18%	ARGVWYYARWSSAVGFDYWGQG	0.23%
QQWQSSHLITFGQGT	0.20%	FNISFHYMHWVRQ	0.09%	VASIYPYYGSSNYADSV	0.16%	ARGVWYYVSLCSHVGLDYWGQG	0.23%
QQWYSFHPITFGQGT	0.20%	FNISGFYMHWVRQ	0.09%	VASIYPYYGSTAYADSV	0.16%	ARGFGIAGRSSAVGFDYWGQG	0.11%
QQWHASLPLTFGQGT	0.14%	FNISYYYIHWVRQ	0.09%	VASIYSYYGSNYYADSV	0.16%	ARGFGIWLVGLLQWFDYWGQG	0.11%
QQWHHSQPITFGQGT	0.14%	FNTPYYYMHWVRQ	0.09%	VASTYPYYAATYYADSV	0.13%	ARGFGIWLVVSAVGFDYWGQG	0.11%
QQWHPSHTITFGQGT	0.14%	FNTSSSYIHWVRQ	0.09%	VAYIYPSYGSPNYADSV	0.13%	ARGFGSTIGYFSAVGFDYWGQG	0.11%
QQWHSAHPITFGQGT	0.14%	FNVSFSYLHWVRQ	0.09%	VAFIYPYYGSTYYADSV	0.11%	ARGFWFYADRTPAVGFDYWGQG	0.11%
QQWHSSHPVTFGQGT	0.14%	FNVSGFYIHWVRQ	0.09%	VASIYPYYGSICYADSV	0.11%	ARGFWFYVGLSAAVGFDYWGQG	0.11%
QQWHSSLPVTFGQGT	0.14%	FNVSSSYIHWVRQ	0.09%	VASIYRYYGSTYYADSV	0.11%	ARGFWLYDGYFSAVGFDYWGQG	0.11%
QQWHSSQRITFGQGT	0.14%	FNFPAYYMHWVRQ	0.04%	VASNYPYYDSSYYADSV	0.11%	ARGFWSYAGTSFRVGIDYWGQG	0.11%
QQWHSSRPITFGQGT	0.14%	FNFSSYYVHWVRQ	0.04%	VAYSYPYYGSTFYADSV	0.11%	ARGFWSYAGWSPAVGFDYWGQG	0.11%
QQWHSSSTLTFGQGT	0.14%	FNIASFYMHWVRQ	0.04%	VAFTYPYYASNRYADSV	0.09%	ARGFWSYARWSLAVGFDYWGQG	0.11%
QQWHSYHSITFGQGT	0.14%	FNIFSYYMHWVRQ	0.04%	VASFYPYYGSPGYADSV	0.09%	ARGFWSYARWSSAVGFDYWGQG	0.11%
QQWHTAHPITFGQGT	0.14%	FNILSFYLHWVRQ	0.04%	VASIFPYYESTYYADSV	0.09%	ARGFWSYDGWSPAAGFDYWGQG	0.11%
QQWHWSHPITFGQGT	0.14%	FNIRSYYMHWVRQ	0.04%	VASIYHYYRSTDYADSV	0.09%	ARGFWSYDGWSPAAGLDYWGQG	0.11%
QQWRSSQPVTFGQGT	0.14%	FNISANYMHWVRQ	0.04%	VASIYPYYGSTNYADSV	0.09%	ARGFWSYDGWSSTVGFDYWGQG	0.11%
QQWSSSHPITFGQGT	0.14%	FNISAYYIHWVRQ	0.04%	VASIYPYYGSTSYADSV	0.09%	ARGFWSYDGYFSAVGFDYWGQG	0.11%
QQWYSSQPVTFGQGT	0.14%	FNISGYYIHWVRQ	0.04%	VASIYSNYGSTYYADSV	0.09%	ARGFWSYQGWSSTVGFDYWGQG	0.11%
QQWYTSHTITFGQGT	0.14%	FNISHGYMHWVRQ	0.04%	VASNYPYYASNRYADSV	0.09%	ARGFWSYTGWTSAVGFDYWGQG	0.11%
QQGHPYDSSTFGQGT	0.07%	FNISLSYMHWVRQ	0.04%	VASTYSYYGYTSYADSV	0.09%	ARGFWYLAGRSSTVGFDYWGQG	0.11%
QQWAGSHPITFGQGT	0.07%	FNISPYYIHWVRQ	0.04%	VAYIYSYYGSVYYADSV	0.09%	ARGFWYNAGLSSTVGFDYWGQG	0.11%
QQWAPSHLITFGQGT	0.07%	FNISSFYSHWVRQ	0.04%	VAFTYPYYDSSYYADSV	0.07%	ARGFWYYIGWTSAVGFDYWGQG	0.11%
QQWDATQPTTFGQGT	0.07%	FNISSTYMHWVRQ	0.04%	VASIYNNYGSMYYADSV	0.07%	ARGIWFYAGLSSAVGLDYWGQG	0.11%
QQWDSSHSKTFGQGT	0.07%	FNISTSYIHWVRQ	0.04%	VASIYPYYDSTYYADSV	0.07%	ARGIWSIAAWSSAVGFDYWGQG	0.11%
QQWHAAHRITFGQGT	0.07%	FNISTYYVHWVRQ	0.04%	VASIYPYYGLSYYADSV	0.07%	ARGIWYFARYSSAVGFDYWGQG	0.11%
QQWHASHPVTFGQGT	0.07%	FNISYFYLHWVRQ	0.04%	VASIYPYYSVIYYADSV	0.07%	ARGIWYNAGLSSTVSFDYWGQG	0.11%
QQWHASNPITFGQGT	0.07%	FNISYYYMHWVRQ	0.04%	VASIYSYYGSTYYADSV	0.07%	ARGLWSLSGRAAFIGFDYWGQG	0.11%
QQWHASQPVTFGQGT	0.07%	FNITFYYVHWVRQ	0.04%	VASLYPYYAFTDYADSV	0.07%	ARGLWSYVGRSFRVGFDYWGQG	0.11%
QQWHAYHPITFGQGT	0.07%	FNITSYYSHWVRQ	0.04%	VASNYLYYGSMYYADSV	0.07%	ARGVCYYAGLSSEVAFDYWGQG	0.11%
QQWHPAHPITFGQGT	0.07%	FNITYFYMHWVRQ	0.04%	VASNYPYYGSTYYADSV	0.07%	ARGVWAYSACSSKLGFDYWGQG	0.11%
QQWHSAHLSTFGQGT	0.07%	FNIYANYVHWVRQ	0.04%	VASTYRYYGATYYADSV	0.07%	ARGVWAYSAWCPKIGFDYWGQG	0.11%
QQWHSSQPITFGQGT	0.07%	FNLFTYYIHWVRQ	0.04%	VAWIYPSYGSTDYADSV	0.07%	ARGVWAYSAWFV*IGFDYWGQG	0.11%
QQWHTSQAITFGQGT	0.07%	FNLSSYYIHWVRQ	0.04%	VAATYPYYGSTYYADSV	0.04%	ARGVWAYSAWFV*NWFDYWGQG	0.11%
QQWHWSDPITFGQGT	0.07%	FNMSFNYMHWVRQ	0.04%	VADIYPYYGSTYYADSV	0.04%	ARGVWAYSAWSSKLGFDYWGQG	0.11%
QQWHWSHQITFGQGT	0.07%	FNMSSHYIHWVRQ	0.04%	VAFTYPYYGSMYYADSV	0.04%	ARGVWFIAGWISAVGFDYWGQG	0.11%
QQWHWSQPVTFGQGT	0.07%	FNMSSYYLHWVRQ	0.04%	VAFTYSYYGSTYYADSV	0.04%	ARGVWFYGGRSSFVGFDYWGQG	0.11%
QQWHWTQPITFGQGT	0.07%	FNMTTSYIHWVRQ	0.04%	VASIHRYYGSTRYADSV	0.04%	ARGVWFYSGWTPTVGFDYWGQG	0.11%
QQWISYHPITFGQGT	0.07%	FNNSSYYMHWVRQ	0.04%	VASIYASYDSTNYADSV	0.04%	ARGVWSIAAWSSAVGFDYWGQG	0.11%
QQWKSARPITFGQGT	0.07%	FNSSSYYMHWVRQ	0.04%	VASIYAYYGSMNYADSV	0.04%	ARGVWSIRWLVFAVGFDYWGQG	0.11%
QQWLSYHPITFGQGT	0.07%	FNSYGYYIHWVRQ	0.04%	VASIYPHYGSMYYADSV	0.04%	ARGVWSIRWLVSAVGFDYWGQG	0.11%
QQWNSSHTLTFGQGT	0.07%	FNTSFYYMHWVRQ	0.04%	VASIYPHYGSTAYADSV	0.04%	ARGVWSLNGLSYVVGFDYWGQG	0.11%
QQWNSSVPITFGQGT	0.07%	FNTSGYYMHWVRQ	0.04%	VASIYPYYGLYYYADSV	0.04%	ARGVWSSLDGLPLVGFDYWGQG	0.11%
QQWPSSHPITFGQGT	0.07%	FNTSSYYLHWVRQ	0.04%	VASIYPYYGSSFYADSV	0.04%	ARGVWSYAARSSAVGFDYWGQG	0.11%
QQWPSSPRITFGQGT	0.07%	FNVSAYYMHWVRQ	0.04%	VASIYPYYGSTKYADSV	0.04%	ARGVWSYAAWAPAVGFDYWGQG	0.11%

Appendix F. NGS analysis of CDRL3, CDRH1, CDRH2, and CDRH3 mIL3Rβ–1*mut* phage pool: Phage display <u>selection 2 – Round 3</u> panning against Fc–fused mIL3Rβ target protein. The most abundant CDRH1, H2, H3, and L3 sequences were identified by NGS. The clones containing the top most frequent CDRH1, H2, H3, and L3 sequences (bold and highlighted in yellow) were obtained by conventional single clone sequencing. This clone was labeled as mIL3Rβ–1*mut* clone and used for generation of affinity–matured mIL3Rβ–1*mut* antibody and further *in vitro* and *in vivo* analysis. The sequences highlighted *red* represent the original unmutated clone from the first round of phage display selections based on NGS analysis. The most abundant CDL3 in the *mutated* pool of phage was indicated as the original unmutated CDRL3. The unmutated CDRH1 was not found in the *mutated* phage pool.

mIL3Rβ–1*mut* phage pool
(Selection 2: Round3 pool)

CDRL3	% Frequency	**CDRH1**	% Frequency	**CDRH2**	% Frequency	**CDRH3**	% Frequency
QQYSYSYYYPITFGQGT	8.8%	FNLSSSFMHWVRQ	16.8%	VASIYSYYGYRSYADSV	7.1%	ARSSSGWYGFDYWGQG	26.7%
QQYSYSHYYPITFGQGT	5.6%	FNLSSSFIHWVRQ	4.9%	VASIYSYYSYTSYADSV	4.1%	ARSSSGRYGFDYWGQG	4.4%
QQYSFSRYNPITFGQGT	2.0%	FNLSSSFLHWVRQ	2.8%	VASIYSHYSYTSYADSV	1.1%	ARSASGWYGFDYWGQG	4.3%
QQYSYSSYYPITFGQGT	1.4%	FNLASSYTHWVRQ	2.5%	VASIYSNYSYTSYADSV	0.9%	ARSSSGWYGLDYWGQG	4.1%
QQYSYSYHYPITFGQGT	1.3%	FNVSSSFMHWVRQ	2.1%	VASIYSYYRYTSYADSV	0.8%	ARSTSGWYGFDYWGQG	3.4%
QQYSYSYYSPITFGQGT	1.1%	FNISSSFMHWVRQ	1.4%	VASIYAYYSYTSYADSV	0.7%	ARSSSGWFGFDYWGQG	2.6%
QQYSYSYSYPITFGQGT	1.0%	FNLTSSFMHWVRQ	1.3%	VASIYSYYSYSSYADSV	0.7%	ARSPSGWYGFDYWGQG	2.4%
QQYSYSYNYPITFGQGT	1.0%	FNFSSSFMHWVRQ	1.2%	VASILSYYPYTSYADSV	0.6%	ARSYSGWYGFDYWGQG	2.3%
QQYSYAYYYPITFGQGT	1.0%	FNLSSSFVHWVRQ	1.1%	VASIYSFYSYTSYADSV	0.6%	ARSFSGWYGFDYWGQG	1.9%
QQYSYSNYYPITFGQGT	1.0%	FNLSYSFMHWVRQ	1.0%	VASIYSYYGYTSYADSV	0.6%	ARSLSGWYGFDYWGQG	1.6%
QQYSYSYYHPITFGQGT	0.9%	FNVSSSFIHWVRQ	0.9%	VASIYSSYSYTSYADSV	0.6%	ARSSSGWYGIDYWGQG	1.4%
QQYTYSYYYPITFGQGT	0.9%	FNLSSSYMHWVRQ	0.8%	VASVYSYYSYTSYADSV	0.5%	ARSSSGFYGFDYWGQG	1.3%
QQYSYSSSYPITFGQGT	0.8%	FNLSSAFMHWVRQ	0.8%	VATTYSAYSYTSYADSV	0.5%	ARSSSGYYGFDYWGQG	1.0%
QQYSYSYYDPITFGQGT	0.7%	FNVSSSFTHWVRQ	0.8%	VATIYSYYSYTSYADSV	0.5%	ARSSSGWHGFDYWGQG	0.8%
QQYSYSYYNPITFGQGT	0.7%	FNLSTSFMHWVRQ	0.8%	VASFYWNHGYISYADSV	0.5%	ARSSSGWYGYDYWGQG	0.8%
QQYSYSFYYPITFGQGT	0.6%	FNFSSSFIHWVRQ	0.7%	VASIYYHYSYTSYADSV	0.4%	ARSSSGWYGVDYWGQG	0.7%
QQYSYSYFHPITFGQGT	0.5%	FNLSASFMHWVRQ	0.6%	VATIYHSPRYTSYADSV	0.4%	ARSSSGWNGFDYWGQG	0.7%
QQYSYSYDYPITFGQGT	0.5%	FNLASSFMHWVRQ	0.6%	VASSYSYYSYTSYADSV	0.4%	ARASSGWYGFDYWGQG	0.7%
QQYSYTYYYPITFGQGT	0.5%	FNISFSFIHWVRQ	0.6%	VASIYSGYSYTSYADSV	0.4%	ARSISGWYGFDYWGQG	0.7%
QQYSYSYFYPITFGQGT	0.5%	FNLPSSFMHWVRQ	0.6%	VASIYSHYGYTSYADSV	0.4%	ARSASGRYGFDYWGQG	0.6%
QQYSYSNYSPITFGQGT	0.5%	FNLSSAFIHWVRQ	0.5%	VASTYSYYSYTSYADSV	0.4%	ARSFSGRYGFDYWGQG	0.6%
QQYSYSYHHPITFGQGT	0.5%	FNLYSSFMHWVRQ	0.5%	VASIYPYYSYTSYADSV	0.4%	ARSPSGRYGFDYWGQG	0.5%
QQYSYDYYAPITFGQGT	0.4%	FNISSSFIHWVRQ	0.5%	VASLYYDYSYTPYADSV	0.4%	ARSVSGWYGFDYWGQG	0.5%
QQYSYSYYFPITFGQGT	0.4%	FNISSSFVHWVRQ	0.5%	VASFYSYYSYTSYADSV	0.4%	ARSLSGRYGFDYWGQG	0.4%
QQYSLSYYYPITFGQGT	0.4%	FNLTSSYMHWVRQ	0.5%	VASIYSEYSYTSYADSV	0.4%	ARSSSGRFGFDYWGQG	0.4%
QQYSYSNFNPITFGQGT	0.4%	FNVTSSFIHWVRQ	0.5%	VASIYSYYSYASYADSV	0.3%	ARSSSGRNGFDYWGQG	0.4%
QQYSYSNYHPITFGQGT	0.4%	FNLSFSFMHWVRQ	0.5%	VASLYSHYSYTSYADSV	0.3%	ARSSSGRYGLDYWGQG	0.4%
QQYSFSYYYPITFGQGT	0.4%	FNLSSYFMHWVRQ	0.5%	VASSYSYYRYTSYADSV	0.3%	ARSSSGRDGLDYWGQG	0.4%
QQYSYSNNYPITFGQGT	0.4%	FNLSSSYIHWVRQ	0.5%	VASIYSYYTYTSYADSV	0.3%	ARSTSGWYGLDYWGQG	0.4%
QQYTYSYYHPITFGQGT	0.4%	FNSSSSFMHWVRQ	0.4%	VASTYSNYSYTSYADSV	0.3%	ARSYSGRYGYDYWGQG	0.4%
QQYSYSYQYPITFGQGT	0.4%	FNFSTSFMHWVRQ	0.4%	VASVYSYYSYSSYADSV	0.3%	ARSSSGWFGLDYWGQG	0.4%
QQYSYSNKSPITFGQGT	0.3%	FNLSSTFIHWVRQ	0.4%	VATIYSYYSYKSYADSV	0.3%	ARSYSGWFGFDYWGQG	0.4%
QQYSYSQYYPITFGQGT	0.3%	FNVSSTFMHWVRQ	0.4%	VASIYSDYSYTSYADSV	0.3%	ARSASGWYGLDYWGQG	0.3%
QQYSYSYGYPITFGQGT	0.3%	FNPSSSFMHWVRQ	0.4%	VATIYFSYMYNSYADSV	0.3%	ARSSTGRYGFDYWGQG	0.3%
QQYSYSKYYPITFGQGT	0.3%	FNLSSSFTHWVRQ	0.4%	VASIYSYYSYTTYADSV	0.3%	ARSYSGRYGFDYWGQG	0.3%
QQYTYSRYYPITFGQGT	0.3%	FNLYSSFIHWVRQ	0.4%	VASGYSYYRYTSYADSV	0.3%	ARSSSGWNGLDYWGQG	0.3%
QQYSYSLYYPITFGQGT	0.3%	FNMSSSFMHWVRQ	0.4%	VASSYSYHSYTSYADSV	0.3%	ARSSSGRSGFDYWGQG	0.3%
QQHSYSSYYPITFGQGT	0.3%	FNVSSSFVHWVRQ	0.4%	VATIYSYHSYTSYADSV	0.3%	ARSTSGRYGFDYWGQG	0.3%
QQYAYSYYYPITFGQGT	0.3%	FNVTSSFMHWVRQ	0.4%	VASLYSYYSYTSYADSV	0.3%	ARGSSGWYGFDYWGQG	0.3%
QQYSYSYYGPITFGQGT	0.3%	FNLASSFIHWVRQ	0.3%	VASVYPYYSYASYADSV	0.3%	ARSLSGWYGLDYWGQG	0.3%
QQYSYSHHYPITFGQGT	0.3%	FNLSSTWMHWVRQ	0.3%	VASIFSYYSYTSYADSV	0.3%	ARSRSGWYGFDYWGQG	0.3%
QQYSYSYYTPITFGQGT	0.3%	FNVYSSFMHWVRQ	0.3%	VASIYPYYSYTAYADSV	0.3%	ARSSSGMYGFDYWGQG	0.3%
QQHSYSYYYPITFGQGT	0.3%	FNHSSSFVHWVRQ	0.3%	VASIYSNYRYTSYADSV	0.3%	ARSASGWFGFDYWGQG	0.3%
QQYSHAYYYPITFGQGT	0.3%	FNISSAFMHWVRQ	0.3%	VASIYSYYSYTAYADSV	0.3%	ARSGSGWYGFDYWGQG	0.3%
QQYSYQYFYPITFGQGT	0.3%	FNLSNSFMHWVRQ	0.3%	VASNYSYYRYTSYADSV	0.3%	ARSSSGRYGIDYWGQG	0.3%
QQYSYSYYKPITFGQGT	0.3%	FNLTYSYMHWVRQ	0.3%	VASNYYYYSYTSYADSV	0.3%	ARSSAGRYGFDYWGQG	0.2%
QQYSYAYYHPITFGQGT	0.3%	FNLSSYFIHWVRQ	0.3%	VASIYSDYSYSSYADSV	0.3%	ARSCSGWYGFDYWGQG	0.2%
QQYAYSYYHPITFGQGT	0.2%	FNLSPSFMHWVRQ	0.3%	VASIYYYYSYTSYADSV	0.3%	ARSSSAWYGFDYWGQG	0.2%
QQYYYSYYYPITFGQGT	0.2%	FNLSSRYIHWVRQ	0.3%	VASIYSSYRYTSYADSV	0.3%	ARSSSGWYGSDYWGQG	0.2%
QQYSYFYYYPITFGQGT	0.2%	FNLSSTFMHWVRQ	0.3%	VASIYSYYSYNSYADSV	0.3%	ARSSSGWFGIDYWGQG	0.2%
QQYSYSYHSPITFGQGT	0.2%	FNHSSSFMHWVRQ	0.3%	VASIYGYYSYTSYADSV	0.3%	ARSFSGWYGLDYWGQG	0.2%
QQYSYSYRYPITFGQGT	0.2%	FNLSSAYMHWVRQ	0.3%	VASVYSAYSYSSYADSV	0.3%	ARSHSGKYGFDYWGQG	0.2%
QQYSFSYHSPITFGQGT	0.2%	FNLSSHFVHWVRQ	0.3%	VASNYSYYSYTSYADSV	0.3%	ARSSSGYYGLDYWGQG	0.2%
QQYSYAYYNPITFGQGT	0.2%	FNLTSSFIHWVRQ	0.3%	VASTYSSYSYTSYADSV	0.3%	ARSLSGWFGFDYWGQG	0.2%
QQYSYSSSSPITFGQGT	0.2%	FNISSSFLHWVRQ	0.3%	VATIYSSYSYTSYADSV	0.3%	ARSNSGWYGFDYWGQG	0.2%
QQYTYSGFWPITFGQGT	0.2%	FNMSASFIHWVRQ	0.3%	VASVLSVYNYTSYADSV	0.2%	ARSSSGLYGFDYWGQG	0.2%
QQYTYSYSYPITFGQGT	0.2%	FNVSSSYMHWVRQ	0.3%	VASIYPYHTYSSYADSV	0.2%	ARSSSGMYGVDYWGQG	0.2%
QQYAYSYYNPITFGQGT	0.2%	FNISSTFMHWVRQ	0.2%	VASIYTYYSYTSYADSV	0.2%	ARSTSGWFGFDYWGQG	0.2%

Appendix G. Anti–mIL3Rα–2 antibody blocked IL3–induced suppression of imatinib activity and inhibited proliferation, induced apoptosis, and disrupted colony formation in CML cells *in vitro*. (A) Anti–mIL3Rα–2 antibody treatment of CJ cells partially attenuated cell viability in a dose–dependent manner *in vitro* (*P < 0.0001). (B) Anti–mIL3Rα–2 antibody inhibited IL3–induced suppression of imatinib activity in a dose–dependent manner *in vitro (*P = 0.0014, **P < 0.0001). (C) Anti–mIL3Rα–2 antibody reverses IL3–induced Imatinib suppression *(*P = 0.0345; ** P < 0.0001), provides an additive effect to Imatinib cytotoxicity (*** P = 0.0165), and reverses the effect of exogenous IL3 on CML cells *in vitro*. Y–axis numbers denote the absorbance (nm) in MTT assay, and X–axis shows multiple treatment combinations. (D) Anti–mIL3Rα–2 reversed IL3 suppression of imatinib activity and promoted apoptosis and cell death in CML cells *in vitro.* Y–axis represents the percentage of apoptotic Annexin V–APC+ cells. X–axis indicates various treatments. (E) Anti–mIL3Rα–2 antibody impaired IL3–induced colony formation capacity of CML cells in the presence of imatinib *in vitro.* Bars represent the mean; error bars indicate mean ± SD; * P < 0.0001; significance of difference analyzed by one-way ANOVA following by Tukey *post hoc* test for multiple comparisons. (F) Western blot analysis of blocking downstream IL3 signaling: anti–mIL3Rα–2 antibody inhibits IL3–induced phosphorylation of STAT5 in CJ cells individually.

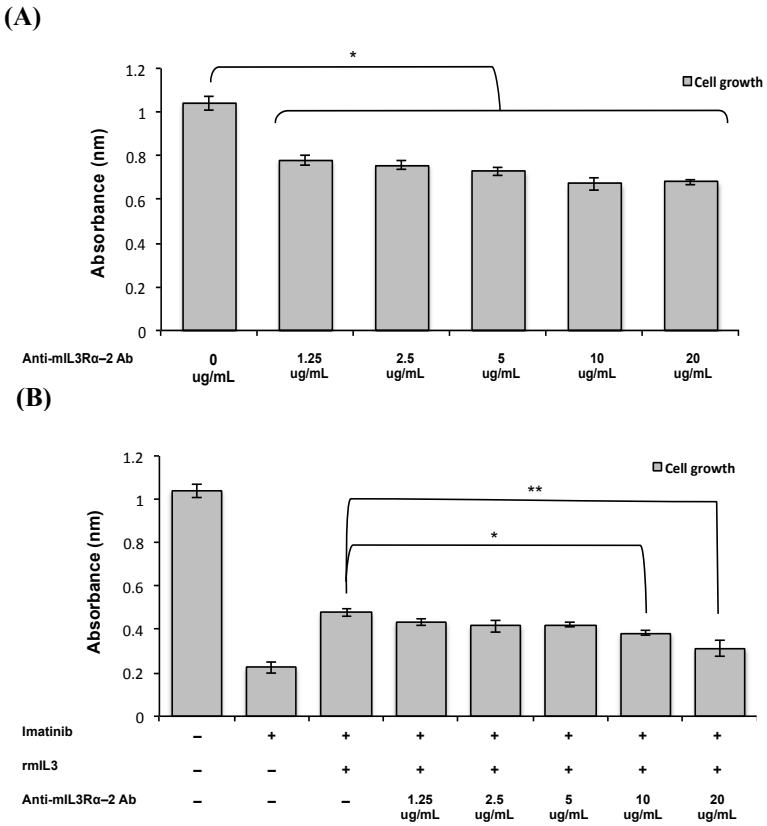

(C)

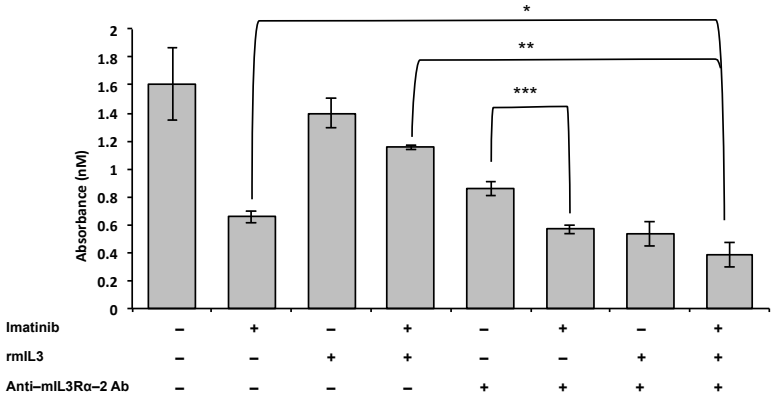
Absorbance (nM)
2
1.8
1.6
1.4
1.2
1
0.8
0.6
0.4
0.2
0
*
**
***
Imatinib – + – + – + – +
rmIL3 – – + + – – + +
Anti–mIL3Rα–2 Ab – – – – + + + +

(D)

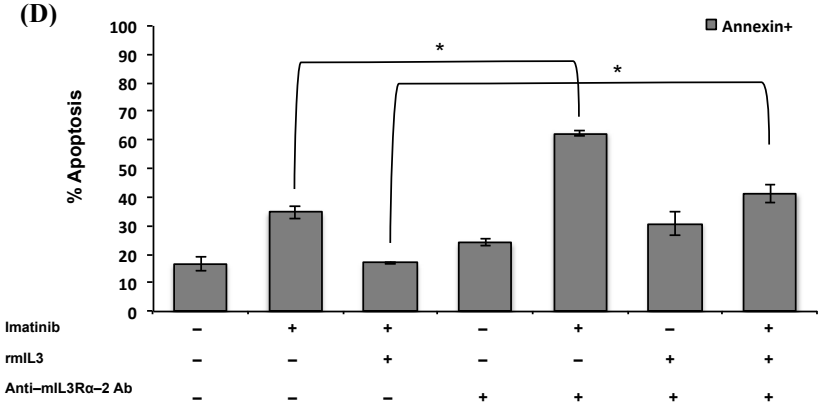
% Apoptosis
Annexin+
100
90
80
70
60
50
40
30
20
10
0
*
*
Imatinib – + + – + – +
rmIL3 – – + – – + +
Anti–mIL3Rα–2 Ab – – – + + + +

(E)

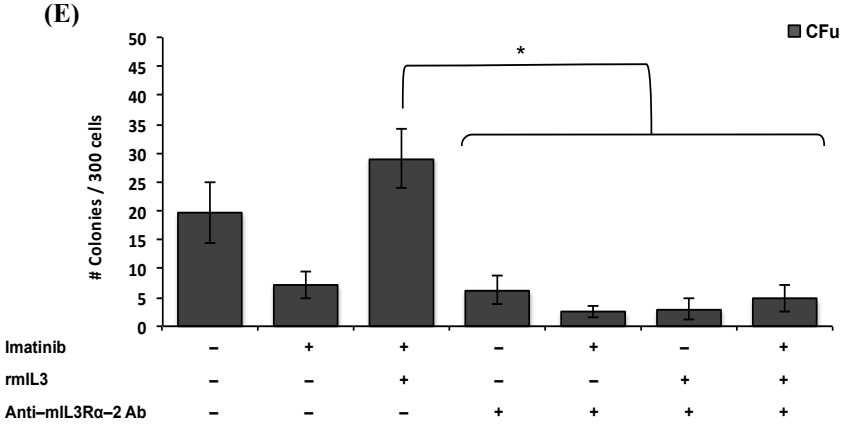
Colonies / 300 cells
CFu
50
45
40
35
30
25
20
15
10
5
0
*
Imatinib – + + – + – +
rmIL3 – – + – – + +
Anti–mIL3Rα–2 Ab – – – + + + +

(F)

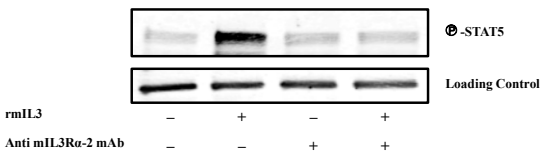
P-STAT5
Loading Control
rmIL3 – + – +
Anti mIL3Rα-2 mAb – – + +

Appendix H. Engraftment of anti–mIL3Rα–2 antibody–treated CJ cells increased disease latency in the mouse model. CJ cells were treated with antibody in the presence or absence of IL3 and / or imatinib at 37ºC for 48 hours and transplanted into sub–lethally irradiated C57BL/6 mice. Survival curves were compared by log rank test (N = 6–8 mice per treatment group). Kaplan–Meier survival curves show (A) A significant decrease in mouse survival in mice transplanted with IL3 and imatinib–treated cells, as compared with untreated or imatinib group; P = 0.0049. (B) Engraftment of cells treated with anti–mIL3Rα–2 antibody with IL3+imatinib lead to significant increase in survival of mice; P = 0.0002. (C–D) Engraftment of cells treated with anti–mIL3Rα–2 antibody treatment resulted in a significant increase in mouse survival as compared with imatinib; P = 0.0069 and P = 0.0022, respectively (E) Engraftment of cells treated with anti–mIL3Rα–2 antibody and exogenous IL3 caused a significant increase in survival of mice, as compared to IL3–treated group; P = 0.0078.

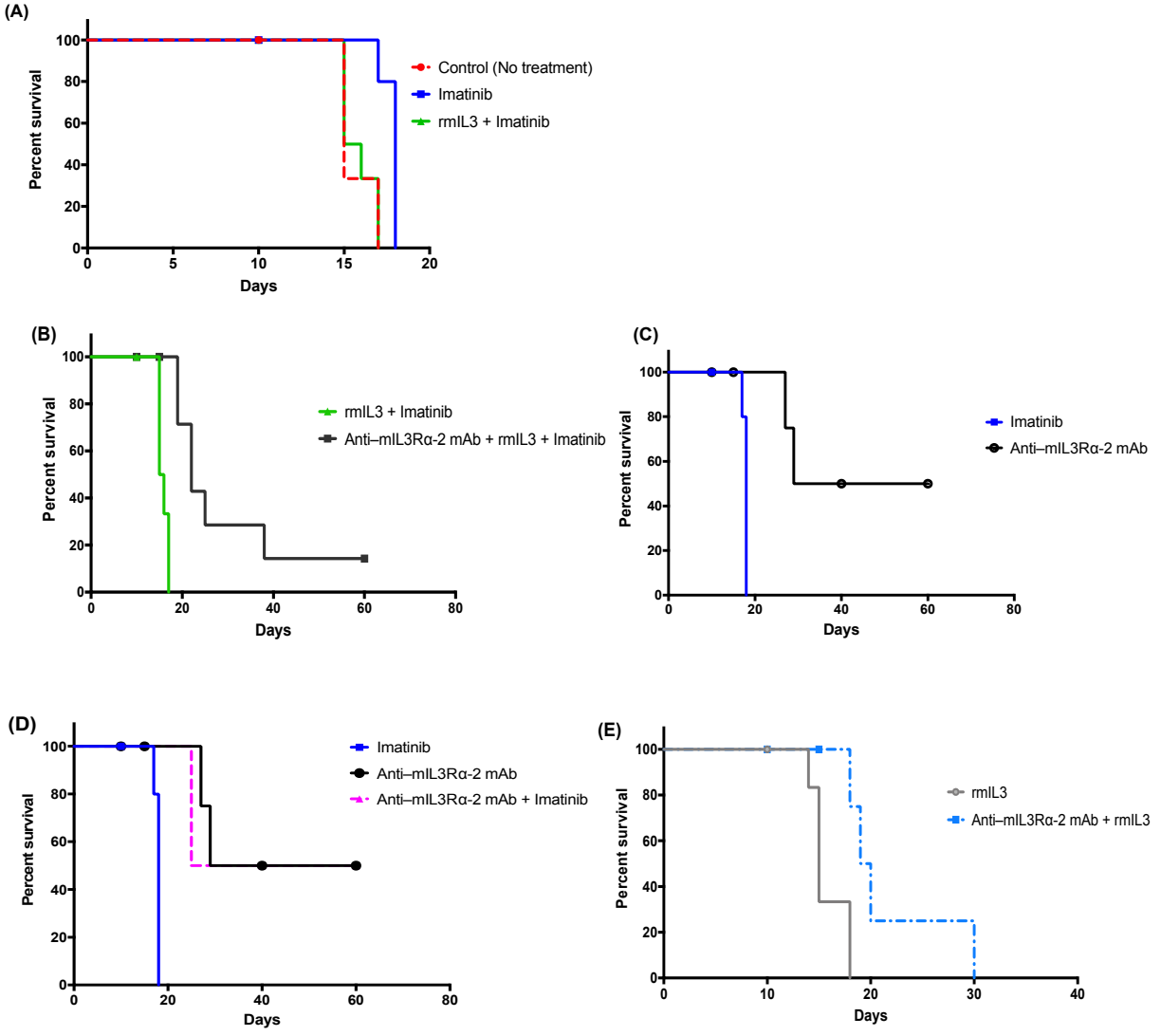

Appendix I. Preliminary analysis of the effect of anti–mIL3Rβ–1 antibody in reversal of IL3–mediated imatinib suppression and inhibition of cell proliferation in human and mouse CML cells *in vitro*. Cells were incubated with 10 µg / mL anti–mIL3Rβ–1 antibody for 3 hours at 37ºC, following by adding IL3 and incubation for 3 hours at 37ºC, and final addition of Imatinib and incubation of cells for 48 hours at 37ºC. Final concentration of cells: 5.0E05 / mL; Cells were evaluated after 48 hours of treatment. Anti–mIL3Rβ–1 antibody reversed the IL3–mediated imatinib suppression. (A) Viability assay on KU–812 human CML cells. Bars represent the mean; error bars indicate Mean ± SD; **P* < 0.0001; (B) MTT assay on CJ cells. Bars represent the mean absorbance; error bars indicate Mean ± SD; **P* = 0.0336; Y–axis numbers denote % cell viability (A) or absorbance (nm) (B). X–axis shows multiple treatment combinations. Data analysis was performed by one-way ANOVA followed by Tukey *post hoc* test for multiple comparisons.

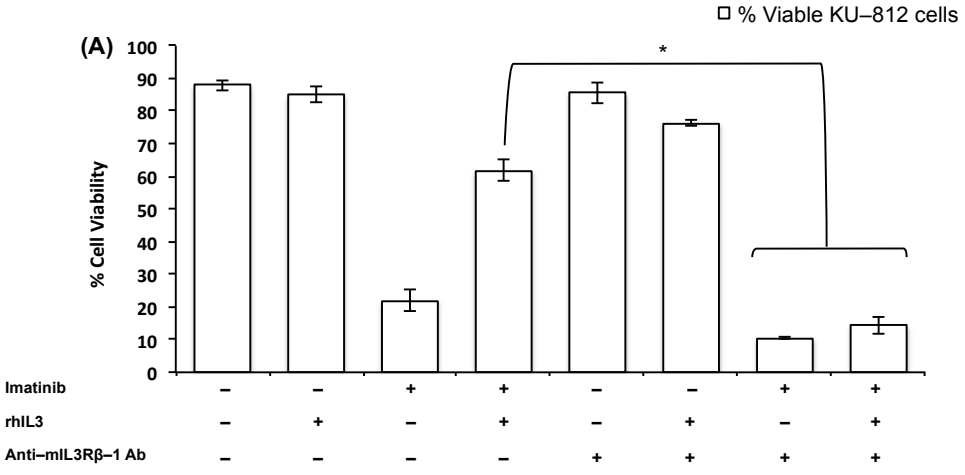

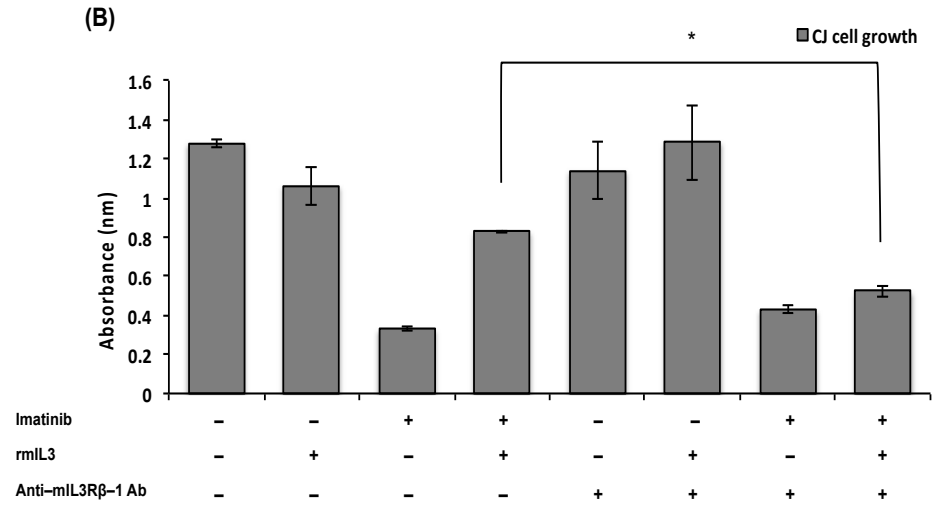

Appendix J. Anti–mIL3Rα–1*mut* antibody induced direct cell killing on mouse CML cells *in vitro*. CJ cells were treated with anti–mIL3Rα–1*mut* antibody ranging 0 – 10 μg / mL at 37ºC for 48 hours. (A) MTT assay shows a direct inhibitory effect of 4–10 ug/mL of antibody on cell proliferation in the absence of exogenous IL3 and imatinib. Y–axis numbers denotes the absorbance (nm) and X–axis indicates antibody titration of 0 – 10 μg / mL; * $P < 0.0001$. (B) Colony formation assay shows that imatinib treatment of cells caused 4–5 fold decrease in colony formation, while anti–mIL3Rα–1*mut* antibody treatment of CJ cells decreased 100–fold decrease in colony formation. Colony forming units (CFU) were analyzed by light microscopy. Y–axis numbers denotes the Cfu / mL and X–axis indicates treatments; * $P < 0.0001$. (C) Control anti–MBP antibody. Control anti–MBP antibody, ranging 0 – 20 μg /mL, did not affect CJ cell proliferation ($P > 0.9$). Y–axis numbers denote the absorbance (nm) and X–axis indicates antibody titration. Bars represent the mean; error bars indicate Mean ± SD; Significance of difference was analyzed by one-way ANOVA followed by Tukey *post hoc* test for multiple comparisons.

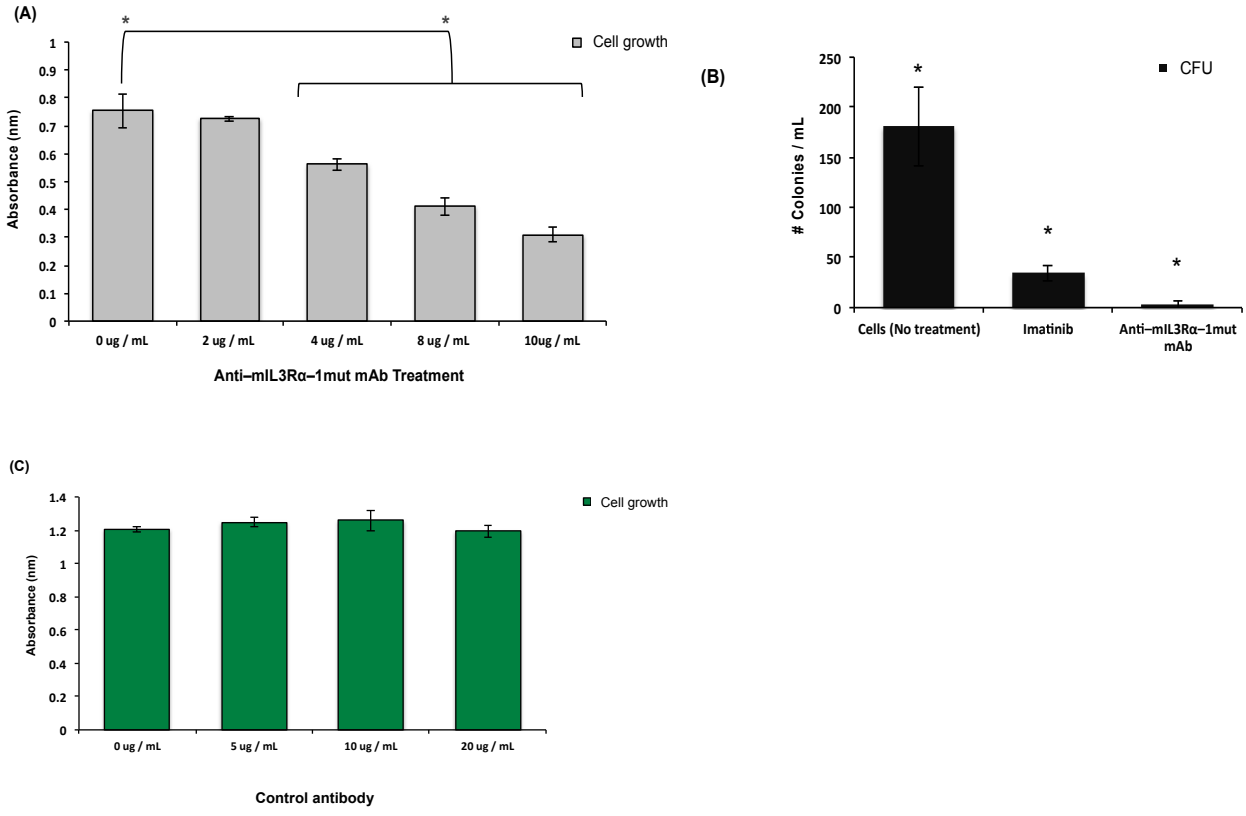

Appendix K. Anti–mIL3Rα–1*mut* antibody induced direct cell apoptosis in CJ cells in the absence of exogenous IL3. Flow cytometry density plot analysis to detect apoptosis and cell death. (A) Unstained untreated CJ cells. Negligible apoptosis and cell death (B–C) Single color controls for flow cytometry analysis. (D–F) Anti–mIL3Rα–1*mut* antibody treatment of CJ cells shows a significant increase in the SYTOX blue positive (dead cells) population. Y–axis represents cells stained with SYTOX blue; X–axis indicates Annexin V APC staining. The density plot gates indicate Q1: SYTOX blue+|APC–, Q2: SYTOX blue–|APC–, Q3: SYTOX blue–|APC+, Q4: SYTOX blue–|APC–; Q2 represents necrotic cells; Q3 is representative of apoptotic cells; $P = 0.0007$ based on three independent data collections and data analysis by unpaired two–tailed *t* test.